



**University of Pavia**

**PhD School: Biomedical Science**

PhD Course Coordinator: Prof. Egidio D'Angelo

Tutor: Prof. Livia Visai

*PhD Thesis*

**Effects on bone remodeling by  
strontium-containing nanoparticles**

PhD Candidate: Francesco Cristofaro

*XXIX Cycle*

Academic year 2015/2016



*PAR INGENIO VIRTUS*

# Table of Contents

<b>1. Abstract .....</b>	<b>1</b>
<b>2. General introduction and objectives of the thesis.....</b>	<b>2</b>
2.1 Bone Tissue .....	2
2.1.1 Molecular mechanisms of osteoblast differentiation and osteogenesis .....	4
2.1.2 Molecular mechanisms of osteoclast differentiation and bone resorption .....	7
2.1.3 The bone remodeling process .....	11
2.1.4 Calcium homeostasis .....	14
2.2 Osteoporosis .....	15
2.2.1 Osteoporosis and microgravity .....	16
2.3 Treating osteoporosis: drug therapies.....	17
2.3.1 Calcium and vitamin D.....	17
2.3.2 Anti-resorptive agents.....	17
2.3.3 Anabolic drugs.....	19
2.3.4 New target in osteoporosis pharmacological treatment.....	20
2.3.5 Nanotechnologies and bone repair in osteoporotic patients .....	21
2.4 The effect of strontium on bone regeneration .....	23
2.4.1 Strontium Ranelate .....	24
2.4.2 Strontium Chloride .....	26
2.4.3 Strontium-containing Hydroxyapatite .....	26
2.5 Objectives of the thesis.....	30
2.6 References .....	31
<b>3. Synthesis and Characterization of Strontium-substituted hydroxyapatite nanoparticles for bone regeneration .....</b>	<b>44</b>
3.1 Introduction .....	44
3.2 Materials and Methods .....	46
3.2.1 HA nanopowders: synthesis and suspensions preparation .....	46
3.2.2 Characterization techniques and procedures .....	46
3.2.3 Biocompatibility studies .....	48
3.2.4 Effect on cell viability and apoptosis of Sr Ranelate, Sr Chloride (SrCl <sub>2</sub> ) and Sr100S ....	49
3.2.5 Statistical analysis.....	49
3.3 Results .....	50

3.3.1 Nanopowders and suspensions characterization.....	50
3.3.2 Cell viability, apoptosis and morphology .....	58
3.4 Discussion .....	62
3.5 Conclusion and Future Perspective .....	67
3.6 References .....	68
<b>4. Effect of Strontium-containing nanoparticles on Bone Remodeling: <i>in vitro</i> cell studies.....</b>	<b>73</b>
4.1 Introduction .....	73
4.2 Materials and Methods .....	75
4.2.1 Cell culture conditions and nanoparticles treatment.....	75
4.2.2 Nanoparticles suspension preparation .....	76
4.2.3 Nanoparticles uptake studies .....	77
4.2.4 Cell viability, apoptosis and morphological analysis .....	78
4.2.5 Enzyme assays for evaluation of differentiation process.....	79
4.2.6 Extracellular Matrix (ECM) deposition and mineralization.....	80
4.2.7 Gene expression.....	83
4.2.8 Statistics .....	84
4.3 Results .....	85
4.3.1 Osteoblasts-like SAOS-2 cell line .....	85
4.3.2 Human Bone Marrow Mesenchymal Stem Cells (hBMMSCs) .....	96
4.3.3 Osteocytes cell line Ocy454 .....	101
4.3.4 Murine macrophage RAW264.7 cell line.....	106
4.4 Discussion .....	108
4.5 Conclusion and Future Perspective .....	118
4.6 References .....	119
<b>5. <i>In vivo</i> effect of gelatin sponge enriched with Sr-hydroxyapatite on ectopic bone formation .....</b>	<b>127</b>
5.1 Introduction .....	127
5.2 Materials and methods.....	130
5.2.1 Materials preparation .....	130
5.2.2 Animals and Surgery .....	130
5.2.3 Harvest and X-ray Imaging .....	130
5.2.4 Histology analysis.....	130

5.2.5 RNA extraction and gene expression .....	131
5.2.6 Statistics .....	133
5.3 Results .....	134
5.3.1 X-ray Imaging.....	134
5.3.2 Histology analysis.....	135
5.3.3 Gene expression.....	136
5.4 Discussion .....	142
5.5 Conclusion and Future Perspective .....	145
5.6 References .....	146
<b>6. Sr-containing nanoparticles as a potential countermeasure for the bone loss induced by microgravity .....</b>	<b>150</b>
6.1 Introduction .....	150
6.2 Materials and Methods .....	153
6.2.1 Isolation, expansion, and culture of hBMMSCs.....	153
6.2.2 Cell Culture Condition and Nanoparticles treatment.....	153
6.2.3 Culture on the RPM .....	154
6.2.4 Resazurin-based assay .....	154
6.2.5 Alkaline Phosphatase (ALP) Activity .....	155
6.2.6 Quantification of calcium – Alizarin Red Staining .....	155
6.2.7 Extraction of ECM proteins and enzyme-linked immunosorbent assay .....	155
6.2.8 Fluorescence microscopy analysis.....	156
6.2.9 Gene expression analyses .....	156
6.2.10 Experiment performed on ISS .....	157
6.2.11 Human Cytokine Antibody Array .....	158
6.2.12 Statistics.....	159
6.3 Results .....	160
6.3.1 FIRST PART: Experiment on simulated microgravity (RPM) .....	160
6.3.2 SECOND PART: Experiment performed on ISS .....	164
6.4 Discussion .....	169
6.5 Conclusion and Future Perspectives.....	172
6.6 References .....	173
<b>7. Summary, closing remarks and future perspectives .....</b>	<b>178</b>
7.1 Summary and address to the aims .....	178

7.2 Closing remarks and Future Perspectives .....	180
<b>8. List of Abbreviations.....</b>	<b>182</b>
<b>9. Aknowledgements .....</b>	<b>186</b>
<b>10. Publications .....</b>	<b>187</b>
<b>11. Curriculum Vitae .....</b>	<b>189</b>

# 1. Abstract

In this thesis, research efforts focused on the development of a new nanosystem for the delivery of strontium to improve bone formation are reported. Strontium-substitute hydroxyapatite nanoparticles were synthesized and deeply physical-chemical characterized. The effect of nanoparticles on bone remodeling was evaluated using four different *in vitro* models that allowed investigations on every single bone cell type: bone marrow mesenchymal stem cells, osteoblasts, osteocytes and osteoclasts. Sr-containing nanoparticles enhanced osteoblasts differentiation by increasing alkaline phosphatase activity, bone matrix deposition and mineralization and gene expression of specific markers for osteogenesis. In addition, Sr-containing nanoparticles inhibited the differentiation of osteoclasts, the cells responsible for bone resorption, by reducing tartrate-resistant acid phosphatase activity and preventing cell fusion and adhesion with inhibition of multinucleated cell formation. Sr-containing nanoparticles affected also the osteocytes differentiation inducing more mature stages and improving their ability to deposit a mineralized bone matrix.

Moving from *in vitro* to *in vivo*, a new material was developed made of gelatin sponge and enriched with Sr-hydroxyapatite and its effect on ectopic bone formation was evaluated in mice. Ectopic bone formation induced by Sr-hydroxyapatite resulted comparable, even greater in some cases, to Bone Morphogenetic Protein 2 (BMP2) effect, a well-known agent with osteinduction properties. Histology analysis and gene expression revealed increased endochondrial ossification induced by Sr-hydroxyapatite. Moreover, Sr-hydroxyapatite enriched sponges improved bone formation enhancing osteogenic-associated gene expression and reducing that related to osteoclasts differentiation.

Finally, the effect of Sr-containing nanoparticles was also studied in simulated and real microgravity conditions showing to be a useful countermeasure to the bone reduction induced by this environment, with lower side effects than pharmacological treatments.



# Chapter 1

---

## 2. General introduction and objectives of the thesis

The change in living conditions during the twentieth century, compared to the previous centuries, has brought major benefits to the welfare and health of mankind. However, the increased life-expectancy, the dynamism of activities (e.g. transportation methods and sport activities), and the growing world population lead to a substantial increase in patients who suffer from damaged, malfunctioning or diseased tissues or body parts. In the case of bone tissue, the increase in the number of elderly people has led to an increase in cases of osteoporosis. Moreover, the normal function of bone tissue can be impaired by many traumatic injuries and some pathological disorders, such as osteoarthritis, osteogenesis imperfecta, and Paget's disease. These malfunctions cause nonunion bone fractures, bone deformation, severe pain, and loss of mobility<sup>1</sup>.

### 2.1 Bone Tissue

Bone tissue is a type of connective tissue. It consists of cells and extracellular matrix, 70% of which is made of inorganic compounds (mostly calcium phosphate). Bone tissue forms the skeleton bones and has support-mechanical function. Moreover, bone tissue is the depot of calcium and phosphorus.

Morphological and functional properties of bone change with age and physical activity and depend on nutritional condition, the influence of endocrine glands, innervation, etc.

Bone is a hard connective tissue with cells, *osteocytes*, distributed in the abundance of matrix that works as support, attachment site, leverage, protection and mineral storage. To obtain great strength and rigidity with some elasticity, the matrix is composed of densely packed collagen fibrils infiltrated with bone mineral as fine crystals of calcium salts resembling *hydroxyapatite* crystals. Mineral constitutes about 65% of the dry weight of bone. The densely packed *collagen fibrils* are primarily type I. There are small amounts of distinctive non-collagenous proteins, e.g., calcium-binding *osteocalcin* and bone *sialo-proteins*. Matrix is strong but dense, thus nutritive fluids cannot diffuse freely through it. Osteocytes, therefore, differ from chondrocytes in having many long processes extending through canaliculi (narrow passages) throughout which they make contact each another and, indirectly, with blood vessels. The cell body lies in a lacuna, in the matrix<sup>2</sup>.

Bone cell types include *osteoblasts*, which build new bone tissue; *osteoclasts*, which break down bone tissue; *osteocytes*, which hold the bone together; and lining cells, which protect the bone.

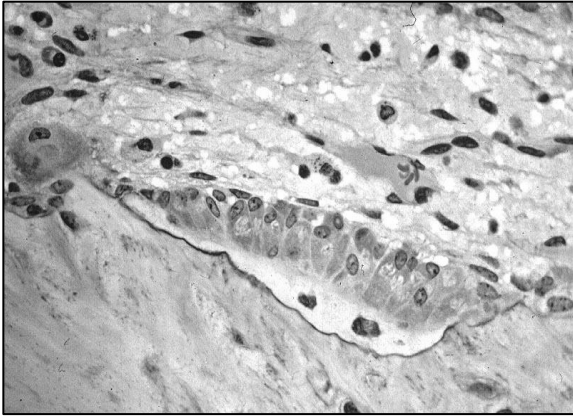


Fig 1.1 - Light micrograph of osteoblasts actively synthesizing osteoid<sup>3</sup>

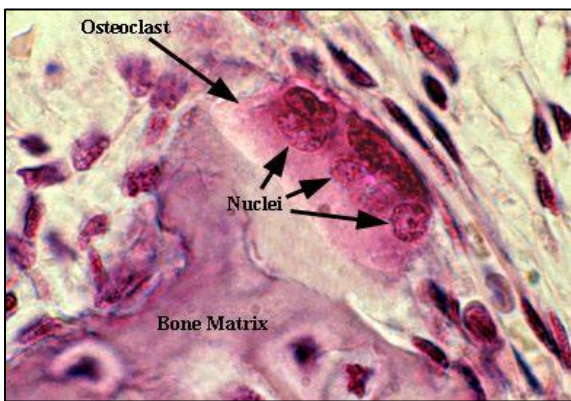


Fig 1.2 - Light micrograph of osteoclast<sup>6</sup>



Fig. 1.3 Transmission electron micrograph of Osteocyte<sup>8</sup>

Osteoblasts are mono nucleated cells that synthesize bone matrix. In the process of bone formation they work in groups of connected cells (individual cells cannot make bone). The group of organized osteoblasts together with the bone matrix made by a unit of cells is usually called the *osteon*. Osteoblasts are specialized, terminally differentiated products of

mesenchymal stem cells<sup>3</sup>. They synthesize very dense, cross-linked collagen, and several additional specialized proteins in much smaller quantities, including osteocalcin and osteopontin, which compose the organic component of the matrix. Osteoclasts are necessary for the maintenance, repair, and remodeling of bones. They disassemble and digest the composite of hydrated protein and mineral at a molecular level by secreting acid and a collagenase, in the process known as bone resorption.

This process also helps regulate the level of blood calcium. Talking about morphology, an osteoclast is a large multinucleated cell and human osteoclasts typically have five nuclei and are about 150-200  $\mu\text{m}$  in diameter<sup>4</sup>. Osteoclasts lie in a small cavity called Howship's lacunae, formed from the digestion of the underlying bone. They form podosomes to attach to

the bone in sealing zones<sup>5</sup>. Osteocytes are non-proliferative, terminally differentiated cells of the

osteoblast lineage. They reside both in the mineralized bone matrix and in newly formed osteoid, locked inside small lacuna spaces in the hard substance of bone and, for obvious reasons, are considered non-migratory. On the other hand, recent studies have proposed that osteocytes are, at some level, motile within their lacuna/canalicular system and that they might be capable of retracting and extending cytoplasmic processes in the canals. They form an extensive syncytial network through small dendritic/cytoplasmic processes in canaliculi<sup>6</sup>.

Throughout life, because of maintaining *mineral homeostasis*, and its features of growth, bone remains in an unending turnover, with selective destruction and replacement - the *remodeling* process.

### **2.1.1 Molecular mechanisms of osteoblast differentiation and osteogenesis**

Osteoblastogenesis describes a process of osteoblast development encompassing initiation, proliferation, differentiation, and maturation.

Osteoblasts are responsible for the deposition of bone matrix and for osteoclasts regulation. They arise from a common pluripotent mesenchymal stem cell (MSC), following timely programmed steps requiring the expression of specific genes, which in turn are under the control of pro-osteogenic pathways. MSCs represent less than 0.01% of the bone marrow cell population and have the capacity to differentiate into osteoblasts, chondrocytes and adipocytes, depending on the transcription factors that regulate the pathway<sup>7</sup>.

MSC differentiation into osteoblasts can be achieved *in vitro* in the presence of vitamin D3, ascorbic acid and  $\beta$ -glycerophosphate. Osteoblast differentiation from MSCs appears to be stimulated by two families of growth factors: the Wnt family members (19 Wnt ligands are encoded in both the human and the mouse genome) and the *bone morphogenetic proteins* (BMPs), which belong to the *transforming growth factor beta* (TGF- $\beta$ ) superfamily. BMPs and Wnt pathways are crucial especially for the early stage of osteoblastogenesis, where they promote MSCs commitment towards an osteo/chondroprogenitor<sup>8</sup>.

Wnts activate three distinct intracellular signaling cascades: the Wnt/ $\beta$ -catenin pathway, the Wnt/ $\text{Ca}^{2+}$  pathway and the Wnt/planar polarity pathway. The Wnt/ $\beta$ -catenin pathway is frequently referred to as the canonical pathway and it promotes cell fate determination, proliferation and survival through the increase of  $\beta$ -catenin levels and alteration of gene expression by the transcription factor Lymphoid enhancer factor/T cell factor (Lef/Tcf). Activation of this signalling pathway occurs with binding of Wnt to *Frizzled* (Fz), a transmembrane receptor, and low-density lipoprotein receptor related protein 5/6 (LRP5/6) co-receptors. LRP5 interacts with proteins from the Wnt family to form a complex with Fz leading to the activation of the canonical Wnt signalling pathway.

In the absence of a Wnt ligand, the cytosolic level of  $\beta$ -catenin is kept low by its phosphorylation and degradation, thereby suppressing the expression of Wnt-responsive genes<sup>9</sup>.

There are contrasting findings about the role of the canonical Wnt pathway, but they have been reconciled recently by Liu *et al* who found that Wnt/ $\beta$ -catenin signalling favors osteogenic commitment in basal medium by inhibiting MSC commitment into adipocytes, but inhibits osteoblast differentiation in osteogenic conditions in human MSC cultures<sup>7,10</sup>.

Osteoblastogenesis requires sequential expression of at least two transcription factors: Runx2/Cbfa1 (*Runt-related transcription factor 2 / core binding factor alpha 1*), a member of the Runt family, and *Osterix* (Osx), a downstream target of Runx2. In the absence of Runx2 and Osx, no osteoblasts are formed.

Runx2 is a master gene of osteoblast differentiation, as demonstrated by the fact that Runx2-null mice are completely deprived of osteoblasts. This leads to bone lack and failure of chondrocytes of cartilage template to undergo hypertrophy<sup>11</sup>.

During embryonic development, Runx2 is expressed just before osteoblast differentiation and only in mesenchymal cells committed to become either chondrocytes or osteoblasts.

Among the several targets downstream of Runx2 there is Osx, also known as Sp7, whose expression in MSC progenitors is stimulated by BMPs and *Insulin-like Growth Factor* (IGF)-1<sup>12</sup>. On the other hand, the lack of LRP5 blocks the expression of Osx and, as a consequence, the cell can acquire a chondrogenic phenotype<sup>13</sup>.

A further transcription factor, *Distal-less homeobox 5* (Dlx5), promotes osteogenesis under the control of many osteogenic signals including BMP-2 and it is highly expressed in the developing skeleton. Dlx5 is phosphorylated by protein kinase A (PKA), which is involved several steps of osteoblast differentiation. It was found that PKA activation increases the protein stability, osteogenic activity and transcriptional activity of Dlx5<sup>14</sup>.

It has been observed that, after the expression of Runx2, there is a proliferation phase, during which osteoblast progenitors acquire bone-specific alkaline phosphatase (ALP) activity. These cells are now pre-osteoblasts, which undergo morphological changes, becoming large, cuboidal cells highly positive for ALP activity and very active in the synthesis of the extracellular matrix (ECM), mainly consisting of *collagen type I* (Col I)<sup>8</sup>.

The late stage of osteoblast differentiation (after around 28 days from beginning of process) is characterized by increased levels of Col I, which is expressed from the beginning of osteoblast differentiation and is the main structural component of bone matrix, and by the production of non-collagenous proteins such as *bone sialo protein* (BOSP I and BOSP II), *osteopontin* (OPN), *osteonectin* (ONT), *osteocalcin* (OCN). OPN (and ALP) is important in stabilizing the matrix, while OCN is a highly carboxylated protein, almost exclusively expressed in bone and it is up-regulated in the late differentiation stage. This stage coincides with the onset of mineralization suggesting that osteocalcin may play a part in the regulation of matrix mineralization<sup>9</sup>.

Mature osteoblast can be eventually trapped in the bone matrix just deposited and mineralized<sup>8</sup>. The function of mature osteoblasts, including the ability to synthesize ECM proteins, requires LRP5 as well as the signalling protein *activating-transcription factor 4* (ATF4). The effects of Wnt co-

receptor LRP5 are linked to its role on the Wnt signalling pathway and the importance of this molecule is confirmed by studies in humans where mutations that inactivate LRP5 were shown to cause osteoporosis<sup>9</sup>.

On the other hand, there are two major cytokines, *Tumor necrosis factor* (TNF)- $\alpha$  and *interleukin* (IL)- $1\beta$  that lead to decrease bone mineral density by inhibiting osteoblast differentiation from pluripotent progenitor cells and bone formation in many inflammatory diseases<sup>15</sup>. TNF- $\alpha$  for instance has been reported to decrease Runx2 expression and promote its degradation<sup>16</sup>.

Osteoblasts that differentiate at the site of formation from precursor cells perform bone formation, which is a slow phase that completes the remodeling cycle by fully replacing the removed bone with new osteoid that eventually mineralizes. Bone formation restores the resorbed matrix by means of deposition of lamellar bone that entraps the more mature osteoblasts in lacunar spaces, where they become osteocytes. At the end of the formation phase, bone has been replaced, but its total amount has not changed. Only in pathological conditions, the activities of osteoclasts and osteoblasts are unbalanced, resulting in an insufficient deposition compared to resorption, as observed in osteoporosis<sup>17</sup>.

The mechanisms inducing the termination of the formation phase remain unclear. Very likely, the major signal is released by osteocytes embedded in the mineralized matrix. This is *sclerostin* (SOST), an LRP5 ligand that prevents the activation of the Wnt signal, thus blocking an important osteoblast inducer<sup>18</sup>.

Thus, the immature bone matrix, uncalcified osteoid, consists of many organic substances, including proteoglycans, non-collagenous matrix proteins, phospholipids, ALP. Those substances can interact with calcium or phosphate, both of which are components of *hydroxyapatite* (HA).

Mineralization is initiated in bone in association with extracellular *matrix vesicles* (MVs). MVs are approximately 30 to 100 nM in diameter, extracellular, membrane-invested particles that are generated by polarized budding and release from the surfaces of osteoblasts. Only a specific region of the outer cell membrane gives rise to MVs<sup>19</sup>. Within the MVs, crystallized HA appears and grows, showing the primary calcification. HA crystals subsequently multiply, forming calcified nodules that expand, fuse, and then calcify expansive matrix<sup>20</sup>.

Once the calcification cascade is begun, matrix vesicles are no longer needed to support mineralization and are consumed by the advancing mineralization front in which performed crystals serve as nuclei for the formation of new crystals. The rate of crystal proliferation is promoted by the availability of  $\text{Ca}^{2+}$ ,  $\text{PO}_4^{3-}$ , and the presence of collagen, and retarded by naturally occurring inhibitors of mineralization such as proteoglycans and several non-collagenous calcium-binding

proteins of bone including bone-Gla protein (osteocalcin), phosphoproteins, osteonectin, and alpha-2HS-glycoproteins<sup>21</sup>.

### **2.1.2 Molecular mechanisms of osteoclast differentiation and bone resorption**

Bone resorption is a multistep process initiated by the proliferation of immature osteoclasts precursors, followed by the commitment of these cells to the osteoclasts phenotype and, finally, the degradation of the organic and inorganic phases of bone by the mature resorptive cells<sup>22</sup>.

The differentiation of osteoclasts from a promyeloid precursor is dependent on a *tumor necrosis factor* (TNF) family cytokine, a *receptor activator of nuclear factor- $\kappa$ B ligand* (RANKL), as well as *macrophage colony stimulating factor* (M-CSF).

M-CSF is a cytokine provided from the microenvironments and it was revealed to be essential because it induces the proliferation of osteoclast precursor cells, supports their survival and upregulates the RANK expression<sup>23</sup>.

In response to M-CSF, hematopoietic stem cells undergo differentiation into *macrophage colony-forming units* (CFU-M, the common precursor cells of macrophages and osteoclasts) and the step from CFU-M to multinucleated osteoclasts is characterized by cell-cell fusion, mainly induced by RANKL and other molecules. Actually, RANKL-RANK signaling directly controls the differentiation process.

RANK is a transmembrane protein and its intracellular domain lacks intrinsic enzymatic activity. In the maturation stage (activation), osteoclasts acquire bone resorbing activity. The signal transduction pathways activated by RANK incorporate the *tumor necrosis receptor-associated factor* (TRAF) family of cytoplasmic adaptor proteins<sup>24</sup>. It was demonstrated that RANK interacts both *in vitro* and *in vivo* in cells with different TRAFs (particularly with TRAFs 1, 2, 3, 5 and 6). Site-directed mutagenesis demonstrated that multiple TRAF binding sites (clustered in two distinct domains in the RANK cytoplasmic tail) exhibited selective binding for different TRAF proteins. In particular, TRAF6 interacts with membrane-proximal determinants distinct from those binding TRAFs 1, 2, 3, and 5<sup>25</sup>. It was reported that targeted disruption of TRAF6 leads to osteopetrosis, which is characterized by increased bone mass owing to reduced bone resorption, with defects in bone remodeling and tooth eruption due to impaired osteoclast function<sup>26</sup>. This highlights a crucial role of TRAF6 as the major adaptor molecule linking RANK to osteoclastogenesis, while the contributions of TRAF2, TRAF3 and TRAF5 seem to be relatively limited.

Among the molecules immediately activated by TRAF6, genetic evidence supports the essential role of NF- $\kappa$ B in osteoclastogenesis. NF- $\kappa$ B is a family of dimeric transcription factors that recognize a common DNA sequence called the  *$\kappa$ B site* and positively regulate the expression of many genes involved in inflammatory and other responses.

NF- $\kappa$ B proteins reside in the cytoplasm of non-stimulated cells but rapidly enter the nucleus upon cell stimulation with a variety of agonists, including RANKL. Thus RANKL and some pro-inflammatory cytokines, including TNF, activate NF- $\kappa$ B and downstream signaling, including c-Fos (a proto-oncogene) and the so called *nuclear factor of activated T-cells, cytoplasmic 1* (NFATc1), to positively regulate osteoclast formation and functions.

NFATc1 has been called the master regulator of osteoclastogenesis and its major role may be (at the early stage) to down-regulate expressions of constitutively active repressors of RANK signaling, rather than induce expression of osteoclastogenic genes.

In order to activate NFATc1, NF- $\kappa$ B is recruited to the NFATc1 promoter immediately after RANKL stimulation. Another molecule that is recruited to the NFATc1 promoter is NFATc2 (*nuclear factor of activated T-cells, cytoplasmic 2*), a member of the NFAT family of transcription factors. NFATc2 preexists before RANKL stimulation and is recruited to the NFATc1 promoter at the same time as NF- $\kappa$ B. NFATc2 and NF- $\kappa$ B cooperatively activate the NFATc1 promoter within minutes of RANKL stimulation<sup>27</sup>.

RANK signaling also activates the transcription factor complex *activating protein 1* (AP-1), which collectively describes a group of structurally and functionally related members of the Jun protein family (c-Jun, JunB and JunD), Fos protein family (c-Fos, FosB, Fra-1 and Fra-2) and ATF protein family (ATFa, ATF2, ATF3, ATF4, B-ATF). Every cell type has a complex mixture of AP-1 dimers with subtly different functions<sup>28</sup>. It was reported that c-Fos is a central regulatory component of AP-1, since Fos-deficient animals lack osteoclasts and develop osteopetrosis<sup>29</sup>.

An AP-1 complex containing c-Fos may cooperate with NFATc1 to enable a robust induction of NFATc1. The so called *auto-amplification phase* occurs only in the case of NFATc1, depends on the calcium signal and requires the recruitment of transcriptional coactivators with histone acetylase activity, such as *CREB-binding protein* (CBP) and *p300/CBP-associated factor* (PCAF), to the NFATc1 promoter. The rate of histone acetylation in the NFATc1 promoter increased gradually after RANKL stimulation and that the high acetylation status was sustained, but this was not observed in the NFATc2 promoter. Methylation of histone H3 lysine 4, which is characteristic of the transcriptionally active locus, is upregulated exclusively in the NFATc1 promoter<sup>27</sup>.

NFATc1 expression levels increase again at late stage, and require c-Fos expression induced by NF- $\kappa$ B, to induce expression of genes involved in osteoclasts resorptive functions such as TRAP (*tartrate-resistant acid phosphatase*; a marker enzyme of osteoclasts), DC-STAMP (*dendritic cell-specific transmembrane protein*; a putative seven-transmembrane spanning protein, essential for the cell-cell fusion of osteoclasts) and *cathepsin K*. Calcitonin receptor,  $\beta$ 3 integrin genes and the *osteoclast-specific immunoreceptor osteoclast associated receptor* (OSCAR) are also regulated by

NFATc1<sup>23,30</sup>. **Figure 1.4** shows a scheme that recapitulates the event in osteoclastogenesis induced by RANKL-RANK interaction.

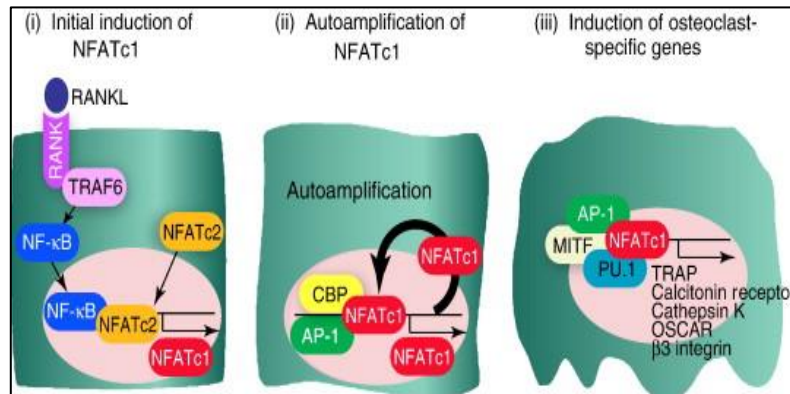


**Fig. 1.4** A schematic diagram of the three stages of osteoclast differentiation governed by NFATc1<sup>23</sup>.

Moreover, it has been shown that NFATc1 cooperates with PU.1 (a transcriptional activator) and *microphthalmia-associated transcription factor* (MITF) on the cathepsin K and the OSCAR promoters. Thus, both PU.1 and MITF, which are thought to be important for the survival of osteoclast precursor cells, also participate in osteoclast-specific gene induction at the terminal stage of differentiation<sup>31</sup>.

As previously said, the auto-amplification of NFATc1 is stimulated by calcium signaling. This is mediated by *immunoreceptor tyrosine-based activation motif* (ITAM), which is necessary for the transduction of the calcium signal in immune cells (**Fig. 1.5**). The activation of ITAM occurs in adaptor molecules such as *DNAX-activating protein 12* (DAP12) and *Fc receptor common  $\gamma$  subunit* (FcR $\gamma$ )<sup>32</sup> in association with costimulatory receptors of the immunoglobulin superfamily, including *triggering receptor expressed in myeloid cells-2* (TREM-2), *signal-regulatory protein  $\beta 1$*  (SIRP  $\beta 1$ ), *paired immunoglobulin-like receptor-A* (PIR-A), and OSCAR

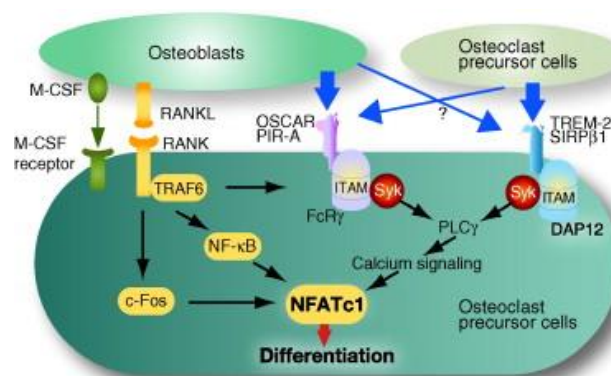


**Fig. 1.5** Cooperation of RANKL and immunoreceptor tyrosine-based activation motif (ITAM) signals in osteoclastogenesis<sup>23</sup>



Phosphorylation of ITAM, stimulated by immunoreceptors and RANKL–RANK interaction, results in the recruitment of *Syk family kinases*, leading to the activation of *phospholipase C $\gamma$*  (PLC $\gamma$ ) and calcium mobilization, which is critical for NFATc1 induction.

Thus, ITAM-mediated calcium signaling, activated through PLC $\gamma$  is indispensable to osteoclastogenesis<sup>31</sup> but osteoclastogenesis cannot be induced by costimulatory signals alone and requires RANKL stimulation.

On the other hand, the production of osteoclasts can be reduced by *osteoprotegerin* (OPG), a soluble decoy receptor for RANKL (also known as OPGL) that strongly inhibits osteoclasts differentiation and function induced by RANKL both *in vitro* and *in vivo*. This inhibitory effect is due to the fact that it can prevent the binding of RANKL to its receptor<sup>5</sup>.

It is the balance between the expression of the stimulator of osteoclastogenesis, RANKL, and of the inhibitor, OPG, that dictates the quantity of resorbed bone.

Both mononuclear and multinuclear osteoclasts can resorb bone, but larger cells seem to be more effective, although there is no direct relationship between the resorption capacity and the number of nuclei. The sequence of cellular events needed for bone resorption is called the *resorption cycle*; this term covers neither the differentiation pathway nor the cellular activities needed to form the multinuclear mature osteoclasts.

Resorption requires different cellular activities that include migration of the osteoclast to the resorption site; attachment of the osteoclast to the bone, polarization and formation of new membrane domains; dissolution of hydroxyapatite; degradation of organic matrix; removal of degradation products from the resorption lacuna; apoptosis of the osteoclasts or return to the non-resorbing stage.

After proliferating in bone marrow, precursors are guided to bone surfaces, near to those sites that are going to be resorbed. There, even if it is not known exactly how resorption sites are determined, it is known that the first sign is the retraction of bone-lining cells. This retraction uncovers osteoid and after its removal by osteoblasts the osteoclasts can attach to the mineralized surface<sup>33</sup>. A specific membrane domain, the *sealing zone*, forms under the osteoclasts, attaches tightly to the bone matrix and seals the resorption site from its surroundings. The molecular interactions at the sealing zone are still unclear but it is known that integrins play an important role in early phases. At least four different integrins are expressed in osteoclasts:  $\alpha_v\beta_3$ ,  $\alpha_v\beta_5$ ,  $\alpha_2\beta_1$  and  $\alpha_v\beta_1$ <sup>34</sup>.

Current data suggest that resorbing osteoclasts contain not only the sealing zone but also at least three other specialized membrane domains: a *ruffled border*, a *functional secretory domain* and a *basolateral membrane*. The ruffled border is a resorbing organelle, and it forms an isolated

resorptive microenvironment between the osteoclast and the underlying bone matrix<sup>5</sup>. This offers a good diffusion barrier between the resorption lacuna and extracellular fluid.

After formation of the ruffled membrane, the osteoclast acidifies an extracellular microenvironment by means of an electrogenic proton pump<sup>35</sup>. The low pH is essential for bone mineral dissolution and the optimized activities of bone degradation enzymes. Intracellular pH is maintained by  $\text{HCO}_3^-/\text{Cl}^-$  exchange at the cell's antiresorptive surface.  $\text{Cl}^-$  ions pass through a ruffled membrane-residing anion channel into the resorptive microenvironment, which achieves a pH approximating 4.5. After solubilization of the mineral phase, several proteolytic enzymes degrade and remove the organic bone matrix, although the detailed sequence of events at the resorption lacuna is still obscure.

The role of two major classes of proteolytic enzymes (*lysosomal cysteine proteinases* and *matrix metalloproteinases*) has been studied most extensively. The high levels both of expression of MMP-9 (gelatinase B) and cathepsin K and of their secretion into the resorption lacuna suggest that these enzymes play a central role in the resorption process<sup>33</sup>.

The degradation products are removed from the resorption lacuna through a transcytosis vesicular pathway from the ruffled border to the functional secretory domain, where they are liberated into the extracellular space.

Some studies have suggested that *TRAP-facilitated fragmentation* of endocytosed material takes place in a specific cellular compartment, since TRAP was found in the transcytosis vesicles of resorbing osteoclasts, and that it can generate highly destructive reactive oxygen species able to destroy collagen and other proteins. These results suggest that bone matrix degradation occurs not only extracellularly in the resorption lacunae but also intracellularly in the transcytosis vesicles<sup>36</sup>.

After the degradation of a "packet" of bone, thus forming a resorption lacuna, osteoclasts depart and are replaced by osteoblasts that, in young individuals, completely restore the previously resorbed bone. The functional cycle of the osteoclast consists of episodes of matrix adherence followed by detachment and movement to a new site of bone degradation. Although the events initiating bone resorption are reasonably well understood, less is known about the signals that arrest the process<sup>22</sup>.

### **2.1.3 The bone remodeling process**

During bone remodeling, mature bone tissue is removed from the skeleton, the so called bone resorption, and new bone tissue is formed by the ossification process. These processes also control the reshaping or replacement of bone following injuries like fractures but also micro-damage, which occurs during normal activity. Remodeling responds also to functional demands of the mechanical loading.

Bone homeostasis involves multiple but coordinated cellular and molecular events<sup>37</sup>. The structure of bones as well as adequate supply of calcium requires close cooperation between osteoblast,

osteoclast and other cell populations present at the bone remodeling sites (ex. immune cells)<sup>38</sup>. Bone metabolism relies on complex signaling pathways and control mechanisms to achieve proper rates of growth and differentiation. These controls include the action of several hormones, including *parathyroid hormone* (PTH), vitamin D, growth hormone, steroids, and calcitonin, as well as several bone marrow-derived membrane and soluble *cytokines* and *growth factors* (ex. M-CSF, RANKL, vascular endothelial growth factor (VEGF), IL-6 family).

In response to appropriate signaling, osteoclasts move to resorb surface of the bone, followed by deposition of bone by osteoblasts. Together, the cells that are responsible for bone remodeling are known as the *basic multicellular unit* (BMU), and the temporal duration (i.e. lifespan) of the BMU is referred to as the bone remodeling period.

An active BMU consists of a leading front of bone-resorbing osteoclasts. Reversal cells, of unclear phenotype, follow the osteoclasts, covering the newly exposed bone surface, and prepare it for deposition of replacement bone. Osteoblasts occupy the tail portion of the BMU and secrete and deposit unmineralized bone matrix known as osteoid and direct its formation and mineralization into mature lamellar bone. This unique spatial and temporal arrangement of cells within the BMU is critical to bone remodeling, ensuring coordination of the distinct and sequential phases of this process: activation, resorption, reversal, formation, and termination, which are discussed below and illustrated schematically in **Fig. 1.6**.

*Activation Phase* — The first stage of bone remodeling involves detection of an initiating remodeling signal. This signal can take several forms, e.g. direct mechanical strain on the bone that results in structural damage or hormone (e.g. estrogen or PTH) action on bone cells in response to more systemic changes in homeostasis.

*Resorption Phase* — Osteoblasts respond to signals generated by osteocytes or direct endocrine activation signals discussed above and recruit osteoclast precursors to the remodeling site. In response to PTH-induced bone remodeling, osteoblasts produce the chemokine monocyte chemoattractant protein-1 (MCP-1) *in vivo*, which is a chemoattractant for osteoclast precursors and enhances RANKL-induced osteoclastogenesis *in vitro*<sup>37</sup>. In addition to recruitment of osteoclast precursors, osteoblast expression of the master osteoclastogenesis cytokines, CSF-1, RANKL, and OPG, is also modulated in response to PTH. OPG expression is reduced, and CSF-1 and RANKL production is increased to promote osteoclast formation and subsequent activity. Matrix metalloproteinases (MMPs), including MMP-13, are also secreted from osteoblasts in response to mechanical and endocrine remodeling signals. MMPs degrade the unmineralized osteoid that lines the bone surface and expose RGD adhesion sites within mineralized bone that are necessary to facilitate osteoclast attachment.

*Reversal Phase* — Following osteoclast-mediated resorption, the Howship lacunae remain covered with undigested demineralized collagen matrix. A mononuclear cell of undetermined lineage removes these collagen remnants and prepares the bone surface for subsequent osteoblast-mediated bone formation. Initially, this “reversal” cell was proposed to be a monocytic phagocyte based on morphological assessment. More recently it was proposed that these cells are both *osteomacs* (osteal macrophage) and mesenchymal bone-lining cells that work together to facilitate events during the reversal phase. The final role of the reversal cells may be to receive or produce coupling signals that allow transition from bone resorption to bone formation within the BMU.

*Formation Phase* — The nature of the coupling signal that coordinates this transition and directs bone formation precisely to sites of bone resorption remains controversial. Initially, it was proposed that the coupling molecule(s) were stored in the bone matrix and liberated during bone resorption. Insulin-like growth factors I and II and TGF- $\beta$  are all such factors, and regulation of active TGF- $\beta$  appears to be a key signal for recruitment of mesenchymal stem cells to sites of bone resorption. However, in mice and humans that have functionally defective osteoclasts, unable to resorb bone, osteoblast bone formation is preserved even in the absence of released matrix-bound growth factors. These observations have led to the hypothesis that osteoclasts produce the coupling factor(s). Several candidate coupling mechanisms have been proposed, including the soluble molecule sphingosine 1-phosphate, secreted by osteoclasts, that induces osteoblast precursor recruitment and promotes mature osteoblast survival. Mechanical stimulation and the endocrine signal PTH can exert bone formation signals via osteocytes. Under resting conditions, osteocytes express sclerostin, that binds to LRP5/6 and directly prevents Wnt signaling. Once mesenchymal stem cells or early osteoblast progenitors have returned to the resorption lacunae, they differentiate and secrete molecules that ultimately form replacement bone. Collagen type I is the primary organic component of bone. Non-collagenous proteins, including proteoglycans, glycosylated proteins such as tissue non-specific alkaline phosphatase, small Integrin-Binding ligand, N-linked Glycoprotein (SIBLING), Gla-containing proteins (matrix Gla protein and osteocalcin), and lipids compose the remaining organic material. For bone to assume its final form, HA is incorporated into this newly deposited osteoid.

*Termination Phase* — When an equal quantity of resorbed bone has been replaced, the remodeling cycle concludes. The termination signal(s) that inform the remodeling machinery to cease work are largely unknown, although a role for osteocytes is emerging. The loss of sclerostin expression, which occurred to initiate osteoblastic bone formation, likely returns toward the end of the remodeling cycle. Following mineralization, mature osteoblasts undergo apoptosis, revert back to a bone-lining phenotype or become embedded in the mineralized matrix, and differentiate into

osteocytes. The resting bone surface environment is reestablished and maintained until the next wave of remodeling is initiated<sup>37</sup>.

An imbalance in the regulation of bone remodeling's two sub-processes, bone resorption and bone formation, results in many metabolic bone diseases, such as osteoporosis.

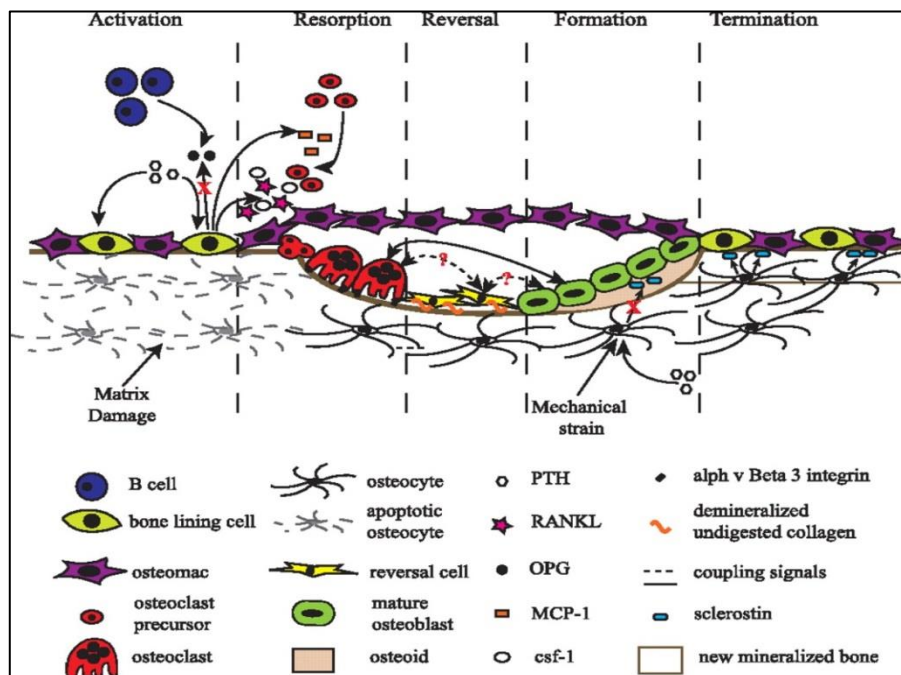


Fig. 1.6 Schematic representation of a BMU and the associated bone-remodeling process<sup>37</sup>

## 2.1.4 Calcium homeostasis

PTH and Vitamin D are two major regulators of mineral metabolism. They play critical roles in the maintenance of calcium and phosphate homeostasis as well as the development and maintenance of bone health. PTH and Vitamin D form a tightly controlled feedback cycle, PTH being a major stimulator of vitamin D synthesis in the kidney while vitamin D exerts negative feedback on PTH secretion. The major function of PTH and major physiologic regulator is circulating ionized calcium. The effects of PTH on gut, kidney, and bone serve to maintain serum calcium within a tight range. In contrast, vitamin D has a stimulatory effect on calcium homeostasis, playing a key role in providing adequate mineral for normal bone formation. Both hormones act in concert with the more recently discovered fibroblast growth factor 23 (FGF23) and klotho, hormones involved predominantly in phosphate metabolism, which also participate in this closely knit feedback circuit<sup>39</sup>.

The plasma ionized calcium concentration is regulated to within very narrow limits (1.3–1.5 mmol/L), despite being the central hub through which calcium is moved from one body compartment to the other. This is achieved by both the parafollicular cells of the thyroid gland, and

the parathyroid glands constantly sensing (i.e. measuring) the concentration of Ca ions in the blood flowing through them. When the Ca concentration rises, the parafollicular cells of the thyroid gland increase their secretion of calcitonin (a proteinaceous hormone) into the blood. At the same time the parathyroid glands reduce their rate of PTH secretion into the blood. The resulting high levels of calcitonin in the blood stimulate the skeleton to remove calcium from the blood plasma, and deposit it as bone. The reduced level of PTH inhibits removal of calcium from the skeleton. The low level of PTH has several other effects: it increases the loss of calcium in the urine, but more importantly inhibit the loss of phosphate ions via that route. Phosphate ions will therefore be retained in the plasma where they form insoluble salts with calcium ions, thereby removing them from the ionized calcium pool in the blood. The low level of PTH also inhibits the formation of calcitriol (1,25 dihydroxyvitamin D<sub>3</sub>) from cholecalciferol (vitamin D<sub>3</sub>) by the kidneys. The reduction in the blood calcitriol concentration acts (comparatively slowly) on the epithelial cells (enterocytes) of the duodenum inhibiting their ability to absorb calcium from the intestinal contents<sup>40</sup>. The low calcitriol level also acts on bone causing the osteoclasts to release less calcium ions into the blood plasma.

When the plasma ionized calcium level is low or falls, the opposite happens. Calcitonin secretion is inhibited and PTH secretion is stimulated, resulting in calcium being removed from bone to rapidly correct the plasma calcium level. The high plasma PTH levels inhibit calcium loss via the urine while stimulating the excretion of phosphate ions via that route. They also stimulate the kidneys to produce calcitriol (a steroid hormone), which enhances the ability of the cells lining the intestine to absorb calcium from the intestinal contents into the blood. The PTH stimulated production of calcitriol also causes calcium to be released from bone into the blood, by the release of RANKL from the osteoblasts. These are, however, a relatively slow processes<sup>40</sup>.

Thus fast short term regulation of the plasma ionized calcium level primarily involves rapid movements of calcium into or out of the skeleton. Longer term regulation is achieved by regulating the amount of calcium absorbed from the intestine<sup>40</sup>.

## **2.2 Osteoporosis**

Osteoporosis is a systemic skeletal condition, characterized by low bone mass, reduced bone strength and microarchitectural loss of the bone tissue<sup>41</sup> (**Fig. 1.7**). The alteration of bone's quantity and quality affects also the mechanical properties of the tissue, leading to an increased risk of fracture, because of the decreased density and increased bone fragility.

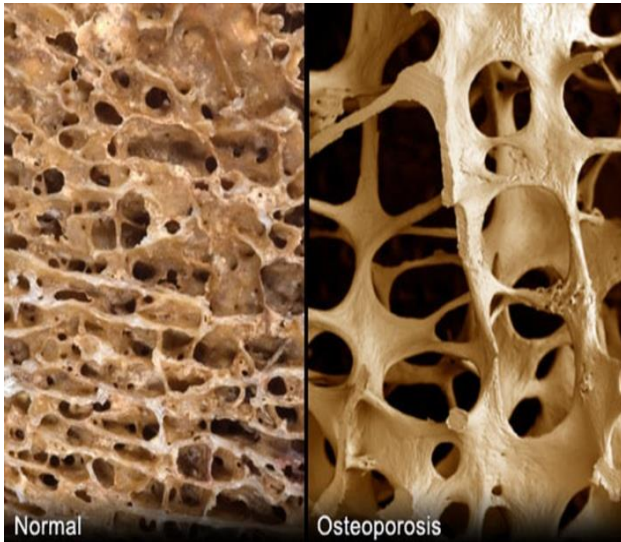


**Fig 1.7 Comparison between normal bone and bone microarchitecture in osteoporotic patients. (Image from free internet access.)**

The disease exists in two forms. Primary osteoporosis consists in loss of bone mass, typically associated with sex hormone deficiency and ageing. In particular, primary osteoporosis can occur in women, during menopause age, because oestrogen levels decrease. Secondary osteoporosis tends to develop in association with chronic diseases, such as hyperthyroidism, gastrointestinal and connective tissue illnesses and pharmacological therapies. For example, osteoporosis represents one of the most common side effects of long-term use of glucocorticoids, as a result of their ability to suppress the

osteoblastic activity.

Other genetic and environmental factors, such as sedentary lifestyle and immobilization, inadequate calcium intake and alcohol and tobacco abuse, can increase the risk of osteoporosis<sup>42,43</sup>.

### **2.2.1 Osteoporosis and microgravity**

It is well known that microgravity influences different biological systems like bone and muscle as well as the heart and brain, and it enhances cancer risk<sup>44</sup>. During their stay at the International Space Station (ISS), astronauts and cosmonauts experience a distinct loss of bone mineral density in the lumbar spine, the pelvis, and the proximal femur, and the extent of bone loss varied up to 20%<sup>45</sup>. In space, the amount of weight that bones must support is reduced to almost zero. At the same time, many bones that aid in movement are no longer subjected to the same stresses that they are subjected to on Earth. Over time, calcium normally stored in the bones is broken down and released into the bloodstream. The high amount of calcium found in astronaut's blood during spaceflight (much higher than on Earth) reflects the decrease in bone density, or bone mass. This drop in density, known as disuse osteoporosis, leaves bone weak and less able to support the body's weight and movement upon return to Earth, putting the astronaut at a higher risk of fracture<sup>44</sup>. This bone loss begins within the first few days in space. The most severe loss occurs between the second and fifth months in space, although the process continues throughout the entire time spent in microgravity. Astronauts regain most of their bone mass in the months following their return from space, but not all of it. The phenomenon of bone loss has been attributed to a reduction in bone formation and an increase in bone resorption<sup>46,47</sup>. Although abundant studies have reported the negative effect of microgravity on bone mass, the underlying mechanisms are still unclear.

## **2.3 Treating osteoporosis: drug therapies**

The principal therapies for osteoporosis treatment fall in two classes, the inhibitors of bone resorption and the stimulators of bone formation. These drugs were developed to solve the alteration in coupling activity, in people affected by osteoporosis. Principal actors in coupling are osteoclasts and osteoblasts, but their activity is associated with the involvement of other systemic molecules and metabolites, such as steroid hormones, parathyroid hormone (PTH), vitamin D, calcitonin, macrophage colony-stimulating factor (M-CSF), osteoprotegerin (OPG), SOST and receptor activator of nuclear factor  $\kappa$ -B ligand (RANKL)<sup>48-50</sup>. Dysregulation of these modulators, however, can lead to an imbalance in coupling, at the beginning, and then to the development of primary osteoporosis, both in postmenopausal women and elderly men<sup>51</sup>.

### **2.3.1 Calcium and vitamin D**

Although calcium and vitamin D supplements administered independently are an insufficient means of treating osteoporosis, nutritional deficiencies of these substances can lead to osteoporosis and other illnesses, such as hyperparathyroidism and hypocalcaemia. Consequently, they have been administered in combination with stand-alone oestrogen, PTH and bisphosphonate therapies. Various studies have also demonstrated mild effects on increasing bone mineral density (BMD) and reducing fracture risk<sup>52</sup>. Calcium also supplements the use of sodium fluoride, shown to stimulate osteoblast proliferation, via Wnt/ $\beta$ -catenin signalling, and to enhance vertebral BMD by 8% for every consecutive year of use, in osteoporotic female patients. However, in the USA, decreased cortical BMD, increased atypical fractures and gastrointestinal issues have prevented approval of sodium fluoride<sup>53,54</sup>. Calcitriol, a metabolite of vitamin D, increases calcium absorption and reduces fracture risk in postmenopausal women, if compared to calcium alone, while also temporarily increasing BMD<sup>55,56</sup>. Clinical therapies for osteoporosis includes dietary supplementation of calcium and vitamin D, in addition to treatment with oestrogen, calcitonin, bisphosphonates, SERMs or fluoride<sup>57,58</sup>.

### **2.3.2 Anti-resorptive agents**

Oestrogen are a group of steroid hormones that play a key role in physiological bone remodelling. Oestrogen binds to  $\alpha$  and  $\beta$  receptors on bone cells, promoting the activity of the osteoblast and consequently the bone formation. These hormones also regulate calcium homeostasis and are involved in the suppression of bone resorption: oestrogen act onto osteoclasts, reducing their formation and their resorptive activity, and onto cytokines, that are involved in resorption supporting, such as IL-1 and TNF<sup>59</sup>. Oestrogen deficiency is the leading cause of osteoporosis in postmenopausal women and elderly men. Decreased levels of these hormones result in a coupling



imbalance, with an increasing in osteoclastogenesis process, which leads to a progressive loss of the trabecular bone. The effects of the postmenopausal oestrogen therapy are controversial: the treatment reduces the development of osteoporotic fractures by approximately 50% and increases the BMD. However, oestrogen receptors, that lie in bone marrow and on immune cells, also interacts with the hormone and there is evidence that a long-term therapy can lead to an increased risk of endometrium hyperplasia, breast cancer, stroke and cardiovascular diseases<sup>52</sup>.

Selective oestrogen receptor modulators (SERMs) were developed as an alternative to oestrogen. These molecules do not have the steroid structure of oestrogen, but their tertiary structure allows them to interact with  $\alpha$  and  $\beta$  receptors, as agonists or antagonists<sup>59</sup>. Raloxifene is a selective oestrogen receptor modulator, that increases the BMD and decreases the risk of vertebral fracture by 30%<sup>60</sup>. Furthermore, if compared to oestrogen, raloxifene decreases the risk of breast cancer, but cardiovascular risk still remains<sup>61</sup>.

Bisphosphonates are analogues of the pyrophosphate. These compounds act specifically on the bone, because of their high affinity for bone minerals. In particular, their phosphate portion interacts with hydroxyapatite crystals and inhibits their growth, aggregation and dissolution. Bisphosphonates determine an increasing of BMD and act also on a specific cell type, the osteoclast. If these nitrogen-containing compounds are present, osteoclasts activity and morphology are altered. In particular, the most evident cellular effects of bisphosphonates are the apoptosis and impairment in recruiting of the osteoclasts, resulting in reduced bone resorption. Many studies have been shown that bisphosphonates, such as alendronate, risedronate and ibandronate, can decrease vertebral and hip fractures by about 50 % and other bone fractures by 20– 25% in osteoporotic patients<sup>62</sup>. However, both oral and intravenous bisphosphonates show side effects, such as the osteonecrosis of the jawbone, atypical femoral fractures and nephrotoxicity; while gastrointestinal adverse effects are limited to oral ones, such as alendronate<sup>63</sup>.

Denosumab is a human monoclonal IgG<sub>2</sub> antibody, which inhibits the receptor activator of nuclear factor  $\kappa$ -B ligand (RANKL). RANKL interacts with the RANK receptor, which is expressed on the surface of the osteoclasts, resulting in enhanced osteoclast development and activity<sup>64,65</sup>. OPG, which is typically secreted by bone marrow<sup>66</sup>, is the natural competitor of RANKL . RANK has a higher binding affinity for RANKL compared to OPG. An imbalance in RANKL/RANK/OPG system allows the development of the osteoporosis and other metabolic diseases of the bone tissue<sup>66</sup>. Denosumab displays a higher specificity and affinity for RANKL than OPG and RANK, encouraging a prolonged antiresorptive effect<sup>67,68</sup>. It promotes a higher BMD at lumbar and hip sites, and effects similar to zoledronate, an intravenous bisphosphonate<sup>69</sup>. A 3-year study has demonstrated that Denosumab is a lot more effective in reduction of the markers of the bone

turnover than other approved compounds, such as bisphosphonates alendronate, risendronate, ibandronate and SERM-raloxifene<sup>70</sup>.

Calcitonin is a peptide hormone, that reduces loss of cancellous bone, while it is relatively ineffective in decreasing cortical bone loss<sup>71</sup>. By binding to calcitonin receptors, osteoclastic activity is diminished and analgesic effects are mediated. Daily administration of low calcitonin doses resulted in a 1 % increase of spinal BMD, whereas high doses were not effective after months of treatment. Actually, salmon calcitonin has been shown to be significantly more efficient than human calcitonin<sup>72,73</sup>. Gastrointestinal disorders have been observed. Combinations of hormone therapy with alendronate, risedronate and calcitonin have shown additive effects in increasing BMD<sup>52</sup>.

### 2.3.3 Anabolic drugs

Current therapies for osteoporosis treatment are focused on maintenance of existing bone mass, limiting the osteoclasts' activity. However, this is not the only option, although a single anabolic drug was approved. The exclusive osteoanabolic agent used for treating severe osteoporosis is PTH in the form of the recombinant human parathyroid hormone rhPTH(1–34), known as Teriparatide<sup>74</sup>. In bone, PTH acts directly on cells of osteoblast lineage (mainly osteoblasts and osteocytes) and indirectly on osteoclasts because only osteoblasts express PTH type I receptor (PTH1R), a transmembrane G-protein coupled receptor. Binding of PTH or rhPTH(1-34) to PTH1R activates two well-defined intracellular signal transduction pathways: the protein kinase A (PKA) pathway, in which G $\alpha$ s stimulates production of cAMP and activation of PKA, and the protein kinase C (PKC) pathway where G $\alpha$ q activates phospholipase C $\beta$  with subsequent formation of diacylglycerol, PKC activation and formation of 1,4,5-inositol trisphosphate. In osteoblasts, PTH regulates most of its target proteins through the PKA pathway. Extensive investigations have been performed to understand the cellular mechanisms by which intermittent injection of PTH increases osteoblast numbers. It has been concluded that, multiple mechanisms, including activating bone lining cells, stimulating osteoblast differentiation from osteoprogenitors, and preventing osteoblast and osteocyte apoptosis, contribute to the anabolic action of PTH<sup>75</sup>.

Results from a phase III trial show that Teriparatide stimulates bone formation, resulting in increased bone mass and strength and the impairment from 53 to 65% of the risk of bone fractures<sup>76</sup>.

**Figure 1.8** shows a scheme that recapitulates the anti-resorptive and anabolic drugs and their mechanisms of action.

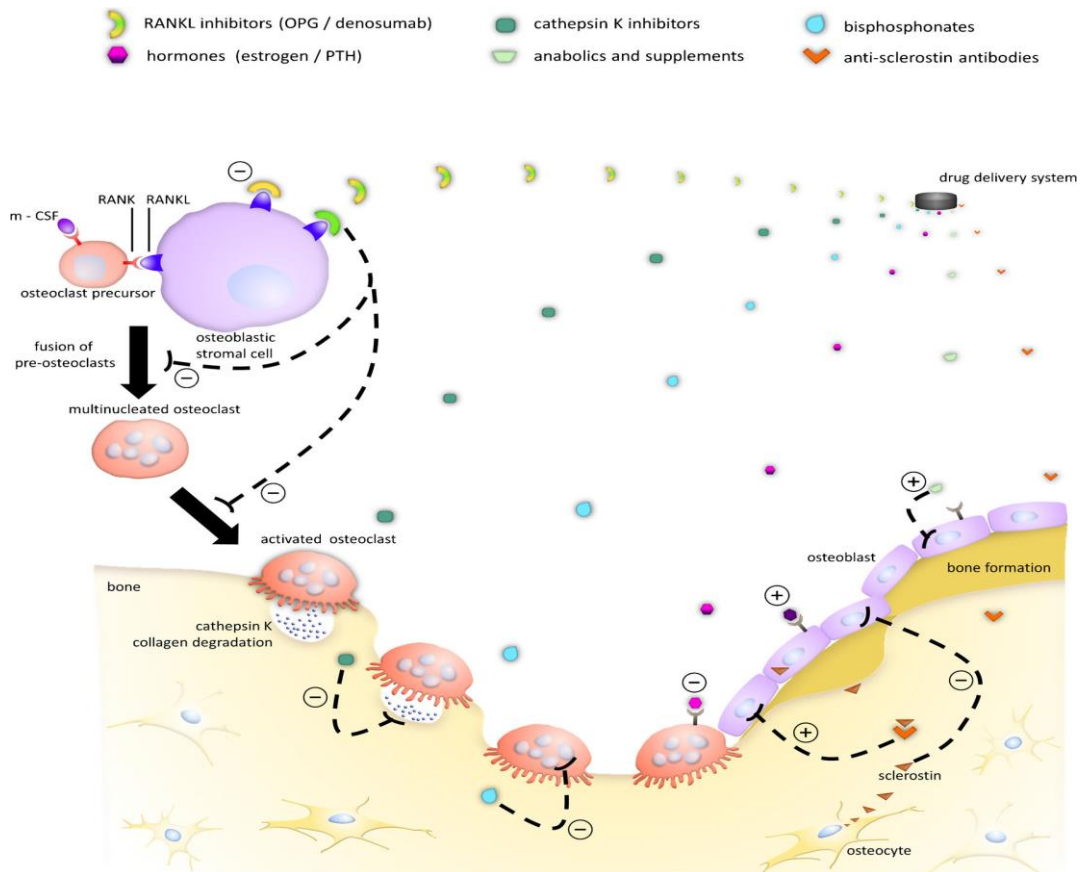


Fig 1.8. Controlled release of different anti-resorptive and anabolic drugs and their mechanisms of action on specific cell types in bone for treatment of osteoporosis<sup>88</sup>

### 2.3.4 New target in osteoporosis pharmacological treatment

Osteocytes synthesize sclerostin in late stages of their differentiation, after the start of bone matrix mineralization<sup>77</sup>. Sclerostin is then transported to the bone surface, where it inhibits the activity of osteoblasts and stimulates their apoptosis<sup>78,79</sup>. Sclerostin has also an autocrine function and upregulates RANKL synthesis in osteocytes, thereby stimulating osteoclastogenesis<sup>80</sup>.

Sclerostin decreases bone formation as it acts as an antagonist of the canonical Wnt-signalling pathway in osteoblasts, thus inhibiting their proliferation, differentiation and viability<sup>81,82</sup>. In the last decade, inhibitors of sclerostin were developed<sup>83</sup>: AMG 785, known as Romosozumab, and blosozumab are humanized monoclonal antibody are currently in clinical development for osteoporosis treatment.

Actually, monoclonal antibodies and other small molecules to inhibit Dkk1 have been investigated as potential treatments of osteoporosis and other bone diseases. Dkk1 is produced by osteocytes, but also by other cells in the body. The relative lack of bone specificity and the reported absence of Dkk1 expression in bones of aged animals, seem to limit Dkk1 inhibitors use in osteoporosis treatment. However, inhibitors of Dkk-1 have been shown to avoid bone loss in a model of

rheumatoid arthritis<sup>84</sup>. In a myeloma model, the inhibition of Dkk-1 prevented the formation of osteolytic lesions and increased bone formation rate<sup>85,86</sup>.

Cathepsin K is a major digestive enzyme that acts in bone resorption, breaking down type I collagen secreted by activated osteoclasts. On the basis of this concept, the use of cathepsin K inhibitors has emerged as a novel therapeutic approach. Odanacatib is currently the most advanced inhibitor of cathepsin K under clinical investigation. Unlike bisphosphonates and other available anti-resorptive agents, Odanacatib does not decrease osteoclast survival, or limit bone formation, and appears to uncouple bone resorption from bone formation. In completed clinical trials in postmenopausal women, the bone formation is maintained and paired with a moderately decreased bone resorption, resulting in an anabolic effect<sup>87-89</sup>.

### **2.3.5 Nanotechnologies and bone repair in osteoporotic patients**

As previously described, high doses of the drugs approved for osteoporosis treatment encourage the risk of occurrence of unpleasant side effects, such as uncontrolled bone formation and tumorigenesis<sup>90,91</sup>. However, also for the future, alternative approaches are available, thanks to the development of the nanotechnologies.

Many nanomaterials are now utilized in the field of orthopaedics and many others are also under investigation. The main purpose is the prevention and treatment of the osteoporosis, through the stimulation of bone repair and regeneration.

Actually, there are many possibilities in this field, concerning the selection of the materials and the techniques that can be used to synthesize the nanomaterials, in scaffold or powder form. Combining different disciplines, such as materials science, nanotechnology and biochemistry, nano-based therapeutics have been developed, especially for a localized delivery in osteoporosis treatments.

The biomaterial designed to for bone regeneration must have basic features. The biomaterial has to be biocompatible, hydrophilic, biofunctional and non-toxic. The scaffold biodegradability shall be required to allow the correct regeneration of the tissue and its chemical and physical features should reflect the organic/inorganic characteristics of the native bone tissue. Moreover, an adequate porous 3D, possibly organized, structure, with a pore size between 200–300  $\mu\text{m}$ , is necessary to encourage cellular adhesion and to guide the infiltration and proliferation of the new forming tissue (osteoconductivity)<sup>92</sup>. The biomaterial has also to possess the ability to recruit progenitor cells and differentiate into desired lineages (osteinductivity) and two other important properties: osteogenicity and osteointegrity<sup>93</sup>.

Several materials satisfy most of the requirements seen above.

The most common platform biomaterials are collagen<sup>94</sup>, which constitutes the organic phase of bone ECM, and ceramic<sup>95</sup>. Among the natural and synthetic polymers, widely used as scaffolding

materials, there are poly(lactic acid) (PLA), poly(glycolic acid) (PGA), and PLGA, that are chosen especially for their design flexibility, the surface modifiability and the functional group availability<sup>96-98</sup>.

However, among these, it seems that an ideal scaffold for bone repair has not been fabricated from pure bioactive ceramics or bioactive polymers. In fact, ceramic is brittle and fragile, while bioactive polymers and collagen fibers have poor mechanical strength, if compared to the ones requested for normal bone function.

Composites, such as nanofibers, nanoparticles (NPs) and nanopores, combine polymers and scaffolding biomaterial. Composites are promising for bone regeneration, because they merge the advantageous properties of different materials, in the nanoscale.

In particular, NPs have been extensively investigated and have shown promise as carriers to deliver drugs<sup>99</sup>, with an increased biostability and bioavailability, proteins and other biomolecules active in the osteogenic pathway.

The most illustrative example of NPs is Nano-Hydroxyapatites (nHAPs). Hydroxyapatite ( $\text{Ca}_{10}(\text{PO}_4)_6(\text{OH})_2$ ; HAp) is the principal inorganic component of the bone, thus nHAPs have been used widely in medical field as an orthopaedic and dental material for bone repair<sup>100</sup>. They are bioactive and biocompatible and possess osteoconductive, non-toxic, non-inflammatory and non-immunogenic properties<sup>101</sup>. Furthermore, NPs of HAp, are also able to interact with osteoblasts and progenitor cells, improving their adhesion, proliferation and differentiation. The inclusion of nHAPs into the biopolymer matrices improves the mechanical properties of the platform and incorporates the features that mimic the nanostructure of natural bone.

Many types of nanomaterials with proved osteogenic properties have been synthesized, such as silver carbon nanotubes, carbon fibers, alumina, cellulose nanocrystals, polyanilines, graphene oxides, nano-diamonds and mesoporous silica-based NPs, and various studies have been published. most trace metals are hypothesized to induce angiogenesis, a process interlinked with osteogenesis<sup>102</sup>.

In addition, NPs can be chemically modified to improve and prolong their therapeutic effect; they also possess anti-microbial properties and enhance mechanical properties of the tissue-engineered scaffolds.

The apatite structure is very tolerant to ionic substitutions. It seems that the incorporation of specific inorganic additives makes the HAp more biocompatible, more similar to native bone matrix, and so an excellent candidate for the future clinical applications<sup>103</sup>. For that purpose, several ions with different properties have been considered to be promising agents. For example, fluoride is an

essential element present in teeth and bones<sup>104</sup> and stimulates the proliferation and differentiation of the osteoblasts *in vitro*<sup>105,106</sup>.

Zinc is an important element, involved in tissue regeneration<sup>107</sup>, especially in proteins and DNA synthesis and cell proliferation<sup>108,109</sup>. In various works, it was reported that zinc, in Zn-HA coatings form, supports osteoblast growth, proliferation and differentiation *in vitro*, and is able to induce an antibacterial effect<sup>109,110</sup>.

The most-know antibacterial agent is silver: in particular, this effect has been reported for Ag-HA coatings<sup>111-113</sup>, against both Gram-positive and Gram-negative bacteria<sup>114</sup>.

In addition to silver NPs, graphene oxide<sup>115</sup> and selenium NPs have been demonstrated to be excellent candidates for anti-microbial applications<sup>116,117</sup>. They seems also promising in osteosarcoma treatment<sup>118</sup>.

One of the most promising elements in Hap-NPs research is strontium (Sr). Sr has a dual effect. It promotes bone cell growth and reduces bone resorption, so it can combat osteoporosis acting on two opposite pathways<sup>119-122</sup>. Moreover, it upregulates ALP activity, OCN, type I collagen and downregulates osteoclast proliferation. Strontium-Hydroxyapatite (Sr-HAp) reveal favourable cell attachment, spreading and growth<sup>103</sup>. It has been established that Sr addition leads to a decrease in the crystallinity of HAp<sup>123</sup>. Although promising, further studies concerning nanomaterials for osteoporosis treatment are needed. Looking further ahead, combinatorial nanoengineered approaches must be explored, in order to realize the ideal system, which provides robust mechanical stability and utilises delivery for accelerate bone regeneration. In this sense, through a combined approach, Liu et al. synthesized a bioactive scaffold of gelatin, fibrin and nHAp, able of a controlled release of BMP-2, necessary for repairing segmental bone fractures<sup>124</sup>.

## **2.4 The effect of strontium on bone regeneration**

Sr is a trace metal in the human body. It is present in nature as a mixture of four stable isotopes: <sup>88</sup>Sr (82.56%), <sup>87</sup>Sr (7.02%), <sup>86</sup>Sr (9.86%) and <sup>84</sup>Sr (0.56%). As other alkaline earth elements, such as calcium (Ca) and magnesium (Mg), Sr forms divalent cations in biological fluids, where it can bind serum and plasma proteins in the same order of magnitude as that of Ca<sup>125</sup>.

More than 99% of total amount of Sr in the body is localized in bone, where it represents only 3.5% of its Ca molar content<sup>125</sup>. Existing some common transport paths, Sr and Ca behave similarly for intestinal absorption, renal tubular re-absorption and accumulation in the bone. Experiments with radio-strontium have proved that this element is removed immediately from the blood flow and then it passes the Haversian capillaries walls by diffusion to reach the bone extracellular fluid.

Finally, Sr deposit in the bone being absorbed on the bone apatite surface or substitute the Ca position in bone crystal<sup>126</sup>. Both Sr and Ca also possess strong bone-seeking properties: that's the reason why Sr can be substituted in the calcium positions of apatite, exerting a beneficial effect on the bone.

Long-term studies have established that, after incorporation into bone, the two elements behave almost identically<sup>125</sup>, although Sr has a larger atomic radius. In the last years, numerous studies focused their attention on Sr potential role in the cure of osteoporosis<sup>127</sup>. *In vitro* and *in vivo* studies, have established that Sr (administered as Sr chloride, ranelate and lactate) increases bone formation and reduces bone resorption, leading to a gain in bone mass and to an improvement of bone mechanical properties in normal animals and humans<sup>121,128</sup>.

#### 2.4.1 Strontium Ranelate

Strontium ranelate (SrR) is a divalent strontium salt of organic ranelic acid<sup>119</sup>. In contrast to other treatments, SrR has a dual mode of action<sup>128-132</sup>. Both *in vitro* and *in vivo*, this compound is considered an uncoupling agent: for example, it was demonstrated that in normal rats, SrR increased bone formation and reduced bone resorption, resulting in increased vertebral bone mass, while preserving bone mineralization<sup>133</sup>.

SrR was shown to act by decreasing bone resorption *in vitro*<sup>128</sup> and the resorbing activity of the osteoclasts<sup>129,132</sup>, by disrupting the cytoskeleton<sup>134</sup>, resulting in a decreasing of osteoclasts marker expression<sup>129</sup>. *In vitro*, it was demonstrated that it also increases the replication of the osteoprogenitor cells and the synthesis of collagen, stimulating the bone formation process<sup>131</sup>. This treatment is associated with the increment of the number of bone-forming sites, which follows the growth of the mechanical resistance and strength of the bone tissue that are significantly correlated with the increase in BMD. Furthermore, this agent enhance the replication of pre-osteoblastic cells and increase many osteoblast markers, such as ALP of MSCs, type-1 collagen and bone sialoprotein, without affecting bone mineralization<sup>130</sup>. All these effects were also found in ovariectomized Sprague-Dawley and Wistar rats<sup>121,135</sup>.

The molecular mechanisms of action of SrR affects bone cells are not yet fully known. It may reduce osteoclastogenesis and increases osteoblastogenesis through different mechanisms. First, it was found that this compound affects the expression of OPG and RANKL, in osteoblastic cells.

Another possible mode of action of SrR may involve the calcium-sensing receptor (CaSR). CaSR is a member of the G-protein coupled receptor (GPCR) family and it is expressed in osteoclasts, osteoblasts and osteocytes<sup>136,137</sup>. With lower affinity than calcium, Sr could act as a full agonist of the bone CaSR, which may be functionally differ from other CaSRs<sup>136,138,139</sup>. In the osteoclast, SrR acts via CaSR increasing osteoclast apoptosis<sup>140</sup>; whereas, in osteoblasts, it activates the mitogen-

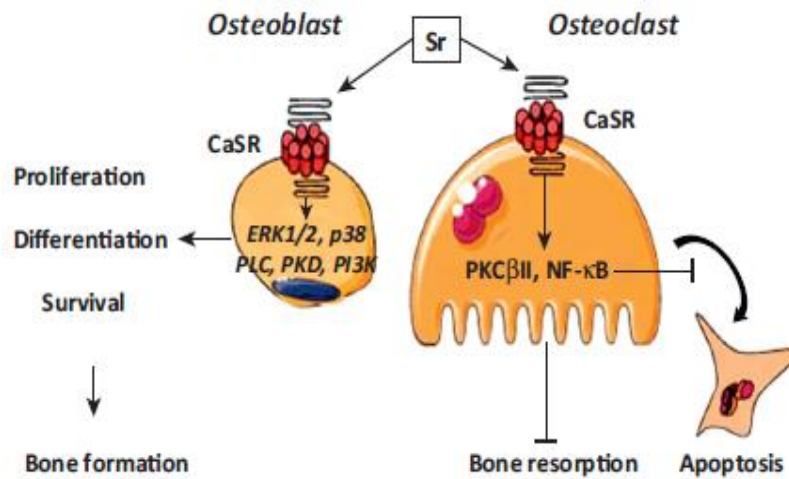


**Figure 1.9** A schematic showing the dual mechanism of action of strontium (Sr): the stimulatory role on bone-forming osteoblast cells and the inhibitory role on bone resorbing osteoclast cells<sup>134</sup>.

activated protein kinase (MAPK) signaling, mediating in part the increased cell replication<sup>141,142</sup> (**Fig. 1.9**). Low doses of this drug were found to increase OPG expression and production and to decrease RANKL expression by osteoblasts *in vitro*<sup>143,144</sup> and this effect is mediated by the CaSR. However, SrR acts also on other osteoblasts receptors, such as GPRC6A, a cation-sensing receptor, whose role is now under investigation.

Recent studies have established the involvement of the calcineurin/NFATc pathway, in response to SrR administration. In osteoblasts, SrR activates Cn/NFATc1 signaling, increasing their replicative activity and inducing the expression of Wnt and the activation of canonical and non-canonical Wnt signaling pathways involved in SrR-induced osteoblastogenesis<sup>141</sup> (**Fig. 1.10**).

Actually, SrR is a new orally active drug, administered for the amelioration of postmenopausal osteoporosis, in order to increase BMD and reduce bone fracture risk, as it was demonstrated through numerous clinical trials. It was proved that it reduces the risk of hip fractures and vertebral compression fractures<sup>145</sup>, especially in postmenopausal women with osteoporosis<sup>120,145</sup>. It also reduces the risk of degenerative bone diseases, regulates the apoptosis of the osteoclasts and improves the metabolism in bone and cartilage tissue<sup>146</sup>.

Recent data have raised significant safety concerns, particularly the risk of myocardial infarction. Combined results of studies on the safety of the medication led the European Medicines Agency (EMA) to add contraindications for those with a history of cardiovascular disease, venous thromboembolism (VTE) and currently uncontrolled hypertension. Safety results showed an increased risk of myocardial infarction (MI) and VTE for individuals with a previous history of those conditions but no increased risk for patients without a prior history. It was found that this strontium-containing compound increases the risk of MI in postmenopausal women<sup>147</sup>.



### 2.4.2 Strontium Chloride

The protective properties of strontium salts on bone were first suggested in 1959, when strontium lactate was reported to decrease bone pain and to increase bone density in a cohort of osteoporotic patients<sup>148</sup>. Further observations found that dietary supplementation with strontium chloride ( $\text{SrCl}_2$ ) tend to increase osteoid surface and to reduce osteoclast numbers in mice<sup>149</sup>, establishing that Sr can act as a direct ‘uncoupler’ of bone turnover<sup>134</sup>.

However, recent studies showed that  $\text{SrCl}_2$  exerts a contained effect on molar basis mineralization, if compared to SrR. This discrepancy may be due to the differing stoichiometry of these two Sr compounds. In fact, SrR chelates two strontium ions per molecule, whereas the  $\text{SrCl}_2$  salt has only one single strontium ion. However, it is possible that the ranelate component of SrR may also have an independent Ca ion chelating action, that could affect mineralization<sup>150</sup>.

Other comparative studies have shown a differential rate in Sr uptaking in bone, after administration of the two different forms of Sr. At low and high Sr doses, ions uptake in the new bone matrix is higher after treatment with SrR, suggesting that this compound promotes greater uptake to bone, if compared with  $\text{SrCl}_2$ .

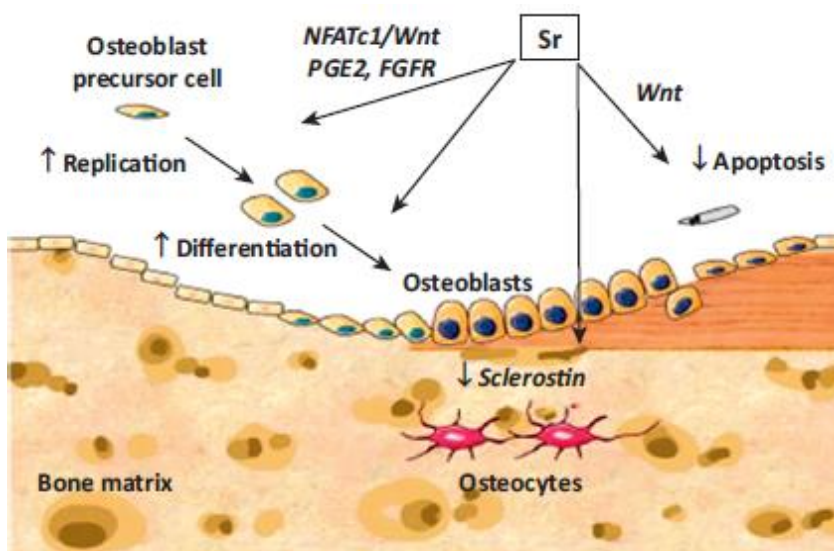


Fig 1.10 A schematic showing how Sr activates osteoblastogenesis: Sr induces increased production of (NFATc)/Wnt signaling, prostaglandin E2 (PGE2), activation of fibroblast growth factor receptor (FGFR) in osteoblastic cells and reduction of SOST express<sup>134</sup>.

### 2.4.3 Strontium-containing Hydroxyapatite

Ceramic drug carriers, in particular hydroxyapatite NPs, are attractive for their ability to provide osteoconductive, space-filling function to the application site, in conjunction with controlled release capability<sup>151</sup>. Ceramic particles are capable of carrying a wide variety of agents for release.

Sr has demonstrated a remarkable versatility, after the advent of the SrR for the treatment of osteoporosis, thus the study of synthetic hydroxyapatites containing Sr may contribute significantly to better understand the effects of Sr in bone mineral.

Sr-HAp produces an increased interest in osteoporotic bone treatment and replacement. Several *in vitro* and *in vivo* studies conducted on Sr-HAps have revealed that they encourage osteoblast proliferation and downregulate osteoclast formation, increasing the ALP activity<sup>152-154</sup>.

Actually, through different analytical methods, many researchers are evaluating the alterations in HAp crystals properties after Sr incorporation and the effects of these substituted apatites at different concentrations.

Li and colleagues reported a decrease in crystallinity and crystal size in several synthetic HAp with 15% Sr relative to Ca<sup>155</sup>. This result was confirmed through X-ray diffraction (XRD), Selected area electron diffraction (SAED), and Transmission Electron Microscopy (TEM) analysis, revealing that the average length of the crystals decreased from 23.3 nm in control to 12.5 in HAp with 15% Sr. This finding was supported by other works. For instance, Aina and collaborators observed a decreased crystallinity and crystal size in HAp with 24% and 67% Sr relative to Ca, using the XRD and Raman Spectroscopy<sup>123</sup>. Although other studies confirmed this result, through XRD and TEM assays, it was also found that crystal size gradually tend to increase with higher Sr contents, reaching values greater than those of control in HAp with 100% Sr<sup>156,157</sup>.

Among others, also the shape and the aggregation level of the HAp crystals is affected by different Sr incorporation. For instance, in the same work of 2007, Li and coworkers proved that the crystals of HAp with 15% Sr were not only smaller, if compared to the control, but also tended to aggregate more, appearing in TEM images as if they were melting to one another<sup>155</sup>.

Similar results were found by Bigi and collaborators, who described the crystals of HAp with up to 50% Sr, as having perturbed shapes and ill-defined edges. Moreover, they noticed not only the decrease in crystal size, but also a linear variation in the lattice constants<sup>156</sup>. It is possible that this difference could result in the formation of crystals with a smaller aspect ratio (length/width) than in control. In fact, Li and coworkers found a decrease in the aspect ratio of crystals of HAp with the low amount of 1.5% Sr. Unfortunately, they could not estimate the aspect ratio of HAp with 15% Sr, because the crystals were too aggregated; however, they suggested that such decrease might be related to a greater effect of inhibitory effect of the Sr on the growth of the crystals along the c-axis direction<sup>155</sup>.

The Sr-HAp has also been found to be highly soluble. An increase in solubility was described for the first time in 1997 by Christoffersen and colleagues, who found that HAp with 10% Sr had a higher solubility than the control<sup>158</sup>. This data was supported by further studies: for example, an

increase in solubility was also seen in HAp with 16.6% and 65% Sr, which presented a significantly higher release of phosphorus than the control, in bicarbonate solution<sup>159</sup>.

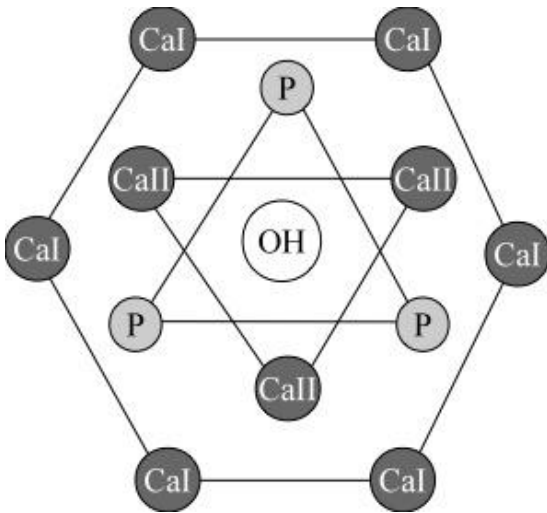


**Fig 1.11** A sketch of the chemical structure of hydroxyapatite. Strontium is preferably incorporated at the CaII position, and this expands the apatite structure, causing destabilization<sup>151</sup>.

Several other changes were described in the structure and composition of the crystal reticle of synthetic Sr-HAp with Sr. Terra and coworkers analyzed in details the effects on Sr in the atomic structure of nanocrystalline Hap, using different assays. They found that Sr can be incorporated into both Ca sites of HAp structure, Ca (I), where the atoms are aligned in long columns, each surrounded by nine oxygen atoms, and Ca (II) site arranged at the apexes of “staggered” equilateral triangles, each surrounded by seven oxygen atoms. Their results show that Ca (I) sites are favored when the Sr content is very low (around 1%), while it displays a gradual preference for Ca (II) sites when the Sr content increases (5% and above). Its occupancy for

the Ca (I) site, at very low concentrations, shows difference in the morphology, whereas such incorporation of Sr in the Ca (II) site lead to a strong local distortion of the lattice, due to variations in bond distances and twist angles<sup>155–157,160</sup> (**Fig. 1.11**).

Also further studies suggest that the morphology of the apatitic crystals is affected by the chemical composition. For instance, a clear shift of the PO<sub>4</sub> peaks to lower wavenumbers was seen by FTIR in HAp with increasing Sr contents, indicating an expansion of the interphosphate anion–anion distance and a decrease in the anion–anion repulsion<sup>156</sup>. The incorporation of Sr in synthetic HAp leads to the loss of OH from the mineral<sup>155,156,159,160</sup>, whereas an increase in the CO<sub>3</sub> content has been described in Sr-HAp<sup>155,161</sup>. Both these aspects were evaluated by FITR.

In 2012, Rokidi and Koutsoukos evaluated the effects of strontium on the crystal growth of octacalcium phosphate (OCP), that may be a transient intermediate for the formation of the bone apatite crystals<sup>162,163</sup>. In supersaturated solution, the presence of Sr was found to decrease the rate of OCP crystal growth, indicating that Sr may stabilize the OCP crystals and delay their transformation into the more stable HAp phase. Another interesting study established that calcium deficient HAp with 10% Sr relative to Ca presented an increase in the negative zeta potential, estimated by dynamic light scattering method. This could suggest that the crystals have a higher surface reactivity, increasing their agglomeration levels, with the organic components of the ECM and with bone cells<sup>162</sup>.

These apatites have been reported to have good compressive strength, similar to human bone compared to the unsubstituted HAps, and to enhance bone mechanical properties<sup>164,165</sup>. Indeed, in ovariectomized rats, Sr-HAp coatings improved the implants integration in the bone tissue<sup>166</sup>. Interestingly, the increase in the net positive charge of strontium-substituted calcium phosphate NPs could potentially increase the gene delivery efficiency through increased interaction of cations on calcium phosphate and the phosphate groups of nucleic acids of the non-viral gene delivery vectors<sup>167</sup>.

## 2.5 Objectives of the thesis

The aim of this thesis was to study the effect of Sr-substituted hydroxyapatite nanoparticles on bone remodeling in *in vitro* and *in vivo* models.

As reported in **Chapter 1**, strontium has been demonstrated to have a dual effect on bone formation and bone resorption. In particular, *in vitro* and *in vivo* evidences demonstrated that strontium containing molecules or biomaterials modulated positively the osteoblast differentiation enhancing and accelerating this process and, on the other hand, an inhibition of osteoclastogenesis and resorptive activity was observed.

In last years, a new idea of delivery of strontium came out. In particular, many authors substituted calcium with strontium ions in hydroxyapatite synthesis. In our study, we obtained a stable suspension of Strontium-substituted hydroxyapatite nanoparticles and we performed several *in vitro* studies on bone remodeling and their ability to induce ectopic bone formation *in vivo*. Finally, we evaluated the effect of Sr-containing nanoparticles on osteoblasts differentiation in microgravity conditions since the absence of the gravity force has been demonstrated to inhibit osteoblastogenesis.

More specifically, the presented research aimed to:

**Chapter 2** – Synthesis of Sr-substituted hydroxyapatite nanopowders and investigation on the effect due to Sr presence within the apatite lattice by a detailed chemical, structural and morphological characterization of the powders. Evaluation of the biocompatibility of nanoparticle stable suspensions of the synthesized powders.

**Chapter 3** – Investigation on the effect of Sr-substitute hydroxyapatite nanoparticles on bone remodelling using *in vitro* different cell models: human osteosarcoma SAOS-2 cell line and mesenchymal stem cells (hBMMSCs) isolated from bone marrow for the osteoblasts differentiation; murine osteocytic Ocy454 cell line for osteocyte differentiation; murine macrophage RAW 264.7 cell line for osteoclast differentiation.

**Chapter 4** – Evaluation of the ectopic bone formation induced by gelatine sponge containing strontium-substitute hydroxyapatite implanted at the periosteal surface of mice femur and comparison to the effect exerted with gelatine sponge containing Bone Morphogenetic Protein 2.

**Chapter 5** – Investigation of the effect exerted with Sr-containing hydroxyapatite nanoparticles on human osteoblasts differentiation in simulated (RPM) and space (ISS) microgravity conditions. We used hBMMSCs cultivated on Random Positioning Machine to simulate microgravity on earth and on International Space Station.

A summary of all data is presented and future research indications are also reported in **Chapter 6**.

## 2.6 References

1. Fernandez-Yague, M. a. *et al.* Biomimetic Approaches in Bone Tissue Engineering: Integrating Biological and Physicomechanical Strategies. *Adv. Drug Deliv. Rev.* **84**, 1–29 (2015).
2. General Histology - Documents - Online Powerpoint Presentation and Document Sharing. *Docfoc.com*
3. Pittenger, M. F. *et al.* Multilineage potential of adult human mesenchymal stem cells. *Science* **284**, 143–147 (1999).
4. Nijweide, P. J., Burger, E. H. & Feyen, J. H. Cells of bone: proliferation, differentiation, and hormonal regulation. *Physiol. Rev.* **66**, 855–886 (1986).
5. Väänänen, H. K., Zhao, H., Mulari, M. & Halleen, J. M. The cell biology of osteoclast function. *J. Cell Sci.* **113** ( Pt 3, 377–381 (2000).
6. Bonewald, L. F. Osteocytes as dynamic multifunctional cells. *Ann. N. Y. Acad. Sci.* **1116**, 281–290 (2007).
7. Fakhry, M., Hamade, E., Badran, B., Buchet, R. & Magne, D. Molecular mechanisms of mesenchymal stem cell differentiation towards osteoblasts. *World J. Stem Cells* **5**, 136–148 (2013).
8. Capulli, M., Paone, R. & Rucci, N. Osteoblast and osteocyte: games without frontiers. *Arch. Biochem. Biophys.* **561**, 3–12 (2014).
9. Caetano-Lopes, J., Canhão, H. & Fonseca, J. E. Osteoblasts and bone formation. *Acta Reumatol. Port.* **32**, 103–10
10. Liu, G. *et al.* Canonical Wnts function as potent regulators of osteogenesis by human mesenchymal stem cells. *J. Cell Biol.* **185**, 67–75 (2009).
11. Komori, T. *et al.* Targeted Disruption of *Cbfa1* Results in a Complete Lack of Bone Formation owing to Maturational Arrest of Osteoblasts. *Cell* **89**, 755–764 (1997).
12. Celil, A. B. & Campbell, P. G. BMP-2 and Insulin-like Growth Factor-I Mediate Osterix (*Osx*) Expression in Human Mesenchymal Stem Cells via the MAPK and Protein Kinase D Signaling Pathways. *J. Biol. Chem.* **280**, 31353–31359 (2005).
13. Hartmann, C. A Wnt canon orchestrating osteoblastogenesis. *Trends Cell Biol.* **16**, 151–158 (2006).
14. Han, Y. *et al.* Protein kinase A phosphorylates and regulates the osteogenic activity of *Dlx5*. *Biochem. Biophys. Res. Commun.* **407**, 461–465 (2011).
15. Ding, J. *et al.* TNF-alpha and IL-1beta inhibit RUNX2 and collagen expression but increase alkaline phosphatase activity and mineralization in human mesenchymal stem cells. *Life Sci.*

- 84**, 499–504 (2009).
16. Gilbert, L. *et al.* Expression of the osteoblast differentiation factor RUNX2 (Cbfa1/AML3/Pebp2alpha A) is inhibited by tumor necrosis factor-alpha. *J. Biol. Chem.* **277**, 2695–2701 (2002).
  17. Teti, A. Bone development: overview of bone cells and signaling. *Curr. Osteoporos. Rep.* **9**, 264–273 (2011).
  18. Moester, M. J. C., Papapoulos, S. E., Löwik, C. W. G. M. & van Bezooijen, R. L. Sclerostin: current knowledge and future perspectives. *Calcif. Tissue Int.* **87**, 99–107 (2010).
  19. Anderson, H. C. Matrix vesicles and calcification. *Curr. Rheumatol. Rep.* **5**, 222–226 (2003).
  20. Hoshi, K. Fine structure of bone matrix calcification. *J. Oral Biosci.* **54**, 19–24 (2012).
  21. Mechanism of mineral formation in bone. *Lab. Invest.* **60**, 320–330 (1989).
  22. Teitelbaum, S. L. Bone Resorption by Osteoclasts. *Science (80-. )*. **289**, 1504–1508 (2000).
  23. Asagiri, M. & Takayanagi, H. The molecular understanding of osteoclast differentiation. *Bone* **40**, 251–264 (2007).
  24. Dougall, W. C. *et al.* RANK is essential for osteoclast and lymph node development. *Genes Dev.* **13**, 2412–2424 (1999).
  25. Galibert, L., Tometsko, M. E., Anderson, D. M., Cosman, D. & Dougall, W. C. The involvement of multiple tumor necrosis factor receptor (TNFR)-associated factors in the signaling mechanisms of receptor activator of NF-kappaB, a member of the TNFR superfamily. *J. Biol. Chem.* **273**, 34120–34127 (1998).
  26. Lomaga, M. A. *et al.* TRAF6 deficiency results in osteopetrosis and defective interleukin-1, CD40, and LPS signaling. *Genes Dev.* **13**, 1015–1024 (1999).
  27. Asagiri, M. *et al.* Autoamplification of NFATc1 expression determines its essential role in bone homeostasis. *J. Exp. Med.* **202**, 1261–1269 (2005).
  28. Hess, J., Angel, P. & Schorpp-Kistner, M. AP-1 subunits: quarrel and harmony among siblings. *J. Cell Sci.* **117**, 5965–5973 (2004).
  29. Johnson, R. S., Spiegelman, B. M. & Papaioannou, V. Pleiotropic effects of a null mutation in the c-fos proto-oncogene. *Cell* **71**, 577–586 (1992).
  30. Boyce, B. F., Xiu, Y., Li, J., Xing, L. & Yao, Z. NF-κB-Mediated Regulation of Osteoclastogenesis. *Endocrinol. Metab.* **30**, 35–44 (2015).
  31. Kim, Y. *et al.* Contribution of nuclear factor of activated T cells c1 to the transcriptional control of immunoreceptor osteoclast-associated receptor but not triggering receptor expressed by myeloid cells-2 during osteoclastogenesis. *J. Biol. Chem.* **280**, 32905–32913 (2005).

32. Koga, T. *et al.* Costimulatory signals mediated by the ITAM motif cooperate with RANKL for bone homeostasis. *Nature* **428**, 758–763 (2004).
33. Bilezikian, J. P., Raisz, L. G. & Martin, T. J. *Principles of Bone Biology: Two-Volume Set.* (Academic Press, 2008).
34. Nesbitt, S. A. & Horton, M. A. Trafficking of matrix collagens through bone-resorbing osteoclasts. *Science* **276**, 266–269 (1997).
35. Baron, A., Lynn, N., Louvard, D. & Courtoy, P. J. Cell-mediated extracellular acidification and bone resorption: evidence for a low pH in resorbing lacunae and localization of a 100-kD lysosomal membrane protein at the osteoclast ruffled border. *J. Cell Biol.* **101**, 2210–2222 (1985).
36. Halleen, J. M. *et al.* Intracellular fragmentation of bone resorption products by reactive oxygen species generated by osteoclastic tartrate-resistant acid phosphatase. *J. Biol. Chem.* **274**, 22907–22910 (1999).
37. Raggatt, L. J. & Partridge, N. C. Cellular and Molecular Mechanisms of Bone Remodeling. *J. Biol. Chem.* **285**, 25103–25108 (2010).
38. Sims, N. A. & Martin, T. J. Coupling the activities of bone formation and resorption: a multitude of signals within the basic multicellular unit. *Bonekey Rep.* **3**, 481 (2014).
39. Khundmiri, S. J., Murray, R. D. & Lederer, E. PTH and Vitamin D. *Compr. Physiol.* **6**, 561–601 (2016).
40. Boron, W. & Boulpaep, E. *Medical Physiology: A Cellular And Molecular Approach.* (2008).
41. Raisz, L. G. Pathogenesis of osteoporosis: concepts, conflicts, and prospects. *J. Clin. Invest.* **115**, 3318–3325 (2005).
42. Rodan, G. A. & Martin, T. J. Therapeutic approaches to bone diseases. *Science* **289**, 1508–14 (2000).
43. South-Paul, J. E. Osteoporosis: part I. Evaluation and assessment. *Am. Fam. Physician* **63**, 897–904,908 (2001).
44. White, R. J. & Averner, M. Humans in space. *Nature* **409**, 1115–1118 (2001).
45. Vico, L., Collet, P., Guignandon, A., Thomas, T. & Rehailia, M. Effects of long-term microgravity exposure on cancellous and cortical weight-bearing bones of cosmonauts. *Lancet* **355**, 1607–1611 (2000).
46. Ulbrich, C. *et al.* The Impact of Simulated and Real Microgravity on Bone Cells and Mesenchymal Stem Cells. **2014**, (2014).
47. Tamma, R. *et al.* Microgravity during spaceflight directly affects in vitro osteoclastogenesis



- and bone resorption. *FASEB J.* **23**, 2549–54 (2009).
48. Lupsa, B. C. & Insogna, K. Bone Health and Osteoporosis. *Endocrinol. Metab. Clin. North Am.* **44**, 517–530 (2015).
  49. Rivadeneira, F. & Makitie, O. Osteoporosis and Bone Mass Disorders: From Gene Pathways to Treatments. *Trends Endocrinol. Metab.* **27**, 262–281 (2016).
  50. Stefanick, M. L. Estrogens and progestins: background and history, trends in use, and guidelines and regimens approved by the US Food and Drug Administration. *Am. J. Med.* **118 Suppl**, 64–73 (2005).
  51. Gennari, L., Merlotti, D. & Nuti, R. Selective estrogen receptor modulator (SERM) for the treatment of osteoporosis in postmenopausal women: focus on lasofoxifene. *Clin. Interv. Aging* **5**, 19–29 (2010).
  52. Overgaard, K., Riis, B. J., Christiansen, C. & Hansen, M. A. Effect of salcatonin given intranasally on early postmenopausal bone loss. *BMJ* **299**, 477–479 (1989).
  53. Tilyard, M. W., Spears, G. F., Thomson, J. & Dovey, S. Treatment of postmenopausal osteoporosis with calcitriol or calcium. *N. Engl. J. Med.* **326**, 357–362 (1992).
  54. Civitelli, R. *et al.* Bone turnover in postmenopausal osteoporosis. Effect of calcitonin treatment. *J. Clin. Invest.* **82**, 1268–1274 (1988).
  55. Langlois, J. A. *et al.* Association between insulin-like growth factor I and bone mineral density in older women and men: the Framingham Heart Study. *J. Clin. Endocrinol. Metab.* **83**, 4257–4262 (1998).
  56. Saaf, M., Hilding, A., Thoren, M., Troell, S. & Hall, K. Growth hormone treatment of osteoporotic postmenopausal women - a one-year placebo-controlled study. *Eur. J. Endocrinol.* **140**, 390–399 (1999).
  57. Chapuy, M. C. & Meunier, P. J. Prevention and treatment of osteoporosis. *Aging (Milano)*. **7**, 164–173 (1995).
  58. Scheiber, L. B. 2nd & Torregrosa, L. Evaluation and treatment of postmenopausal osteoporosis. *Semin. Arthritis Rheum.* **27**, 245–261 (1998).
  59. Lufkin, E. G. *et al.* Treatment of postmenopausal osteoporosis with transdermal estrogen. *Ann. Intern. Med.* **117**, 1–9 (1992).
  60. Rizzoli, R. *et al.* Continuous treatment with odanacatib for up to 8 years in postmenopausal women with low bone mineral density: a phase 2 study. *Osteoporos. Int.* **27**, 2099–2107 (2016).
  61. Overgaard, K. & Riis, B. J. Nasal salmon calcitonin in osteoporosis. *Calcified tissue international* **55**, 79–81 (1994).

62. Asafo-Adjei, T. A., Chen, A. J., Najarzadeh, A. & Puleo, D. A. Advances in Controlled Drug Delivery for Treatment of Osteoporosis. *Curr. Osteoporos. Rep.* (2016). doi:10.1007/s11914-016-0321-4
63. Farrier, A. J. *et al.* New anti-resorptives and antibody mediated anti-resorptive therapy. *Bone Joint J.* **98–B**, 160–165 (2016).
64. Kong, Y.-Y. *et al.* OPGL is a key regulator of osteoclastogenesis, lymphocyte development and lymph-node organogenesis. *Nature* **397**, 315–323 (1999).
65. Mandema, J. W., Zheng, J., Libanati, C. & Perez Ruixo, J. J. Time course of bone mineral density changes with denosumab compared with other drugs in postmenopausal osteoporosis: a dose-response-based meta-analysis. *J. Clin. Endocrinol. Metab.* **99**, 3746–3755 (2014).
66. Anastasilakis, A. D. *et al.* Denosumab versus zoledronic acid in patients previously treated with zoledronic acid. *Osteoporos. Int.* **26**, 2521–2527 (2015).
67. Bekker, P. J. *et al.* A single-dose placebo-controlled study of AMG 162, a fully human monoclonal antibody to RANKL, in postmenopausal women. 2004. *J. Bone Miner. Res.* **20**, 2275–2282 (2005).
68. Kearns, A. E., Khosla, S. & Kostenuik, P. J. Receptor activator of nuclear factor kappaB ligand and osteoprotegerin regulation of bone remodeling in health and disease. *Endocr. Rev.* **29**, 155–192 (2008).
69. Bekker, P. J. *et al.* The effect of a single dose of osteoprotegerin in postmenopausal women. *J. Bone Miner. Res.* **16**, 348–360 (2001).
70. Min, H. *et al.* Osteoprotegerin reverses osteoporosis by inhibiting endosteal osteoclasts and prevents vascular calcification by blocking a process resembling osteoclastogenesis. *J. Exp. Med.* **192**, 463–474 (2000).
71. Carstens, J. H. J. & Feinblatt, J. D. Future horizons for calcitonin: a U.S. perspective. *Calcif. Tissue Int.* **49 Suppl 2**, S2-6 (1991).
72. Francis, M. D. & Valent, D. J. Historical perspectives on the clinical development of bisphosphonates in the treatment of bone diseases. *J. Musculoskelet. Neuronal Interact.* **7**, 2–8 (2007).
73. Marini, F. & Brandi, M. L. Pharmacogenetics of osteoporosis. *Best Pract. Res. Clin. Endocrinol. Metab.* **28**, 783–793 (2014).
74. Wang, H. *et al.* Recombinant human parathyroid hormone related protein 1-34 and 1-84 and their roles in osteoporosis treatment. *PLoS One* **9**, e88237 (2014).
75. Zhu, J. *et al.* Amphiregulin-EGFR Signaling Mediates the Migration of Bone Marrow Mesenchymal Progenitors toward PTH- Stimulated Osteoblasts and Osteocytes. *PLoS One* **7**,

e50099 (2012).

76. Neer, R. M. *et al.* Effect of Parathyroid Hormone (1-34) on Fractures and Bone Mineral Density in Postmenopausal Women with Osteoporosis. *N. Engl. J. Med.* **344**, 1434–1441 (2001).
77. Poole, K. E. S. *et al.* Sclerostin is a delayed secreted product of osteocytes that inhibits bone formation. *FASEB J.* **19**, 1842–1844 (2005).
78. Winkler, D. G. *et al.* Osteocyte control of bone formation via sclerostin, a novel BMP antagonist. *EMBO J.* **22**, 6267 LP-6276 (2003).
79. van Bezooijen, R. L. *et al.* Sclerostin is an osteocyte-expressed negative regulator of bone formation, but not a classical BMP antagonist. *J. Exp. Med.* **199**, 805–14 (2004).
80. Wijenayaka, A. R. *et al.* Sclerostin stimulates osteocyte support of osteoclast activity by a RANKL-dependent pathway. *PLoS One* **6**, (2011).
81. Van Bezooijen, R. L. *et al.* Wnt but not BMP signaling is involved in the inhibitory action of sclerostin on BMP-stimulated bone formation. *J. Bone Miner. Res.* **22**, 19–28 (2007).
82. Semenov, M., Tamai, K. & He, X. SOST is a ligand for LRP5/LRP6 and a Wnt signaling inhibitor. *J. Biol. Chem.* **280**, 26770–26775 (2005).
83. Ke, H. Z., Richards, W. G., Li, X. & Ominsky, M. S. Sclerostin and Dickkopf-1 as therapeutic targets in bone diseases. *Endocr. Rev.* **33**, 747–783 (2012).
84. Diarra, D. *et al.* Dickkopf-1 is a master regulator of joint remodeling. *Nat. Med.* **13**, 156–163 (2007).
85. Heath, D. J. *et al.* Inhibiting Dickkopf-1 (Dkk1) removes suppression of bone formation and prevents the development of osteolytic bone disease in multiple myeloma. *J. Bone Miner. Res.* **24**, 425–436 (2009).
86. Fulciniti, M. *et al.* Anti-DKK1 mAb (BHQ880) as a potential therapeutic agent for multiple myeloma. *Blood* **114**, 371–379 (2009).
87. Eisman, J. A. *et al.* Odanacatib in the treatment of postmenopausal women with low bone mineral density: three-year continued therapy and resolution of effect. *J. Bone Miner. Res.* **26**, 242–51 (2011).
88. Bone, H. G. *et al.* Odanacatib, a cathepsin-K inhibitor for osteoporosis: A two-year study in postmenopausal women with low bone density. *J. Bone Miner. Res.* **25**, 937–947 (2010).
89. Stoch, S. A. *et al.* Effect of the cathepsin K inhibitor odanacatib on bone resorption biomarkers in healthy postmenopausal women: two double-blind, randomized, placebo-controlled phase I studies. *Clin. Pharmacol. Ther.* **86**, 175–82 (2009).
90. Carragee, E. J., Hurwitz, E. L. & Weiner, B. K. A critical review of recombinant human bone

morphogenetic protein-2 trials in spinal surgery: emerging safety concerns and lessons learned. *Spine J.* **11**, 471–491 (2011).

91. Ehnert, S. *et al.* Transforming growth factor beta1 inhibits bone morphogenic protein (BMP)-2 and BMP-7 signaling via upregulation of Ski-related novel protein N (SnoN): possible mechanism for the failure of BMP therapy? *BMC Med.* **10**, 101 (2012).
92. Fricain, J. C. *et al.* A nano-hydroxyapatite--pullulan/dextran polysaccharide composite macroporous material for bone tissue engineering. *Biomaterials* **34**, 2947–59 (2013).
93. Narayanan, G., Vernekar, V. N., Kuyinu, E. L. & Laurencin, C. T. Poly (lactic acid)-based biomaterials for orthopaedic regenerative engineering ☆. (2016). doi:10.1016/j.addr.2016.04.015
94. Keogh, M. B., O' Brien, F. J. & Daly, J. S. A novel collagen scaffold supports human osteogenesis—applications for bone tissue engineering. *Cell Tissue Res.* **340**, 169–177 (2010).
95. López-Álvarez, M., Rodríguez-Valencia, C., Serra, J. & González, P. Bio-inspired Ceramics: Promising Scaffolds for Bone Tissue Engineering. *Procedia Eng.* **59**, 51–58 (2013).
96. Mikos, A. G. *et al.* Preparation and characterization of poly(l-lactic acid) foams. *Polymer (Guildf)*. **35**, 1068–1077 (1994).
97. Langer, R. & Vacanti, J. P. Tissue engineering. *Science (80-. )*. **260**, 920–926 (1993).
98. Ma, P., Zhang, R., Xiao, G. & Franceschi, R. Engineering new bone tissue in vitro on highly porous poly(alpha-hydroxyl acids)/hydroxyapatite composite scaffolds. *J Biomed Mater Res* **54**, 284–93 (2001).
99. Rawat, M., Singh, D., Saraf, S. & Saraf, S. Nanocarriers: promising vehicle for bioactive drugs. *Biol. Pharm. Bull.* **29**, 1790–8 (2006).
100. Fujii, E. *et al.* Selective protein adsorption property and characterization of nano-crystalline zinc-containing hydroxyapatite. *Acta Biomater.* **2**, 69–74 (2006).
101. Murugan, R. & Ramakrishna, S. Bioresorbable composite bone paste using polysaccharide based nano hydroxyapatite. *Biomaterials* **25**, 3829–3835 (2004).
102. Lakhkar, N. J. *et al.* Bone formation controlled by biologically relevant inorganic ions: Role and controlled delivery from phosphate-based glasses. *Adv. Drug Deliv. Rev.* **65**, 405–420 (2013).
103. Yin, P., Feng, F., Lei, T. & Jian, X. Colloidal-sol gel derived biphasic FHA/SrHA coatings. *Surf. Coatings Technol.* **207**, 608–613 (2012).
104. WANG, Y. Between Science and Art: Questionable International Relations Theories. *Japanese J. Polit. Sci.* **8**, 191–208 (2007).

105. Kim, H.-W., Kim, H.-E. & Knowles, J. C. Fluor-hydroxyapatite sol–gel coating on titanium substrate for hard tissue implants. *Biomaterials* **25**, 3351–3358 (2004).
106. Hahn, B.-D. *et al.* Effect of fluorine addition on the biological performance of hydroxyapatite coatings on Ti by aerosol deposition. *J. Biomater. Appl.* **27**, 587–594 (2013).
107. Prasad, A. S. Zinc: An overview. *Nutrition* **11**, 93–99 (1995).
108. Andrews, M. & Gallagher-Allred, C. The role of zinc in wound healing. *Adv. Wound Care* **12**, 137–138 (1999).
109. Wang, X., Ito, A., Sogo, Y., Li, X. & Oyane, A. Zinc-containing apatite layers on external fixation rods promoting cell activity. *Acta Biomater.* **6**, 962–968 (2010).
110. Stanić, V. *et al.* Synthesis, characterization and antimicrobial activity of copper and zinc-doped hydroxyapatite nanopowders. *Appl. Surf. Sci.* **256**, 6083–6089 (2010).
111. Shimazaki, T. *et al.* In vivo antibacterial and silver-releasing properties of novel thermal sprayed silver-containing hydroxyapatite coating. *J. Biomed. Mater. Res. - Part B Appl. Biomater.* **92**, 386–389 (2010).
112. Simchi, A., Tamjid, E., Pishbin, F. & Boccaccini, A. R. Recent progress in inorganic and composite coatings with bactericidal capability for orthopaedic applications. *Nanomedicine Nanotechnology, Biol. Med.* **7**, 22–39 (2011).
113. Chen, Y. *et al.* Anti-bacterial and cytotoxic properties of plasma sprayed silver-containing HA coatings. *J. Mater. Sci. Mater. Med.* **19**, 3603–3609 (2008).
114. Feng, Q. L. *et al.* Antibacterial effects of Ag-HAp thin films on alumina substrates. *Thin Solid Films* **335**, 214–219 (1998).
115. Li, X. *et al.* Boron nitride nanotube-enhanced osteogenic differentiation of mesenchymal stem cells. *J. Biomed. Mater. Res. B. Appl. Biomater.* **104**, 323–329 (2016).
116. Stevanovic, M. *et al.* 45S5Bioglass(R)-based scaffolds coated with selenium nanoparticles or with poly(lactide-co-glycolide)/selenium particles: Processing, evaluation and antibacterial activity. *Colloids Surf. B. Biointerfaces* **132**, 208–215 (2015).
117. Shameli, K. *et al.* Silver/poly (lactic acid) nanocomposites: preparation, characterization, and antibacterial activity. *Int. J. Nanomedicine* **5**, 573–579 (2010).
118. Stolzoff, M. & Webster, T. J. Reducing bone cancer cell functions using selenium nanocomposites. *J. Biomed. Mater. Res. A* **104**, 476–482 (2016).
119. Marie, P. J., Felsenberg, D. & Brandi, M. L. How strontium ranelate, via opposite effects on bone resorption and formation, prevents Osteoporosis. *Osteoporos. Int.* **22**, 1659–1667 (2011).
120. Reginster, J. Y. *et al.* Strontium ranelate reduces the risk of nonvertebral fractures in

- postmenopausal women with osteoporosis: Treatment of Peripheral Osteoporosis (TROPOS) study. *J. Clin. Endocrinol. Metab.* **90**, 2816–22 (2005).
121. Dahl, S. G. *et al.* Incorporation and distribution of strontium in bone. *Bone* **28**, 446–453 (2001).
  122. Ni, G. X. *et al.* Strontium-containing hydroxyapatite (Sr-HA) bioactive cement for primary hip replacement: an in vivo study. *J. Biomed. Mater. Res. B. Appl. Biomater.* **77**, 409–415 (2006).
  123. Aina, V. *et al.* Sr-containing hydroxyapatite: morphologies of HA crystals and bioactivity on osteoblast cells. *Mater. Sci. Eng. C. Mater. Biol. Appl.* **33**, 1132–1142 (2013).
  124. Liu, Y. *et al.* Segmental bone regeneration using an rhBMP-2-loaded gelatin/nanohydroxyapatite/fibrin scaffold in a rabbit model. *Biomaterials* **30**, 6276–6285 (2009).
  125. Pors Nielsen, S. The biological role of strontium. *Bone* **35**, 583–8 (2004).
  126. Davies, D. R., Bassingthwaite, J. B. & Kelly, P. J. Transcapillary exchange of strontium and sucrose in canine tibia. *J. Appl. Physiol.* **40**, 17–22 (1976).
  127. YANG, F. *et al.* Strontium Enhances Osteogenic Differentiation of Mesenchymal Stem Cells and In Vivo Bone Formation by Activating Wnt / Catenin. *Stem Cells* **29**, 981–991 (2011).
  128. Marie, P. J. Optimizing bone metabolism in osteoporosis: insight into the pharmacologic profile of strontium ranelate. *Osteoporos. Int.* **14 Suppl 3**, S9-12 (2003).
  129. Baron, R. & Tsouderos, Y. In vitro effects of S12911-2 on osteoclast function and bone marrow macrophage differentiation. **450**, 11–17 (2002).
  130. Barbara, A., Delannoy, P., Denis, B. G. & Marie, P. J. Normal matrix mineralization induced by strontium ranelate in MC3T3-E1 osteogenic cells. *Metabolism.* **53**, 532–7 (2004).
  131. Canalis, E., Hott, M., Deloffre, P., Tsouderos, Y. & Marie, P. J. The divalent strontium salt S12911 enhances bone cell replication and bone formation in vitro. *Bone* **18**, 517–523 (1996).
  132. Takahashi, N., Sasaki, T., Tsouderos, Y. & Suda, T. S 12911-2 Inhibits Osteoclastic Bone Resorption In Vitro. *J. Bone Miner. Res.* **18**, 1082–1087 (2003).
  133. Ammann, P. *et al.* Strontium ranelate improves bone resistance by increasing bone mass and improving architecture in intact female rats. *J. Bone Miner. Res.* **19**, 2012–20 (2004).
  134. Bonnelye, E., Chabadel, A., Saltel, F. & Jurdic, P. Dual effect of strontium ranelate: stimulation of osteoblast differentiation and inhibition of osteoclast formation and resorption in vitro. *Bone* **42**, 129–38 (2008).
  135. Morohashi, T., Sano, T., Harai, K. & Yamada, S. Effects of strontium on calcium

- metabolism in rats. II. Strontium prevents the increased rate of bone turnover in ovariectomized rats. *Jpn. J. Pharmacol.* **68**, 153–159 (1995).
136. Brown, E. M. & Lian, J. B. New insights in bone biology: unmasking skeletal effects of the extracellular calcium-sensing receptor. *Sci. Signal.* **1**, pe40 (2008).
  137. Chang, W. *et al.* Expression and signal transduction of calcium-sensing receptors in cartilage and bone. *Endocrinology* **140**, 5883–5893 (1999).
  138. Quarles, L. D. Cation sensing receptors in bone: a novel paradigm for regulating bone remodeling? *Journal of bone and mineral research : the official journal of the American Society for Bone and Mineral Research* **12**, 1971–1974 (1997).
  139. Coulombe, J., Faure, H., Robin, B. & Ruat, M. In vitro effects of strontium ranelate on the extracellular calcium-sensing receptor. *Biochem. Biophys. Res. Commun.* **323**, 1184–1190 (2004).
  140. Hurtel-Lemaire, A. S. *et al.* The calcium-sensing receptor is involved in strontium ranelate-induced osteoclast apoptosis. New insights into the associated signaling pathways. *J. Biol. Chem.* **284**, 575–584 (2009).
  141. Fromiguet, O. *et al.* Calcium sensing receptor-dependent and receptor-independent activation of osteoblast replication and survival by strontium ranelate. *J. Cell. Mol. Med.* **13**, 2189–2199 (2009).
  142. Chattopadhyay, N., Quinn, S. J., Kifor, O., Ye, C. & Brown, E. M. The calcium-sensing receptor (CaR) is involved in strontium ranelate-induced osteoblast proliferation. *Biochem. Pharmacol.* **74**, 438–47 (2007).
  143. Atkins, G. J., Welldon, K. J., Halbout, P. & Findlay, D. M. Strontium ranelate treatment of human primary osteoblasts promotes an osteocyte-like phenotype while eliciting an osteoprotegerin response. *Osteoporos. Int.* **20**, 653–64 (2009).
  144. Brennan, T. C. *et al.* Osteoblasts play key roles in the mechanisms of action of strontium ranelate. *Br. J. Pharmacol.* **157**, 1291–300 (2009).
  145. Meunier, P. J. *et al.* Strontium ranelate: dose-dependent effects in established postmenopausal vertebral osteoporosis--a 2-year randomized placebo controlled trial. *J. Clin. Endocrinol. Metab.* **87**, 2060–2066 (2002).
  146. Mentaverri, R. *et al.* The calcium sensing receptor is directly involved in both osteoclast differentiation and apoptosis. *FASEB J. Off. Publ. Fed. Am. Soc. Exp. Biol.* **20**, 2562–2564 (2006).
  147. Agency, E. M. PRAC recommends suspending use of Protelos / Osseor ( strontium ranelate ) Recommendation by PRAC to be considered by CHMP for final opinion. **44**, 1–2 (2014).

148. Pemmer, B. *et al.* Increased strontium uptake in trabecular bone of ovariectomized calcium-deficient rats treated with strontium ranelate or strontium chloride. *J. Synchrotron Radiat.* **18**, 835–841 (2011).
149. Marie, P. J. & Hott, M. Short-term effects of fluoride and strontium on bone formation and resorption in the mouse. *Metabolism.* **35**, 547–551 (1986).
150. Wornham, D. P., Hajjawi, M. O., Orriss, I. R. & Arnett, T. R. Strontium potently inhibits mineralisation in bone-forming primary rat osteoblast cultures and reduces numbers of osteoclasts in mouse marrow cultures. *Osteoporos. Int.* **25**, 2477–2484 (2014).
151. Barry, M., Pearce, H., Cross, L., Tatullo, M. & Gaharwar, A. K. Advances in Nanotechnology for the Treatment of Osteoporosis. *Curr. Osteoporos. Rep.* **14**, 87–94 (2016).
152. Panzavolta, S. *et al.* Setting properties and in vitro bioactivity of strontium-enriched gelatin-calcium phosphate bone cements. *J. Biomed. Mater. Res. A* **84**, 965–972 (2008).
153. Boanini, E., Torricelli, P., Fini, M. & Bigi, A. Osteopenic bone cell response to strontium-substituted hydroxyapatite. *J. Mater. Sci. Mater. Med.* **22**, 2079–2088 (2011).
154. Gentleman, E. *et al.* Biomaterials The effects of strontium-substituted bioactive glasses on osteoblasts and osteoclasts in vitro. *Biomaterials* **31**, 3949–3956 (2010).
155. Li, Z. Y. *et al.* Chemical composition, crystal size and lattice structural changes after incorporation of strontium into biomimetic apatite. *Biomaterials* **28**, 1452–1460 (2007).
156. Bigi, A., Boanini, E., Capuccini, C. & Gazzano, M. Strontium-substituted hydroxyapatite nanocrystals. *Inorganica Chim. Acta* **360**, 1009–1016 (2007).
157. O'Donnell, M. D., Fredholm, Y., de Rouffignac, A. & Hill, R. G. Structural analysis of a series of strontium-substituted apatites. *Acta Biomater.* **4**, 1455–1464 (2008).
158. Christoffersen, J., Christoffersen, M. R., Kolthoff, N. & Bärenholdt, O. Effects of strontium ions on growth and dissolution of hydroxyapatite and on bone mineral detection. *Bone* **20**, 47–54 (1997).
159. Verberckmoes, S. C. *et al.* Effects of strontium on the physicochemical characteristics of hydroxyapatite. *Calcif. Tissue Int.* **75**, 405–415 (2004).
160. Terra, J. *et al.* The structure of strontium-doped hydroxyapatite: an experimental and theoretical study. *Phys. Chem. Chem. Phys.* **11**, 568–577 (2009).
161. Zhang, W. *et al.* Effects of strontium in modified biomaterials. *Acta Biomater.* **7**, 800–808 (2011).
162. Querido, W., Rossi, A. L. & Farina, M. The effects of strontium on bone mineral: A review on current knowledge and microanalytical approaches. *Micron* **80**, 122–134 (2015).



163. Crane, N. J., Popescu, V., Morris, M. D., Steenhuis, P. & Ignelzi, M. A. J. Raman spectroscopic evidence for octacalcium phosphate and other transient mineral species deposited during intramembranous mineralization. *Bone* **39**, 434–442 (2006).
164. Guo, D., Xu, K., Zhao, X. & Han, Y. Development of a strontium-containing hydroxyapatite bone cement. *Biomaterials* **26**, 4073–4083 (2005).
165. Landi, E. *et al.* Sr-substituted hydroxyapatites for osteoporotic bone replacement. *Acta Biomater.* **3**, 961–969 (2007).
166. Li, Z. *et al.* The morphology and lattice structure of bone crystal after strontium treatment in goats. *J. Bone Miner. Metab.* **28**, 25–34 (2010).
167. Hanifi, A., Fathi, M. H. & Mir Mohammad Sadeghi, H. Effect of strontium ions substitution on gene delivery related properties of calcium phosphate nanoparticles. *J. Mater. Sci. Mater. Med.* **21**, 2601–2609 (2010).



# Chapter 2

---

## 3. Synthesis and Characterization of Strontium-substituted hydroxyapatite nanoparticles for bone regeneration

### 3.1 Introduction

Calcium phosphate ceramics, *e.g.* hydroxyapatite  $\text{Ca}_{10}(\text{PO}_4)_6(\text{OH})_2$  (HA) and tricalcium phosphate  $\text{Ca}_3(\text{PO}_4)_2$  (TCP), are widely employed in the field of bone tissue engineering due to their controlled biodegradability and excellent biocompatibility<sup>1-4</sup>. Pure HA possesses a bi-pyramidal hexagonal crystal structure (space group  $\text{P6}_3/\text{m}$ ,  $a = b = 9.418 \text{ \AA}$ ,  $c = 6.884 \text{ \AA}$ ,  $\alpha = \beta = 90^\circ$ ,  $\gamma = 120^\circ$ ) where  $\text{PO}_4^{3-}$  tetrahedrons are regularly placed on two basal planes at  $1/4$  and  $3/4$  of the  $c$ -axis. Considering a unit cell, ten  $\text{Ca}^{2+}$  ions are located within two non-equivalent interstitial sites, four M(1) sites aligned to the  $c$ -axis at the cell edges and six M(2) sites forming two staggered equilateral triangles, placed above the phosphate basal plane. Within this triangular channel along the  $c$ -axis the two OH groups are placed<sup>5</sup>.

The mineralized phase of bones, as well as enamel and dentin, is associated to nano-sized crystallites of calcium deficient HA<sup>6</sup>, partially enriched by a large variety of substitutional ions. For example, one of the most common isomorphous ion replacement consists in the carbonation of HA through the substitution of  $\text{PO}_4^{3-}$  or  $\text{OH}^-$  by  $\text{CO}_3^{2-}$  groups, up to  $\sim 7\% \text{ wt}$ <sup>7,8</sup>. In addition, biological apatites can also rearrange the presence of  $\text{Mg}^{2+}$ ,  $\text{Sr}^{2+}$ ,  $\text{F}^-$ ,  $\text{Cl}^-$  or  $\text{HPO}_4^{2-}$ <sup>9-12</sup> within their crystal structure, influencing the biological behaviour of the material. In particular, strontium is strictly related to the bone response to osteoporosis, by promoting new tissue growth and decreasing its resorption<sup>13</sup>.

Most studies point out that the incorporation of Sr in the bone occurs quite rapidly (within the first two weeks)<sup>14</sup>; XRD shows the distortions of the bone mineral crystals unit cell caused by Sr, confirming the incorporation of such alkaline ion into the crystalline lattice. Since then, after the development of the promising drug strontium ranelate (SrR) (Protelos®, Servier), different types of studies were performed from mapping Sr in bones and teeth, to studying the incorporation of Sr into bone mineral (in particular in the crystal surface and lattice) and the decrease in calcium content, up to evaluate the effects of Sr in synthetic HA<sup>15</sup>. SrR is currently used in the treatment of post-menopausal osteoporosis<sup>16</sup>, although its prescription has been recently restricted to the acute medical cases because of cardiovascular side effects<sup>17</sup>. SrR shows a dual beneficial action,

enhancing the pre-osteoblastic cells differentiation and inhibiting the osteoclastic cells formation and functionality<sup>18</sup>.

In a previous work<sup>19</sup>, strontium has been shown to completely replace calcium ions in both non-equivalent interstitial sites. Due to the ionic radius difference ( $\text{Ca}^{2+} = 0.100 \text{ nm}$ ,  $\text{Sr}^{2+} = 0.118 \text{ nm}$ ), the presence of strontium results in a general perturbation of the lattice, increasing the cell parameters and modifying the mean size of the crystal domains<sup>20</sup>. In addition, previous *in vitro* and *in vivo* studies of the biological reactivity of Sr-substituted HA embedded in scaffolds like coatings on titanium components<sup>21-23</sup>, gels<sup>24</sup>, membranes<sup>25</sup> or tablets<sup>26</sup> in terms of cell vitality, proliferation and morphology have shown the osteogenic effect of Sr-HA. If these studies are relevant because they present potential effects that the incorporation of Sr could have on bone mineral, so far no studies were performed to develop and characterize stable suspension of strontium-substituted HA nanoparticles as a vector for Sr ions delivery for bone tissue engineering applications. For *in vitro* biocompatibility studies, a suitable agent must be selected to produce stable aqueous suspensions, avoiding nanoparticles flocculation<sup>27,28</sup> and growth by Ostwald ripening-like process. In addition, the dispersant should not have any effect on the test system, such as cell lines, microorganisms and animals. Bovine Serum Albumin (BSA) is a biological and mimic fluid and in a previous study was used as dispersant agent to obtain stable nanoparticles suspension<sup>29</sup>, preventing toxic effects due to powder agglomeration. Therefore, in this work, BSA has been used for preparing nanoparticles suspension for biocompatibility evaluation.

In this chapter we present the synthesis of Sr-substituted HA nanopowders and studies about the effect of Sr presence within the apatite lattice by a detailed chemical, structural and morphological characterization of the powders. The synthesized Sr-containing HA nanopowders were then used to produce stable suspensions, analyse their efficiency on osteoblast viability and understand their suitability as nano-carriers for Sr delivery in the stimulation of bone tissue regeneration. In this sense, the effect of Sr-containing HA nanoparticles on cell viability was compared with that induced by strontium ranelate and strontium chloride.

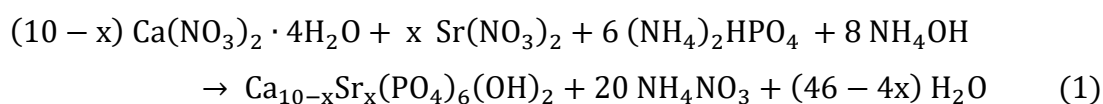
Data presented in this chapter came from a collaboration with Department of Industrial Engineering – University of Trento, Italy and are part of a publication that includes Figures 2.1, 2.2, 2.3, 2.4, 2.5, 2.6, 2.7, 2.8 and 2.9:

Frasnelli M, Cristofaro F, Sglavo VM, Dirè S, Callone E, Ceccato R, Bruni G, Icaro Cornaglia A, Visai L; Strontium-substituted hydroxyapatite nanoparticles for bone regeneration; *Material Science and Engineering C*; 71(2017) 653-662. doi: 10.1016/j.msec.2016.10.047

## 3.2 Materials and Methods

### 3.2.1 HA nanopowders: synthesis and suspensions preparation

HA nanopowders containing various  $\text{Sr}^{2+}$  amount were synthesized by aqueous precipitation method, as reported in a previous work by Bigi et al. <sup>19</sup>. High-purity calcium nitrate tetrahydrate ( $\text{Ca}(\text{NO}_3)_2 \cdot 4\text{H}_2\text{O}$ , 99% w, Sigma Aldrich A.C.S. reagent), strontium nitrate anhydrous ( $\text{Sr}(\text{NO}_3)_2$ , 98% w, Alfa Aesar) and ammonium phosphate dibasic ( $(\text{NH}_4)_2\text{HPO}_4$ , >99.0% w, Fluka), were respectively used to prepare the Ca+Sr nitrate solutions (50 mL, 1.08 M overall) and the phosphate solutions (50 ml, 0.65 M), adjusted at pH 10 with  $\text{NH}_4\text{OH}$  (30% v). The synthesis was carried out in  $\text{N}_2$  constant flow, to avoid as much as possible the carbonatation phenomena, adding drop-wise the phosphate solution to the nitrate solution at  $90^\circ\text{C}$  under stirring. The solution was stirred at  $90^\circ\text{C}$  in  $\text{N}_2$  static atmosphere for 5 h; then, the white precipitate was centrifuged three times (10000 rpm for 10 min), washed and finally dried at  $80^\circ\text{C}$  overnight. The expected reaction is:



The strontium content in the final HA powder was tailored changing the relative amount of  $\text{Ca}(\text{NO}_3)_2 \cdot 4\text{H}_2\text{O}$  and  $\text{Sr}(\text{NO}_3)_2$  in the nitrate solutions, to obtain a Sr/(Sr+Ca) molar ratio of 0, 5, 10, 25, 50, 75 and 100%; pure HA and Sr-substituted HA nanopowders were labelled as Ca100 and SrX (X = molar amount of Sr), respectively.

To establish the best ratio between albumin and powder, different concentrations were tested. The best preparation was obtained by adding 5 mg of powder to 4 mL of 5% BSA (Sigma-Aldrich) aqueous solution. The suspension was sonicated for 1 h at  $45^\circ\text{C}$  using LBS2 sonicator bath (FALC Instruments) with an operation frequency of 40 kHz and then diluted with Phosphate Buffer Solution (PBS). The obtained suspensions were labelled adding the suffix "S" to the powder label (e.g., SrXS).

### 3.2.2 Characterization techniques and procedures

*Inductively coupled plasma optical emission spectrometry (ICP-OES):* The synthesized powders purity and composition were determined by ICP-OES (Spectro Ciros Vision CCD, 125-770 nm) using hydroxyapatite ultrapure standard (Reagent Grade, Sigma-Aldrich) and a 1000 ppm Sr standard (BHD SpectroSol). All samples and standards were dissolved in ultrapure nitric acid (70%v) and diluted in pure water from reverse osmosis (conductivity < 0.1  $\mu\text{S}/\text{cm}$ ), adding Cs (100

g/L) as ionization suppressor. The emission lines chosen for the analysis were 393.366 nm for Ca, 216.596 nm for Sr and 178.287 nm for P.

*Fourier transform infrared spectroscopy (FTIR):* FTIR spectra were acquired in transmission mode using an Avatar Thermo FTIR spectrometer on KBr pellets in the range of 4000-400  $\text{cm}^{-1}$  (resolution = 4  $\text{cm}^{-1}$ , 64 scans). With the aim to investigate the interaction between nanopowders and bovine serum albumin (BSA), ATR-FTIR spectra were recorded on the suspensions previously lyophilized. Physical mixtures were also prepared merely blending 5 mg of each synthesized nanopowder with 200 mg of BSA to be compared with the data collected on the suspensions. ATR-FTIR spectra were recorded in the 4000–650  $\text{cm}^{-1}$  range (resolution = 4  $\text{cm}^{-1}$ , 256 scans) using a Nicolet FT-IR iS10 Spectrometer (Nicolet, Madison, WI, USA) equipped with a ZnSe plate ATR (Attenuated Total Reflectance) sampling accessory.

*Nitrogen sorption:*  $\text{N}_2$  physisorption analyses were carried out on a Micromeritics ASAP 2010 analyser. Specific surface area (SSA) and volume pore distributions were calculated from  $\text{N}_2$  adsorption/desorption isotherms applying BET equation and BJH model, respectively.

*X-ray diffraction:* The mineralogical composition of the synthesized Sr-HA powders was analysed by XRD using a Rigaku DMAX III 4057A2 diffractometer, working at 40 kV and 30 mA (Cu  $K_\alpha$ : 1.5418978 Å). All data were collected in the range  $2\theta = 10^\circ$ - $60^\circ$ , with step size of  $0.03^\circ$  and dwell time of 10 s/step. Spectra were analysed by the Rietveld-method-based software MAUD (2.53 version), using PDF cards #09-0432 - Calcium-hydroxyapatite and #33-1348 - Strontium-hydroxyapatite as structural models.

*Solid state nuclear magnetic resonance (NMR):*  $^{31}\text{P}$  and  $^1\text{H}$  solid state NMR analysis were carried out with a Bruker 300WB instrument. Samples were packed in 4 mm  $\text{ZrO}_2$  rotors, which were spun by air flow at 11 kHz under Magic Angel Spinning (MAS) conditions. The  $^{31}\text{P}$  SP-MAS experiments were recorded at the frequency of 121.49 MHz, with a single pulse sequence under the following conditions:  $\pi/2$  pulse of 3.6  $\mu\text{s}$ , recycle delay 300 s, 16 scans, using high-power proton decoupling during signal acquisition. The  $^{31}\text{P}$  cross-polarization spectra ( $^{31}\text{P}$  CP-MAS) were recorded with a contact time of 0.5 ms, 100 scans. In both cases, ammonium dihydrogen phosphate  $\text{NH}_4\text{H}_2\text{PO}_4$  was used as secondary reference. The  $^1\text{H}$  MAS experiments were run at frequency of 300.13 MHz,  $\pi/2$  pulse of 5  $\mu\text{s}$ , recycle delay 5 s, 16 scans. Pure ethanol was used as secondary reference.

*Transmission electron microscopy:* In order to investigate the powder size and morphology, 5 mg of powder were dissolved in acetone and sonicated for 10 min; 10  $\mu\text{L}$  of the suspension were deposited on a formvar coated copper grid (Electron Microscopy Sciences), allowing solvent evaporation

overnight. Images of each sample were acquired by Zeiss EM 10 transmission electron microscope operating at 80 kV.

*Dynamic light scattering (DLS):* Hydrodynamic diameter and  $\zeta$  potential of nanoparticle suspensions kept at 37°C for 1, 3, 7, 14 and 30 days were measured using DLS technique with Zetasizer Nano-ZS90 (Malvern Instruments).

### 3.2.3 Biocompatibility studies

*Cell culture condition:* The human osteosarcoma cell line SAOS-2 was acquired from the American Type Culture Collection (HTB85, ATCC, Manassas, VA, USA). The cells were cultured in McCoy's 5A modified medium (Lonza) with L-glutamine (Lonza) supplemented with 15% fetal bovine serum (EuroClone), 1% sodium pyruvate (Lonza), 1% antibiotics (Lonza) and 0.2% amphotericin B (Lonza). Cells were cultured at 37°C with 5% CO<sub>2</sub>, routinely trypsinized after confluency, counted and seeded. The cells were treated with three concentrations (6.25 µg/mL, 62.5 µg/mL and 625 µg/mL) of each suspension in the culture medium. The cells were treated for 1, 3 and 7 days changing medium two times per week. Untreated cells were used as negative control.

*Cell apoptosis:* To determine the induction of cell apoptosis by the nanoparticle suspensions, SAOS-2 cells were labelled using the PSVue480™ cell stain according to the manufacturer's instructions (Molecular Targeting Technologies, Inc.). PSVue480™ dye detects apoptosis by targeting the loss of phospholipid asymmetry in the plasma membrane that is an early event in apoptosis, independent of cell type, resulting in the exposure of phosphatidylserine (PS) residues at the outer plasma membrane leaflet<sup>30</sup>. SAOS-2 cells were seeded on glass coverslips (Thermo Scientific) with a density of 5x10<sup>4</sup> cells/cm<sup>2</sup> and incubated with H<sub>2</sub>O<sub>2</sub> (positive controls; 100 mM for 18 h), without suspensions (negative controls) and with 6.25 µg/mL, 62.5 µg/mL and 625 µg/mL of each suspension for 1 and 7 days. At the end of each culture condition, the cells were stained with PSVue480™ solution prepared according to manufacturer's instructions. Samples were then counterstained with a Hoechst 33342 solution (2 µg/mL) to target the cellular nuclei and observed under a fluorescence optical microscope (Nikon Eclipse 80i).

*MTT test:* Mitochondrial activity was evaluated using 3-(4,5-dimethylthiazole-2-yl)-2,5-diphenyl tetrazolium bromide (MTT) test (Sigma-Aldrich). The viability assay was carried out at day 1, 3 and 7 (end of the culture period) as previously reported<sup>31</sup>. Aliquots of 100 µL were sampled and their absorbance was measured at reference wavelengths of 595 nm and 650 nm by a microplate reader (BioRad Laboratories, Hercules, CA, USA).

*Resazurin-based assay:* The resazurin-based assay was used to estimate the number of viable cells by measuring the reduction of resazurin into resorufin. Resazurin solution (Sigma-Aldrich) was added as one-tenth of culture volume to each well of the plate, which was then incubated for 3 h at

37°C and 5% CO<sub>2</sub>. Optical measurements were run on aliquots of 100 µL by a microplate reader (BioRad Laboratories, Hercules, CA, USA) at reference wavelengths of 600 nm and 690 nm at day 1, 3 and 7 (end of the culture period) on treated and untreated cells. A cell viability standard curve was used to express the results as number of alive cells.

*Scanning electron microscopy (SEM)*: Treated and untreated cells morphology was investigated by SEM after 1 and 7 days treatment; samples were fixed with 2.5% v glutaraldehyde solution in 0.1 M Na-cacodylate buffer (pH=7.2) for 1 h at 4°C, washed with Na-cacodylate buffer and then dehydrated at room temperature in a gradient ethanol series up to 100%. To obtain a complete dehydration, samples were lyophilized for 3 h. Samples were then sputtered with gold and observed using a Zeiss EVO-MA10 (Carl Zeiss, Oberkochen, Germany) SEM.

#### **3.2.4 Effect on cell viability and apoptosis of Sr Ranelate, Sr Chloride (SrCl<sub>2</sub>) and Sr100S**

To compare cell apoptosis induced by Sr ranelate, SrCl<sub>2</sub> and Sr100S, SAOS-2 cells untreated or treated with Sr100S, Sr ranelate (Selleckchem) and SrCl<sub>2</sub> (Sigma) for 24h were labelled for apoptosis using the PSVue480™ cell stain, as already described previously. Moreover, cell viability was evaluated after 1, 3 and 7 days of treatment using MTT test, as already reported above. In particular, several concentrations of the three strontium-containing compounds were tested in order to treat cells with the same concentrations of Sr<sup>+2</sup> ions: 0, 0.156, 0.3125, 0.625, 1.25, 2.5, 5, 10 mM.

#### **3.2.5 Statistical analysis**

In all quantitative tests, cell treatments were performed in triplicate and the results of three independent experiments were considered. In order to compare the viability results between treated and untreated cells at day 1, 3 and 7, the one-way analysis of variance (ANOVA) with post hoc Bonferroni test was applied, with a significance level of 0.05.



### 3.3 Results

#### 3.3.1 Nanopowders and suspensions characterization

The chemical analysis of the synthesized nanopowders shows a slight  $\text{Sr}^{2+}$  deficiency compared with the nominal values, especially for the lowest Sr contents (Tab. 2.1). Conversely, the measured (Ca+Sr)/P ratio is in the range of 1.771 - 1.537 for Sr5 and Sr75, respectively, very close to the stoichiometric Ca/P ratio for pure HA, equal to 1.667.

Sample	Ca100	Sr5	Sr10	Sr25	Sr50	Sr75	Sr100
$\text{Sr}^{2+}$ nominal content, mol%	0	5	10	25	50	75	100
Sr/(Ca+Sr), mol%	0.0	4.2	7.4	21.3	45.2	74.2	100.0
(Ca+Sr)/P, at. ratio	1.743	1.771	1.614	1.670	1.652	1.537	1.570

Tab. 2.1: Strontium content in the synthesized Sr-HA nanopowders and calculated metals-to-phosphorus atomic ratio (measured by ICP-OES).

Despite such limited compositional differences, FT-IR spectra of Sr-HA samples (**Fig. 2.1**) are in good agreement with the characteristic  $\text{PO}_4^{3-}$  and  $\text{OH}^-$  vibrations in the HA lattice reported in the literature<sup>32</sup>. The absence of the doublet at 1466 and 1411  $\text{cm}^{-1}$ , associated to  $\text{CO}_3^{2-}$  groups<sup>33</sup>, proves the efficiency of the reaction conditions used here; conversely, the presence of adsorbed water is shown by the very broad signals around 3440  $\text{cm}^{-1}$  and 1630  $\text{cm}^{-1}$ .

From a qualitative point of view, the phosphate bands are affected by progressive signal shifts to lower wavenumbers with increasing  $\text{Sr}^{2+}$  content. For instance, broad  $\nu_3$  signals observed at 1092 and 1034  $\text{cm}^{-1}$  in Ca100 shift to 1076 and 1028  $\text{cm}^{-1}$  in Sr100, respectively. Analogously, from Ca100 to Sr100,  $\nu_1$  moves from 962 to 947  $\text{cm}^{-1}$  and the two signals attributed to  $\nu_4$  (sharp) shift from 602 and 565  $\text{cm}^{-1}$  to 594  $\text{cm}^{-1}$  and 561  $\text{cm}^{-1}$ , respectively. Finally, the very weak  $\nu_2$  signal is found at 472  $\text{cm}^{-1}$  for Ca100 and at 463  $\text{cm}^{-1}$  in Sr100 nanopowders, respectively. Conversely, the signals related to HA-lattice OH groups are observed at 3572  $\text{cm}^{-1}$  (stretching) and 633  $\text{cm}^{-1}$  (bending) in all samples, although they gradually vanish at higher Sr content.

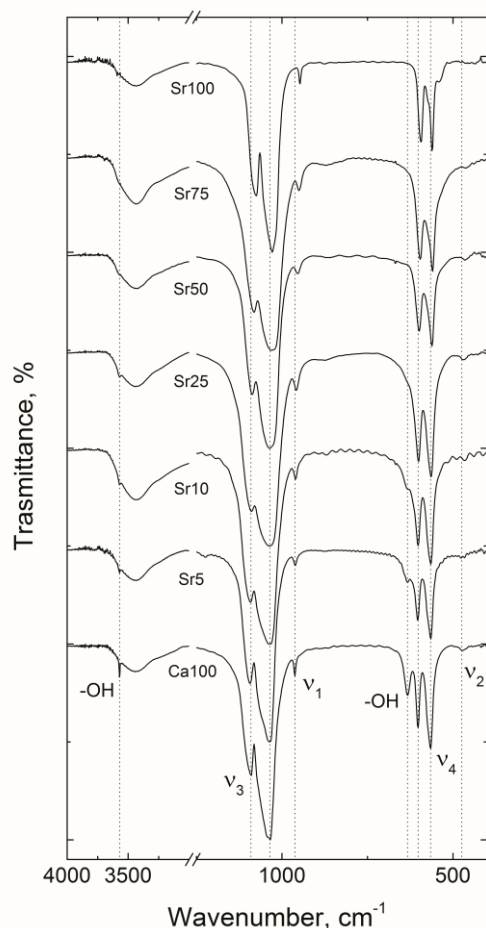


**Fig. 2.1** FT-IR spectra of the synthesized Sr-Hydroxyapatite nanopowder. Vertical dotted lines are referred to the frequencies of interest in the Ca100 spectrum. Published figure.

Further and more accurate information can be obtained by observing the signals in the 500-700  $\text{cm}^{-1}$  range, including the two peaks due to  $\text{PO}_4^{3-}$   $\nu_4$  band and the OH bending vibration ( $\delta$  OH-) at 633  $\text{cm}^{-1}$ . In particular, the most intense peak around 565  $\text{cm}^{-1}$  gradually broadens and then for Sr100 it shrinks revealing two shoulders at 573 and 538  $\text{cm}^{-1}$ , this latter assigned to  $\text{HPO}_4^{2-}$  groups<sup>33</sup>. To quantify these changes, according to the literature<sup>34</sup>, the profile fitting analysis of signals in the 500-700  $\text{cm}^{-1}$  range was performed with six components accounting for hydroxyl groups, surface and internal phosphate groups (Tab. 2.2). Deconvolution and peaks integration were performed on spectra whose intensity was normalized by the corresponding  $\nu_3$  signal at  $\sim 1092 \text{ cm}^{-1}$ .

Sample	surface HPO <sub>x</sub>		internal PO <sub>4</sub> <sup>3-</sup> (1)		internal PO <sub>4</sub> <sup>3-</sup> (2)		internal PO <sub>4</sub> <sup>3-</sup> (3)		surface PO <sub>x</sub>		δ OH <sup>-</sup>	
	Pos., ±2 cm <sup>-1</sup>	Rel. Area, %	Pos., ±2 cm <sup>-1</sup>	Rel. Area, %	Pos., ±2 cm <sup>-1</sup>	Rel. Area, %	Pos., ±2 cm <sup>-1</sup>	Rel. Area, %	Pos., ±2 cm <sup>-1</sup>	Rel. Area, %	Pos., ±2 cm <sup>-1</sup>	Rel. Area, %
Ca100	538	0.4	565	34.6	574	18.1	602	16.7	606	3.0	633	27.4
Sr5	537	8.2	564	29.1	574	18.1	603	22.6	616	3.7	634	18.4
Sr10	540	6.4	563	19.8	571	26.0	602	22.6	614	8.3	635	17.0
Sr25	538	4.2	563	34.4	573	11.4	600	30.9	610	5.6	633	13.6
Sr50	538	8.3	561	25.2	571	21.5	598	22.7	604	12.4	633	9.9
Sr75	538	17.0	559	25.5	572	12.1	595	25.5	603	13.8	633	6.0
Sr100	538	9.1	561	35.0	573	9.5	593	26.6	599	14.3	633	5.4

Tab. 2.2 FTIR signals deconvolution in the range 500-700 cm<sup>-1</sup> (PO43- v4 domain and OH bending δ) using components proposed in <sup>34</sup>. For each component, position and integrated area (as percentage of total signal area) have been reported.

Representative TEM nanopowder micrographs are reported in **Fig. 2.2** showing rod shape geometry with different size and aggregation state. The smallest structures (major axis around  $45 \pm 14$  nm) were observed in Ca100 sample and the nanopowders appeared well separated. In Sr-containing samples enhanced aggregation is observed with an increase in particle size if compared to Ca100 sample. In particular, Sr-containing powders show a more elongated morphology and the length of major axis increases with Sr amount up to  $124 \pm 42$  nm for Sr100 (Tab. 2.6).

The N<sub>2</sub> adsorption-desorption isotherms collected on all samples (**Fig. 2.3**) are characterized by a IIb-type curve with an H3 hysteresis loop and no plateau at high pressures.

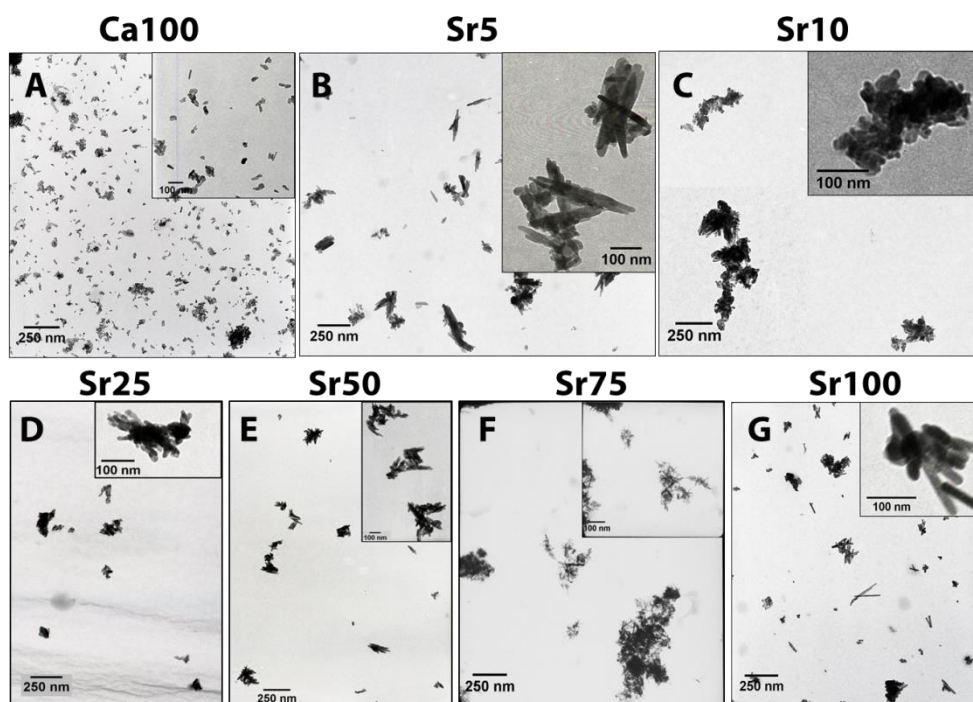
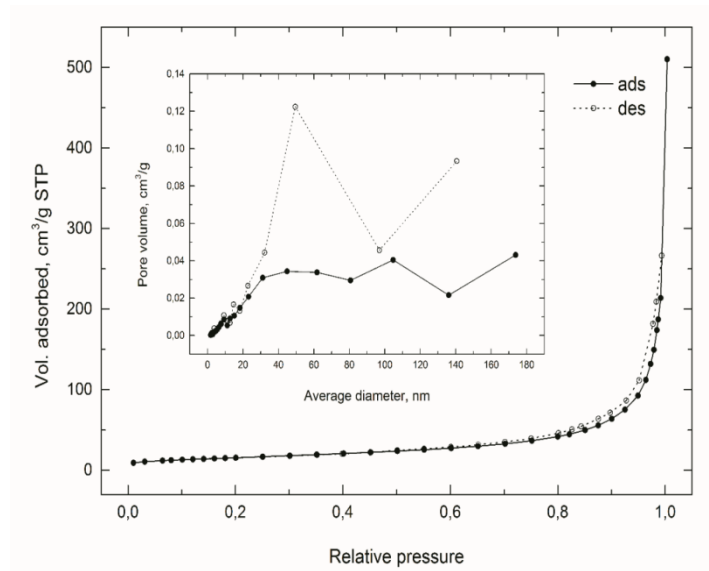
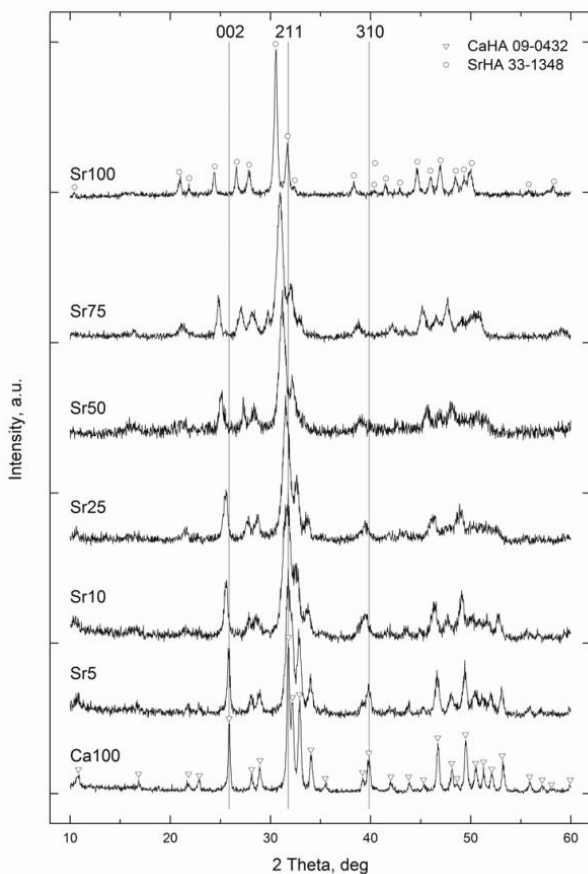


Fig. 2.2 Representative TEM images of HA nanopowders doped with increasing concentrations of Sr. In detail: Ca100 (a), Sr5 (b), Sr10 (c), Sr25 (d), Sr50 (e), Sr75 (f) and Sr100 (g), respectively. The scale bar shown represents 250 nm in all panels and 100 nm in all inserts (Published). Published figure.



**Fig. 2.3 Representative N<sub>2</sub> adsorption (full circle, straight line) and desorption (empty circle, dashed line) isotherms (Sr50 composition). In the top box, corresponding pore size distribution. Published figure.**



**Fig. 2.4 XRD patterns of the synthesized Sr-Hydroxyapatite nanopowders. Vertical dotted lines highlight Ca100 main reflection (211), and planes (002) and (310), respectively normal and parallel to the c axis. Published figure.**

These features are representative of meso- and macro-porous materials constituted by aggregated non-isomorphic particles. The corresponding pore size distribution confirms the presence of a broad range of pores larger than 180-200 Å. By increasing the Sr amount, specific surface area and total pore volume show a fluctuating trend scattered around 50 m<sup>2</sup>/g and 0.300 cm<sup>3</sup>/g, respectively. It is interesting to observe that the measured SSA well scales with the average particles dimension (D) determined by TEM analysis through the well know relationship

$$D = \psi / (\rho_{th} SSA) \quad (2)$$

where  $\rho_{th}$  is the theoretical density (equal to 3.08 g/cm<sup>3</sup> for CaHA, 3.84 g/cm<sup>3</sup> for SrHA) and  $\psi$  is a shape factor equal to ~ 6; assuming SSA = 50 m<sup>2</sup>/g, one can obtain D = 31 nm for CaHA and

39 nm for SrHA. Such values well compare with particles size shown in Tab. 2.3 considering the wide scatter observed especially for larger Sr content. This also confirms that the synthesized nanoparticles are dense and that the considered porosity is substantially related to voids among particles.

XRD patterns collected on synthesized nanopowders are shown in **Fig 2.4**. The two endpoints of the composition series (i.e., Ca100 and Sr100) display quite sharp peaks that are perfectly matched by pure calcium-hydroxyapatite (JCPDS no: 09-0432) and pure strontium-hydroxyapatite (JCPDS no: 33-1348) phases. Conversely, the remaining compositions show reflections at intermediate positions, according to the increasing amount of  $\text{Ca}^{2+}$  substituted by  $\text{Sr}^{2+}$ . At the same time, the peak width increases and the signal-to-noise ratio decreases along the series, as expected for a nanocrystalline material. The average crystallite sizes calculated using the Warren-Averbach method confirm this observation; values are included in the 20-30 nm interval for the intermediate samples, reaching 52 nm (Ca100) and 41 nm (Sr100) for the two limit structures (Tab. 2.3). Moreover, true density ( $\rho$ ) of the powders have been calculated from the refined cell parameters ( $a$  and  $c$ ), following the above equation:

$$\rho = \frac{MW \cdot Z}{V_{\text{cell}} \cdot N_A} = \frac{MW \cdot Z}{a^2 c \sin(\pi/3) \cdot N_A} \quad (3)$$

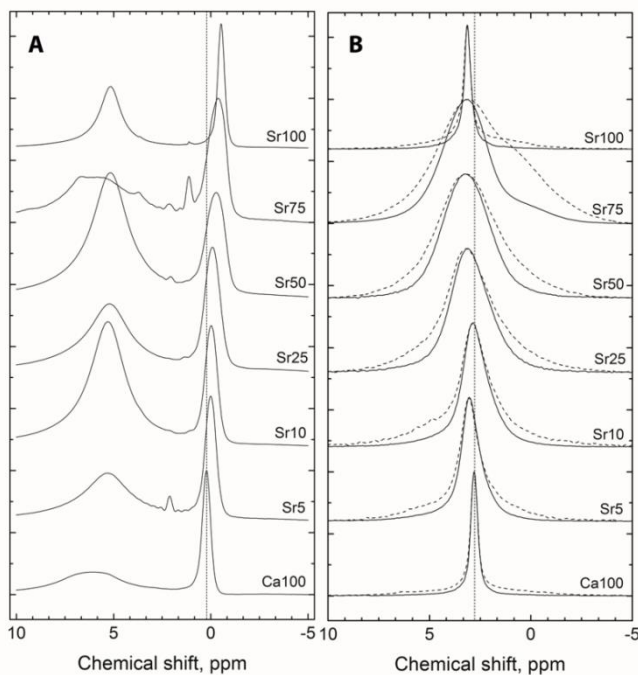


**Fig. 2.5** Solid state NMR spectra of the synthesized Sr-Hydroxyapatite nanopowder. In detail: a)  $^1\text{H}$  MAS; b)  $^{31}\text{P}$  SP-MAS (straight line) and  $^{31}\text{P}$  CP-MAS (dashed line). Vertical dotted lines show the Ca100 main signals. Published figure.

where MW is the molecular weight, based on the ICP chemical composition of each powders, Z is the number of atoms contained into the unit cell, equal to 2,  $N_A$  is the Avogadro constant, equal to  $6.022 \cdot 10^{23} \text{ mol}^{-1}$ , and  $V_{\text{cell}}$  is the volume of the unit cell taking into account the trigonal structure of the Hydroxyapatite. The resulting data slightly exceed (+ 2-6%) the corresponding values extrapolated from the theoretical densities based on stoichiometric HA (i.e. (Sr+Ca)/P at. Ratio = 1.67).

Sample	(002)	(310)	Cell parameters and crystallite size (XS)				True density
	Position, $\pm 0.03$ deg	Position, $\pm 0.03$ deg	a, $\text{\AA}$	c, $\text{\AA}$	c/a, $\pm 0.001$	XS, $\pm 1$ nm	$\rho$ , $\pm 0.01$ g/cm <sup>3</sup>
Ca100	25.87	39.85	$9.423 \pm 0.001$	$6.881 \pm 0.001$	0.730	52	3.23
Sr5	25.81	39.80	$9.435 \pm 0.003$	$6.899 \pm 0.002$	0.731	31	3.30
Sr10	25.63	39.64	$9.461 \pm 0.004$	$6.921 \pm 0.003$	0.732	19	3.20
Sr25	25.57	39.45	$9.507 \pm 0.005$	$6.974 \pm 0.004$	0.734	30	3.38
Sr50	25.18	39.17	$9.609 \pm 0.008$	$7.087 \pm 0.007$	0.738	25	3.57
Sr75	24.82	38.76	$9.668 \pm 0.005$	$7.166 \pm 0.004$	0.741	19	3.72
Sr100	24.40	38.32	$9.776 \pm 0.002$	$7.289 \pm 0.002$	0.746	41	3.93

**Tab. 2.3: XRD (002) and (310) peaks position for the synthesized nanopowders; unit cell parameters, crystallite sizes and true density obtained by XRD pattern refinement are also shown.**

<sup>1</sup>H MAS NMR signals (**Fig 2.5a**) are quite resolved, with a sharp peak at 0.22 ppm (Ca100) assigned to OH groups in HA crystal lattice<sup>35</sup>, which presents a high-field shift and an increase in asymmetry with increasing Sr<sup>2+</sup> content. Furthermore, the proton spectra show the broad water resonance around 5-7 ppm and up to three additional small sharp peaks, randomly observable at 1-3 ppm, probably due to surface adsorbed water<sup>36</sup>. The lineshape analyses of OH peaks was performed in the range -2.0-1.5 ppm by introducing a central main component and two minor side components and the results are reported in Tab. 2.4.

Sample	S <sub>1</sub>			crystalline OH			S <sub>2</sub>		
	$\delta$ , $\pm 0.05$ ppm	FWHM, $\pm 15$ Hz	Rel. Area, %	$\delta$ , $\pm 0.05$ ppm	FWHM, $\pm 15$ Hz	Rel. Area, %	$\delta$ , $\pm 0.05$ ppm	FWHM, $\pm 15$ Hz	Rel. Area, %
Ca100	-0.29	70	1.3	0.22	144	81.7	0.73	187	17.1
Sr5	-0.28	243	13.3	0.01	187	70.7	0.64	227	16.0
Sr10	-0.35	188	4.8	-0.02	218	80.8	0.76	216	14.4
Sr25	-0.44	265	8.3	-0.07	268	77.8	0.95	278	13.9
Sr50	-0.60	152	10.1	-0.21	322	77.0	0.91	250	12.9
Sr75	-0.63	167	16.6	-0.22	302	78.0	0.71	130	5.5
Sr100	-0.83	115	5.5	-0.53	117	76.9	-0.10	193	17.6

**Tab 2.4: Profile fitting analysis of OH signal (range -2.0–1.5 ppm) in 1H MAS NMR spectra, using a central main component (lattice OH) and two minor side components (S1 and S2)**

<sup>31</sup>P SP-MAS NMR experiments show a behaviour consistent with previous evidences achieved by FT-IR and XRD analysis: the spectra (**Fig. 2.5b**, solid line), contain a resolved peak at 2.80 ppm (Ca100), which progressively broadens and shifts to lower fields for increasing Sr<sup>2+</sup> amount, before narrowing again for Sr100 sample. This tendency is emphasized in the <sup>31</sup>P CP-MAS NMR spectra (**Fig. 2.5b**, dashed line), where the additional polarization from protons allows to identify a main sharp signal, associable with internal PO<sub>4</sub><sup>3-</sup> groups, and two broad overlapped resonances leading to shoulders at 3.13 and 2.51 ppm (Ca100) related with -PO<sub>x</sub> and -HPO<sub>x</sub> surface groups<sup>37</sup>. Consequently, <sup>31</sup>P SP spectra deconvolution was performed employing these components (Tab.

2.5). The results point out the low-field shift and broadening of the internal  $\text{PO}_4^{3-}$  component up to 50% of strontium load. Further increase of  $\text{Sr}^{2+}$  content leads to linewidth reduction and moves back the signal towards high fields. Unfortunately, no clear trends can be observed for the minor components.

Sample	surface $\text{PO}_x$			internal $\text{PO}_4^{3-}$			surface $\text{HPO}_x$		
	$\delta$ , $\pm 0.05$ ppm	FWHM, $\pm 6$ Hz	Rel. Area, %	$\delta$ , $\pm 0.05$ ppm	FWHM, $\pm 6$ Hz	Rel. Area, %	$\delta$ , $\pm 0.05$ ppm	FWHM, $\pm 6$ Hz	Rel. Area, %
Ca100	3.13	93	25.8	2.80	43	53.0	2.51	74	21.2
Sr5	4.48	300	9.4	3.03	116	77.7	2.27	146	12.9
Sr10	4.71	222	1.9	2.89	148	79.9	2.10	193	18.2
Sr25	5.13	291	7.5	3.22	214	57.4	2.05	290	35.1
Sr50	5.82	331	4.3	3.21	316	90.5	0.39	296	5.2
Sr75	4.83	338	21.2	3.17	270	62.6	0.72	417	16.2
Sr100	3.46	111	24.5	3.14	39	52.7	2.91	82	22.8

**Tab. 2.5: Profile fitting analysis of 31P SP-MAS NMR spectra in the range -5.0–10.0 ppm using a central main component (internal  $\text{PO}_4$ ) and two minor side components (surface  $\text{PO}_x$  and  $\text{HPO}_x$ ).**

The hydrodynamic diameter (Tab. 2.6) determined on nanoparticle suspensions by DLS at different times is always about twice the size determined by TEM, clearly increasing from Ca100S to Sr100S. No evident trend was recorded for  $\zeta$  potential as a function of Sr content, the values being always quite scattered and ranging between -5.3 mV and -8.4 mV. The same values of hydrodynamic diameter and  $\zeta$  potential were obtained at each measurement performed up to 30 days from preparations suggesting no apparent changes.

	DLS	TEM
Sample	Hydrodynamic diameter, nm	Rod-shape length, Nm
Ca100S	$98 \pm 30$	$45 \pm 14$
Sr5S	$126 \pm 26$	$72 \pm 15$
Sr10S	$157 \pm 31$	$83 \pm 24$
Sr25S	$207 \pm 64$	$98 \pm 17$
Sr50S	$228 \pm 77$	$113 \pm 32$
Sr75S	$224 \pm 54$	$121 \pm 22$
Sr100S	$228 \pm 91$	$124 \pm 42$

**Tab. 2.6: Hydrodynamic diameter measured by DLS technique on nanopowder suspensions and particle length from TEM observations. Published figure.**

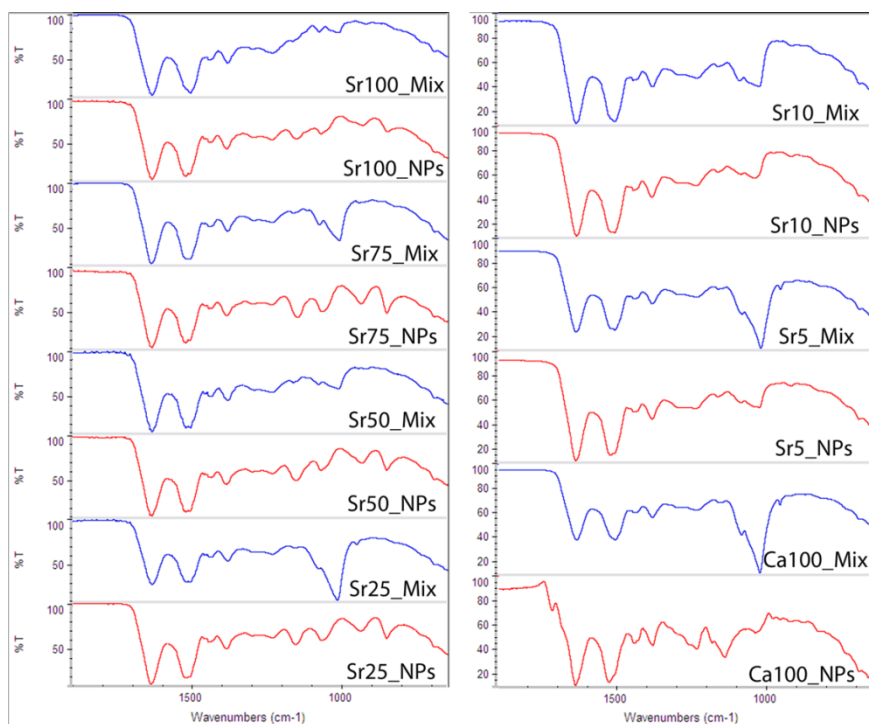


**Fig. 2.6 FT-IR spectra analysis of the interaction between the different types of HA and BSA. The study was performed with FT-IR spectra analysis on physical mixtures (Mix) and on NPs suspensions (NPs) of Ca100 , Sr5, Sr10, Sr25, Sr50, Sr75 and Sr100, respectively. Published figure.**

The FTIR spectra recorded on the suspensions were significantly different from those corresponding to the mere physical mixtures (**Fig. 2.6**). The main differences concern the phosphate group peaks, the  $\nu_3$  signals intensity decreasing with Sr load; a new peak is also evident at about  $1074\text{ cm}^{-1}$  in the suspensions spectra. In addition, two new peaks at  $941$  and  $858\text{ cm}^{-1}$  appear in Sr25S, Sr50S, Sr75S and Sr100S spectra.



### 3.3.2 Cell viability, apoptosis and morphology

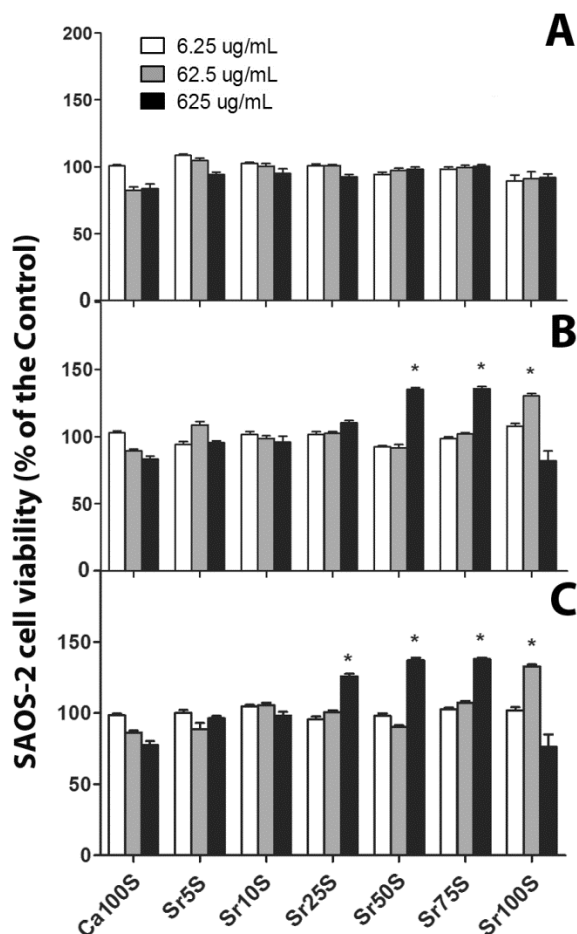


**Fig. 2.7** Dose- and time-dependent effect of the different types of nanoparticles suspensions on SAOS-2 cell viability. SAOS-2 cells were treated with three increasing concentrations of each type of nanoparticles dispersed in 0.5% BSA at three different times: 1 (panel a), 3 (panel b) and 7 (panel c) days, respectively. Results of MTT test are expressed as percentage related to untreated cells set as 100%. Level of significance: \*  $p < 0.05$ . Published figure.

Cell viability determined by the MTT test is shown in **Fig. 2.7** for SAOS-2 cells incubated with increasing suspension concentrations at 1, 3 and 7 days. The data are shown considering 100% viability when no nanoparticles are present. The viability is generally positively influenced by the presence of larger suspension load at longer incubation times. After 24 h, no significant differences ( $p > 0.05$ ) are observed between untreated or treated cells regardless the type of the suspension (**Fig. 2.7a**). After 3 days of culture, viability is 30% higher in samples treated with Sr50S (625  $\mu\text{g/mL}$ ), Sr75S (625  $\mu\text{g/mL}$ ) and Sr100S (62.5  $\mu\text{g/mL}$ ) (**Fig. 2.7b**). After 1 week, an increment from 25% up to 37% is observed in sample treated with Sr25S (625  $\mu\text{g/mL}$ ), Sr50S (625  $\mu\text{g/mL}$ ), Sr75S (625  $\mu\text{g/mL}$ ) and Sr100S (62.5  $\mu\text{g/mL}$ ) (**Fig. 2.7c**). These above-mentioned increments are statistically significant ( $p < 0.05$ ).

Cell proliferation increases in samples treated with larger Sr amount (Sr25S,

Sr50S, Sr75S and Sr100S). Similar results were obtained by using the Resazurin-based test.

In order to evaluate cell apoptosis caused by nanoparticle suspensions treatment, PSVue® 480 and Hoechst staining were performed at 24 h (**Fig. 2.8**). After 24h, as expected, SAOS-2 cells exhibit a clear green fluorescence after hydrogen peroxide treatment, showing high level of apoptosis. Green fluorescence in  $\text{H}_2\text{O}_2$  treated sample is very intense to cover the blue fluorescence of Hoechst. Conversely, fluorescent analysis of untreated and treated cells are negative after staining with PSVue480™ reagent, indicating that all treatments do not induce cell apoptosis. Similar data were obtained after 7 days treatment.

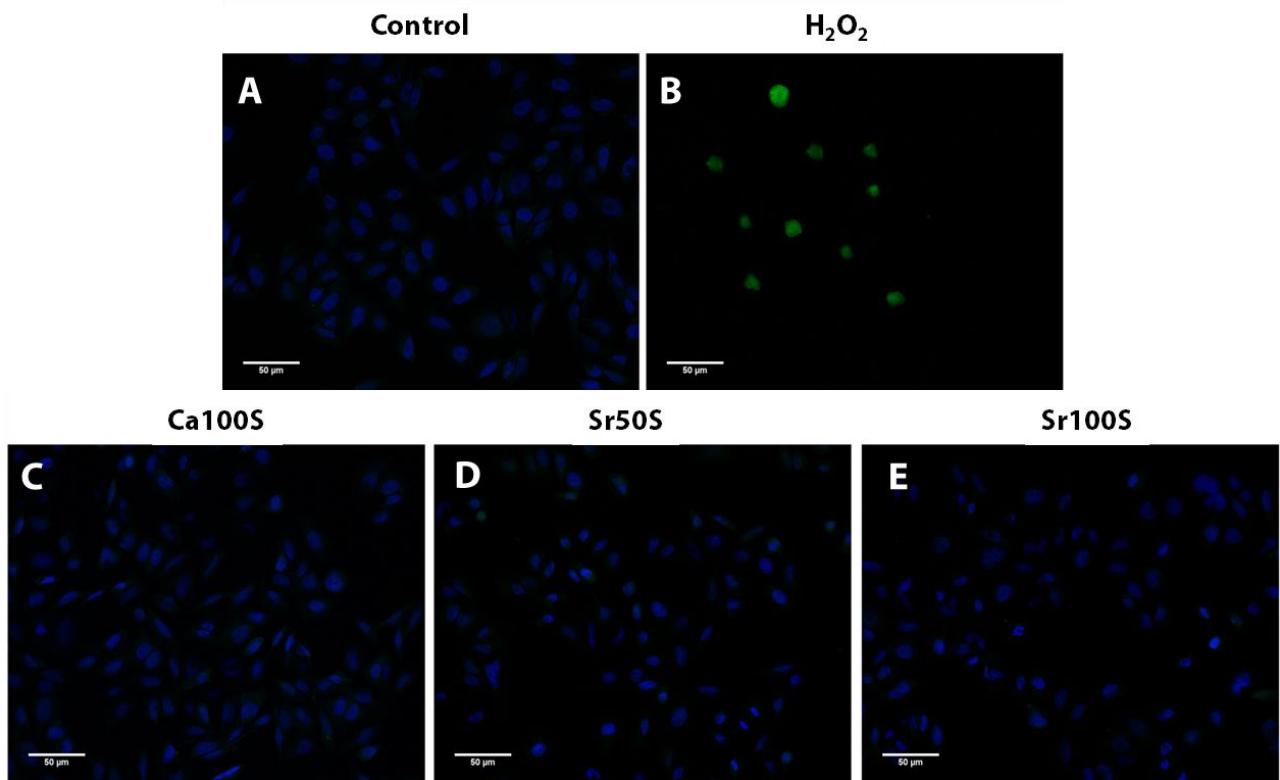


**Fig. 2.8** Fluorescent images of the apoptosis assay. SAOS-2 cells were cultured for 24 h under different conditions as indicated: untreated (Control, A) and treated cells with hydrogen peroxide (B), 1250 μg/mL of Ca100\_NPs (C), Sr50\_NPs (D) and Sr100\_NPs (E), respectively. PSVue480™ (green) reagent was used to evaluate apoptotic cells. Nuclei were counterstained with Hoechst 33342 (blue). The scale bar shown represents 50 mm in all panels. Published figure.

SEM images were recorded on control cells and cells treated with 625 μg/mL. **Figure 2.9** shows representative images of cells untreated and treated with Ca100S, Sr50S and Sr100S at 1 and 7 days of culture. As expected, in all samples, the typical SAOS-2 cells morphology is shown and no differences were observed between treated and untreated cells.

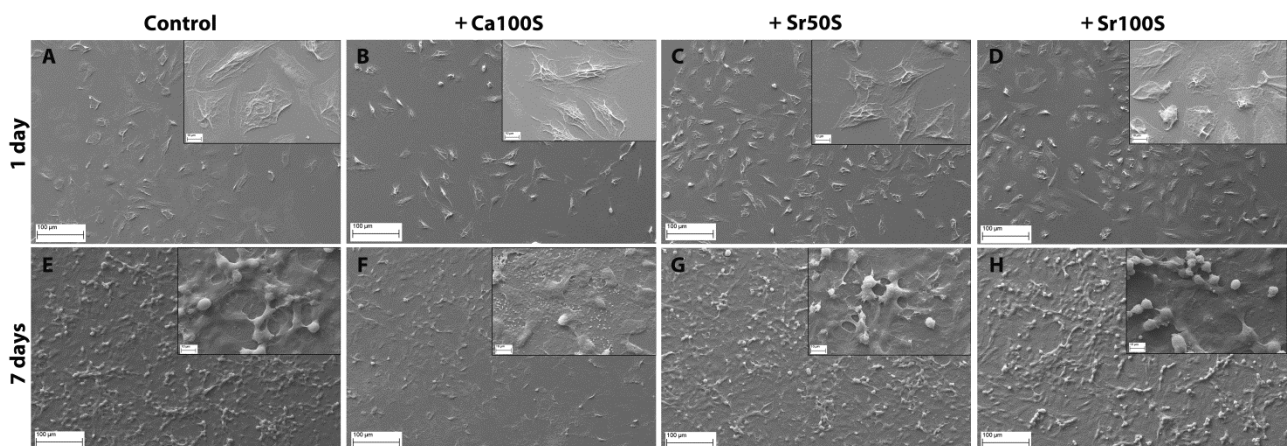


**Fig. 2.9** Representative SEM images of untreated and treated SAOS-2 cells with nanoparticles suspensions. Images were taken after 1 (a, b, c and d) and 7 (e, f, g and h) days of treatment in the following conditions: untreated (a and e) and treated cells with 1250 μg/mL of Ca100S (b and f), Sr50S (c and g) and Sr100S (d and h), respectively. The scale bar shown represents 100 mm in all panels and 10 mm in all inserts. Published figure.

In order to compare the effect on cell viability and apoptosis of three strontium containing compounds, several concentrations of strontium ranelate, strontium chloride and Sr100S were tested with SAOS-2 cells. In particular, **Fig. 2.10** shows results related to cell apoptosis evaluated after 24h through PSVue staining (**Fig. 2.10a**) and cell proliferation evaluated by MTT test at 1, 3 and 7 days of treatment (**Fig. 2.10b**). Intense green fluorescence was observed in strontium ranelate treated samples, in a dose-dependent manner. For strontium chloride treated samples, a reduced number of apoptotic cells was determined if compared to strontium ranelate. For samples treated with Sr100S, a negligible green fluorescence was observed for all the tested concentrations.

Apoptosis results were corroborated by cell viability evaluated with MTT test performed after 1 day. In fact, percentage of live cells detected in Sr100S and strontium chloride samples were comparable to untreated cells for all the tested concentrations. On the contrary, for strontium ranelate treated samples, a decrease in percentage of cell viability was measured in a dose-dependent manner. After 3 days, a more evident decrease in cell viability induced by Strontium ranelate was observed; a slightly increase was observed in Sr100S samples treated with 0.625 and 1,25 mM of  $\text{Sr}^{+2}$  whereas no differences in cell viability was observed in strontium chloride treated samples. After 7 days, a significant increase in cell proliferation was observed for Sr100S treated samples reaching a peak at 1.25mM of  $\text{Sr}^{+2}$ ; while strontium chloride seems not to affect cell viability, strontium ranelate, instead, reduced cell viability significantly in a dose-dependent manner.

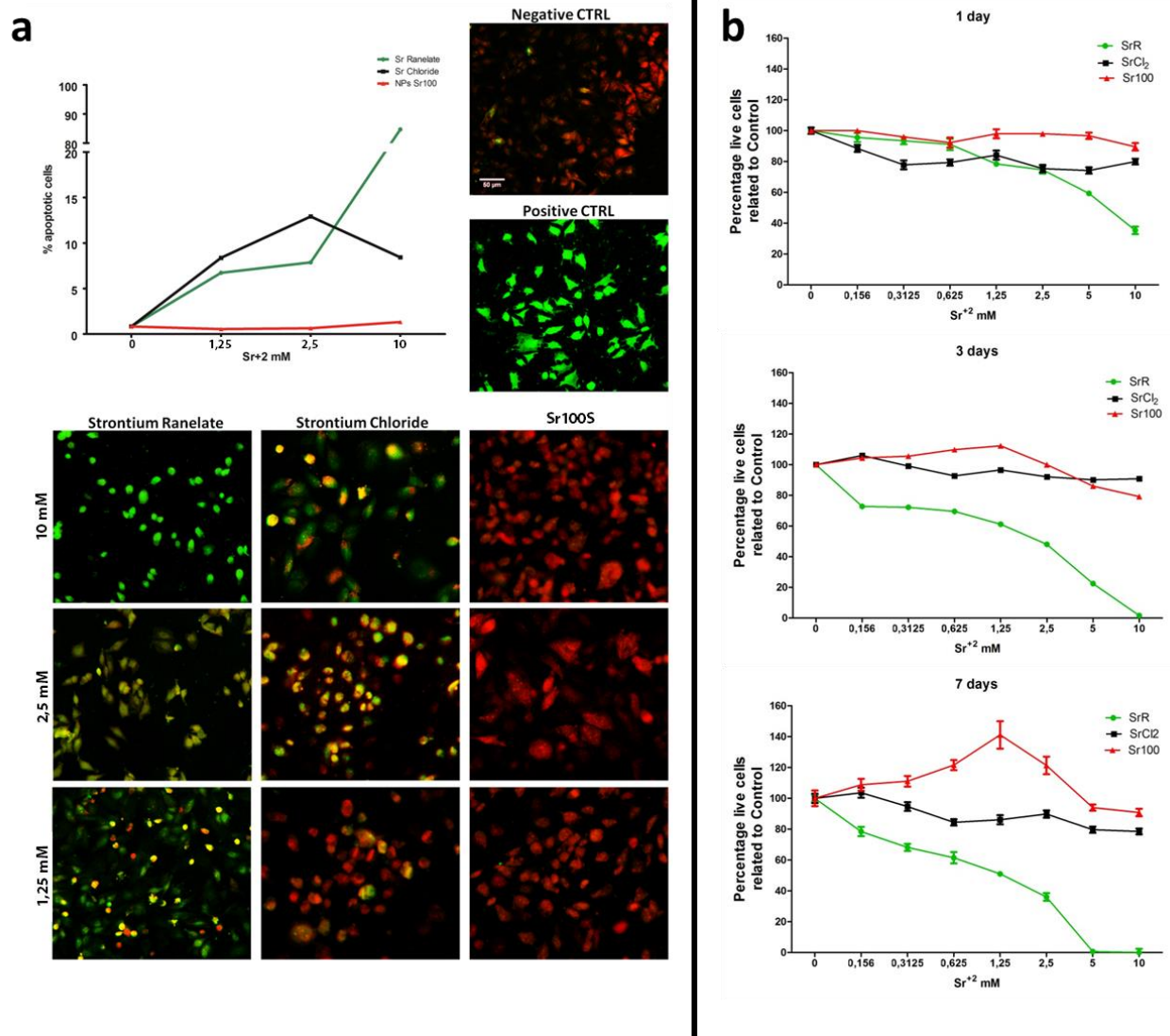


**Fig.2.10** Effect of three different strontium containing compounds on SAOS-2 apoptosis and proliferation. a) Apoptosis evaluation by PSVue 480 staining (green) of SAOS-2 cells untreated (Negative Ctrl) and incubated for 24h with Strontium Ranelate, Strontium Chloride and Sr100 nanoparticles to a Sr<sup>+2</sup> ions final concentration of 10, 2,5 and 1,25 mM and with hydrogen peroxide (Positive control). Nuclei were counterstained with propidium Iodide (red). Diagram indicates mean and SEM of apoptotic cells percentage counted in 5 different field of three different experiments. b) Cell viability evaluated by MTT test at 1, 3 and 7 days of culture in absence and presence of different concentration of Strontium Ranelate, Strontium Chloride and Sr100 nanoparticles. Diagrams indicate mean and SEM of 3 different experiments

### 3.4 Discussion

The structural characterization of the nanopowders carried out by FTIR, XRD and NMR clearly points out valuable differences accounted for by the replacement of calcium with strontium.

$\text{Ca}^{2+} \rightarrow \text{Sr}^{2+}$  substitution leads to a progressive modification of the particle shape along a preferential direction, i.e. parallel to *c*-axis, as observed in the TEM micrographs (**Fig. 2.2**). At the same time, the crystalline cell is coherently subjected to an anisotropic linear growth that involves *c* parameter more than *a* parameter (Tab. 2.3). The effect is further underlined observing the growing trend of *c/a* ratio, where linear regression supplies very good fittings of the experimental data. If such values are plotted as a function of the particle length distribution obtained by TEM (**Fig. 2.11**), a logarithmic-like dependence is found: for limited amount of Sr the crystal elongation highly influences the final particle size, the effect being more limited for larger Sr content.

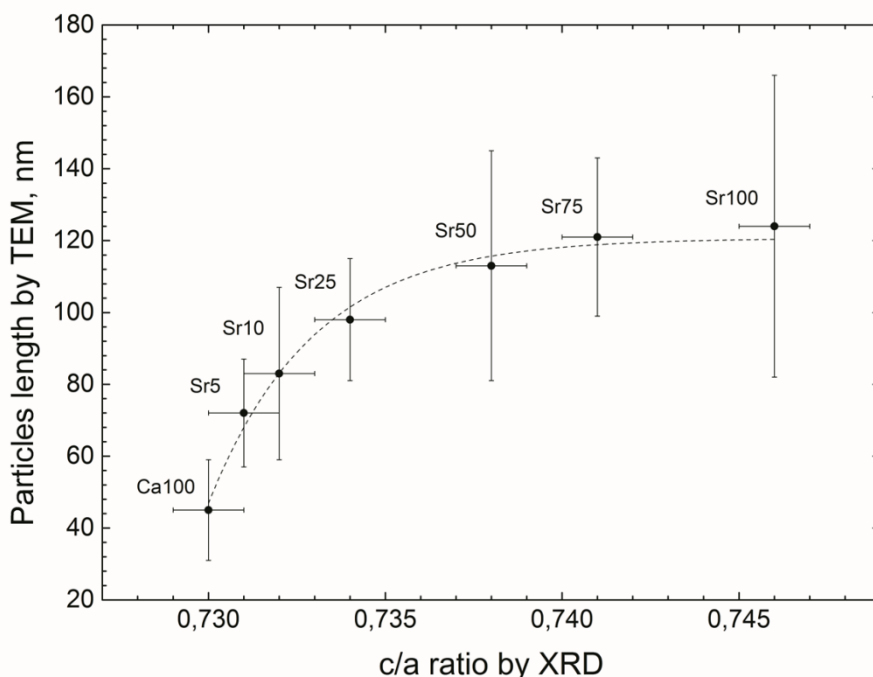


**Fig. 2.11** Correlation between the nanoparticle length (by TEM), and the cell parameters *c/a* ratio (by XRD pattern refinement) increasing the Sr content in the synthesized HA nanopowders.

Strontium causes drastic modifications in the local chemical environment of the apatitic functional groups,  $\text{PO}_4$  and crystalline OH, resulting in clearly observable changes in FT-IR and NMR spectra. The OH bending signal ( $\delta$  OH:  $633 \text{ cm}^{-1}$ ) intensity reduction with Sr load is clearly pointed out by the deconvolution of FT-IR bands in the range  $500\text{-}700 \text{ cm}^{-1}$  (Tab. 2.2). The values of  $\delta$  OH integrated area well relate with the *c/a* ratio (**Fig. 2.12**) showing an exponential decrease with increasing cell deformation. It has to be recalled that hydroxyl groups are located along the *c*-axis,

within interstices shaped by three M(2)-type cations forming planar triangles, perpendicular to the O-H bonds. The contemporary presence of both  $\text{Sr}^{2+}$  and  $\text{Ca}^{2+}$  ions in the M(2) positions generates a strong perturbation in the lattice in terms of ionic radius and electronegativity. Moreover, the anisotropic elongation of the crystalline cells along the *c*-axis entails a decrease in spatial density of O-H bonds, i.e. more limited bonds per unit volume. These conditions probably affect the hydroxyl vibrational mode, causing the reduction of the corresponding FT-IR absorption signal. The modified structural environment affects also the crystalline OH signals in  $^1\text{H}$  MAS NMR spectra, leading to a shift towards higher fields with increasing Sr amount (Tab. 2.4).

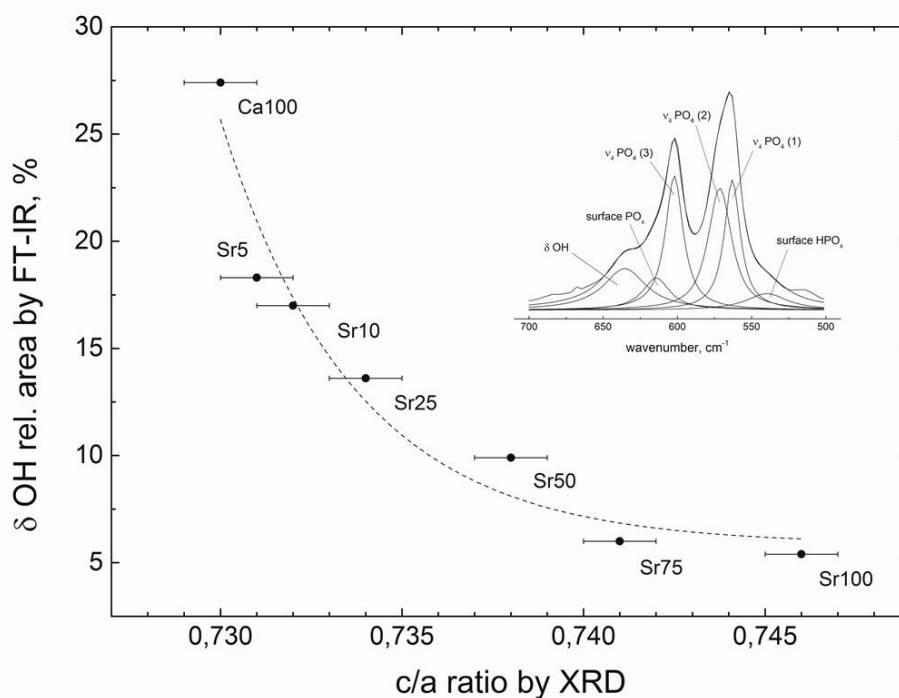
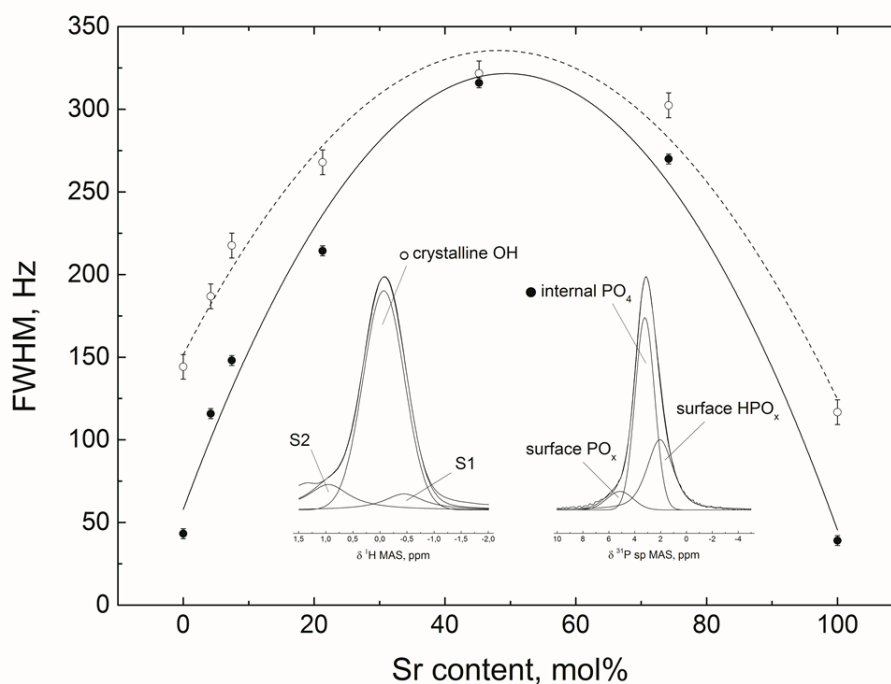


Fig. 2.12 Correlation between relative area of OH bending signal ( $\delta$  OH-, obtained by deconvolution of  $\nu_4$  FT-IR band), and cell parameters *c/a* ratio (obtained by XRD pattern refinement) increasing the Sr content in the synthesized HA nanopowders. In the top right corner, representative example of  $\nu_4$  FT-IR deconvolution with six components (Sr10 composition).

The deconvoluted FT-IR  $\nu_4$ - $\text{PO}_4$  components (1) and (3) (internal  $\text{PO}_4$ :  $565$  and  $602$   $\text{cm}^{-1}$ ) shift to lower wavenumbers following a linear trend with Sr content. Such vibrational frequency decrease has been already accounted for in previous works<sup>38</sup> by considering the energy loss of some P-O bonds, upon the increase of the reciprocal distance between the  $\text{PO}_4$  groups, as a consequence of the lattice expansion. For the same reason, the  $^{31}\text{P}$  SP-MAS signals of internal  $\text{PO}_4$  (Tab. 2.5) present a low-field shift.

One last comment regarding the Sr influence can be drawn by observing the line broadening (as FWHM) of the deconvoluted main components of  $^{31}\text{P}$  SP-MAS (internal  $\text{PO}_4$ ) and  $^1\text{H}$  MAS (crystalline OH) signals, reported as a function of Sr amount in **Fig. 2.13**. Since NMR is extremely sensitive to the different chemical environments surrounding a specific element, it is quite clear that the lower presence of substitutional ion ( $\text{Sr}^{2+}$  or  $\text{Ca}^{2+}$ ) is perceived by the remaining HA lattice ( $\text{Ca}^{2+}$  or  $\text{Sr}^{2+}$ ) as a point defect. The maximum disorder (i.e., the maximum line broadening) is reached for the Sr50 composition, where Sr and Ca atoms are in equal number and they both constitute defects. This short-range variability seems to prevent also crystallization, leading to broader and noisier XRD spectra and smaller crystallite size than in Ca100 and Sr100 limit structures.



**Fig. 2.13** Line broadening (FWHM) of the deconvoluted main components of  $^1\text{H}$  MAS spectra (crystalline OH, empty circles and dotted line) and of  $^{31}\text{P}$  SP-MAS spectra (internal  $\text{PO}_4$ , full circles and straight line) as a function of Sr content in the synthesized HA nanopowders. On the bottom, representative example of  $^1\text{H}$  SP-MAS (left) and  $^{31}\text{P}$  SP-MAS (right) signal deconvolution with three components (Sr25 composition).

However, XRD and NMR results do not provide any evidence of the formation of distinct mono-cation phases. Both XRD and NMR spectra show a gradual evolution between the two limit compositions, Ca100 and Sr100, thus proving the homogeneity of the synthesized nanopowders and the complete solubility of strontium in HA lattice.

The nanopowder surface features, such as SSA and total pore volume, and the components related to surface  $\text{HPO}_x$  and  $\text{PO}_x$  groups in FT-IR and NMR spectra, seem to depend to a lower extent on

Sr content, showing scattered values and apparently no regular trends. Wang et al.<sup>39</sup> recently stated that natural and synthetic apatites are coated by an amorphous hydrated layer. The surface phosphate groups randomly interact with the adsorbed water molecules, whose amount depends on the storing conditions. Such aleatory contribution, which can be removed only by drying, precludes a more detailed analysis of the Sr effect on the nanopowder surface properties.

In order to perform *in vitro* biocompatibility studies, nanoparticles were dispersed with BSA fluid. Albumin is one of the most representative proteins in human blood and one of its functions is to bind hydrophobic molecules and carry them through the body tissues. To promote the bond between nanopowders and the protein, a physical treatment consisting of heating and sonication was performed here. The thermal treatment promotes a partial denaturation of the protein that, losing its natural folding, exposes more functional groups to bind hydroxyapatite crystals<sup>40</sup>; conversely, sonication destroys nanopowders aggregates thus allowing a more efficient surface bond with the protein molecules.

This interaction was investigated using IR technique revealing modifications of the peaks related to phosphate groups (**Fig. 2.6**) suggesting a potential role in the interaction with BSA. Other differences were observed in IR spectra although further investigations are necessary for a deeper understanding of the interaction.

The  $\text{Ca}^{2+} \rightarrow \text{Sr}^{2+}$  substitution influences the hydrodynamic diameter, which is always twice the particles size determined by TEM analysis. A certain contribution of BSA on the hydrodynamic diameter has to be considered, which, however, does not account for the formation of any aggregate. The evaluation of suspensions stability by measuring  $\zeta$  potential revealed the presence of negative charges on the nanoparticles surface with no valuable differences among the different suspensions.  $\zeta$  potential was also separately measured by DLS for nanopowders and BSA in water and values around zero were obtained. Therefore, the negative values determined for the suspensions suggest BSA rearrangement upon the interaction with nanoparticles surface, which results in exposing negative charges to the solvent and in the suspension stabilization<sup>41</sup>.

Nanoparticle suspensions exhibit high biocompatibility as confirmed by viability results and cell morphology evolution. Nanoparticles composition, dose and culture time influence cells proliferation. In general, the proliferation increases in samples treated with nanoparticles containing larger Sr content and after longer incubation times. These results suggest a specific correlation between Sr concentration in the medium and cell viability: for samples treated with Sr100S, the cell proliferation increase was observed at concentration of 62.5  $\mu\text{g}/\text{mL}$  whereas similar increments were detected in samples treated with Sr25S, Sr50S or Sr75S at concentration 10 time larger (625  $\mu\text{g}/\text{mL}$ ). Moreover, since in Ca100S treated samples the number of live cells was comparable to that



detected in the untreated sample, the positive effect on osteoblasts proliferation is only due to the presence of Sr. Conversely, samples treated for 3 or 7 days with Sr100S at 625  $\mu\text{g}/\text{mL}$  show a non-statistically significant cell viability decrease ( $p>0.05$ ). Since no apoptosis was observed in these samples, the effect is likely to be related to the cell proliferation rate and not to the cell death, or to an excessive Sr treatment that could activate other metabolisms leading to a cell proliferation decrease. Further studies are needed to clarify this point. Scaffolds made by HA containing 7% Sr have been reported to affect osteoblast proliferation with an increasing observed from 3 days of treatment onwards<sup>22,26</sup> but there are no data about the real amount of Sr whereby cells were treated. Instead, in works where Sr ranelate was used, the concentration that has a positive effect on osteoblast proliferation is around  $1\text{mM}$ <sup>16,42,43</sup> and that is comparable with Sr concentration treatments in our study calculated using ICP results. The molecular mechanism is not well known but some evidence showed that strontium seems activate Calcium Sensing Receptor which is involved in cell proliferation<sup>44</sup>.

Starting from the effective dose of Sr100S on cell proliferation, we compared the nanoparticles effect with other two strontium-containing compounds: strontium ranelate and strontium chloride. Strontium ranelate, as already said, is a drug used for osteoporosis treatment whereas strontium chloride was used since some observations pointed out that dietary supplementation with this salt tend to increase osteoid surface and to reduce osteoclast numbers in mice<sup>45</sup>. We tested the three strontium-containing compounds at different concentrations keeping constant the final  $\text{Sr}^{+2}$  concentration in the culture media. We observed a strong induction of apoptosis and cell death in strontium ranelate treated samples that was not observed with strontium chloride or Sr100S treated samples. However, strontium chloride did not affected cell proliferation, whereas an increment in SAOS-2 proliferation was evaluated in Sr100S treated cells, either after 3 or 7 days, confirming the cell viability data (**Fig.2.7**).

These results suggest that through the three tested samples Sr-containing hydroxyapatite nanoparticles showed higher biocompatibility and positive effect on cell proliferation. It can be highlighted that is not only the presence of  $\text{Sr}^{+2}$  ions in the media that promote cell proliferation but especially how this element is administered to cells. Moreover, these data suggest that Sr-containing hydroxyapatite nanoparticles can improve the Sr delivery to bone tissue and enhance its positive effects.

### 3.5 Conclusion and Future Perspective

In the present work, strontium-substituted hydroxyapatite nanopowders were systematically synthesized by aqueous precipitation in the range of 0-100 mol% Sr. One single crystalline phase is always obtained, Ca and Sr occupying the same lattice position in the HA structure. The replacement of  $\text{Ca}^{2+}$  by  $\text{Sr}^{2+}$  ions with different ionic radius and electronegativity leads to the nanopowders modification at different structural levels. Pure Sr-HA and Ca-HA nanopowders are characterized by larger crystallite size (50 – 60 nm) with respect to intermediate compositions (20-30 nm). As for powder morphology, a progressive and strongly anisotropic growth along *c* direction is induced by Sr. Correspondingly, crystalline unit cells are subjected to an expansion which is larger along *c* than along *a*; this causes functional group rearrangements, responsible for weaker P-O bonds and, above all, for evident OH spatial density changes and their local environment.

The synthesized powders can be easily used for the preparation of water suspensions with the addition of Bovine Serum Albumin. Such biological protein interacts positively with the nanopowders surface, stabilizing the suspension and avoiding the formation of any aggregate.

The produced suspensions are biocompatible with no apoptotic effect on osteoblast cells. Suspensions prepared with nanopowders containing larger Sr amount clearly promote osteoblast viability and proliferation. Moreover, we demonstrated that Sr-containing hydroxyapatite nanoparticles have higher biocompatibility and stimulatory effect on osteoblasts proliferation if compared with Strontium ranelate and Strontium Chloride

The obtained results point out that strontium-substituted hydroxyapatite nanoparticles could be potentially used to delivery Sr to bone tissue and promote its regeneration, as component of bone substitute synthetic materials, additive for pharmaceutical preparation or food supplementary for systemic distribution.

### 3.6 References

1. Dorozhkin, S. V. Self-Setting Calcium Orthophosphate Formulations: Cements, Concretes, Pastes and Putties. *Int. J. Mater. Chem.* **1**, 1–48 (2012).
2. Champion, E. Sintering of calcium phosphate bioceramics. *Acta Biomater.* **9**, 5855–5875 (2013).
3. Frasnelli, M. & Sglavo, V. M. Effect of Mg(2+) doping on beta-alpha phase transition in tricalcium phosphate (TCP) bioceramics. *Acta Biomater.* **33**, 283–9 (2016).
4. Narayanan, R., Seshadri, S. K., Kwon, T. Y. & Kim, K. H. Calcium phosphate-based coatings on titanium and its alloys. *J. Biomed. Mater. Res. Part B Appl. Biomater.* **85B**, 279–299 (2008).
5. Zahn, D. & Hochrein, O. On the composition and atomic arrangement of calcium-deficient hydroxyapatite: An ab-initio analysis. *J. Solid State Chem.* **181**, 1712–1716 (2008).
6. Gómez-Morales, J., Iafisco, M., Delgado-López, J. M., Sarda, S. & Drouet, C. Progress on the preparation of nanocrystalline apatites and surface characterization: Overview of fundamental and applied aspects. *Prog. Cryst. Growth Charact. Mater.* **59**, 1–46 (2013).
7. McElderry, J.-D. P. *et al.* Crystallinity and compositional changes in carbonated apatites: Evidence from (31)P solid-state NMR, Raman, and AFM analysis. *J. Solid State Chem.* **206**, 192–198 (2013).
8. Heslop, D. D., Bi, Y., Baig, A. A., Otsuka, M. & Higuchi, W. I. A comparative study of the metastable equilibrium solubility behavior of high-crystallinity and low-crystallinity carbonated apatites using pH and solution strontium as independent variables. *J. Colloid Interface Sci.* **289**, 14–25 (2005).
9. Laurencin, D. *et al.* Magnesium incorporation into hydroxyapatite. *Biomaterials* **32**, 1826–37 (2011).
10. Lijuan, X., Liyun, J., Chengdong, X. & Lixin, J. Effect of different synthesis conditions on the microstructure, crystallinity and solubility of Mg-substituted hydroxyapatite nanopowder. *Adv. Powder Technol.* **25**, 1142–1146 (2014).
11. Cox, S. C., Jamshidi, P., Grover, L. M. & Mallick, K. K. Preparation and characterisation of nanophase Sr, Mg, and Zn substituted hydroxyapatite by aqueous precipitation. *Mater. Sci. Eng. C. Mater. Biol. Appl.* **35**, 106–14 (2014).
12. Abert, J., Bergmann, C. & Fischer, H. Wet chemical synthesis of strontium-substituted hydroxyapatite and its influence on the mechanical and biological properties. *Ceram. Int.* **40**, 9195–9203 (2014).
13. Ratnayake, J. T. B., Mucalo, M. & Dias, G. J. Substituted hydroxyapatites for bone

regeneration: A review of current trends. *J. Biomed. Mater. Res. - Part B Appl. Biomater.* 1–15 (2016). doi:10.1002/jbm.b.33651

14. Kinney, E. & McCollum, E. A study of the rate of deposition and paths of absorption of strontium in the rat. *J. Pharmacol.* **22**, 165–176 (1922).
15. Querido, W., Rossi, A. L. & Farina, M. The effects of strontium on bone mineral: A review on current knowledge and microanalytical approaches. *Micron* **80**, 122–134 (2015).
16. Barbara, A., Delannoy, P., Denis, B. & Marie, P. Normal matrix mineralization induced by strontium ranelate in MC3T3-E1 osteogenic cells. *Metabolism* **53**, 532–537 (2004).
17. Grosso, A., Douglas, I., Hingorani, A., MacAllister, R. & Smeeth, L. Post-marketing assessment of the safety of strontium ranelate; a novel case-only approach to the early detection of adverse drug reactions. *Br. J. Clin. Pharmacol.* **66**, 689–94 (2008).
18. Bonnelye, E., Chabadel, A., Saltel, F. & Jurdic, P. Dual effect of strontium ranelate: stimulation of osteoblast differentiation and inhibition of osteoclast formation and resorption in vitro. *Bone* **42**, 129–38 (2008).
19. Bigi, A., Boanini, E., Capuccini, C. & Gazzano, M. Strontium-substituted hydroxyapatite nanocrystals. *Inorganica Chim. Acta* **360**, 1009–1016 (2007).
20. Li, Z. Y. *et al.* Chemical composition, crystal size and lattice structural changes after incorporation of strontium into biomimetic apatite. *Biomaterials* **28**, 1452–1460 (2007).
21. Li, Y. *et al.* The effect of strontium-substituted hydroxyapatite coating on implant fixation in ovariectomized rats. *Biomaterials* **31**, 9006–9014 (2010).
22. Capuccini, C. *et al.* Strontium-substituted hydroxyapatite coatings synthesized by pulsed-laser deposition: In vitro osteoblast and osteoclast response. *Acta Biomater.* **4**, 1885–1893 (2008).
23. Abdel-Aal, E. A. Inserting of strontium during coating of hydroxyapatite compound on titanium substrate. *Int. J. Nanoparticles* **4**, 77 (2011).
24. Raucci, M. G., Giugliano, D., Alvarez-Perez, M. a. & Ambrosio, L. Effects on growth and osteogenic differentiation of mesenchymal stem cells by the strontium-added sol-gel hydroxyapatite gel materials. *J. Mater. Sci. Mater. Med.* **26**, 90 (2015).
25. Kitayama, S. *et al.* Regeneration of rabbit calvarial defects using biphasic calcium phosphate and a strontium hydroxyapatite-containing collagen membrane. *Clin. Oral Implants Res.* **0**, 1–9 (2015).
26. Capuccini, C. *et al.* Interaction of Sr-doped hydroxyapatite nanocrystals with osteoclast and osteoblast-like cells. *J. Biomed. Mater. Res. A* **89**, 594–600 (2009).
27. Holthoff, H., Egelhaaf, S. U., Borkovec, M., Schurtenberger, P. & Sticher, H. Coagulation Rate Measurements of Colloidal Particles by Simultaneous Static and Dynamic Light Scattering.

*Langmuir* **12**, 5541–5549 (1996).

28. Lauten, R. A., Kjøniksen, A.-L. & Nyström, B. Colloid Polymer Interactions and Aggregation in Aqueous Mixtures of Polystyrene Latex, Sodium Dodecyl Sulfate, and a Hydrophobically Modified Polymer: A Dynamic Light Scattering Study. *Langmuir* **17**, 924–930 (2001).
29. Risi, G. *et al.* In vitro study of multiwall carbon nanotubes (MWCNTs) with adsorbed mitoxantrone (MTO) as a drug delivery system to treat breast cancer. *RSC Adv.* **4**, 18683 (2014).
30. van Engeland, M., Nieland, L. J. W., Ramaekers, F. C. S., Schutte, B. & Reutelingsperger, C. P. M. A review on an apoptosis detection system based on phosphatidylserine exposure. *Cytometry* **31**, 1–9 (1998).
31. Saino, E. *et al.* In Vitro Enhancement of SAOS-2 Cell Calcified Matrix Deposition onto Radio Frequency Magnetron Sputtered Bioglass-Coated Titanium Scaffolds. *Tissue Eng. Part A* **16**, 995–1008 (2010).
32. Koutsopoulos, S. Synthesis and characterization of hydroxyapatite crystals: a review study on the analytical methods. *J. Biomed. Mater. Res.* **62**, 600–12 (2002).
33. Kaflak, A. & Kolodziejcki, W. Complementary information on water and hydroxyl groups in nanocrystalline carbonated hydroxyapatites from TGA, NMR and IR measurements. *J. Mol. Struct.* **990**, 263–270 (2011).
34. Šupová, M. Substituted hydroxyapatites for biomedical applications: A review. *Ceram. Int.* **41**, 9203–9231 (2015).
35. Kolmas, J. & Kolodziejcki, W. Inverse  $31\text{P} \rightarrow 1\text{H}$  NMR cross-polarization in hydrated nanocrystalline calcium hydroxyapatite. *Chem. Phys. Lett.* **554**, 128–132 (2012).
36. Munarin F *et al.* Micro- and nano-hydroxyapatite as active reinforcement for soft biocomposites. *Int J Biol Macromol* **Jun**, 199–209 (2015).
37. Kolmas, J., Ślósarczyk, A., Wojtowicz, A. & Kolodziejcki, W. Estimation of the specific surface area of apatites in human mineralized tissues using  $31\text{P}$  MAS NMR. *Solid State Nucl. Magn. Reson.* **32**, 53–58 (2007).
38. Fowler, B. O. Infrared studies of apatites. II. Preparation of normal and isotopically substituted calcium, strontium, and barium hydroxyapatites and spectra-structure-composition correlations. *Inorg. Chem.* **13**, 207–214 (1974).
39. Wang, Y. *et al.* Water-mediated structuring of bone apatite. *Nat. Mater.* **12**, 1144–1153 (2013).
40. Guillermo Picò. Thermodynamic aspects of thermal stability of human serum albumin. *Biochem. Mol. Biol. Int.* **36**, 1017–1023 (1995).

41. Salis, A. *et al.* Measurements and Theoretical Interpretation of Points of Zero Charge / Potential of BSA Protein. *Langmuir* **27**, 11597–11604 (2011).
42. Takahashi, N., Sasaki, T., Tsouderos, Y. & Suda, T. S 12911-2 Inhibits Osteoclastic Bone Resorption In Vitro. *J. Bone Miner. Res.* **18**, 1082–1087 (2003).
43. Lariboisiere, H. & Cultures, C. The Divalent Strontium Salt S12911 Enhances Bone Cell. *Bone* **18**, 517–523 (1996).
44. Chattopadhyay, N., Quinn, S. J., Kifor, O., Ye, C. & Brown, E. M. The calcium-sensing receptor (CaR) is involved in strontium ranelate-induced osteoblast proliferation. *Biochem. Pharmacol.* **74**, 438–47 (2007).
45. Marie, P. J. & Hott, M. Short-term effects of fluoride and strontium on bone formation and resorption in the mouse. *Metabolism.* **35**, 547–551 (1986).



# Chapter 3

---

## 4. Effect of Strontium-containing nanoparticles on Bone Remodeling: *in vitro* cell studies

### 4.1 Introduction

Bone is a metabolically active tissue that is constantly being repaired and renewed throughout life by the process of bone remodelling. It has been estimated that approximately 10% of the adult skeleton is being remodelled at any one time. Together, the cells that are responsible for bone remodeling are known as the *basic multicellular unit* (BMU), and the temporal duration (i.e. lifespan) of the BMU is referred to as the bone-remodeling period. The mechanism, which triggers this process, is unclear, but it has been speculated that some chemotactic factors, released from areas of skeletal micro-damage, may play a role.

Bone remodelling starts with attraction of osteoclast precursors to the site, which is to be resorbed. In response to activation of a surface receptor called RANK (receptor activator of nuclear factor kappa B) by the RANK ligand (RANKL), expressed on osteoblasts, osteocytes and bone marrow stromal cells, osteoclast precursors start to differentiate and fuse together to form multinucleated cells<sup>1</sup>. In addition to RANKL, another factor produced by osteoblasts, the M-CSF-1, is required for osteoclast formation<sup>2,3</sup>.

After maturation, the osteoclast attaches to the bone surface by forming a sealing zone, demarcated by the so-called actin ring, and starts to secrete hydrochloric acid and proteolytic enzymes into the space underneath the sealing zone through a specialized membrane called the ruffled border.

When the process is complete, osteoclasts are removed from the bone surface and undergo the “reversal phase”, a programmed cell death phase, which heralds the start of bone formation.

Bone formation begins with the attraction of osteoblast precursors to the site, which has undergone resorption. Expression of the transcription factors Runx2, Dlx5 and Msh homeobox homologue-2 (Msx2) is required to push the precursor cells toward the osteoblast lineage. Osteoblast precursors differentiate into mature cells in response to the transcription factors Runx2 and Osx and several components of the Wnt signalling pathway, which binds to the promoter of several osteoblast specific genes such as osteocalcin, type-I collagen and alkaline phosphatase, causing the cells to assume an osteoblast-like phenotype<sup>4-7</sup>. LRP5 is another key regulator of bone formation that stimulates bone formation, when activated by the Wnt protein family. Wnt proteins stimulate



effects on bone formation are antagonized by a protein, known as Sclerostin, which is produced by osteocytes.

Mature osteoblasts lay down uncalcified bone matrix (osteoid) onto the bone surface and, after a period of about 10 days, this calcifies to form mature mineralized bone. The enzyme ALP, which is produced by osteoblasts, plays an important role in promoting mineralization by degrading pyrophosphate, a natural inhibitor of mineralization that is present in extracellular fluid. ALP is released from normal osteoblasts and used clinically as a biochemical marker of bone formation<sup>8</sup>. During bone formation, some osteoblasts are trapped within bone matrix and differentiate into osteocytes, which are thought to be responsible for sensing the effects of mechanical strain on the skeleton. They produce various signaling molecules, such as prostaglandins and nitric oxide in response to mechanical loading<sup>9</sup>. They also produce SOST, which is a negative regulator of bone formation, dentin matrix protein 1 (DMP1), which regulates mineralization of bone, and FGF23, which is involved in phosphate homeostasis<sup>10</sup>.

An imbalance in the regulation of bone remodeling's two sub-processes, bone resorption and bone formation, results in many metabolic bone diseases, such as osteoporosis.

Many are the technologies developed to modulate this complex process. Here, we demonstrate the effect of Strontium-containing nanoparticles on bone remodeling using several *in vitro* cell models such as osteoblasts, osteocytes and osteoclasts. In particular, the osteosarcoma cell line SAOS-2 and human Mesenchymal Stem Cells isolated from Bone Marrow were used to evaluate the effects of Strontium-containing nanoparticles on osteoblasts differentiation. A murine osteocytic cell line Ocy454 was used to study the effect on osteocytes, while with the murine macrophage RAW264.7 cell line we investigated the effects of nanoparticles on osteoclasts differentiation.

## 4.2 Materials and Methods

### 4.2.1 Cell culture conditions and nanoparticles treatment

#### *SAOS-2 cell line*

The human osteosarcoma cell line SAOS-2 was acquired from the American Type Culture Collection (HTB85, ATCC, Manassas, VA, USA). The cells were cultured in McCoy's 5A modified medium (Lonza) with L-glutamine (Lonza) supplemented with 15% fetal bovine serum (EuroClone), 1% sodium pyruvate (Lonza), 1% antibiotics (Lonza) and 0.2% amphotericin B (Lonza). Cells were cultured at 37°C with 5% CO<sub>2</sub>, routinely trypsinized after confluency, counted and seeded for experiments. To induce differentiation to mature osteoblasts, to the previously described medium 10<sup>-7</sup> M dexamethasone and 5mM β-glycerophosphate were added. Ascorbic acid, another osteogenic supplement, is already present in McCoy's 5A medium so it was not added. After seeding, cells were kept in proliferative medium for 48h and then replaced with osteogenic medium and changed two times per week for 21 days.

#### *Human Bone Marrow Mesenchymal Stem Cells (hBMMSCs)*

The design of this study was approved by the Institutional Review Board of the Fondazione IRCCS Policlinico San Matteo and the University of Pavia (2011).

Bone Marrow (BM) aspirates were harvested from healthy pediatric hematopoietic stem cell donors after obtaining written informed consent. Thirty milliliters of BM from each donor was assigned to BM-MSC generation; heparin was added as an anticoagulant. Mononuclear cells were isolated from BM aspirates (30 mL) by Ficoll density gradient centrifugation (density, 1.077 g/mL; Lymphoprep, Nycomed Pharma, Oslo, Norway) and plated in non-coated 75- to 175-cm<sup>2</sup> polystyrene culture flasks (Corning Costar, Celbio, Milan, Italy) at a density of 16 · 10<sup>4</sup> cells/cm<sup>2</sup>. Cells were cultured in Mesencult medium (Stem Cell Technologies, Vancouver, Canada) supplemented with 2mM L-glutamine, 50 µg/mL gentamycin, and 10% fetal calf serum. Cultures were maintained at 37°C in a humidified atmosphere containing 5% CO<sub>2</sub>. After 48 h, non-adherent cells were discarded and culture medium was replaced twice a week. After reaching 80% confluence as a minimum, the cells were harvested and replated for expansion at a density of 4000 cells/cm<sup>2</sup> until the fifth passage. The colony-forming unit fibroblast assay (CFU-F) was performed as described previously<sup>11</sup>. CFU-F formation was examined after 12 days of incubation in a humidified atmosphere (37°C, 5% CO<sub>2</sub>); the clonogenic efficiency was calculated as the number of colonies per 10<sup>6</sup> BM mononuclear cells seeded. According to the International Society for Cellular Therapy on the nomenclature of mesenchymal progenitors, the cells cultured for this study were defined as multipotent stromal cells.

To phenotypically characterize BM-MSCs and to define their purity, FACS analysis was performed as previously described<sup>11</sup>. After reaching 80% confluence at a minimum, the cells were harvested and re-plated for expansion at a density of  $2.5 \cdot 10^4$  cells/cm<sup>2</sup>. The cells were cultured at 37°C, 5% CO<sub>2</sub>, and three fifths of the medium was renewed every 3 days.

A density of  $5 \cdot 10^5$  cells/cm<sup>2</sup> was used for experiments. After seeding cells were kept in proliferative medium for 48h and then osteoblasts differentiation was induced using an osteogenic medium for 28 days:  $\alpha$ -MEM (Invitrogen, Paisley, PENN) supplemented with 10% fetal bovine serum, 50  $\mu$ g/mL penicillin-streptomycin, 2% L-glutamine, 2% Sodium Pyruvate,  $10^{-7}$  M dexamethasone, 50  $\mu$ g/mL ascorbic acid, and 5 mM b-glycerophosphate<sup>12</sup>.

#### *Osteocytes cell line Ocy454*

Osteocytic cell line Ocy454 was generated by Dr Paola Divieti Pajevic from mouse long bones<sup>13</sup> and single cell subclone of Ocy454 cells was used<sup>14</sup>. The routine culturing conditions to maintain the Ocy454 osteocytic phenotype were twice weekly sub-passages (1:5) for up to 4 months at 33°C with 5% CO<sub>2</sub> from a frozen stock. Cells were cultured in complete growth medium made of  $\alpha$ -MEM with 10% fetal bovine serum and 50  $\mu$ g/mL penicillin-streptomycin. For differentiation experiments, Ocy454 were seeded with a cell density of  $10 \cdot 10^5$  cells/mL. No differentiation/mineralization media or other additives were used. Three days post plating, media was changed and cells were moved to 37°C incubator with 5% CO<sub>2</sub>. Thereafter, media was changed every 2-3 days. Routine Paola Divieti Pajevic laboratory (School of dental medicine, Molecular and cell biology – Boston University) time points for osteocytic phenotype is 2 weeks in culture medium at 37°C.

#### *Murine macrophage RAW264.7 cell line*

RAW264.7 cells, a murine macrophage cell line, were purchased from American Type Culture Collection (Rockville, MD, USA). The cells were maintained in Dulbecco's modified Eagle's medium (DMEM) containing 50  $\mu$ g/mL penicillin-streptomycin, 2% L-glutamine and 10% fetal bovine serum at 37°C in a humidified atmosphere with 5% CO<sub>2</sub>. For all experiments, the cells were grown to 80–90% confluency and were subjected to no more than 20 cell passages. To induce the differentiation in osteoclasts, cells were treated with 50ng/mL of recombinant RANKL (Miltenyi Biotec) for 9 days changing medium every 3 days.

#### **4.2.2 Nanoparticles suspension preparation**

To obtain a stable suspension, 5 mg of sterile powders (Ca100, Ca50Sr50 and Sr100) were added to 4 mL 5% sterile BSA solution. The suspension was sonicated for 90 minutes at 45°C, using LBS2

sonicator bath (FALC Instruments), with an operation frequency of 40 kHz and mechanical stirring. The suspension was then diluted with Phosphate Buffer Solution (PBS) and filtered with 0.45  $\mu\text{m}$  filters. NPs suspensions were suspended again in culture medium at the concentrations indicated for each type of experiment.

### 4.2.3 Nanoparticles uptake studies

#### *Confocal Laser Scanning Microscopy (CLSM)*

In order to study NPs uptaking, Ca100\_NPs and Sr100\_NPs were conjugated with fluorescein isothiocyanate (FITC). To do this, 1 mL of 625  $\mu\text{g}/\text{mL}$  NPs suspension was re-suspended in 250  $\mu\text{L}$  of 1  $\text{mg}/\text{mL}$  FITC solution in sodium carbonate-bicarbonate buffer. Solutions were incubated for 2 hours, at room temperature, with gentle stirring. After this time, samples were centrifuged at  $10^4 \times g$  for 30 minutes and then washed with PBS twice. The FITC-NPs were re-suspended in proliferative medium. SAOS-2 cells and hBMMSCs were seeded onto glass coverslips with a cell density of  $3 \times 10^4$  cell/mL and, after 24 hours, SAOS-2 cells were treated with FITC-NPs solutions for 2, 6 and 24 hours, whereas hBMMSCs for 24h. At the incubation times, the glass coverslips were washed with PBS to remove not internalized FITC-NPs and cells were fixed with 4% (w/v) paraformaldehyde (PFA) solution in 0.1 M phosphate buffer (pH 7.4), for 30 min at  $4^\circ\text{C}$ , and washed with PBS three times. Actin staining was performed using 10  $\mu\text{g}/\text{mL}$  phalloidin, labelled with tetramethylrhodamine (TRITC) (Sigma), and nuclei counterstained with a Hoechst 33342 solution (2  $\mu\text{g}/\text{mL}$ ). Samples have been examined using a confocal laser scanning microscope (Leica TCS SP2, Leica Instruments, Germany), acquiring images every 1.5  $\mu\text{m}$  till 100  $\mu\text{m}$  of depth. Rhodamine fluorescence was excited at 540 nm and measured at 565 nm; whereas FITC fluorescence was excited at 488 nm and measured at 491–586nm. Instead, DAPI fluorescence was excited at 405 nm and measured at 420–480 nm.

In order to study the uptaking pathway used by SAOS-2 cells to internalize NPs, cells were seeded onto glass coverslips with a cell density of  $3 \times 10^4$  cell/mL and, after 24 hours, cells were incubated with medium containing different endocytosis inhibitors and then maintained for 2 h at  $37^\circ\text{C}$  with 5% of  $\text{CO}_2$ -air. The inhibitors used were 3mM amiloride (Sigma-Aldrich), 35  $\mu\text{M}$  chlorpromazine (Sigma-Aldrich) and 22.5  $\mu\text{M}$  indomethacin (Sigma-Aldrich). The dose of each inhibitor was chosen taking into account the previous data carried out in different studies, as reported in literature<sup>15-21</sup>. After 2 h of treatment with these inhibitors, medium was replaced with medium containing 675  $\mu\text{g}/\text{mL}$  FITC-NPs, 40  $\mu\text{M}$  amiloride or 35  $\mu\text{M}$  chlorpromazine or 22.5  $\mu\text{M}$  indomethacin. After 24 h, the medium was removed and the cells were fixed and observed to CLSM following the procedure described above.

### *Flow Cytometry*

In order to evaluate the endocytosis pathway for nanoparticles uptake, SAOS-2 cells were seeded in 6-well culture plates at a density of  $2.5 \times 10^5$  cells/mL and the same procedure with inhibitors and FITCH-NPs as described above was performed. After 24 hours with NPs treatment, the culture medium was removed and the cells were trypsinized and analysed to PARTEC PAS II cytofluorimeter acquiring data in linear or log mode, to evaluate the FITC-NPs incorporation. FITC fluorescence was excited at 488 nm and measured using the Partec PAS II flow cytometer. Three control types were carried out in parallel: (a) Negative control, which corresponds to cells without inhibitors and without FITC-NPs, (b) Control Ca100\_NPs, which corresponds to cells treated with Ca100\_NPs without inhibitors and (c) Control Sr100\_NPs, which corresponds to cells treated with Sr100\_NPs without inhibitors. All data were elaborated using Flowmax dedicated software.

### *Inductively coupled plasma optical emission spectrometry (ICP-EOS)*

In order to evaluate quantitatively nanoparticles uptake, SAOS-2 cells were seeded in  $175\text{cm}^2$  tissue culture flasks, untreated and treated with Ca100 and Sr100 at a concentration of  $625\ \mu\text{g/mL}$  and incubated for 24h. Afterwards, medium was removed; cells were trypsinized, counted and washed two times with PBS and one time quickly with pure water. All the samples and the standards were dissolved in ultrapure nitric acid (70%v) and diluted in pure water from reverse osmosis (conductivity  $<0.1\ \mu\text{S/cm}$ ), adding Cs (100 g/L) as ionization suppressor. The synthesized powders purity and composition were determined by ICP-EOS (Spectro Ciros Vision CCD, 125-770 nm) using hydroxyapatite ultrapure standard (Reagent Grade, Sigma-Aldrich) and a 1000 ppm Sr standard (BHD SpectroSol). Emission lines chosen were 366 nm for Ca and 596 nm for Sr.

#### **4.2.4 Cell viability, apoptosis and morphological analysis**

##### *3-(4,5-dimethylthiazol-2-yl)-2,5-diphenyltetrazolium bromide Assay*

To measure the viability of cells untreated and treated with nanoparticles, the mitochondrial activity was evaluated using 3-(4,5-dimethylthiazole-2-yl)-2,5-diphenyl tetrazolium bromide (MTT) test (Sigma-Aldrich). At indicated time points, the viability assay was performed as previously reported<sup>22</sup>. Aliquots of  $100\ \mu\text{L}$  were sampled, and the related absorbance values were measured at 595 nm and 655 nm, using the iMark Microplate Reader (BioRad Laboratories). The viability assay was performed for the times indicated on treated and untreated cells (Control). A standard curve of cell viability was used to express the results as number of live cells.

### *Resazurin-based assay*

The resazurin-based assay was used to estimate the number of viable cells in NPs treated/untreated cells by measuring the reduction of resazurin into resorufin. Resazurin solution (Sigma-Aldrich) was added as one-tenth of culture volume, and then cells were incubated for 3 h at 37°C with 5% CO<sub>2</sub>. Optical measurements were run on aliquots of 100 µL by a microplate reader (BioRad Laboratories, Hercules, CA, USA) at reference wavelengths of 600 nm and 690 nm. A cell viability standard curve was used to express the results as number of live cells.

### *PSVue480™ staining*

To determine the induction of cell apoptosis by the nanoparticle suspensions, BMMSCs were labelled using the PSVue480™ cell stain according to the manufacturer's instructions (Molecular Targeting Technologies, Inc.). PSVue480™ dye detects apoptosis by targeting the loss of phospholipid asymmetry in the plasma membrane that is an early event in apoptosis, independent of cell type, resulting in the exposure of phosphatidylserine (PS) residues at the outer plasma membrane leaflet<sup>23</sup>. BMMSCs were seeded on glass coverslips (Thermo Scientific) with a density of 3x10<sup>4</sup> cells/cm<sup>2</sup> and incubated with H<sub>2</sub>O<sub>2</sub> (positive control; 100 mM for 18 h), without suspension (negative control) and with 6.25, 31.25, 62.5, 312.5 and 625 µg/mL of each NPs suspension for 1 and 7 days, respectively. At the end of each culture condition, the cells were stained with PSVue480™ solution prepared according to the manufacturer's instructions. Samples were then counterstained with a Hoechst 33342 solution (2 µg/mL) to target the cellular nuclei and observed under a fluorescence optical microscope (Nikon Eclipse 80i).

### *Morphological analysis*

In order to study cell morphology of untreated and NPs treated cells, after 24h of treatment, cells were paraformaldehyde fixed, as described above, permeabilized with 0.1% Triton X-100 for 1 h at room temperature (RT) and incubated with FITCH conjugated antibody against β-tubulin (Invitrogen) for 90 min at RT, then incubated with phalloidin conjugated with TRICH (Sigma) for 45 min. Finally, nuclei were counterstained with Hoechst 33342 solution (2 µg/mL) and samples were observed under a fluorescence optical microscope (Nikon Eclipse 80i).

## **4.2.5 Enzyme assays for evaluation of differentiation process**

### *Alkaline Phosphatase (ALP) Activity*

In order to study osteoblasts differentiation, ALP activity was determined using a colorimetric end point assay<sup>24</sup>. The assay measures the conversion of the colorless substrate p-nitrophenol phosphate

(pNPP) by the enzyme ALP to the yellow product p-nitrophenol; the rate of color change corresponds with the amount of enzyme present in solution. The test was performed as previously described<sup>25</sup> on cells cultured in presence or absence of NPs at the indicated time points. Samples were run in triplicate and compared with the calibration curve of p-nitrophenol standards. The enzyme activity was expressed as micromoles of p-nitrophenol produced per minute per milligram of enzyme.

#### *Tartrate-resistant acid phosphatase (TRAP) activity*

In order to study the effect of NPs on osteoclast differentiation, TRAP activity of the enzyme released in the culture medium by untreated and treated RAW264.7 cells was performed. To do that, 30  $\mu$ l of culture medium were incubated for 30 min at 37°C with 30  $\mu$ l of 600 mM sodium acetate buffer (pH 5.5) containing L-ascorbic acid (17.6 mg/ml), sodium tartrate dehydrate (9.2 mg/ml), disodium 4-nitrophenylphosphate (3.6 mg/ml), Triton X-100 (0.3%), EDTA (6 mM), and NaCl (600 mM). The reaction was terminated by addition of 30  $\mu$ l of NaOH (300 mM) and the absorbance at 405 nm was measured by microplate reader (BioRad Laboratories, Hercules, CA, USA).

TRAP histochemical staining of the cells cultured for 10 days in absence and presence of Ca100 and Sr100 NPs was performed using a leukocyte acid phosphatase kit (Sigma-Aldrich). The cultured cells were paraformaldehyde fixed then stained for TRAP activity according to the manufacturer's instructions.

#### **4.2.6 Extracellular Matrix (ECM) deposition and mineralization**

##### *Alizarin Red Staining*

To analyze calcium (Ca) deposition by untreated and NPs treated at the indicated time points, cells were rinsed with PBS, fixed for 30 min at 4°C with 4% PFA and stained for 10 min with 40 mM Alizarin Red S (pH 4.2, Sigma-Aldrich)<sup>26</sup>. Then, samples were washed three times with water and one time with PBS for 10 minutes and pics of the well were taken or observed at microscope. Alizarin Red S staining was released from the cell matrix by incubation in 10% cetylpyridinium chloride (Sigma-Aldrich) in 10 mM sodium phosphate (pH 7.0), for 15 min and the absorbance measured at 562 nm.

In order to study the effect of Sr100 NPs on bone matrix calcification of Ocy454 cells culture in the presence of the calcium sensing receptor inhibitor NPS2143 hydrochloride (Sigma), osteocytes were cultured in absence/presence of Sr100 NPs, and in absence/presence of the inhibitor for 7 days. Moreover, in other two samples treatment with inhibitor was performed only during the first

three days of culture and from the fourth to the seventh day. At the end of culture, cells were fixed with 4% paraformaldehyde and stained with Alizarin Red as described previously.

#### *Calcium–cresolphthalein complexone assay*

The calcium content of NPs treated and untreated cells, was assayed to quantify the amount of mineralized matrix present and was measured using a Calcium Fast kit (Mercury SPA, Naples, Italy) according to the manufacturer's instructions. The colorimetric end point assay measures the amount of purple-coloured calcium–cresolphthalein complexone complex formed when cresolphthalein complexone binds to free calcium in an alkaline solution<sup>27</sup>. Briefly, 1 mL of 1N HCl was added to each sample at the end of the culture and incubated for 24 h at 4°C to release calcium into solution. The sample supernatant was diluted 1:10 with the Assay Working Solution previously prepared by mixing equal parts of calcium-binding reagent and calcium buffer reagent provided by the kit. Ca<sup>2+</sup> standards in concentrations ranging from 0 to 10 mg/mL were prepared from dilutions of a 100 mg/mL stock solution of Ca<sup>2+</sup>. The absorbance reading was performed at 595nm with a microplate reader (BioRad Laboratories) using 100 µL of standard or sample placed into individual wells of a 96-well plate. Samples were run in triplicate and compared against the standard solution calibration curve.

#### *Scanning Electron Microscopy (SEM) and Energy dispersive X-ray spectroscopy (EDS) analysis*

In order to evaluate Sr incorporation in bone matrix, SAOS-2 cells were seeded on plastic cell culture coverslip disks (Thermanox Plastic, Nalge Nunc International, New York, NY) and cultured for 21 days in presence of 62.5 µg/ml of Sr100 and Ca100 NPs, in proliferative and osteogenic conditions. At the end of the culture time, cells were fixed with 2.5% (v/v) glutaraldehyde solution in 0.1 M sodium cacodylate buffer (pH 7.2) for 1 h at 4°C. Afterwards, samples were washed with sodium cacodylate buffer and then dehydrated at room temperature, in an ethanol gradient series up to 100%. To obtain a complete dehydration, samples were lyophilized for 3 h. Finally, the samples were observed using a scanning electron microscope Zeiss EVO-MA10 (Carl Zeiss, Oberkochen, Germany) and Elemental maps of Ca, P and Sr were obtained using Energy dispersive X-ray spectroscopy (EDSdetector X-max 50 mm<sup>2</sup>, Oxford instruments, Oxford, U.K.)

#### *Extraction of ECM proteins and enzyme-linked immunosorbent assay*

At the end of the culture period, in order to evaluate the amount of ECM produced, the samples were washed extensively with sterile PBS to remove culture medium, and then incubated with sterile lysis buffer made of 20mM Tris-HCl, 4M GuHCl, 10mMEDTA, 0.066% [w/v] sodium



dodecyl sulfate [SDS], pH 8.0 and frozen and thawed several times to allow the cell lysis and ECM disruption. After that, the total protein concentration of samples was evaluated with the BCA Protein Assay Kit (Pierce Biotechnology, Inc., Rockford, IL).

Calibration curves to measure type-I and -III collagens, decorin (DEC), osteopontin, osteocalcin, osteonectin, fibronectin (FN) and ALP were performed. Microtiter wells were coated with increasing concentrations of each purified protein, from 10 ng to 2 mg, in coating buffer (50mM Na<sub>2</sub>CO<sub>3</sub>, pH 9.5) overnight at 4°C. Control wells were coated with BSA as a negative control. To measure the ECM amount of each protein by ELISA, microtiter wells were coated, overnight at 4°C, with 100 µL of the previously extracted ECM (20 µg/mL in coating buffer). After three washes with PBS containing 0.1% (v/v) Tween 20, the wells were blocked by incubating with 200 µL of PBS containing 2% (w/v) BSA for 2 h at 22°C. The wells were subsequently incubated for 1.5 h at 22°C with 100 µL of the anti-type-I and -III collagens, antidecorin, anti-osteopontin, anti-osteocalcin, anti-onectin and anti-ALP rabbit polyclonal antisera (1:500 dilution in 1% BSA), kindly provided by L. Fisher. The same dilution was used for the anti-FN rabbit polyclonal IgG. After washing, the wells were incubated for 1 h at 22°C with 100µL of horseradish peroxidase (HRP)-conjugated goat anti-rabbit IgG (1:1000 dilution in 1% BSA). The wells were finally incubated with 100 mL of the development solution (phosphate-citrate buffer with o-phenylenediamine dihydrochloride substrate). The color reaction was stopped with 100 µL of 0.5 M H<sub>2</sub>SO<sub>4</sub>, and the absorbance values were measured at 490nm with a microplate reader (BioRad Laboratories). An underestimation of the absolute protein deposition is possible because the sample buffer, used for matrix extraction, contained sodium dodecyl sulfate, which may interfere with the protein adsorption during ELISA.

#### *Immunostaining of ECM proteins*

At the end of culture time, untreated and NPs treated samples were fixed with 4% (w/v) paraformaldehyde solution in 0.1M phosphate buffer (pH 7.4) for 30 min at 4°C and washed with PBS three times. For immunological studies, paraformaldehyde fixed cells were blocked by incubating with PAT (PBS containing 1% [w/v] bovine serum albumin and 0.02% [v/v] Tween 20) for 2 h at room temperature and washed. Anti-type-I collagene and anti-osteocalcin rabbit polyclonal antisera were used as the primary antibodies diluted to 1:500 in PAT. The incubation with the primary antibodies was performed overnight at 4°C, whereas the negative controls were incubated with PAT alone. The samples and the negative controls were washed and incubated with Alexa-Fluor-488 goat anti-rabbit IgG (HþL; Invitrogen) at a dilution of 1:750 in PAT for 1 h at room temperature. At the end of the incubation, the samples were washed in PBS, counterstained

with a Hoechst solution (2 µg/mL) to target the cellular nuclei, and then washed. The images were taken by the Fluorescence microscope (Leica Microsystems, Bensheim, Germany) equipped with a digital image capture system at 40X magnification.

#### 4.2.7 Gene expression

Total RNA from samples cultured in presence and absence of NPs, was extracted with the RNeasy Plus Mini Kit (Qiagen) and retrotranscribed into cDNA with the iScript cDNA Synthesis Kit (BioRad Laboratories) as previously reported<sup>25</sup>. Quantitative reverse-transcription polymerase chain reaction (qRT-PCR) analysis was performed in a 48-well optical reaction plate using a MiniOpticon Real-Time PCR System (BioRad Laboratories). Oligonucleotide primers were designed with gene sequences published in GenBank and are indicated in Table 3.1 and 3.2. Reactions were performed in 20 µL with 2 µL of cDNA, 10 µL Brilliant SYBER Green qPCR Master Mix (Stratagene, La Jolla, CA), 0.4 µL of each primer, and 7.2 µL H<sub>2</sub>O. PCR conditions were as follows: 3 min at 95°C, 40 cycles of 5 sec at 95°C, and 23 sec at 60°C. Gene expression was normalized to the 18S housekeeping gene expression. Each sample was analyzed in triplicate and correlated against a standard curve. The reaction mixture, without cDNA, was used as a negative control in each run.

<b>Gene</b>	<b>Forward primer</b>	<b>Reverse Primer</b>
<b><i>IBSP</i></b>	5'-GGGCAGTAGTGACTCATCCG-3'	5'-TCAGCCTCAGAGTCTTCATCTTC-3'
<b><i>ALP</i></b>	5'- ACCTCGTTGACACCTGGAAG-3'	5'- CCACCATCTCGGAGAGTGAC-3'
<b><i>COL1A1</i></b>	5'-TGTAAGCGGTGGTGGTTATG-3'	5'-GGTAGCCATTCCTTGAAG-3'
<b><i>COL3A1</i></b>	5'-TGGATCAGATGGTCTTCCA-3'	5'-TCTCCATAATACGGGGCAA-3'
<b><i>DCN</i></b>	5'-CGAGTGGTCCAGTGTTCTGA-3'	5'-AAAGCCCCATTTCAATTCC-3'
<b><i>RUNX2</i></b>	5'-ACAGTAGATGGACCTCGGGA-3'	5'-ATACTGGGATGAGGAATGCG-3'
<b><i>BMP2</i></b>	5'-AACGGACATTCGGTCCTTGC-3'	5'-CGCAACTCGAACTCGCTCAG-3''
<b><i>OCN</i></b>	5'-GGCAGCGAGGTAGTGAAGAG-3'	5'-CTGGAGAGGAGCAGAACTGG-3'
<b><i>18S</i></b>	5'-GTAACCCGTTGAACCCATT-3'	5'-CCATCCAATCGGTAGTAGCG-3'

Tab. 3.1 Primers used for qRT-PCRs for expression of human genes

<b>Gene</b>	<b>Forward primer</b>	<b>Reverse Primer</b>
<i>OCN</i>	5'-CGCTCTGTCTCTCTGACCTC-3'	5'-GACTGAGGCTCCAAGGTAGC-3'
<i>DMP1</i>	5'-AGGACTCCACAGACACCACA-3'	5'-GGGTATCTTGGGCACTGTTT-3'
<i>IBSP</i>	5'- AACGAACAAG GCATAAACGGCACCA-3'	5'- CTTGCCCTGCCTTCCGGTCT-3'
<i>RANKL</i>	5'-GCTGGGCCAAGATCTCTAAC-3'	5'-GTAGGTACGCTTCCCGATGT-3'
<i>SOST</i>	5'-GCCTCATCTGCCTACTTGTG-3'	5'-CTGTGGCATCATTCTGAAG-3'
<i>ACP5</i>	5'-CATTGAGGACAAAGGCCCTG-3'	5'-TGTACCGTGGGTCAGGAGT-3'
<i>CTSK</i>	5'-GCCACGCTTCTATCCGAAA-3'	5'-ACTGGGTGTCCAGCATTTCC-3'
<i>CD44</i>	5'-GAATTCTGCGCCCTCGGTT-3'	5'-TGGAATACACCTGCGTAGCG-3'
<i>NFATc1</i>	5'-GGTAACTCTGTCT TTCTAACCTTAAGCTC-3'	5'-GTGATGACCCAG CATGCACCAGTCACAG-3'
<i>18S</i>	5'-TCAAGAACGAAAGTCGGAGG-3'	5'-GGACATCTAAGGGCATCAC-3'

Tab. 3.2 Primers used for qRT-PCRs for expression of murine genes

#### 4.2.8 Statistics

Each experiment was repeated three times. Quantitative results are expressed as the mean  $\pm$  standard error of the mean (SEM). In order to compare the results between untreated, Ca100, Ca50Sr100 and Sr100 treated samples, the one-way analysis of variance (ANOVA) with post hoc Bonferroni test was applied, with a significance level of 0.05.

## 4.3 Results

### 4.3.1 Osteoblasts-like SAOS-2 cell line

#### *Nanoparticles uptake studies*

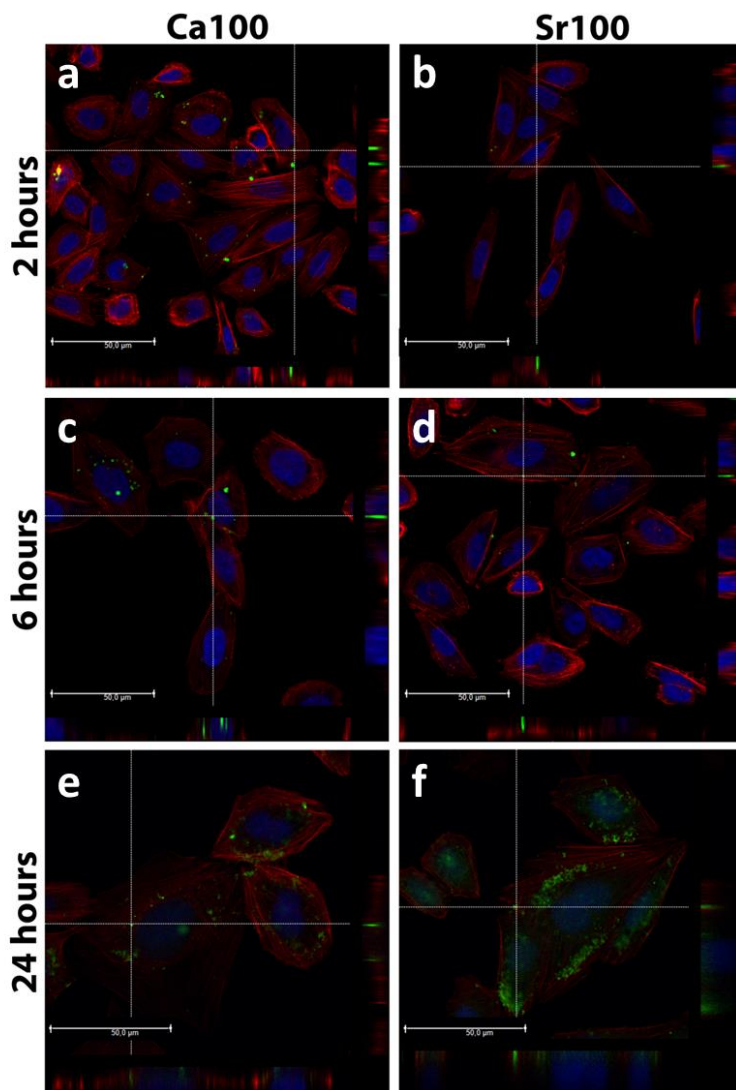


**Fig. 3.1** Nanoparticles Uptaking kinetic. Representative CLSM images and orthogonal projection of SAOS-2 cells incubated for 2 (a,b), 6 (c,d) and 24 (e,f) hours with Ca100 (a, c, e) and Sr100 (b, d, f) nanoparticles conjugated with FITCH (green). Actin filaments were stained with phalloidine-TRITC (red) and nuclei counterstained with Hoechst 33342 (blue). Magnification 40X, scale bars represent 50 $\mu$ m.

To evaluate Ca100 and Sr100 nanoparticles internalization into cells, NPs suspended in BSA were labelled with FITC in order to make them visible by fluorescence.

**Figure 3.1** is a representative image of CLSM of SAOS-2 cells treated with 62.5  $\mu$ g/mL FITC-NPs for 2, 6 and 24 hours: nuclei and actin filaments were stained with Hoechst 33342 and Phalloidin-TRITC, respectively. In the figure, orthogonal projections are also reported.

As the figure shows, after 2 h of treatment few NPs are visible, but slightly more in Ca100 treated samples: in particular the orthogonal projections seem to show the Ca100-NPs co-localization with actin filaments at the cell membrane level (**Fig. 3.1a and b**). No NPs were observed inside cells in both types of samples. After 6 h, the number of internalized NPs is higher than those observed at shorter times, especially in

Ca100 treated sample. Also after 6 hours most of NPs are localized on cell membrane but some of them appear to be underneath the actin filaments indicating a complete internalization (**Fig. 3.1c and d**). After 24 h, a significant higher number of NPs were observed inside the cells of both samples (**Fig. 3.1e and f**). These data seem to suggest that NPs are uptake by cells in a time course manner and that the complete internalization occurs between 6h and 24h. Moreover, a different

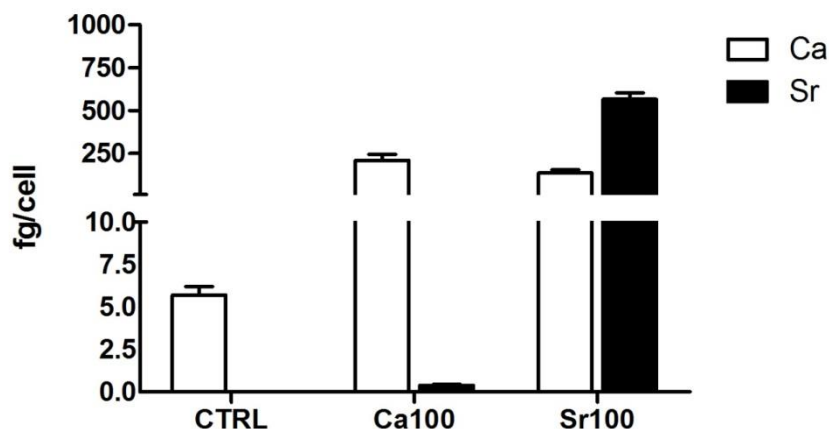


**Fig. 3.2** Ca and Sr intracellular amounts evaluated by ICP-OES analysis in untreated (Ctrl) and treated SAOS-2 cells with Ca100 and Sr100 nanoparticles, after 24h. Bars represent fg/cell for each element.

behaviour was observed for the two types of NPs: Ca100 seems to be uptake at a shorter time than Sr100, probably due to the difference in NPs size.

To get deeper, a quantitative evaluation of intracellular amount of Ca and Sr was evaluated at 24 h in untreated, Ca100 and Sr100 treated samples. **Figure 3.2** shows the femtograms per cell of each element as detected by ICP-EOS technique. The graph shows that the amounts of calcium detected in Ca100 and Sr100 treated samples were similar but 50 times higher than untreated cells, whereas strontium was 1000 times greater in Sr100 treated samples if compared to Ca100 treated ones (in untreated samples no strontium was detected). These data confirm the complete NPs uptake occurs after 24h and, surprisingly, the amounts of Ca detected in Ca100 and Sr100 treated cells were comparable, suggesting that Sr addition induces an intracellular calcium increase.

In order to study the mechanisms involved in NPs internalization, SAOS-2 cells were pre-incubated with three inhibitors, as described in materials and methods section (pag 77). After the pre-incubation, new media containing FITCH conjugated NPs and the inhibitors were added and incubated for further 24h. At the end, all samples were qualitatively observed with CLSM (**Figure 3.3**). The same experiment was performed using flow cytometry to measure the NPs fluorescence using FloMax<sup>®</sup> 2.2 Software (**Figure 3.4**). In particular, to calculate the percentage of inhibition, signals obtained from cells treated with NPs in presence of inhibitors were compared with the fluorescence of cells treated with NPs but in absence of inhibitors (**Fig. 3.4a**). Fluorescence peaks analysis revealed that amiloride strongly reduced the uptake of Ca100 by 73% ( $p < 0.001$ ) whereas the reduction was around 34% with Sr100 ( $p < 0.01$ ), whereas no significant decreases were observed in samples treated with chlorpromazine and indomethacin, for both nanosystems ( $p > 0.05$ ) (**Fig. 3.4b**). These data are confirmed by CLSM observation where a smaller amount of green fluorescence was observed in cells treated with amiloride, especially in Ca100 treated samples (**Fig. 3.3**). Again no significant differences were observed in cells treated with Chlorpromazine and

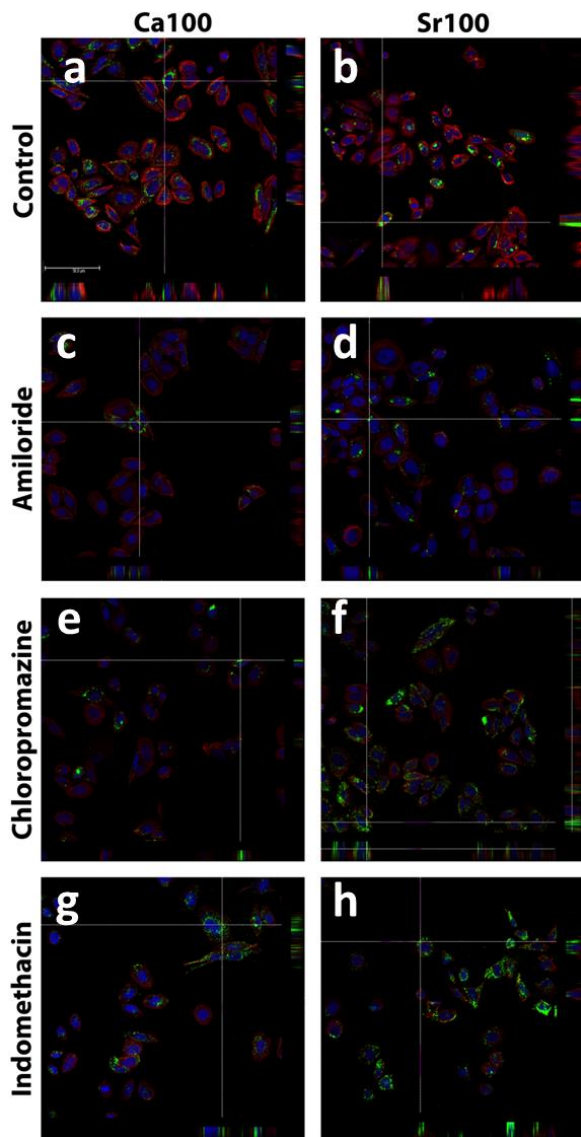


**Fig. 3.3 Nanoparticles uptake pathways.** Representative CLSM images and orthogonal projection of SAOS-2 cells incubated with Ca100 (a, c, e, g) and Sr100 (b, d, f, h) nanoparticles in absence (a, b) and in presence of uptake inhibitors: amiloride (c, d), chlorpromazine (e, f) and indomethacin (g, h). Actin filaments were stained with phalloidine-TRITC (red) and nuclei counterstained with Hoechst 33342 (blue). Magnification 20X, scale bars represent 50 $\mu$ m.

Indometacin cells, endorsing the quantitative results (Fig. 3). A cell viability evaluation was also carried out with FloMax<sup>®</sup> software, in order to evaluate the percentages of live cells in those samples untreated/treated with inhibitors in the presence/absence of NPs showing a range of 82%–94% with no significant statistical differences. This datum confirms that the uptake process is not related to the possible cytotoxic effect exerted by the selected inhibitors. Based on the previous indicated results, we may suggest that macropinocytosis is the uptake mechanism involved in cell internalization of Ca100 and Sr100 NPs.

#### *Effect of NPs on Osteoblasts differentiation*

After uptake studies that revealed some details about NPs internalization, further experiments were performed in order to evaluate the effect exerted by NPs on osteoblasts differentiation. To do that, we evaluated the extracellular matrix deposition in terms of proteins and mineralization quantification, ALP activity and expression of specific bone marker genes of SAOS-2 cells untreated/treated with Ca100 and Sr100 for 21 days in 2 different culture medium conditions, proliferative and osteogenic media, respectively.

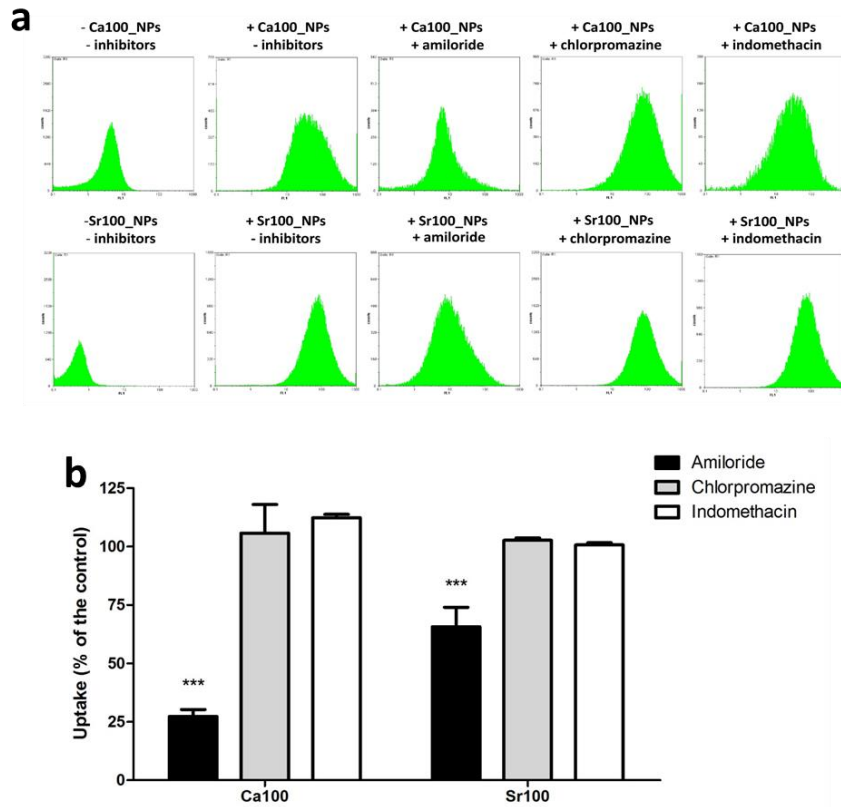


**Fig. 3.4** Nanoparticles uptake pathways. Quantitative determination by flow cytometry of nanoparticles uptake in presence of uptake inhibitors. a) Peaks of NPs fluorescence; b) Percentage of NPs uptake obtained comparing fluorescence from inhibitors treated samples with inhibitor untreated samples. Bars represent percentage of nanoparticles uptake related to positive control (uptake in absence of inhibitors). Statistical analysis performed against the positive control, \*\*\* $p < 0.001$ .

**Figure 3.5** shows results related to ALP activity and protein expression. In particular, an increase of enzyme activity was observed for Sr100 treated cells in both types of culture conditions ( $p < 0.001$ ) (**Fig. 3.5a**). The level of ALP activity was higher in osteogenic on respect to proliferative medium. In particular, a slight increase was observed also in Ca100 treated samples ( $p < 0.001$ ) if related to untreated samples. These data are confirmed by observation with a fluorescence microscope: a more intense and diffuse green fluorescence was observed in Sr100 treated samples in comparison to untreated and Ca100 treated samples (**Fig. 3.5b**). These results suggest a stimulatory effect of Sr100 on ALP protein expression and activity, possibly promoting osteoblasts differentiation.

The most important activity related to osteoblasts task is their ability to synthesize and deposit a mineralized extracellular matrix. **Figure 3.6** shows results related to mineralization, in particular Alizarin Red stained samples of untreated/treated with Ca100 and Sr100 SAOS-2 cells (**Fig. 3.6A-F**) and their quantitative evaluation (**Fig. 3.6G**). Alizarin Red staining is specific for calcium deposits as shown by red spots observed only in samples cultured in osteogenic conditions (**Fig. 3.6A-C**). No red staining was observed in samples cultured in proliferative conditions (**Fig. 3.6D-F**). Moreover in Sr100 treated samples a higher number of larger red spots were observed in comparison to the control and Ca100 treated samples. Quantitative results obtained by the calcium–cresolphthalein complexone assay confirmed the previous data (**Fig. 3.6G**) showing an increase of Ca deposition in Sr100 treated samples cultured in osteogenic conditions ( $p < 0.001$ ). Quantitative data related to samples cultured in proliferative conditions are not shown since no calcium was detected.

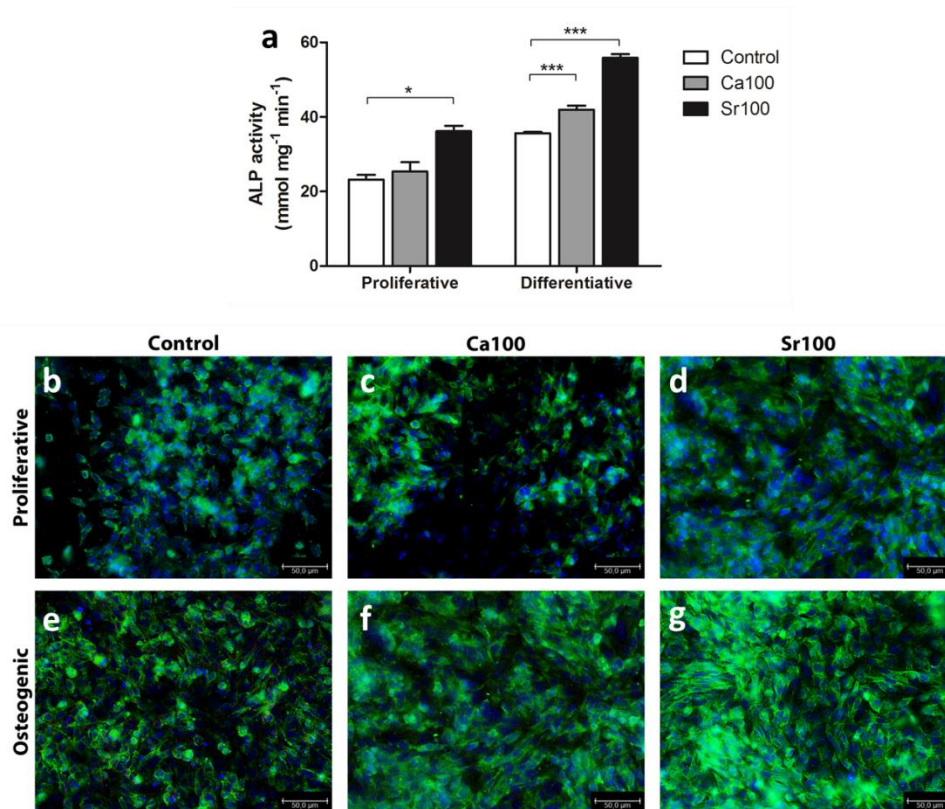


**Fig. 3.5** Effect of nanoparticles treatment on ALP activity and expression in SAOS-2 cells. a) ALP specific activity in SAOS-2 cells untreated (control) and treated with Ca100 and Sr100 nanoparticles for 21 days, cultured in proliferative and osteogenic conditions. Bars represent mean and SEM of three experiments (\* $p < 0.05$ , \*\* $p < 0.01$ , \*\*\* $p < 0.001$ ); (from b to g) representative fluorescence images of ALP immunostaining (green) in sample cultured for 21 days in proliferative (b, c, d) and osteogenic (e, f, g) conditions, in absence (b, e) and presence of Ca100 (c, f) and Sr100 (d, g) nanoparticles. Nuclei were counterstained with Hoechst 33342 (blue). Magnification 20X, scale bars represent 50 $\mu$ m.



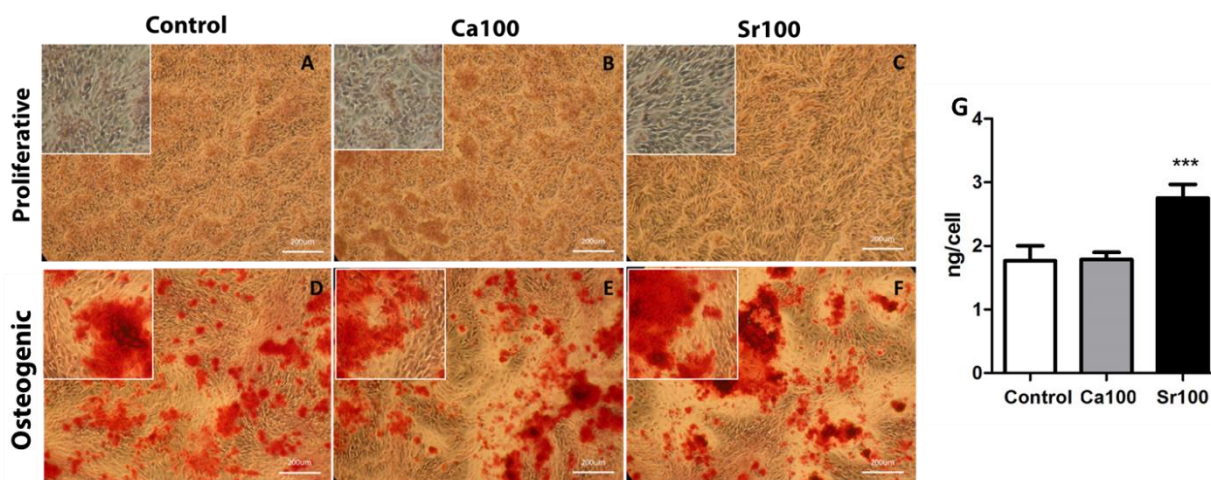


**Fig. 3.6** Effect of nanoparticles on bone matrix mineralization by SAOS-2 cells. (From A to F) Representative images at optical microscope of SAOS-2 cells cultured for 21 days in proliferative (A, B, C) and osteogenic (D, E, F) conditions, in absence (A-D) and presence of Ca100 (B, E) and Sr100 (C, F) nanoparticles and stained with Alizarin Red S for calcium deposits visualization. Magnification 10X (insert 20X), scal bars represent 50 $\mu$ m. G) Quantitative evaluation of calcium deposited by SAOS-2 after 21 days in absence (Control) and presence of Ca100 and Sr100 nanoparticles in osteogenic condition, by Calcium-cresolphthalein complexone method. Bars represent mean and SEM of three experiments, statistical analysis performed against control (\*\*\*) $p < 0.001$ ).

To study the effect of Sr100-NPs in comparison to strontium-containing salts on calcium deposition, SAOS-2 cells were treated with different amounts of Sr100 nanoparticles, Strontium Chloride and Strontium Ranelate in osteogenic conditions. **Figure 3.7** shows the absorbance of Alizarin Red stained samples after cetylpyridinium dissolution and Alizarin red stained wells of untreated/treated cells with 1.25 mM  $\text{Sr}^{+2}$  concentrations using the three different compounds. 1.25 mM is the  $\text{Sr}^{+2}$  concentration used for all the SAOS-2 differentiation experiments corresponding to 62.5  $\mu\text{g}/\text{mL}$  of Sr100 nanoparticles. An higher mineralization was observed in Sr100 treated samples for  $\text{Sr}^{+2}$  concentrations ranging from 0.156 mM to 2.5mM (**Fig. 3.7a**). At higher  $\text{Sr}^{+2}$  concentrations, an absorbance decrease was observed in all samples treated with the three Sr-containing compounds indicating a negative effect which resulted dose-dependent for Sr on bone matrix mineralization, especially for Strontium Ranelate. A more detailed analysis on bone matrix mineralization was performed by SEM measurements with energy dispersive microanalysis. **Figure 3.8** shows spectra, SEM micrography, maps of Ca, P and Sr and relative quantitative evaluation of untreated/treated with Ca100 and Sr100 SAOS-2 cells in proliferative (**Fig. 3.8a**) and osteogenic (**Fig. 3.8b**) conditions, respectively. In samples cultured in proliferative conditions no differences were observed (Fig. 8a is representative for all of the three samples). On the contrary, a significant difference was observed for samples cultured in osteogenic medium, in particular between untreated/treated samples with Ca100 and Sr100 (**Fig. 3.8b**). Significant increase in P and Ca peaks intensity was recorded. Interestingly, Sr peaks were detected in Sr-treated samples (yellow arrows

in Fig. 8b) that are absent in the other samples. This result suggests that Sr, which has been administered by nanoparticles, is deposited by cells in bone matrix. Quantitative evaluation of this deposition was measured around 1%.

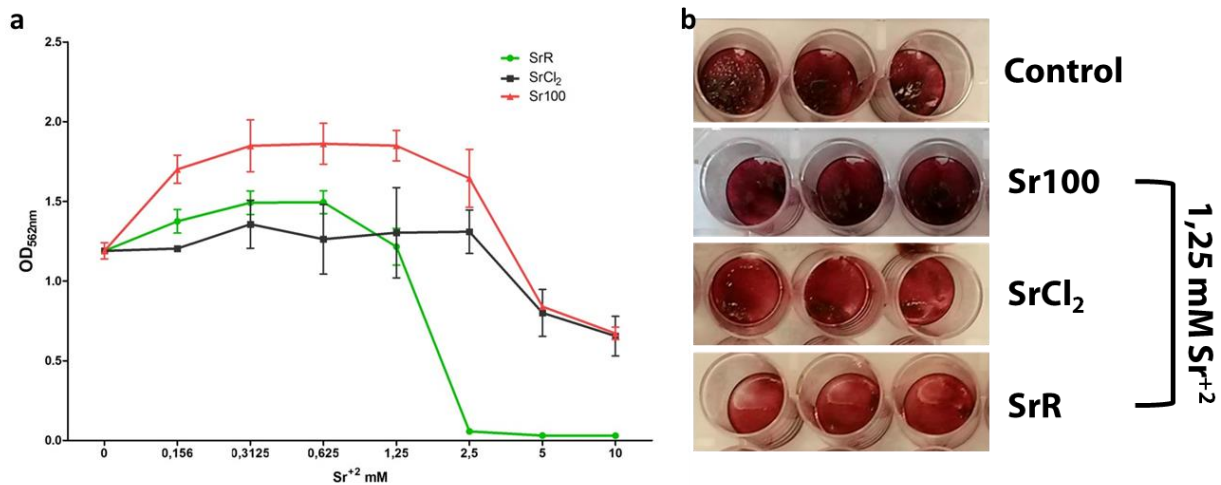


**Fig. 3.7** Effect of three different strontium-containing compounds on bone matrix mineralization. (a) Quantitative evaluation of Alizarin Red staining after cetylpyridinium dissolution of calcium deposited by SAOS-2 cells cultured for 21 days in osteogenic condition in absence and in presence of different concentrations of Strontium Ranelate, Strontium Chloride and Sr100 nanoparticles. Diagram represent mean and SEM of three different experiments. (b) Pics of Alizarin Red stained wells of SAOS-2 cells untreated (Control) and treated for 21 days in osteogenic condition with Sr100 nanoparticles, SrCl<sub>2</sub> and Strontium ranelate at a Sr<sup>+2</sup> concentration of 1,25 mM, the concentration used in differentiation experiments.

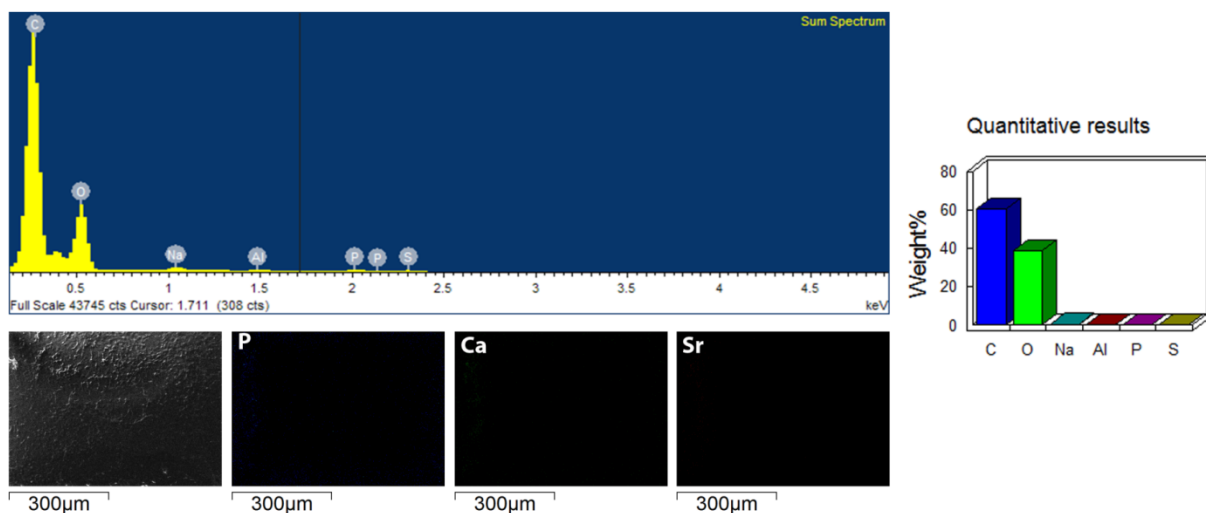


**Fig. 3.8a** Strontium determination in extracellular matrix. EDX spectrum, elemental maps and quantitative element results of SAOS-2 cultured in proliferative condition for 21 days. Showed results are representative of untreated, Ca100 and Sr100 nanoparticles treated samples.

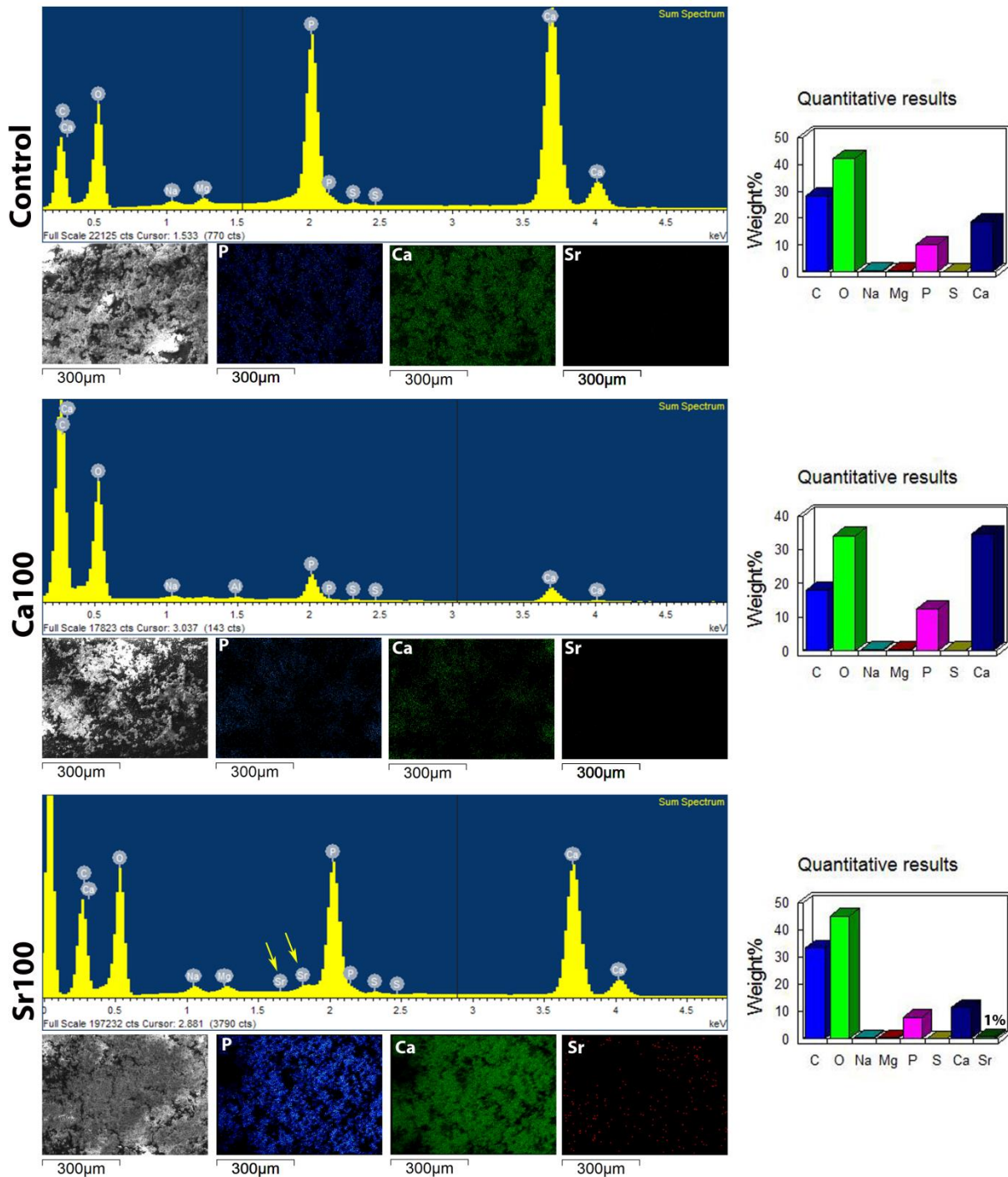


**Fig. 3.8b** Strontium determination in extracellular matrix. EDX spectra, elemental maps and quantitative element results of SAOS-2 cultured in osteogenic conditions for 21 days in absence (Control) and presence of Ca100 and Sr100 nanoparticles, yellow arrows point out Sr peaks.

Bone matrix proteins deposited by untreated and NPs treated SAOS-2 cells was also evaluated by ELISA assay. **Figure 3.9** shows results expressed as ratio of protein amounts measured in treated samples relate to untreated ones. An increase in deposition of all the tested proteins was detected in Sr100 treated samples cultured in both culture conditions. This increase was observed for type-I collagen, the main constituent of bone matrix, but also for bone marker proteins like ALP, OCN, DEC, OPN and ONT and the adhesive hFN. **Figure 3.10** shows immunolocalization of Osteocalcin

and Osteopontin in samples cultured in proliferative and osteogenic conditions, in the absence/presence of nanoparticles. Regarding osteocalcin deposition, it is possible to see a different localization of this protein in the 2 culture conditions: in particular in osteogenic medium, the green fluorescence seems to be localized in specific spots whereas in samples cultured in proliferative conditions a more diffuse fluorescence was observed. Also for osteopontin deposition, a more diffuse green fluorescence was observed in samples cultured in osteogenic conditions. No big differences, in terms of osteopontin expression, were observed between nanoparticles untreated and treated samples.

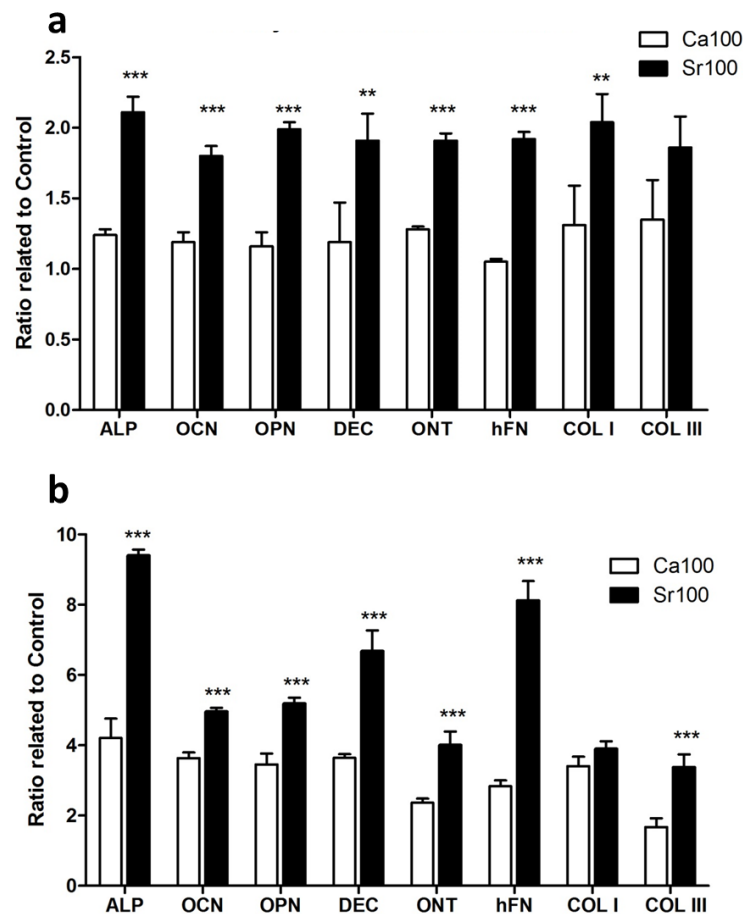


**Fig. 3.9** Effect of nanoparticles on extracellular matrix proteins deposition. Extracellular matrix proteins deposited by SAOS-2 cells cultured in proliferative (a) and osteogenic (b) conditions for 21 days in absence (control) and presence of Ca100 and Sr100 nanoparticles determined by ELISA assay. Results are expressed as ratio of treated samples related to control. Bars represent mean and SEM of three different experiments, statistical analysis performed between normalized Sr100 samples against normalized Ca100 samples (\*\* $p < 0,01$ , \*\*\* $p < 0,001$ )

Gene expression of specific markers of osteoblasts differentiation was evaluated in samples cultured in proliferative and osteogenic conditions, in absence/presence of NPs. **Figure 3.11** shows results of genes whose a significant difference was observed; fold increases were normalized to untreated samples. Regarding proliferative conditions, an increase in *ALP*, *COL1A1* and *OCN* gene expression in Sr100 treated samples was observed. In osteogenic conditions, the same genes were found up-regulated by Sr100 treatment together with *BMP2* and *DCN*. The expression of genes related to osteoblasts differentiation and ECM proteins seems to be positively affected by Sr treatment.

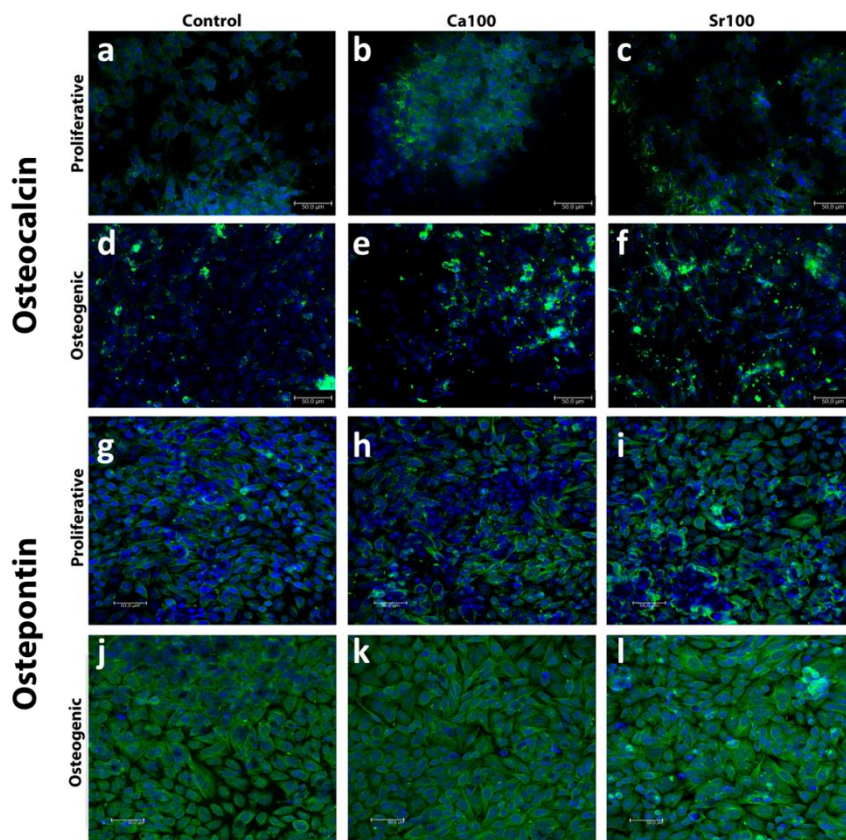


**Fig. 3.10** Effect of nanoparticles on extracellular matrix proteins deposition. Representative fluorescence images of samples immuno-stained (green) for osteocalcin (a – f) and osteopontin (g – l) deposited from SAOS-2 cells after 21 days in proliferative (a, b, c, g, h, i) and osteogenic (d, e, f, j, k, l) conditions in absence (a, d, g, j) and presence of Ca100 (b, e, h, k) and Sr100 (c, f, I, l) nanoparticles. Nuclei were counterstained with Hoechst 33342 (blue). Magnification 20X, scale bars represent 50µm..

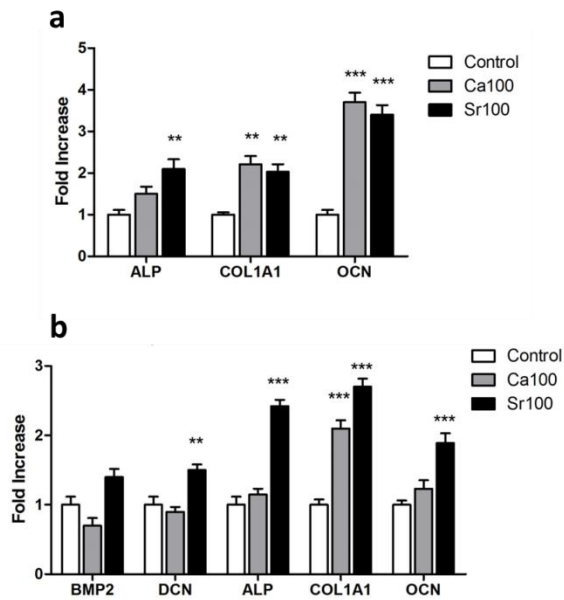


**Fig. 3.11** Gene expression of indicated bone specific markers as determined by qRT-PCR. SAOS-2 cells were cultured for 21 days in proliferative (a) and differentiative (b) condition in absence (Control) and presence of Ca100 and Sr100 nanoparticles. Relative expression was normalized on control. Bars indicated mean and SEM of three different experiments. Statistical analysis was performed against control (\*\*p<0,01, \*\*\*p<0,001)

### 4.3.2 Human Bone Marrow Mesenchymal Stem Cells (hBMMSCs)

#### *Cell viability, apoptosis, morphological observation and NPs uptake analysis*

A preliminary study about cell viability and apoptosis of hBMMSCs following treatment with different concentrations of Ca100 and Sr100 nanoparticles was performed to evaluate the cytotoxicity of NPs and to choose the effective concentration to be used in the succeeding experiments.

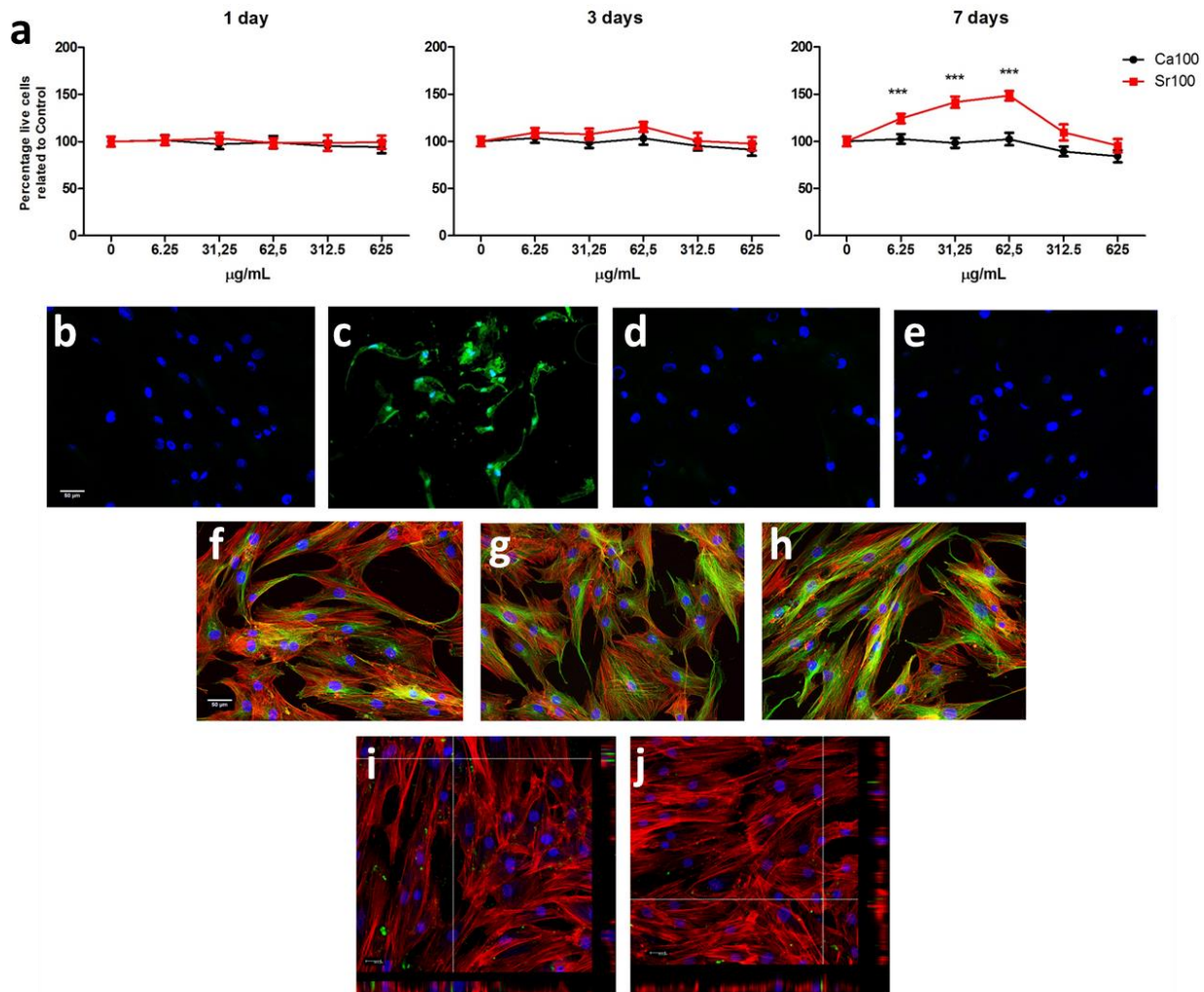


**Fig. 3.12** Effect of nanoparticles on BMMSCs viability, apoptosis and morphology. **a)** hBMMSCs viability evaluated by MTT test of untreated (control), Ca100 and Sr100 nanoparticles at different concentration after 1, 3 and 7 days. Results are expressed as percentage related to control, diagrams represent mean and SEM of three different experiments. Statistical analysis performed between normalized Sr100 samples against normalized Ca100 samples (\*\*\*p<0,001); **(b-e)** BMMSCs apoptosis evaluated by PSVue 480 staining (green) on untreated **(b)** cells, hydrogen peroxide **(c)**, 62,5 µg/mL Ca100 **(d)** and 62,5 µg/mL Sr100 **(e)** nanoparticles treated cells for 24h; **(f-h)** β-tubulin (green) and actin (red) filaments staining of untreated **(f)**, 62,5 µg/mL Ca100 **(g)** and 62,5 µg/mL Sr100 **(h)** nanoparticles treated hBMMSCs for 24h; **(i, j)** Representative CLSM images and orthogonal projection of hBMMSCs incubated for 24h with 62,5 µg/mL Ca100 **(i)** and 62,5 µg/mL Sr100 **(j)** nanoparticles conjugated with FITCH. Nuclei were counterstained with Hoechst 33342 (blue). All scale bars represent 50µm.

**Figure 3.12a** shows cell viability results obtained by MTT test of hBMMSCs treated with increased concentrations of Ca100 and Sr100 NPs for 1, 3 and 7 days, respectively. After 1 and 3 days, no differences between treated and untreated cells were observed, whereas, after 7 days, an increase around 20-50% in cell proliferation was observed in samples treated with concentrations ranging between 3.25 and 62.5  $\mu\text{g/mL}$  of Sr100 NPs ( $p < 0.001$ ). For higher Sr100 concentrations and for all Ca100 tested concentrations, no differences in cell viability were observed related to untreated samples ( $p > 0.05$ ).

In **Figure 3.12b-e**, PSVue 480 staining of 62.5  $\mu\text{g/mL}$  Ca100 (**Fig. 3.12d**) and Sr100 (**Fig. 3.12e**) treated samples are shown together with untreated (**Fig. 3.12b**) and  $\text{H}_2\text{O}_2$  treated (**Fig. 3.12c**) samples to evaluate cell apoptosis. The same analysis was performed for samples treated also with other nanoparticles concentrations, but no differences were observed related to those shown.  $\text{H}_2\text{O}_2$  treated samples were used as positive control, while untreated cells as negative control. No apoptosis was detected after 24h for both types of nanoparticles treatments at all concentrations since no green fluorescence was observed.

After 24h, cell morphology was evaluated in untreated and treated samples with 62.5  $\mu\text{g/mL}$  Ca100 or Sr100. To do that,  $\beta$ -tubulin and actin filaments were stained in green and in red, respectively. No significant differences were observed between untreated (**Fig. 3.12f**) and treated cells with Ca100 (**Fig. 3.12g**) and Sr100 (**Fig. 3.12h**), showing the typical fibroblast like morphology of hBMMSCs. Successively, nanoparticles uptake was evaluated after 24h. **Figure 3.12i-j** shows CLSM micrographs of hBMMSCs incubated with 62.5  $\mu\text{g/mL}$  of Ca100 (**Fig. 3.12i**) and Sr100 (**Fig. 3.12j**) of nanoparticles conjugated with FITCH. As already observed with SAOS-2 cells, after 24h FITCH-NPs were detected inside cells with no significant differences between Ca100 or Sr100 treatments.

#### *Effect of NPs on osteoblastic differentiation*

Effect of NPs on differentiation in osteoblasts was evaluated on cells cultured for 28 days in proliferative and osteogenic medium. **Figure 3.13a** shows ALP specific activity measured in samples of hBMMSCs treated with different concentrations of Ca100 and Sr100 NPs, cultured in osteogenic (continuous lines) and proliferative medium (dashed lines). Significant increase in ALP activity was observed in samples treated with 31.25 and 62.5  $\mu\text{g/mL}$  of Sr100 NPs in osteogenic conditions ( $p < 0.01$ ), whereas no differences were observed between Ca100 treated and untreated cells ( $p > 0.05$ ). For higher concentrations of Sr100 treatment, a significant decrease of ALP activity and a higher number of adipocytes (data not shown) were observed. Cells cultured in



proliferative conditions, in absence/presence of nanoparticles, did not show any differences in terms of ALP activity (dashed lines).

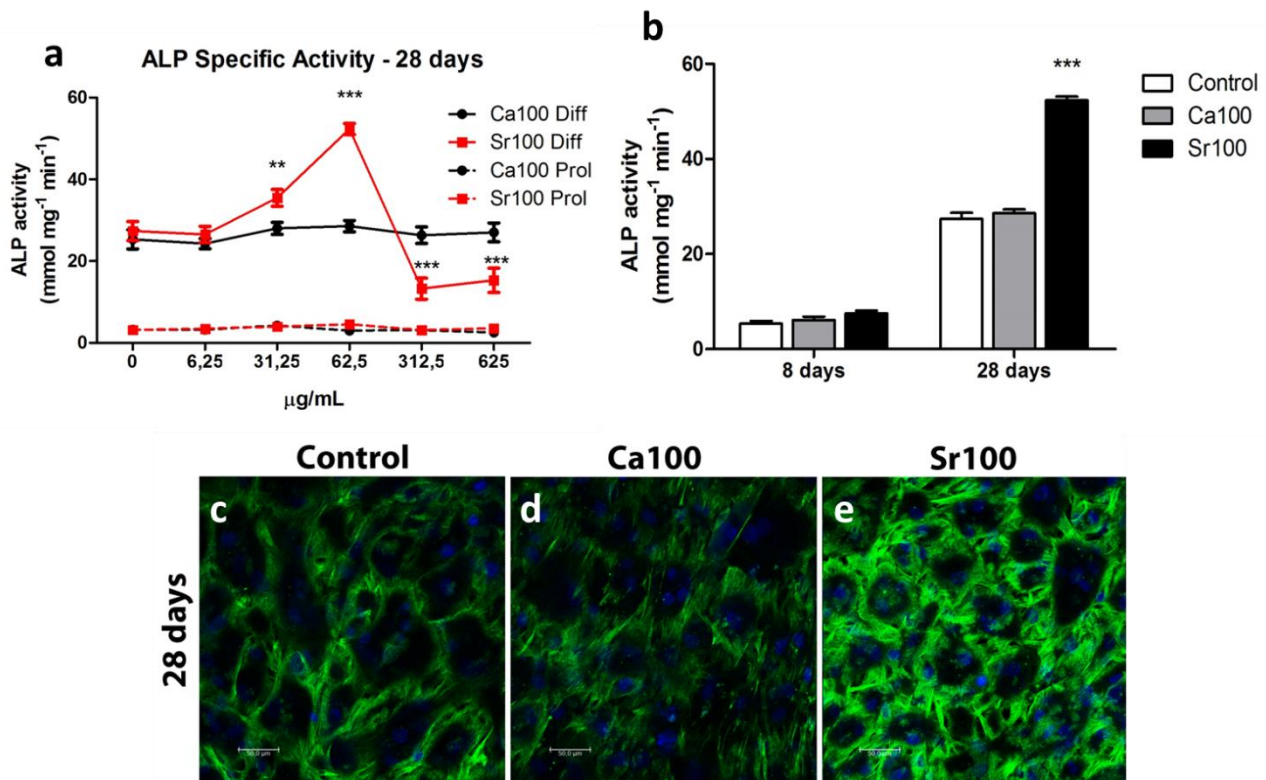


**Fig. 3.13** Effect of nanoparticles on ALP activity and deposition. a) ALP specific activity of untreated (control), Ca100 and Sr100 nanoparticles treated hBMMSCs for 28 days in osteogenic conditions. Results are expressed as percentage related to control. Diagrams represent mean and SEM of three different experiments. Statistical analysis performed between normalized Sr100 samples against normalized Ca100 samples (\*\* $p < 0,01$ , \*\*\* $p < 0,001$ ); b) ALP specific activity of untreated (control), Ca100 and Sr100 treated hBMMSCs for 8 and 28 days in osteogenic conditions. Bars indicate mean and SEM of three different experiments, statistical analysis were performed against control (\*\*\* $p < 0,001$ ); c) representative fluorescence images of ALP immunostaining (green) in sample cultured for 28 days in osteogenic condition, in absence (c) and presence of Ca100 (d) and Sr100 (e) nanoparticles. Nuclei were counterstained with Hoechst 33342 (blue). Magnification 40X, scale bars represent 50µm.

Since the 62.5 µg/mL showed the higher increase of cell proliferation and ALP activity, we choose to use this concentration for the succeeding studies.

**Figure 3.13b** shows ALP values of hBMMSCs differentiated for 8 and 28 days in absence and presence of Ca100 and Sr100 nanoparticles in osteogenic conditions. Data at 28 days confirmed the previous observations, whereas no differences were observed after 8 days when differentiation process seems to be not affected by nanoparticles treatment. Enzyme activity results were confirmed by immunolocalization of ALP observed by fluorescence microscope as shown in **Figure 3.13c-e**, where a more intense and diffuse green fluorescence was observed in Sr100 treated samples.

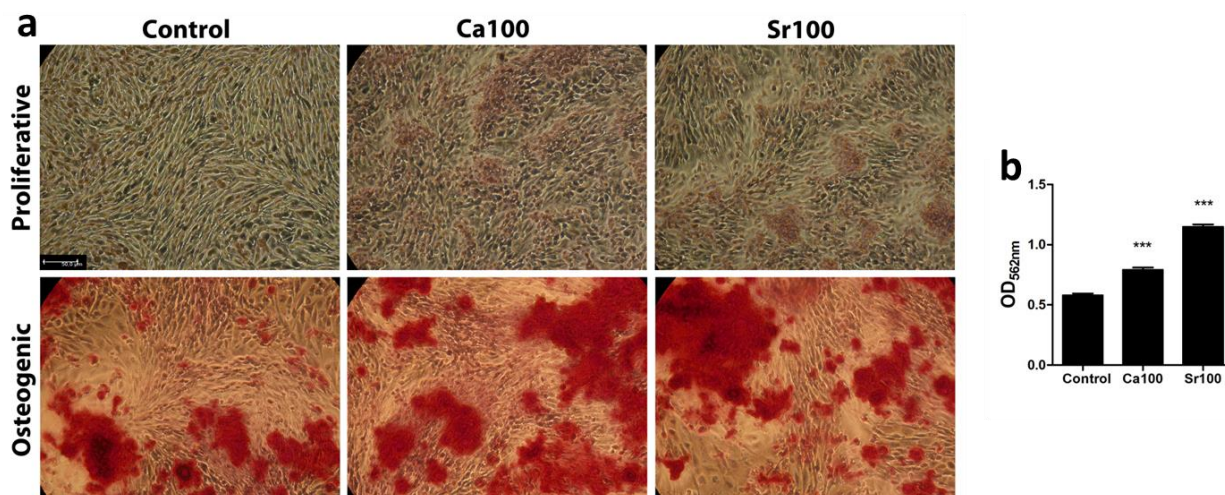


**Fig. 3.14** Effect of nanoparticles on bone matrix mineralization by hBMSCs. a) Representative images at optical microscope of hBMSCs cultured for 28 days in proliferative and osteogenic conditions, in absence and presence of Ca100 (b) and Sr100 nanoparticles and stained with Alizarin Red S for calcium deposits visualization. Magnification 10X, scale bars represent 50µm. b) Quantitative evaluation of Alizarin Red staining after cetylpyridinium dissolution of calcium deposited by hBMSCs cultured for 28 days in absence (Control) and presence of Ca100 and Sr100 nanoparticles in osteogenic condition. Bars represent mean and SEM of three experiments, statistical analysis performed against control (\*\*p<0,001)

Additional evaluation about NPs effect on calcified bone matrix after 28 days of treatment in proliferative and osteogenic conditions was evaluated. **Figure 3.14** shows Alizarin Red stained samples (**Fig. 3.14a**) and quantification of Alizarin red stained deposits after cetylpyridinium dissolution (**Fig. 3.14b**). An intense red staining in samples cultured in osteogenic conditions was observed unlikely to those cultured in proliferative conditions. Moreover, in Ca100 and Sr100 treated samples, a higher number and larger calcium deposits were observed and it was confirmed by absorbance reading at 562 nm after cetylpyridinium dissolution (**Fig. 3.14b**). These data suggest a positive effect of nanoparticles treatment, especially of Sr100, on bone matrix mineralization.

ECM proteins deposition was evaluated after 28 days in samples cultured in proliferative and osteogenic conditions in absence/presence of Ca100 and Sr100 nanoparticles by ELISA assay (**Fig. 3.15a**) and immunolocalizations of type-I collagen and osteocalcin were performed in samples cultured in osteogenic conditions (**Fig. 3.15b**). An increase of all tested proteins was observed in Sr100 treated samples cultured in osteogenic conditions. Instead, no differences were observed in those cultured in proliferative conditions. Quantitative results were corroborated by immunofluorescence observations, where a more intense and diffuse green fluorescence was observed for both the immunostained proteins.

In order to complete the panel of nanoparticles effects on osteoblasts differentiation from hBMSCs, gene expression of untreated and treated cells with Ca100 and Sr100 was evaluated after 28 days of culture in proliferative and osteogenic conditions. **Figure 3.16** shows results related

to genes, which showed significant differences. In proliferative conditions, the increase in *COL1A1* expression was observed in treated samples ( $p < 0.001$ ) while no differences of *ALP* gene expression was observed, confirming the enzyme activity results. A different situation was observed in samples cultured in osteogenic conditions where an increase of *ALP*, *COL3A1*, *Integrin binding Sialoprotein (IBSP)*, *OCN*, *DCN* and *RUNX2* were observed in treated samples showing a higher expression values for samples treated with Sr100 nanoparticles.

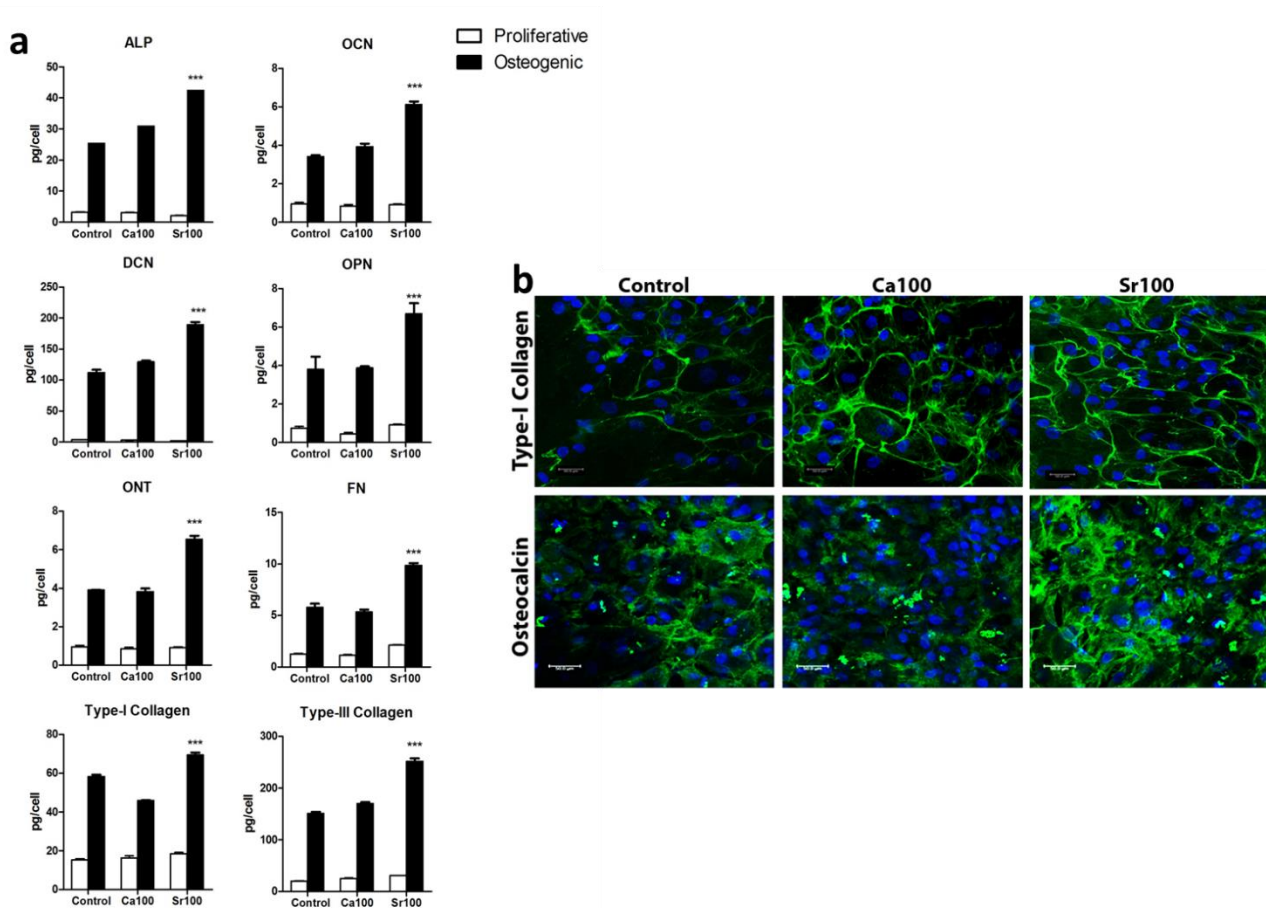


**Fig. 3.15** Effect of nanoparticles on extracellular matrix proteins deposition. a) Extracellular matrix proteins deposited by hBMSCs cultured in osteogenic condition for 28 days in absence (control) and presence of Ca100 and Sr100 nanoparticles determined by ELISA assay. Bars represent mean and SEM of three different experiments, statistical analysis performed against control (\* $p < 0,05$ , \*\* $p < 0,01$ , \*\*\* $p < 0,001$ ); b) Representative fluorescence images of samples immuno-stained (green) for type-I collagen and osteocalcin deposited by hBMSCs cultured for 28 days in osteogenic conditions in absence (Control) and presence of Ca100 and Sr100 nanoparticles. Nuclei were counterstained with Hoechst 33342 (blue). Magnification 20X, scale bars represent 50 $\mu$ m.

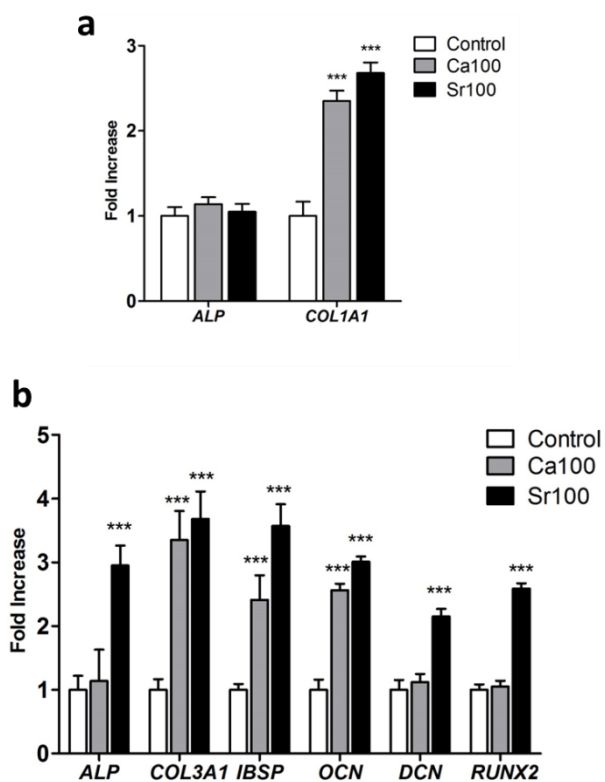


**Fig. 3.16** Gene expression of indicated bone specific markers as determined by qRT-PCR. hBMMSCs were cultured for 28 days in proliferative (a) osteogenic (b) conditions in absence (Control) and presence of Ca100 and Sr100 nanoparticles. Relative expression was normalized on control. Bars indicate mean and SEM of three different experiments. Statistical analysis was performed against control (\*\*p<0,001).

### 4.3.3 Osteocytes cell line Ocy454

#### *Effect of NPs on osteocytes differentiation and activity*

After the study of NPs effects on osteoblasts differentiation, influence of NPs on osteocytes was evaluated. To do that, we used an osteocyte cell line Ocy454 generated and kindly provided by Dr. Paola Divieti Pajevic (School of dental medicine, Molecular and cell biology – Boston University). Briefly, mice expressing the green fluorescent protein (GFP) under the control of dentin matrix protein 1 (8-kb DMP1-GFP) were mated with mice carrying a ubiquitously expressed SV40 large T antigen, and osteocytes

were isolated from the long bones of 4-week-old double transgenic mice. Two criteria were used to select mature osteocytic cell line: sorted GFP-positive were required to 1) have high levels of production of known osteocytic genes (*SOST* and *DMP1*) at the early time point of 14 days at the semipermissive temperature in the

absence of differentiation and 2) respond to the known effects of PTH stimulation by suppression of *SOST* and increased expression of *RANKL*. This method provided a heterogeneous population of DMP1-GFP-positive cells, which are known to be a mixture of cells with various degrees of *SOST* and *DMP1* expression depending on their age/maturation. From this population a more homogenous population called Ocy454 was obtained from single cell sub-clone isolation. Ocy454 cells have the same osteocyte marker expression and hormonal (PTH, PGE2, and shear stress) response<sup>13</sup>.

First of all, the 625 µg/mL concentration of nanoparticles was used for the experiments with Ocy454 since no effect in terms of bone mineralization was observed in sample treated with lower nanoparticles concentrations (data not shown). **Figure 3.17** shows Alizarin Red staining results of samples untreated and treated with Ca100, Ca50Sr50 and Sr100 nanoparticles for 3, 7 and 10 days, respectively. Bone matrix mineralization seems to be affected by nanoparticles treatment: in particular, after 7 days red spots were visible in treated samples (**Fig. 3.17a**) while no mineralization was detected in control; after 10 days, the treated samples showed a more intense

and diffuse red staining if compared to control. This increase was observed especially for strontium treated samples in a dose-dependent manner. Qualitative observations were confirmed by quantitative evaluation of absorbance values of Alizarin red stained calcium deposits after cetylpyridinium dissolution.

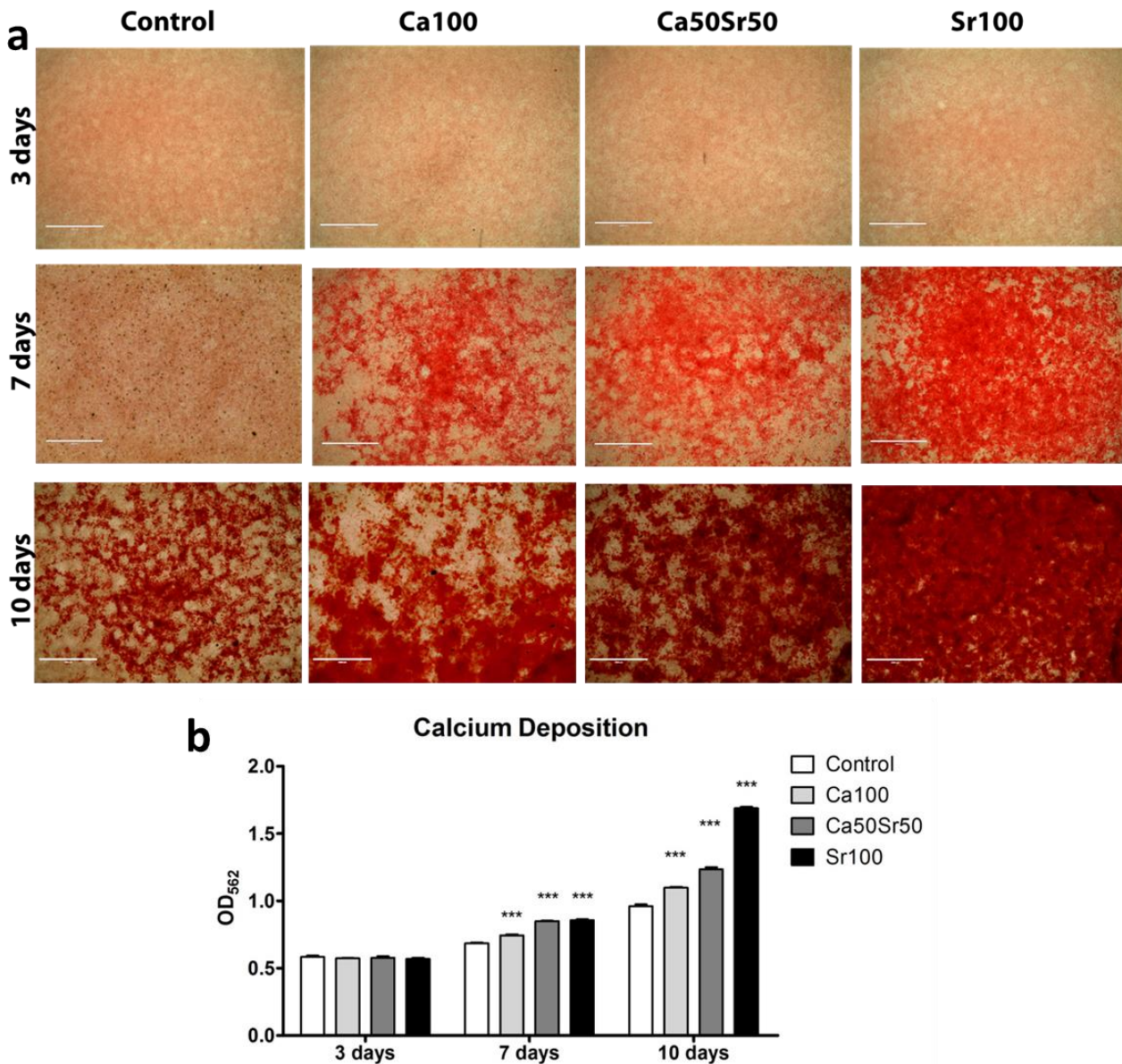


**Fig. 3.17** Effect of nanoparticles on bone matrix mineralization by osteocytes. Representative images at optical microscope of Ocy454 osteocytes cultured for 3, 7 and 10 days at 37°C, in absence (Control) and presence of Ca100, Ca50Sr50, and Sr100 nanoparticles and stained with Alizarin Red S for calcium deposits visualization. Magnification 10X, scale bars represent 100µm. **b**) Quantitative evaluation of Alizarin Red staining after cetylpyridinium dissolution of calcium deposited by Ocy454 osteocytes cultured for 3, 7 and 10 days in absence (Control) and presence of Ca100, Ca50Sr50 and Sr100 nanoparticles at 37°C. Bars represent mean and SEM of three experiments, statistical analysis was performed against control (\*\*p<0,001).

Beyond influence of nanoparticles on bone matrix mineralization, gene expression of untreated and nanoparticles treated samples was evaluated at 3, 7 and 10 days of treatment, respectively. **Figure 3.18** shows expression of *OCN*, *RANKL*, *DMP1*, *IBSP* and *SOST* in treated samples, normalized to untreated sample, over the time. An increase for all tested genes, except for *RANKL*, was observed in treated sample, especially for Sr100 treated ones. A different behaviour was observed for *RANKL*, where Sr treatment induced a decrease in gene expression at 3 and 7 days. **Figure 3.19** shows a similar gene expression results in a more detailed manner. It is noteworthy the *IBSP* expression after 7 days was around 250 times higher in Sr100 treated samples if compared to the other samples. Moreover, for all tested genes, strontium treatment seems to work in a dose-dependent way: Ca50Sr50 seems to be an intermediate condition between Ca100 and Sr100. The expression of the specific osteocytic marker *SOST*, was detected only after 10 days and an up-regulation in Sr100 treated samples was observed, suggesting a later differentiated stage induced by Sr treatment.

Preliminary results about possible molecular mechanisms involved in Sr100 nanoparticles action on Ocy454 were obtained using NPS2143 hydrochloride inhibitor, a selective CaSR antagonist. In particular, bone matrix mineralization was evaluated in samples untreated and treated for 7 days with Sr100 and NPS2143 hydrochloride Inhibitor. **Figure 3.20** shows representative images of

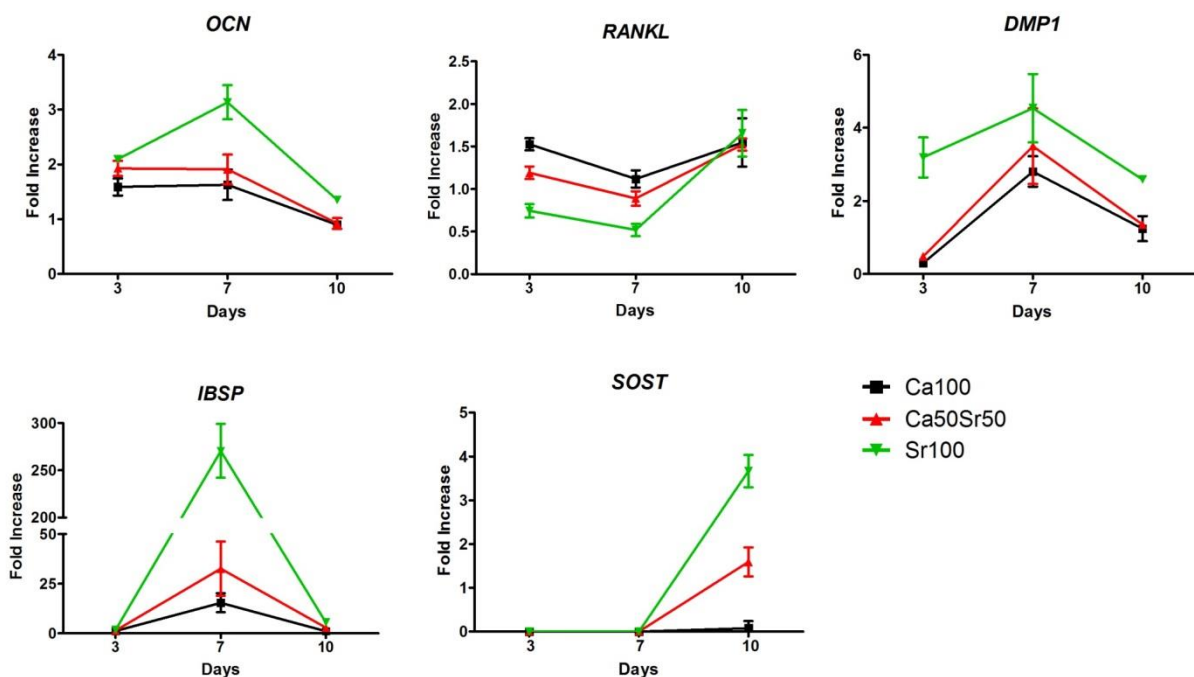


**Fig. 3.18** Gene expression over the time of indicated genes determined by qRT-PCR. Ocy454 were cultured for 3, 7 and 10 days at 37°C in absence and presence of Ca100, Ca50Sr50 and Sr100 nanoparticles. Relative expression was normalized against untreated samples.

Alizarin Red stained samples (**Fig. 3.20a-d**) and quantitative evaluation of Alizarin Red stained calcium deposits after cetylpyridium dissolution. Treatment with inhibitor reduces drastically bone matrix mineralization both in the presence and in the absence of Sr100 nanoparticles.

Additionally, we treated cells with Sr100 nanoparticles for 7 days while inhibitor treatment was performed only from day 1<sup>st</sup> to day 3<sup>rd</sup> and from day 4<sup>th</sup> to day 7<sup>th</sup> and then Alizarin red staining was used to evaluate bone matrix mineralization (**Fig. 3.21**). We observed that samples treated in the first three days of culture with inhibitor, showed a similar bone matrix mineralization level of samples treated with inhibitor for all the 7 days (**Fig. 3.21a-b**). On the other hand, samples treated with NPS2143 hydrochloride inhibitor in the last three days of differentiation showed bone matrix mineralization similar to samples without inhibitor (**Fig. 3.21c-d**). Since no bone matrix mineralization was observed in untreated and treated samples at day 3 (**Fig. 3.17a**), the mineral deposition observed in the latter samples occurred from day 3 to day 7.

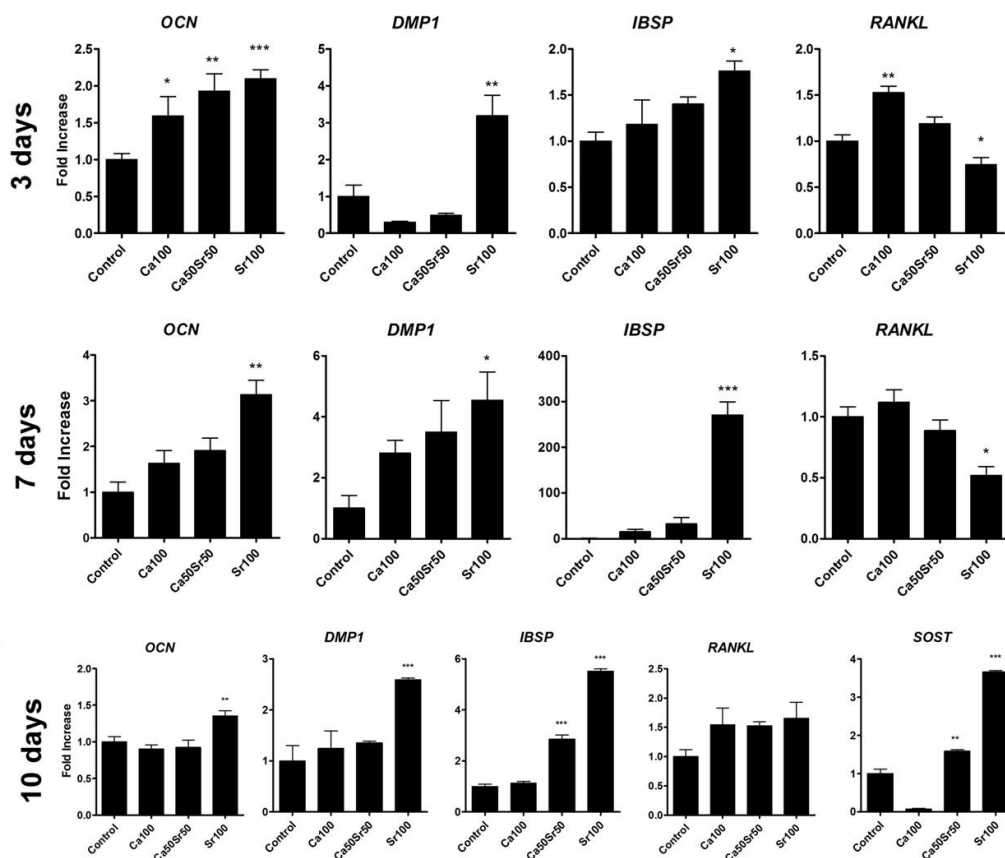


**Fig. 3.19** Gene expression of indicated genes determined by qRT-PCR. Ocy454 were cultured for 3, 7 and 10 days at 37°C in absence and presence of Ca100, Ca50Sr50 and Sr100 nanoparticles. Relative expression was normalized against untreated samples. Bars indicated mean and SEM of three different experiments. Statistical analysis was performed against control (\* $p < 0,05$ ; \*\* $p < 0,01$ ; \*\*\* $p < 0,001$ ).

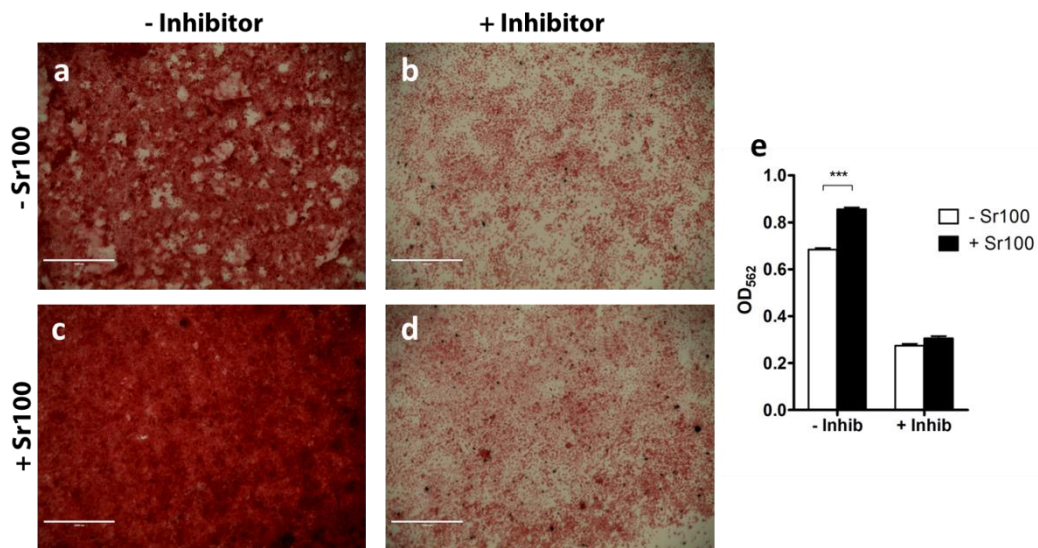


Fig. 3.20 Effect of nanoparticles in presence of CaR inhibitor on bone matrix mineralization. (a – d) Representative images at optical microscope of Alizarin Red S stained samples of Ocy454 osteocytes cultured for 7 days in absence (a, c) and presence (b, d) of NPS 2143 hydrochloride, in absence (a, b) and presence (c, d) of Sr100 nanoparticles. Magnification 10X, scale bars represent 100µm. e) Quantitative evaluation of Alizarin Red staining after cetylpyridinium dissolution of calcium deposited by Ocy454 Osteocytes cultured for 7 days in absence and presence of NPS 2143 hydrochloride, in absence and presence of Sr100 nanoparticles. Bars indicate mean and SEM of three different experiments. Statistical analysis was performed between nanoparticles treated samples against untreated ones (\*\*\*) $p < 0,001$ .

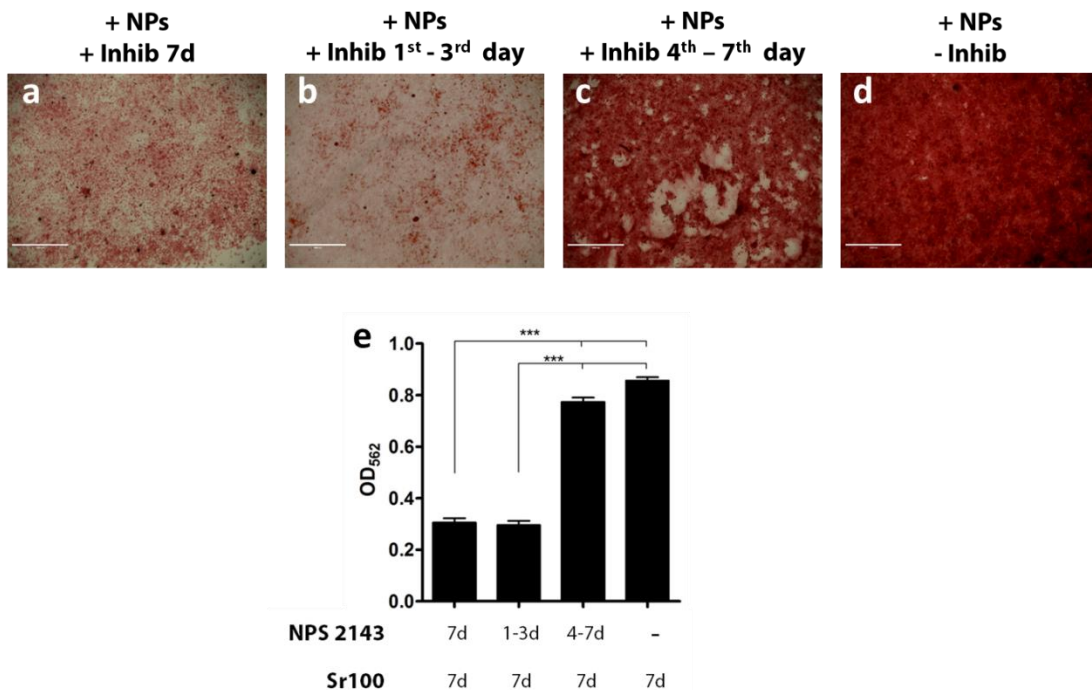
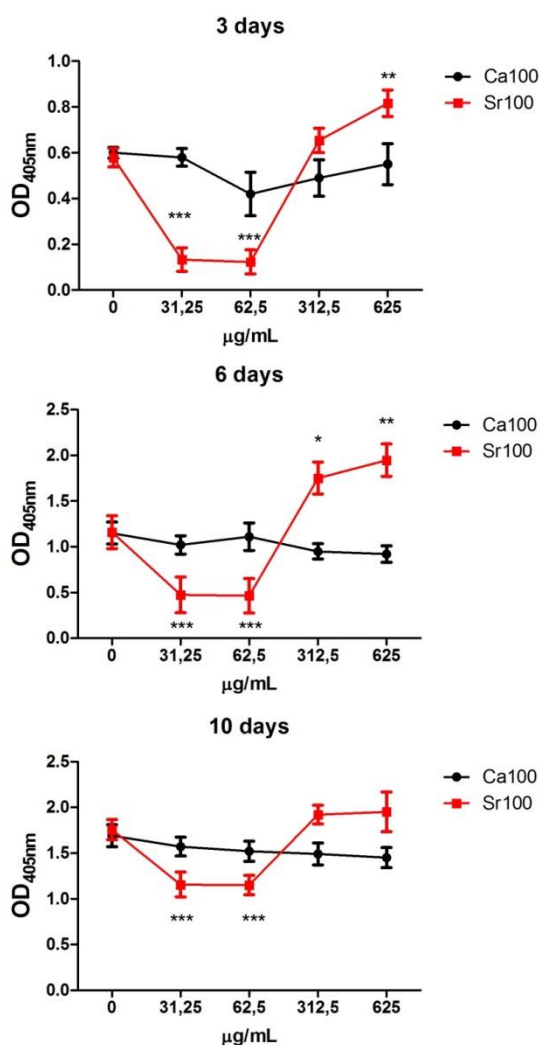


Fig. 3.21 Effect of nanoparticles on bone matrix mineralization deposited by Ocy454 treated at different time points with CaR inhibitor. (a – d) Representative images at optical microscope of Alizarin Red S stained samples of Ocy454 cultured for 7 days in presence of Sr100 nanoparticles, in absence (d) and presence of NPS 2143 hydrochloride for 7 days (a), from day 1 to day 3 (b) and from day 4 to day 7 (c) of culture. Magnification 10X, scale bars represent 100µm. e) Quantitative evaluation of Alizarin Red staining after cetylpyridinium dissolution of calcium deposited by Ocy454 cultured for 7 days in presence of Sr100 nanoparticles, in absence and presence of NPS 2143 hydrochloride for 7 days, from day 1 to day 3 and from day 4 to day 7 of culture. Bars indicate mean and SEM of three different experiments. Statistical analysis was performed between all groups (\*\*\*) $p < 0,001$ .



#### 4.3.4 Murine macrophage RAW264.7 cell line



**Fig. 3.22** Effect of nanoparticles on osteoclasts differentiation. TRAP enzyme activity of RAW 264.7 cells cultured for 3, 6 and 10 days in presence of 50ng/mL RANKL, in absence (control) and presence of different concentration of Ca100 and Sr100 nanoparticles. Diagrams indicate mean and SEM of three different experiments. Statistical analysis was performed on Sr100 treated samples against Ca100 ones (\* $p < 0,05$ , \*\* $p < 0,01$ , \*\*\* $p < 0,001$ )

The murine macrophage RAW264.7 cell line, treated with soluble RANKL for osteoclasts differentiation, was the last *in vitro* model used to study the effect of nanoparticles on bone remodelling. Preliminary studies were performed to assess the best concentration of RANKL to obtain multinucleated TRAP positive cells. In particular, a range of concentrations was tested and 50 ng/mL was selected and used for the following experiments (data not shown).

To study the effect of Ca100 and Sr100 nanoparticles on osteoclasts differentiation, NPs concentrations from 31.25 to 625 µg/mL were tested with RAW264.7 cultured in presence of 50 ng/mL of RANKL for 3, 6 and 10 days, respectively. TRAP enzyme was used as osteoclasts differentiation marker and its activity in the cell culture media was evaluated (**Fig. 3.22**). At all three tested times, samples treated with 31.25 and 62.5 µg/mL of Sr100 nanoparticles showed a decrease in TRAP activity ( $p < 0.001$ ), whereas for higher doses of Sr100 NPs concentration an opposite effect was observed. No differences were observed for Ca100 treated samples at all tested concentrations. Starting from these results, 62.5 µg/mL was used for the following experiments.

To evaluate the effects on osteoclasts differentiation of Ca100 and Sr100 nanoparticles,

RAW264.7 were cultured for 10 days in absence/presence of 50 ng/mL of RANKL and then treated with Ca100 and Sr100 NPs. After 10 days of culture, samples were fixed with paraformaldehyde, stained for TRAP and nuclei counterstained with Hoechst 33342 (**Fig. 3.23**). Samples cultured in the presence of RANKL showed multinucleated TRAP positive cells (**Fig. 3.23b**) whereas for samples cultured in absence of RANKL, no positive TRAP cells were observed (**Fig. 3.23a**).

Samples treated with Ca100 showed small osteoclasts-like cells (**Fig. 3.23c**) whereas Sr100 treated samples showed very few multinucleated cells (**Fig. 3.22d**). Treatment with nanoparticles induced a reduction in osteoclasts size ( $p < 0.001$ ) and the number of nuclei per osteoclasts ( $p < 0.001$ ) whereas only Sr100 treatment reduced significantly the number of osteoclasts per well ( $p < 0.001$ ) (**Fig. 3.22e**). Multinucleated cells with at least three nuclei were counted as osteoclasts.

Gene expression of five osteoclasts specific markers were evaluated in untreated/treated cells with Ca100 and Sr100, being cultured for 10 days in presence of RANKL. **Figure 3.24** shows relative gene expression normalized to samples at time zero. Expression of Acid Phosphatase 5 (*ACP5*), *CD44* and *NFATc1* were down-regulated by Sr100 treatment while no differences were observed for Cathepsin K (*CTSK*) gene expression between untreated and treated samples.

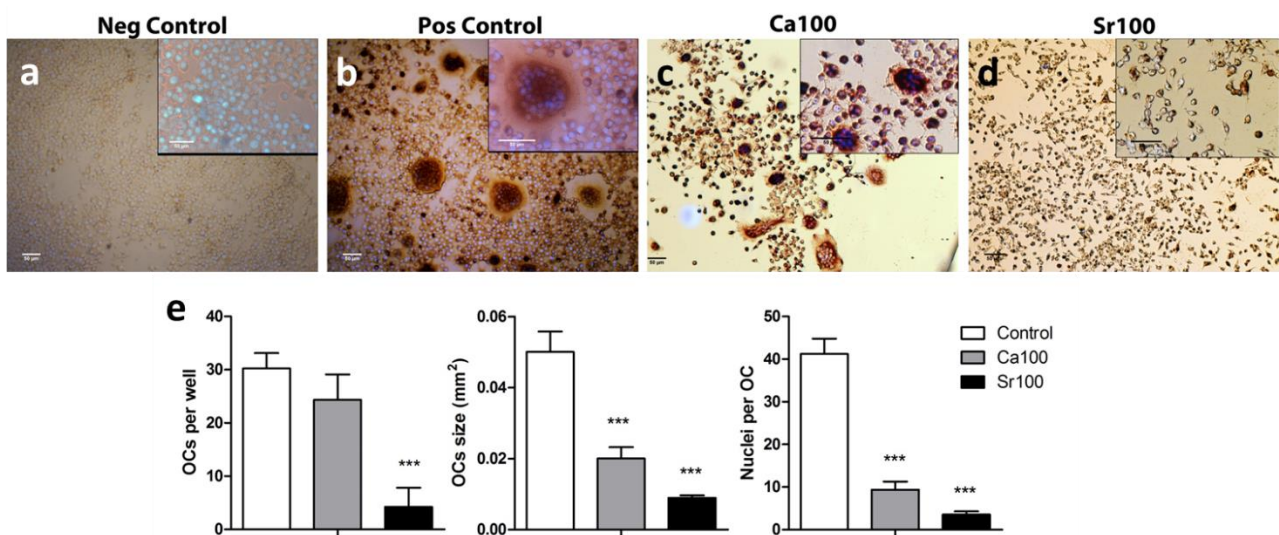


**Fig. 3.23** Effect of nanoparticles on osteoclasts differentiation and morphology. (a-d) Representative images of TRAP stained RAW 264.7 cells cultured in absence (a) and presence (b-d) of RANKL, in absence (b) and presence of Ca100 (c) and Sr100 (d) nanoparticles. Magnification 10X (insert 20X), scale bars indicate 50µm; e) Number, size and nuclearity of osteoclasts-like cells from RAW 264.7 cultured for 10 days in presence of RANKL, in absence (control) and presence of Ca100 and Sr100 nanoparticles. Bars indicate mean and SEM of three different experiments. Statistical analysis was performed against control (\*\*\*) $p < 0.001$ .

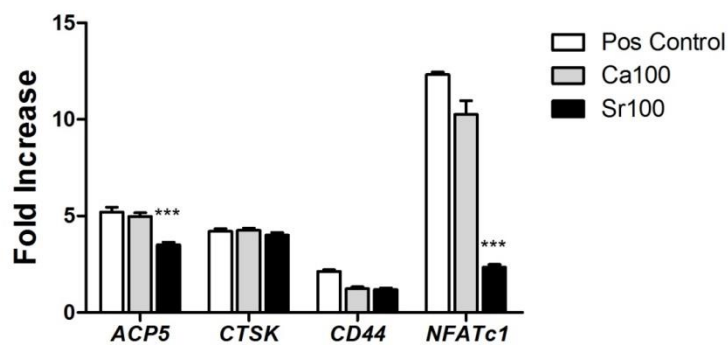


**Fig. 3.24** Gene expression of indicated osteoclasts specific markers as determined by qRT-PCR. RAW264.7 cells were cultured for 10 days in presence of RANKL (Pos Control) and treated with Ca100 and Sr100 nanoparticles. Relative expression was normalized on samples at time zero. Bars indicated mean and SEM of three different experiments. Statistical analysis was performed against control (\*\*\*) $p < 0.001$

## 4.4 Discussion

The effect of strontium containing nanoparticles on bone remodeling was evaluated *in vitro*. We used four *in vitro* models to mimic bone cells and to study the effect of NPs treatment on their activity and differentiation. The first two *in vitro* models were osteoblasts-like SAOS-2 cell line and human Mesenchymal Stem cells isolated from Bone Marrow. These two cell types allowed us to study the effect of the nanoparticles on osteoblasts differentiation and activity.

SAOS-2 is a cell line widely used to study osteoblasts differentiation due to their ability to produce mineralized bone matrix and the expression of several osteoblasts markers like RUNX2, OCN, BMP2 and ALP<sup>28</sup>. Due to their ability to grow indistinctly, we used SAOS-2 cells for preliminary studies about NPs cytocompatibility, dose-dependence and NPs uptake studies. After the evaluation of cell proliferation induced by NPs described in the previous chapter, we studied the interaction between nanoparticles and osteoblasts-like SAOS-2 cells investigating the nanoparticles uptake and the pathway involved in this process. One of the most important issue in the field of nanotechnology is the size effect on the bio-distribution, kinetic of release, and cellular uptake of nanoparticles<sup>29,30</sup>. In our studies, we demonstrated that NPs internalization occurs after 24h with different times for Ca100 and Sr100 nanoparticles. Ca100 seems to be uptake by cells in a shorter time, probably due to their smaller size. The uptake pathway activated by NPs seems to be the macropinocytosis since the presence of the inhibitor amiloride produced a significant reduction of FITC-NPs internalization. Macropinocytosis comprises a series of events initiated by extensive plasma membrane reorganization or ruffling to form an external macropinocytic structure that is then enclosed and internalized. Macropinosomes share many features with phagosomes and both are distinguished from other forms of pinocytic vesicles by their large size, morphological heterogeneity and lack of coat structures<sup>31</sup>. Macropinocytosis is dependent on microtubule function because these elements are involved in plasma membrane ruffling and also are necessary for transport of GTPases that mediate macropinocytosis to specific plasma membrane domains where they can be activated<sup>32</sup>. The pronounced effect of amiloride, which inhibits macropinocytosis by lowering submembranous pH and preventing Rac1 and Cdc42 signaling<sup>33</sup>, demonstrates that this endocytosis mechanism is the main process for NPs entry into SAOS-2 cells. Moreover, the dimensions of Ca100 and Sr100 NPs fit perfectly with macropinosomes that have a diameter in a range of 0.2 to 5  $\mu\text{m}$ <sup>34</sup>. Another inhibitor that we used is Chlorpromazine, an inhibitory drug known to interfere with clathrin-mediated endocytosis, by disrupting the assembly of the clathrin lattice, forming the endocytic pit at the plasma membrane<sup>19</sup>. The average diameter of the clathrin-coated vesicles is around 100 nm<sup>35</sup>. Finally, the third used inhibitor, indomethacin, blocks the internalization of caveolae and the return of plasmalemmal vesicles<sup>10,18</sup>. These pathway vesicles

have an approximate diameter of 60 nm in size<sup>36</sup>. In both cases, diameters of vesicle are much smaller than Ca100 and Sr100 NPs, and this can explain why these pathways were not involved in NPs uptake.

From a quantitative point of view, we evaluated Ca100 and Sr100 NPs uptake measuring amount of intracellular Ca and Sr elements in untreated and treated samples. Knowing the amount of nanoparticles we added in the culture media, we calculated an 80% uptake of nanoparticles by cells. Although the most interesting result is the Ca amount increase we found in Sr100 NPs treated samples. In fact, while in Ca100 treated cells the intracellular Ca increase could be related to nanoparticles uptake, in Sr100 treated ones the intracellular Ca amount increase seems to be a direct consequence of the Sr treatment. Calcium ions are regulators of many cellular processes; notably, these include the events that will decide the fate of a cell: survival, proliferation, motility, apoptosis, and differentiation<sup>37</sup>. One of these processes is the cell proliferation. Increases in cytosolic free calcium concentration are associated with the progression through the cell cycle: the exit from quiescence in early G1 phase, the G1/S transition, and other checkpoints during S and M phases<sup>38,39</sup>. Calcium exerts its regulatory role by acting as a ubiquitous allosteric activator or inhibitor of several intracellular enzymes in the cytosol, in the organelles, and in the nucleus. Some proteins (calcium binding proteins), other than enzymes, bind to calcium with different affinities and act as calcium buffers, thus limiting its diffusion. Other proteins do not have intrinsic enzymatic activity but, after their interaction with the ion, regulate calcium-dependent enzymes and ion channels. The best known example is calmodulin, probably the most relevant calcium decoder for cell proliferation: it regulates, among others, the family of calcium-calmodulin dependent kinases type II (CaMKII) and several membrane channels. A great amount of data points out to a direct involvement of CaMKII at several transition points during cell cycle progression<sup>39</sup>. Calcium-dependent enzymes also regulate the activation of several nuclear factors involved in the DNA division machinery, for example cdk and cyclins<sup>40</sup>. The observed increase of intracellular Ca in Sr treated samples, could be directly correlated with the detected increase of proliferation. Further investigations are needed to clarify and confirm this point but this increase could be related also to the results observed on cells differentiation.

A similar behaviour to SAOS-2 cells was observed also on hBMMSCs proliferation treated with Sr100 for 7 days. In particular, the increase in proliferation was observed after 7 days of treatment confirming an already documented *in vitro* effect of strontium on cell proliferation after long treatment<sup>41-43</sup>. Higher doses of Sr did not affect cell proliferation and neither induced cell apoptosis or death confirming nanoparticles high cytocompatibility. hBMMSCs morphology was not affected by nanoparticles treatment and, also with these cells, complete NPs uptake was detected after 24h.

A temporal and functional pattern of gene expression characterizes the osteoblast maturation process, which can be divided into proliferation, differentiation, and mineralization stages<sup>44</sup>. Strontium treatment not only affects osteoblast cellular proliferation, but also increased expression of bone marker genes during differentiation and mineralization, and enhances calcified matrix deposition. The first parameter that was taken into account was the ALP activity. ALP expression has been demonstrated to increase during osteoblasts differentiation and decrease when cells reach very late differentiation stage through osteocytes<sup>45</sup>. Enzyme activity increase was observed in Sr treated sample both in SAOS-2 or hBMMSCs culture, at the end of the differentiation process. ALP increase was also observed in SAOS-2 cells cultured without osteogenic factors while in proliferative conditions very low ALP activity was detected in untreated and nanoparticles treated hBMMSCs. This is because SAOS-2 cells even if not cultured in the presence of osteogenic factors show pre-osteoblasts features, like a basal ALP activity<sup>28</sup>, while hBMMSCs if not cultured in presence of osteogenic factors, keep their characteristic of stem cells. Besides the increased ALP activity, also an increase in ALP gene transcription and translation were observed in strontium treated samples. At the end of culture, in Sr100 treated SAOS-2 and hBMMSCs cells, increased expression of *ALP* gene was observed together with an increase in ALP protein deposition, as evaluated by ELISA assay. ALP is recognized as an important component in hard tissue formation and it is highly expressed in mineralized tissue cells. Osteoblast cells grown with ascorbic acid sequentially express osteoblastic marker proteins such as ALP and then form a mineralized ECM as a consequence of osteoblastic differentiation. The importance of ALP in the mineralization of ECM has been previously reported<sup>46</sup>. Its mechanism of action is not completely known, but it appears to promote both the local concentration of inorganic phosphate, a mineralization promoter, and to decrease the concentration of extracellular pyrophosphate, an inhibitor of mineral formation<sup>46</sup>.

In order to study the effect of nanoparticles on ECM deposition, the fundamental bone matrix constituents such as type-I and -III collagen, decorin, osteopontin, osteocalcin, osteonectin, and fibronectin were investigated. In both SAOS-2 and hBMMSCs samples, a higher deposition of these proteins were detected at the end of culture time. Similar increments were found in SAOS-2 cells cultured in proliferative and osteogenic conditions while, regarding hBMMSCs, differences in protein deposition were detected only in samples cultured in osteogenic conditions. The Sr100 treatment increased the deposition of type-I collagen in SAOS-2 cells cultured in proliferative conditions and in hBMMSCs cultured in osteogenic conditions. Bone type-I collagen is the most abundant protein in the bone matrix and is known to be up-regulated at the proliferation stage of osteoblasts<sup>44,47</sup>. Type-III collagen and decorin are known to be associated with type-I collagen<sup>48</sup> and higher amount of these proteins were found in Sr100 treated samples. Appreciable differences for

other bone matrix proteins such as osteonectin, fibronectin, osteopontin and osteocalcin were observed between Sr100 treated and untreated or treated with Ca100 samples. All of these ECM proteins are organic components of bone and are implicated in bone formation and remodelling. Osteopontin is known to play an important role in cell attachment<sup>49</sup> and calcification of mineralized tissue<sup>50</sup>, whereas osteocalcin<sup>51</sup> is the most recently identified secreted ECM protein. Osteonectin is a calcium and collagen-binding ECM glycoprotein and also acts as a modulator of cell–matrix interactions<sup>52</sup>. The role of fibronectin is important considering that it is reported to promote both cell adhesion and proliferation in many cell types<sup>52,53</sup>. In view of these information, macroscopic increases in *in vitro* protein levels of ALP (that makes the phosphate available for calcification), osteopontin (that anchors bone cells via their  $\alpha_v\beta_3$  integrin to the mineralized bone surface), osteocalcin (a marker of formed bone tissue), and type-I and -III collagens (the major organic components of bone matrix produced by osteoblasts) were more evident for osteoblasts treated with Sr100 nanoparticles. All together these results suggest that the main effect of Sr100 NPs is a greater efficiency in promoting bone ECM deposition.

Interestingly, the qRT-PCR analysis showed an increase of bone markers gene expression both in SAOS-2 and hBMMSCs cells treated with Sr100 NPs. Genes related to ECM proteins like *COL1A1*, *COL3A1*, *OCN*, *DCN* were up-regulated by Sr100 treatment supporting proteins results. Together with these genes, in hBMMSCs also the *IBSP* was found up-regulated by nanoparticles treatment, especially by Sr100 nanoparticles. *IBSP* gene codify for bone sialo protein (BOSP), which is a significant component of the bone ECM and is suggested to constitute approximately 8% of all non-collagenous proteins found in bone and cementum. Furthermore, we decided to evaluate the gene expression level of *RUNX2*, also known as core binding factor 1 (cbfa1; subsequently renamed Runx2 as runt-related transcription factor 2)<sup>54</sup>. Runx2 is a transcriptional factor involved in osteoblastic and skeletal morphogenesis. Runx2 has an essential role in the maturation of osteoblasts by binding to its target promoters and enhancers of various other bone-specific target genes, including collagen type-I, osteopontin, and bone sialoprotein through its runt homology domain<sup>55,56</sup>. The *RUNX2* gene expression is strictly correlated with the cell ability to differentiate towards osteoblasts and it was enhanced by Sr100 nanoparticles treatment of hBMMSCs cultured in osteogenic conditions. Since Runx2 is considered the transcriptional target of Wnt/ $\beta$ -catenin pathway<sup>57</sup>, its up-regulation in Sr100 treated samples is in line with previous works where it was demonstrated that Sr enhances bone formation *in vitro* and *in vivo* through Wnt/ $\beta$ -catenin pathway<sup>58</sup>.

In summary, the increased transcription of these genes could indicate that Sr100 nanoparticles drive a more rapid commitment of stem cells toward osteoblastic differentiation.

The increases in transcript levels of the *IBSP*, *OSC*, and *DCN* genes and in the deposition of osteopontin, osteonectin and osteocalcein were supported by the mineralization data. Quantitative analysis of the calcium mineral content in ECM deposited at the end of the culture time in SAOS-2 and hBMMSCs samples showed an increase around 1.5 and 2 times of mineralization in Sr100 treated samples. Mineralization of ECM is the most important feature of the bone matrix and Sr100 nanoparticles seems to improve calcium deposition as shown by Alizarin Red staining. It is quite clear that in both *in vitro* models, mineralization occurred only in presence of osteogenic factors and not in proliferative medium. Moreover, we compared the effect on ECM mineralization of Sr100 nanoparticles with strontium ranelate and strontium chloride. To do that, we used different concentration on these three strontium-containing compounds to ensure the same doses of Sr<sup>+2</sup> to SAOS-2 cells. The results suggested that samples treated with Sr100 nanoparticles presented a more calcified matrix than those cultured in presence of strontium ranelate and strontium chloride. It has been already reported that strontium can enhance ECM mineralization *in vitro* and that it is used by cells in ECM mineralization<sup>59,60</sup>. Also in our study we demonstrated that SAOS-2 cells deposited strontium in the ECM, suggesting that after Sr100 nanoparticles uptake, strontium takes part to the mineral deposition. In this way, the ECM deposited by Sr100 treated osteoblasts resulted enriched in strontium and this could reduce its resorption by osteoclasts. It has been already demonstrated that osteoclasts-like cells viability, differentiation and resorption activity is reduced when they are cultured on scaffolds made of strontium enriched coatings<sup>61</sup>.

In summary, all these results about the effects of nanoparticles on osteoblasts differentiation suggest that Sr100 NPs improved SAOS-2 and hBMMSCs proliferation and their differentiation towards mature osteoblasts. The treatment with Sr100 nanoparticles enhanced ECM proteins deposition and the process of matrix mineralization. We observed a whole positive effect of Sr100 nanoparticles on osteoblasts viability, differentiation and activity.

The *in vitro* effect of strontium on bone remodelling is widely investigated with osteoblasts and osteoclasts cultures. Not many data are present in literature about the effect on osteocytes because of less available *in vitro* models to study this cell type. We studied the effect of Sr100 nanoparticles on the osteocyte cell line Ocy454 produced and kindly provided by Dr. Paola Divieti Pajevic. In particular, they generated a novel osteocytic cell line Ocy454 that recapitulates known *in vivo* osteocytic functions without the requirement for long term high density cultures and in the absence of differentiation medium. These cells were isolated from long bones of double transgenic mice expressing both a GFP under the *DMP1* promoter and a temperature-sensitive large T antigen. These cells can be cultured for a long period of time at permissive conditions (33 °C) without losing

their phenotypic characteristics and then can rapidly recapitulate a mature osteocytic phenotype after 10–12 days in culture at semipermissive conditions (37 °C). As expected for an osteocyte, these cells express high levels of *SOST*/sclerostin, *DMP1*, *Phex*, and *E11*, whereas they have undetectable levels of the osteoblastic marker keratocan at all time points. Thus, in contrast to currently available osteocytic cell lines (MLO-Y4 and IDG-SW3 for example), the uniqueness of these cells is their expression of mature osteocytic genes in the absence of differentiation factors at early time points, suggesting that these cells display a mature osteocytic phenotype in a shorter experimental time frame<sup>13</sup>. All these features make Ocy454 a perfect model to study the effect of Sr100 nanoparticles also on osteocytes differentiation.

In the first instance, we observed increased bone matrix mineralization by Ocy454 treated with Sr100 nanoparticles if compared to Control, Ca100 and Ca50Sr50 nanoparticles. This data suggests that Sr100 nanoparticles enhanced the calcium deposition not only during earlier osteoblasts differentiation stages, as observed with hBMMSCs, but even in later maturation of osteoblasts toward osteocytes. However, we observed that the Sr100 nanoparticles effective dose on Ocy454 was ten times higher than the one effective on hBMMSCs. At lower doses, in fact, no effect on bone matrix mineralization was observed. This could be due to a different uptaking rate between the two cell types or to a different Sr dosage necessary to observe an effective effect.

Results that are more interesting were obtained by qRT-PCR analysis, where several osteocytic marker genes were evaluated. Osteocytes do not normally express alkaline phosphatase but do express osteocalcin<sup>62</sup> and, in Sr100 treated Ocy454, higher expression of *OCN* and *IBSP* were detected. Related to bone matrix mineralization is *DMP1* expression that was up-regulated by treatment with Sr100 nanoparticles if compared to untreated, or Ca100 and Ca50Sr50 treated Ocy454 cells. *DMP1* is a protein that has been recently proposed as Small, Integrin-Binding Ligand, N-linked Glycoprotein. The members of this family also include bone sialoprotein, osteopontin, dentin sialophosphoprotein and they share similar biochemical features, such as the presence of relatively large amounts of sialic acid and phosphate and the RGD cell-binding sequence. All of these family members can bind to hydroxyapatite and can be detected in blood<sup>63</sup>. Because *DMP1* is very acidic and secreted into the extracellular matrix during the formation and mineralization of bone and dentin, it is generally believed that *DMP1* plays an important role in the initiation of mineralization<sup>64</sup>, moreover *DMP1* has been demonstrated to be expressed and secreted by osteocytes in bone<sup>65</sup>. For these reasons, its expression is related to the osteocytes maturation stage and, of course, to the bone mineralization.

Even if osteoblasts and osteoclasts are cells responsible of bone formation and bone resorption, osteocytes collaborate to the bone remodelling process secreting several factors that modulate



osteoblasts and osteoclasts differentiation. One of those is RANKL, the most responsible factor that induce the osteoclastogenesis. Many are the evidences that osteocytes regulate bone homeostasis through RANKL expression<sup>66</sup> and in our study we found a down-regulation of *RANKL* gene expression by Sr100 nanoparticles if compared to control, Ca100 and Ca50Sr50 nanoparticles treated samples. These findings suggest that Sr100 nanoparticles could inhibit osteoclasts differentiation by decreasing RANKL expression and its release by osteocytes.

An osteocytes specific marker is, indeed, sclerostin, transcribed by *SOST* gene. Sclerostin functions as an antagonist of canonical Wnt signaling, whereby GSK-3 $\beta$ <sup>2</sup>-stimulated, ubiquitin-mediated breakdown of  $\beta$ -catenin is alleviated, resulting in its nuclear translocation, and binding to transcription factors of the T-cell factor/lymphoid enhancer factor family, to induce the transcription of growth-associated genes<sup>67</sup>. Non-canonical Wnt signaling does not involve  $\beta$ -catenin translocation to the nucleus<sup>68</sup>. Sclerostin binds to the extracellular domains of the Wnt co-receptors LRP5, LRP6, and LRP4 and disrupts extracellular Wnt-induced Frizzled/LRP complex formation thus providing a molecular mechanism by which loss of sclerostin function may lead to conditions such as sclerostosis<sup>69</sup>. In our study, *SOST* expression resulted to be up-regulated by Sr100 nanoparticles unlike other studies where strontium ranelate was demonstrated to increase the Wnt canonical pathway and decrease sclerostin expression in human osteoblasts<sup>70</sup>. To best of our knowledge, no data are reported about the effect of strontium on sclerostin expression by osteocytes. The observed increase in *SOST* expression could indicate a more mature stage of differentiation induced by Sr100 nanoparticles.

Many studies demonstrated that Strontium Ranelate acts on bone cells in part via the CaSR<sup>71,72</sup>, so we started to investigate if Sr100 nanoparticles exert their action through the same receptor. To do this, we used an antagonist of CaSR, NPS 2143 hydrochloride, that blocks increments in cytoplasmic Ca<sup>2+</sup> concentrations elicited by activation of the CaSR<sup>73</sup>. After 7 days, Ocy454 cultured in the presence of NPS 2143 hydrochloride showed a significant decrease in bone matrix mineralization, highlighting the important role of this receptor in bone matrix mineralization<sup>74</sup>. When Ocy454 were cultured in presence of NPS 2143 hydrochloride and Sr100 nanoparticles, no differences in bone matrix mineralization were observed related to samples cultured in the absence of NPs. This could be explained by the fact that nanoparticles could act through the CaSR inhibited by NPS 2143 hydrochloride. On the other hand, the involvement of other receptors cannot be excluded since bone matrix mineralization is strictly correlated to the CaSR that, when inhibited, covers the effect of possible other pathways activated by Sr100 nanoparticles. It is reasonable that CaSR is not the only one involved in Sr100 nanoparticles stimuli, since many evidences demonstrated the role of other cation sensing receptors in strontium ranelate activation<sup>75</sup>. These data

are not sufficient to establish the molecular mechanisms activated by Sr100 nanoparticles that needs to be more addressed in future studies.

Further investigations showed that, when NPS 2143 hydrochloride was added to osteocytes sub-sequentially to 3 days Sr100 nanoparticles pre-incubation, the inhibitory effects of bone matrix mineralization was not observed and the amount of calcium deposition was comparable with samples cultured in absence of NPS 2143 hydrochloride. This suggests that Sr100 nanoparticles, in the first three days, activated the pathway promoting an increased mineralization, probably also through the CaSR, and the subsequent treatment with NPS 2143 did not affect the calcium deposition. NPS 2143 hydrochloride is one of the calcilytic drugs proposed for osteoporosis treatment<sup>76-78</sup>, since they stimulate the secretion of PTH by parathyroid cells and decrease renal excretion of Ca<sup>2+</sup>. Three calcilytic compounds progressed into phase II studies in postmenopausal women with osteoporosis (T score  $\leq$  2.5). Although all these calcilytic compounds showed efficacy as anabolic agents in the ovariectomized rat model<sup>79</sup>, the results in humans have been disappointing<sup>80</sup>. Because calcilytics are known to be tissue nonselective, it is possible that their actions on skeletal CaSR could blunt the ability of elevated PTH to stimulate bone formation<sup>81</sup>. In this sense, a pre-treatment with Sr100 nanoparticles could reduce the negative effect of calcilytic drugs on bone cells and, moreover, Sr100 nanoparticles and calcilytic drug could work synergically as new osteoporosis treatment for an improved bone matrix deposition. We are aware that these are only preliminary results but they are very promising for the development of a new osteoporosis treatment.

The last *in vitro* model used to study the effect of Sr100 nanoparticles on bone remodelling, was the murine macrophage RAW264.7 cell line that, when cultured in presence of RANKL, exhibits several osteoclasts features<sup>82</sup>. Osteoclasts, in fact, are bone-resorbing cells that differentiate from macrophage precursors in response to receptor activator of NF- $\kappa$ B, RANKL. *In vitro* models of osteoclasts differentiation are principally based on primary cell cultures, which are poorly suited to molecular and transgene studies due to the limitations associated with the use of primary macrophage. RAW264.7 is a macrophage cell line with the capacity to form osteoclast-like cells<sup>82</sup>. In our study, we differentiated RAW264.7 with soluble RANKL and evaluated the effect of Ca100 and Sr100 nanoparticles on osteoclastogenesis.

Lower concentrations of Sr100 NPs (31.25 and 62.5  $\mu$ g/mL) showed an inhibitory effect on TRAP activity, whereas an opposite effect was observed for higher Sr100 nanoparticles concentrations, if compared to control. No differences with control were observed in Ca100 treated samples. The increased TRAP activity in samples treated with higher concentration of Sr100 nanoparticles could

be due to macrophage activation. TRAP enzyme, in fact, has been demonstrated to be expressed also in activated macrophage, both in human and rats<sup>83,84</sup>. Moreover, no multinucleated cells were observed in those samples.

After 10 days, the number of multinucleated cells was significantly reduced by Sr100 nanoparticles. Moreover, osteoclasts size and number of nuclei per cells was significantly reduced by both types of nanoparticles, especially for Sr100 ones, if compared to control. These results were confirmed by *NFATc1* expression that was significantly down-regulated in cells treated with Sr100 nanoparticles. NFATc1 is a master regulator of osteoclastogenesis and it induces the formation of multinucleated osteoclasts as well as expression of fusion-mediating molecules such as the d2 isoform of vacuolar ATPase V<sub>o</sub> domain (Atp6v0d2) and the dendritic cell-specific transmembrane protein (DC-STAMP)<sup>85</sup>. Cell-cell fusion is an essential process for the development of multinucleated cells such as giant cell macrophages and osteoclasts. Fusion-mediated giant cell formation is critical for osteoclasts maturation; and without these cells, bone resorption is inefficient<sup>86,87</sup>. Mononuclear cells appear to recognize each other and fuse to form multinuclear cells and cell-surface molecules are thought to play a fusion-mediating role. NFATc1, a member of the NFAT family of transcription factors, is up-regulated during RANKL-induced osteoclastogenesis<sup>88</sup>. Recently, it was reported that ectopic expression of NFATc1 causes precursors to undergo efficient osteoclasts differentiation in the absence of RANKL, and that NFATc1-deficient embryonic stem cells fail to differentiate into osteoclasts in response to RANKL<sup>88</sup>, suggesting that NFATc1 acts as a master regulator of osteoclastogenesis. In addition to the important role for NFATc1 in osteoclasts differentiation, recent data indicate that NFATc1 appears to be involved in osteoclast functions such as bone resorption<sup>89</sup>. Indeed, previous reports have shown that NFATc1 regulates TRAP, cathepsin K, c-Src, and  $\beta$ 3 integrin<sup>88</sup>, which are known to be involved in resorption activity.

In samples treated with Ca100 and Sr100 nanoparticles, *CD44* expression was observed to be down-regulated if compared to untreated cells. CD44 is a cell surface glycoprotein known to bind osteopontin, an important non-collagen protein present in the bone matrix that aids in osteoclasts attachment<sup>90</sup>. Antibodies to CD44 inhibited *in vitro* osteoclast-like cell formation from mouse bone marrow precursors<sup>91</sup>. After 10 days, in Ca100 and Sr100 nanoparticles treated samples, a lower number of osteoclasts, especially in Sr100 treated ones, were observed and this could be correlated to a reduced expression of proteins involved in cell adhesion, like CD44.

Expression of *ACP5* and *CTSK* was also evaluated as osteoclastogenesis markers. While Ca100 and Sr100 nanoparticles showed no effect on *CTSK* expression, a down-regulation in *ACP5* expression was detected in Sr100 treated samples. This result confirms TRAP activity and staining (*ACP5* transcribes for TRAP enzyme). In fact, Sr100 nanoparticles reduced the expression and activity of

TRAP enzyme if compared to Ca100 nanoparticles treated and untreated samples. Both *ACP5* and *CTSK* are up-regulated by RANKL treatment<sup>92</sup>, but only *ACP5* resulted be affected by Sr100 nanoparticles.

In summary, Sr100 nanoparticles seem to inhibit osteoclastogenesis by reduction of fusion-mediating molecules, like NFATc1, and proteins important for cell adhesion, like CD44. This leads to less number and smaller osteoclasts-like cells and reduction in TRAP activity. Further investigations are necessary to confirm these results and studies on osteoclasts activity need to be performed to assess the effect of Sr100 nanoparticles on resorption activity.

## 4.5 Conclusion and Future Perspective

In this chapter we presented results showing the effect of hydroxyapatite (Ca100) and Sr-substitute hydroxyapatite (Sr100) nanoparticles on bone remodelling, using *in vitro* models.

We reported a stimulatory effect of Sr100 nanoparticles on osteoblasts differentiation, using SAOS-2 cell line and human mesenchymal stem cells isolated from bone marrow. In particular, Sr100 nanoparticles accelerate and improve the commitment of cell to differentiate toward osteoblasts and increase the extracellular bone matrix deposition and mineralization that resulted enriched in strontium. The exact molecular mechanism activated by Sr100 nanoparticles is still unknown and needs to be addressed in future studies. Preliminary results suggest an involvement of Wnt/ $\beta$ -catenin pathway since some factors related to this pathway were up-regulated by Sr100 nanoparticles. Deeper investigations are necessary to confirm this hypothesis.

On the other hand, Sr100 nanoparticles reduced the differentiation of osteoclasts, the cells responsible of bone matrix resorption, suggested by observed reduction of TRAP expression, cell fusion and adhesion with the result to inhibit the multinucleated cells formation. These preliminary data need to be confirmed by resorption activity assays to endorse the inhibition effect of Sr100 nanoparticles on osteoclasts differentiation.

Osteoblasts and osteoclasts differentiation is concerted also by osteocytes. In our studies, we demonstrated that Sr100 nanoparticles push the osteocytes differentiation toward more mature differentiated stages and improve their ability to deposit extracellular matrix. A modulation in released molecules that influence osteoblasts and osteoclasts differentiation was observed with a decrease of *RANKL* expression and an increase of *SOST*. Preliminary results about the molecular mechanism involved in this process, suggest a role of calcium sensing receptor and in particular the possibility to use Sr100 nanoparticles to reduce the negative effect of calcilytics drugs. Also in this sense, further investigations are necessary to clarify how Sr100 nanoparticles influence osteocytes metabolism.

## 4.6 References

1. Dougall, W. C. *et al.* RANK is essential for osteoclast and lymph node development. *Genes Dev.* **13**, 2412–2424 (1999).
2. Van Wesenbeeck, L. *et al.* The osteopetrotic mutation toothless (tl) is a loss-of-function frameshift mutation in the rat *Csf1* gene: Evidence of a crucial role for CSF-1 in osteoclastogenesis and endochondral ossification. *Proc. Natl. Acad. Sci. U. S. A.* **99**, 14303–14308 (2002).
3. Wiktor-Jedrzejczak, W. *et al.* Total absence of colony-stimulating factor 1 in the macrophage-deficient osteopetrotic (op/op) mouse. *Proc. Natl. Acad. Sci. U. S. A.* **87**, 4828–4832 (1990).
4. Ducy, P., Zhang, R., Geoffroy, V., Ridall, A. L. & Karsenty, G. *Osf2/Cbfa1*: A Transcriptional Activator of Osteoblast Differentiation. *Cell* **89**, 747–754 (1997).
5. Glass, D. A. *et al.* Canonical Wnt signaling in differentiated osteoblasts controls osteoclast differentiation. *Dev. Cell* **8**, 751–764 (2005).
6. Hu, H. *et al.* Sequential roles of Hedgehog and Wnt signaling in osteoblast development. *Development* **132**, 49–60 (2005).
7. Nakashima, K. *et al.* The novel zinc finger-containing transcription factor Osterix is required for osteoblast differentiation and bone formation. *Cell* **108**, 17–29 (2002).
8. Gomez, B. *et al.* Monoclonal antibody assay for measuring bone-specific alkaline phosphatase activity in serum. *Clin. Chem.* **41**, 1560 LP-1566 (1995).
9. Burger, E. H. & Klein-Nulend, J. Mechanotransduction in bone--role of the lacuno-canalicular network. *FASEB J.* **13 Suppl**, S101-12 (1999).
10. van Bezooijen, R. L. *et al.* Sclerostin is an osteocyte-expressed negative regulator of bone formation, but not a classical BMP antagonist. *J. Exp. Med.* **199**, 805–14 (2004).
11. Bernardo, M. E. *et al.* Human bone marrow derived mesenchymal stem cells do not undergo transformation after long-term in vitro culture and do not exhibit telomere maintenance mechanisms. *Cancer Res.* **67**, 9142–9 (2007).
12. Bernardo, M. E. *et al.* Optimization of in vitro expansion of human multipotent mesenchymal stromal cells for cell-therapy approaches: further insights in the search for a fetal calf serum substitute. *J. Cell. Physiol.* **211**, 121–30 (2007).
13. Spatz, J. M. *et al.* The Wnt Inhibitor Sclerostin Is Up-regulated by Mechanical Unloading in Osteocytes in Vitro \*. *J. Biol. Chem.* **290**, 16744–16758 (2015).
14. Wein, M. N. *et al.* HDAC5 Controls MEF2C - Driven Sclerostin Expression in Osteocytes. *J. bone Miner. Res.* **30**, 400–411 (2015).
15. Linares, J. *et al.* Endocytic mechanisms of graphene oxide nanosheets in osteoblasts,

hepatocytes and macrophages. *ACS Appl. Mater. Interfaces* **6**, 13697–13706 (2014).

16. Maruyama, K. *et al.* Endocytosis of Multiwalled Carbon Nanotubes in Bronchial Epithelial and Mesothelial Cells. *Biomed Res. Int.* e793186 (2015). doi:10.1155/2015/793186, 10.1155/2015/793186
17. West, M. A., Bretscher, M. S. & Watts, C. Distinct endocytotic pathways in epidermal growth factor-stimulated human carcinoma A431 cells. *J. Cell Biol.* **109**, 2731–2739 (1989).
18. Smart, E. J., Estes, K. & Anderson, R. G. W. Inhibitors That Block Both the Internalization of Caveolae and the Return of Plasmalemmal Vesicles. *Cold Spring Harb. Symp. Quant. Biol.* **60**, 243–248 (1995).
19. Mis-assembly of clathrin lattices on endosomes reveals a regulatory switch for coated pit formation. *J. Cell Biol.* **123**, 1107–1117 (1993).
20. Bhowmick, T., Berk, E., Cui, X., Muzykantov, V. R. & Muro, S. Effect of flow on endothelial endocytosis of nanocarriers targeted to ICAM-1. *J. Control. Release Off. J. Control. Release Soc.* **157**, 485–492 (2012).
21. Mäger, I., Langel, K., Lehto, T., Eiríksdóttir, E. & Langel, U. The role of endocytosis on the uptake kinetics of luciferin-conjugated cell-penetrating peptides. *Biochim. Biophys. Acta* **1818**, 502–511 (2012).
22. Saino, E. *et al.* In Vitro Enhancement of SAOS-2 Cell Calcified Matrix Deposition onto Radio Frequency Magnetron Sputtered Bioglass-Coated Titanium Scaffolds. **16**, (2010).
23. van Engeland, M., Nieland, L. J. W., Ramaekers, F. C. S., Schutte, B. & Reutelingsperger, C. P. M. A review on an apoptosis detection system based on phosphatidylserine exposure. *Cytometry* **31**, 1–9 (1998).
24. Saino, E. *et al.* In vitro calcified matrix deposition by human osteoblasts onto a zinc-containing bioactive glass. *Eur. Cell. Mater.* **21**, 59–72; discussion 72 (2011).
25. Saino, E. *et al.* In Vitro Enhancement of SAOS-2 Cell Calcified Matrix Deposition onto Radio Frequency Magnetron Sputtered Bioglass-Coated Titanium Scaffolds. *Tissue Eng. Part A* **16**, 995–1008 (2010).
26. Gregory, C. A., Gunn, W. G., Peister, A. & Prockop, D. J. An Alizarin red-based assay of mineralization by adherent cells in culture: comparison with cetylpyridinium chloride extraction. *Anal. Biochem.* **329**, 77–84 (2004).
27. Cohen, S. A. & Sideman, L. Modification of the o-cresolphthalein complexone method for determining calcium. *Clin. Chem.* **25**, 1519–20 (1979).
28. Anderson, H. C. *et al.* The Bone-Inducing Agent in Saos-2 Cell Extracts and Secretions. *Cells Mater.* **8**, 89–98 (1998).

29. Feczak, T. Comparison of the preparation of PLGA – BSA nano- and microparticles by PVA , poloxamer and PVP. *Colloids Surfaces A Physicochem. Eng. Asp.* **319**, 188–195 (2008).
30. Lu, F., Wu, S., Hung, Y. & Mou, C. Size Effect on Cell Uptake in Well-Suspended , Uniform Mesoporous Silica Nanoparticles. *Communications* 1408–1413 (2009).
31. Jones, A. T. Macropinocytosis : searching for an endocytic identity and a role in the uptake of cell penetrating peptides. *J. Cell. Mol. Med.* **11**, 670–684 (2007).
32. Kruth, H. S. *et al.* Macropinocytosis Is the Endocytic Pathway That Mediates Macrophage Foam Cell Formation with Native Low Density Lipoprotein. *J. Biol. Chem.* **280**, 2352–2360 (2005).
33. Koivusalo, M. *et al.* Amiloride inhibits macropinocytosis by lowering submembranous pH and preventing Rac1 and Cdc42 signaling. *J. cell* **188**, 547–563 (2010).
34. Falcone, S. *et al.* Macropinocytosis: regulated coordination of endocytic and exocytic membrane traffic events. *J. Cell Sci.* **119**, 4758–4769 (2006).
35. Marsh, M. & McMahon, H. T. The structural era of endocytosis. *Science* **285**, 215–220 (1999).
36. Parton, R. G. & Simons, K. The multiple faces of caveolae. *Nat. Rev. Mol. Cell Biol.* **8**, 185–194 (2007).
37. Berridge, M. J., Bootman, M. D. & Lipp, P. Calcium - a life and death signal. *Nature* **395**, 645–648 (1998).
38. Berridge, M. J. Calcium signalling and cell proliferation. *BioEssays* **17**, 491–500 (1995).
39. Kahl, C. R. & Means, A. R. Regulation of Cell Cycle Progression by Calcium / Calmodulin-Dependent Pathways. *Endocr. Rev.* **24**, 719–736 (2016).
40. Santella, L. The Role of Calcium in the Cell Cycle : Facts and Hypotheses. *Biochem. Biophys. Res. Commun.* **324**, 317–324 (1998).
41. Capuccini, C. *et al.* Strontium-substituted hydroxyapatite coatings synthesized by pulsed-laser deposition: In vitro osteoblast and osteoclast response. *Acta Biomater.* **4**, 1885–1893 (2008).
42. Capuccini, C. *et al.* Interaction of Sr-doped hydroxyapatite nanocrystals with osteoclast and osteoblast-like cells. *J. Biomed. Mater. Res. A* **89**, 594–600 (2009).
43. Raucci, M. G., Giugliano, D., Alvarez-Perez, M. a. & Ambrosio, L. Effects on growth and osteogenic differentiation of mesenchymal stem cells by the strontium-added sol–gel hydroxyapatite gel materials. *J. Mater. Sci. Mater. Med.* **26**, 90 (2015).
44. Owen, T. A. *et al.* Progressive development of the rat osteoblast phenotype in vitro: reciprocal relationships in expression of genes associated with osteoblast proliferation and differentiation during formation of the bone extracellular matrix. *J. Cell. Physiol.* **143**, 420–30 (1990).



45. Beloti, M. M. & Rosa, A. L. Osteoblast Differentiation of Human Bone Marrow Cells Under Continuous and Discontinuous Treatment with Dexamethasone. *Braz Dent J.* **16**, 156–161 (2005).
46. Torii, Y., Hitomi, K., Yamagishi, Y. & Tsukagoshi, N. Demonstration of alkaline phosphatase participation in the mineralization of osteoblasts by antisense RNA approach. *Cell Biol. Int.* **20**, 459–464 (1996).
47. Selvamurugan, N., Kwok, S., Vasilov, A., Jefcoat, S. C. & Partridge, N. C. Effects of BMP-2 and pulsed electromagnetic field (PEMF) on rat primary osteoblastic cell proliferation and gene expression. *J. Orthop. Res.* **25**, 1213–20 (2007).
48. Quarles, L. D., Yohay, D. A., Lever, L. W., Caton, R. & Wenstrup, R. J. Distinct proliferative and differentiated stages of murine MC3T3-E1 cells in culture: An in vitro model of osteoblast development. *J. Bone Miner. Res.* **7**, 683–692 (1992).
49. Azari, F. *et al.* Intracellular precipitation of hydroxyapatite mineral and implications for pathologic calcification. *J. Struct. Biol.* **162**, 468–79 (2008).
50. van Dijk, S., D’Errico, J. A., Somerman, M. J., Farach-Carson, M. C. & Butler, W. T. Evidence that a non-RGD domain in rat osteopontin is involved in cell attachment. *J. Bone Miner. Res.* **8**, 1499–506 (1993).
51. Denhardt, D. T. & Guo, X. Osteopontin: a protein with diverse functions. *FASEB J.* **7**, 1475–82 (1993).
52. Grzesik, W. J. & Robey, P. G. Bone matrix RGD glycoproteins: immunolocalization and interaction with human primary osteoblastic bone cells in vitro. *J. Bone Miner. Res.* **9**, 487–96 (1994).
53. Krämer, A. *et al.* Adhesion to fibronectin stimulates proliferation of wild-type and bcr/abl-transfected murine hematopoietic cells. *Proc. Natl. Acad. Sci. U. S. A.* **96**, 2087–92 (1999).
54. Kojima, H., Uede, T. & Uemura, T. In vitro and in vivo effects of the overexpression of osteopontin on osteoblast differentiation using a recombinant adenoviral vector. *J. Biochem.* **136**, 377–86 (2004).
55. Komori, T. Regulation of Osteoblast Differentiation by Transcription Factors. *J. Cell. Biochem.* **1239**, 1233–1239 (2006).
56. Stock, M., Otto, F. & Lu, M. Upstream and Downstream Targets of RUNX Proteins. *J. Cell. Biochem.* **18**, 9–18 (2003).
57. Gaur, T. *et al.* Canonical WNT signaling promotes osteogenesis by directly stimulating Runx2 gene expression. *J. Biol. Chem.* **280**, 33132–40 (2005).
58. YANG, F. *et al.* Strontium Enhances Osteogenic Differentiation of Mesenchymal Stem Cells and In Vivo Bone Formation by Activating Wnt / Catenin. *Stem Cells* **29**, 981–991 (2011).

59. Atkins, G. J., Welldon, K. J., Halbout, P. & Findlay, D. M. Strontium ranelate treatment of human primary osteoblasts promotes an osteocyte-like phenotype while eliciting an osteoprotegerin response. *Osteoporos. Int.* **20**, 653–64 (2009).
60. Kokesch-himmelreich, J. *et al.* ToF-SIMS analysis of osteoblast-like cells and their mineralized extracellular matrix on strontium enriched bone cements. *Biointerphases* **8**, (2013).
61. Gentleman, E. *et al.* Biomaterials The effects of strontium-substituted bioactive glasses on osteoblasts and osteoclasts in vitro. *Biomaterials* **31**, 3949–3956 (2010).
62. Clarke, B. Normal Bone Anatomy and Physiology. *Clin J Am Soc Nephrol* **3**, S131–S139 (2008).
63. Feng, J. Q. *et al.* The Dentin Matrix Protein 1 ( Dmp1 ) is Specifically Expressed in Mineralized , but not Soft , Tissues during Development. *J. Dent. Reserach* **82**, 776–780 (2003).
64. Butler, W. T. & Ritchie, H. The nature and functional significance of dentin extracellular matrix proteins. *Int. J. Dev. Biol.* **179**, 169–179 (1995).
65. Kalajzic, I. *et al.* Dentin matrix protein 1 expression during osteoblastic differentiation , generation of an osteocyte GFP-transgene. *Bone* **35**, 74–82 (2004).
66. Nakashima, T. *et al.* Evidence for osteocyte regulation of bone homeostasis through RANKL expression. *Nat. Med.* **17**, 1231–1234 (2011).
67. BEHRENS, J. *et al.* Functional interaction of beta-catenin with the transcription factor LEF-1. *Nature* **382**, 638–642 (1996).
68. Kubota, T., Michigami, T. & Ozono, K. Wnt signaling in bone metabolism. *J. Bone Miner. Metab.* **27**, 265–271 (2009).
69. Seme, M. SOST Is a Ligand for LRP5 / LRP6 and a Wnt Signaling Inhibitor \*. *J. Biol. Chem.* **280**, 26770–26775 (2005).
70. Rybchyn, M. S., Slater, M., Conigrave, A. D. & Mason, R. S. An Akt-dependent Increase in Canonical Wnt Signaling and a Decrease in Sclerostin Protein Levels Are Involved in Strontium Ranelate-induced Osteogenic Effects in Human. *J. Biol. Chem.* **286**, 23771–23779 (2011).
71. Chattopadhyay, N., Quinn, S. J., Kifor, O., Ye, C. & Brown, E. M. The calcium-sensing receptor (CaR) is involved in strontium ranelate-induced osteoblast proliferation. *Biochem. Pharmacol.* **74**, 438–47 (2007).
72. Brown, E. M. Is the calcium receptor a molecular target for the actions of strontium on bone? *Osteoporos. Int.* **14 Suppl 3**, S25-34 (2003).
73. Nemeth, E. F. *et al.* Calcilytic Compounds : Potent and Selective Ca<sup>2+</sup> Receptor Antagonists That Stimulate Secretion of Parathyroid Hormone. *J. Pharmacol. Exp. Ther.* **299**, 323–331 (2001).

74. Takaoka, S., Yamaguchi, T., Yano, S., Yamauchi, M. & Sugimoto, T. The Calcium-sensing Receptor ( CaR ) is Involved in Strontium Ranelate-induced Osteoblast Differentiation and Mineralization. *Horm Metab Res* **42**, 627–631 (2010).
75. Pi, M. & Quarles, L. D. A novel cation-sensing mechanism in osteoblasts is a molecular target for strontium. *J. Bone Miner. Res.* **19**, 862–9 (2004).
76. Nemeth, E. F. The search for calcium receptor antagonists (calcilytics). *J. Mol. Endocrinol.* **29**, 15–21 (2002).
77. Silve, J. & Bushinsky, D. Harnessing the parathyroids to create stronger bones. *Curr Opin Nephrol Hypertens* **13**, 471–6 (2004).
78. Widler, L. Calcilytics: antagonists of the calcium-sensing receptor for the treatment of osteoporosis. *Future Med. Chem.* **3**, 535–547 (2011).
79. Gowen, M. *et al.* Antagonizing the parathyroid calcium receptor stimulates parathyroid hormone secretion and bone formation in osteopenic rats. *J. Clin. Invest.* **105**, 1595–1604 (2000).
80. Nemeth, E. F., Ph, D., Scientist, C. & Shoback, D. Calcimimetic and calcilytic drugs for treating bone and mineral-related disorders. *Best Pract. Res. Clin. Endocrinol. Metab.* **27**, 373–384 (2013).
81. Dvorak-ewell, M. M. *et al.* Osteoblast Extracellular Ca<sup>2+</sup> -Sensing Receptor Regulates Bone Development, Mineralization, and Turnover. *J. bone Miner. Res.* **26**, 2935–2947 (2011).
82. Cuetara, B. L. V., Crotti, T. N., O'Donoghue, A. J. & Mchugh, K. P. Cloning and characterization of osteoclast precursors from the RAW264.7 cell line. *Vitr. Cell Dev Biol Anim* **42**, 182–188 (2010).
83. How, J., Brown, J. R., Saylor, S. & Rimm, D. L. Macrophage expression of tartrate-resistant acid phosphatase as a prognostic indicator in colon cancer. *Histochem cell Biol* **142**, 195–204 (2014).
84. Hayman, A. R., Macary, P., Lehner, P. J. & Cox, T. M. Tartrate-resistant Acid Phosphatase ( Acp 5 ): Identification in Diverse Human Tissues and Dendritic Cells. *J. Histochem. Cytochem.* **49**, 675–683 (2001).
85. Kim, K., Lee, S.-H., Ha Kim, J., Choi, Y. & Kim, N. NFATc1 induces osteoclast fusion via up-regulation of Atp6v0d2 and the dendritic cell-specific transmembrane protein (DC-STAMP). *Mol. Endocrinol.* **22**, 176–85 (2008).
86. Zhang, R. *et al.* Bone Resorption by Osteoclasts. *Science (80-. )*. **289**, 1504–1508 (2000).
87. Walsh, M. C. *et al.* Osteoimmunology: Interplay Between the Immune System and Bone Metabolism. *Annu. Rev. Immunol.* **24**, 33–63 (2006).
88. Takayanagi, H. *et al.* Induction and activation of the transcription factor NFATc1 (NFAT2)

- integrate RANKL signaling in terminal differentiation of osteoclasts. *Dev. Cell* **3**, 889–901 (2002).
89. Komarova, S. V, Pereverzev, A., Shum, J. W., Sims, S. M. & Dixon, S. J. Convergent signaling by acidosis and receptor activator of NF-kappaB ligand (RANKL) on the calcium/calcineurin/NFAT pathway in osteoclasts. *Proc. Natl. Acad. Sci. U. S. A.* **102**, 2643–8 (2005).
90. Weber, G. F., Ashkar, S., Glimcher, M. J. & Cantor, H. Receptor-ligand interaction between CD44 and osteopontin (Eta-1). *Science* **271**, 509–12 (1996).
91. Kania, J. R., Kehat-Stadler, T. & Kupfer, S. R. CD44 antibodies inhibit osteoclast formation. *J. Bone Miner. Res.* **12**, 1155–64 (1997).
92. Day, C. J. *et al.* Gene array identification of osteoclast genes: differential inhibition of osteoclastogenesis by cyclosporin A and granulocyte macrophage colony stimulating factor. *J. Cell. Biochem.* **91**, 303–15 (2004).



# Chapter 4

---

## **5. *In vivo* effect of gelatin sponge enriched with Sr-hydroxyapatite on ectopic bone formation**

### **5.1 Introduction**

Bone substitute materials are commonly used to restore lost or defective bone under the original treatment concept of guided bone regeneration (GBR). The new generation of these materials would isolate the bone defect site from non-osteogenic soft tissue, the bone substitute would maintain a three-dimensional scaffold to support the osteogenic cells and tissue during bone healing. However, a hypothesis as such remains speculative, since the mechanisms of bone healing and regeneration have not been sufficiently described. Different types of biomaterials are used as bone substitutes and optimizations, for the predictable outcomes of these biomaterials, require a proper understanding of the interactions between the substitute materials with the local host environment. This includes the influence of the biomaterial properties on the early cellular and molecular events that determine the onset of tissue healing and may eventually affect the overall defect restitution.

To hasten the translational lag from laboratory to clinical studies in bone tissue engineering, we used a hemostatic gelatin sponge, a longstanding US Food and Drug Administration (USFDA)-approved material, as a scaffold to repair bone defects. Skeletal defects, which can be caused by irradiation, trauma, nonunion, disease (e.g., osteoporosis), and/or tumor resection, require complicated reconstruction efforts using bone grafts<sup>1,2</sup>. Bone graft source approaches commonly include autografts, allografts, artificial bones, and more. Autografts, the current gold standard for bone graft procedures, are used to enhance bone-healing, spinal fusion, and fracture repair. However, autografts require a secondary operation to remove material from the donor site, which increases post-operative pain and impacts surgical success. Allografts, often cadaver tissue, do not require a secondary operation, but there is a limited supply of material and a minimal but genuine risk of disease transmission<sup>3</sup>. Engineered artificial bones are a very viable alternative because they are durable, biocompatible, osteoconductive, and osteoinductive<sup>1,4,5</sup>.

In order to decrease the safety concerns and ameliorate the translational gap between laboratory studies and clinical applications, several biomaterials and related products widely used in clinical applications can be investigated for their potential as bone tissue engineering scaffolds. Here, we examine the use of gelatin sponges in just such a role. Gelatin sponges are sterile, water-insoluble,

malleable, and absorbable. They are easily obtained, inexpensive, biocompatible, and are not known to induce allergic reactions or other harmful side effects<sup>6</sup>. Gelatin sponges have been demonstrated as a suitable *in vitro* model for producing 3-dimensional (3D) human and bovine chondrocyte cultures<sup>7-9</sup>. Some studies have demonstrated the usefulness of gelatin sponges as a carrier or an implant for repairing gingival depressions and bone defects<sup>10-13</sup> and the suitability of gelatin sponge as a carrier or an implant for bone regeneration.

To estimate the effect of strontium hydroxyapatite on ectopic bone formation, BMP2 was used as positive control, since its osteoinduction effect is already known and widely demonstrated. Bone BMPs are a subfamily of the TGF- $\beta$  superfamily. They have been identified for as important factors in the growth and differentiation of mesenchymal cells into chondrocytic and osteoblastic lineages. This process occurs through a series of signal transduction steps that influence and regulate gene expression<sup>14</sup>. BMPs are stored in the extracellular matrix of various bone tissue, osteoprogenitor cells, osteoblasts, chondrocytes and other bone related cells. During bone repair and remodeling the BMPs are released leading to the signal transduction and bone formation<sup>15</sup>. The BMP focused on in this study is BMP-2 due to its role in skeletal repair and regeneration<sup>16</sup>.

BMP-2 signals through serine/threonine kinase receptors consisting of type I and type II receptors. The type I receptors include Alk3 and Alk6, and bind BMP ligands. The type II receptors have been identified as BMPR-II and type II/IIB activating receptors. Once the ligand binds, type I receptors recruits the type II receptors initiating the BMP signaling cascade<sup>16</sup>. The type I receptor phosphorylates Smad1/5/8 proteins, which play a central role in the translocation of the BMP signal to the nucleus. Once phosphorylated Smad1 associates with related proteins and translocates into the nucleus where it regulates and affects gene transcription. Because BMP-2 has such a powerful role in the formation of bone, there are a number of molecular mechanisms that regulate it. Two important BMP-2 agonists include Gremlin and Noggin<sup>16</sup>. Gremlin, a member of the Dan family of BMP agonists, is able to bind and block BMP-2. Gremlin primarily functions by modulating early limb growth through inhibiting chondrogenesis and apoptosis<sup>17</sup>. Noggin binds directly to BMPs, creating a complex, which can no longer bind to the cell surface receptors, and stopping the signal from beginning. BMPs stimulate Noggin secretion in mesenchymal cells, but may act as a negative feedback control in cell differentiation<sup>18</sup>. In addition to agonists, there are a number of mechanisms to block the transduction. Overall, there are many mechanisms to regulate the expression of BMP-2. This regulation is important because of the degree of importance that BMP-2 plays in bone formation and growth.

In this chapter, we demonstrated the ectopic bone formation induced by gelatin sponge enriched with Strontium hydroxyapatite and BMP2 in mice. In particular, we implanted sponges at the periosteal surface of femur and after 16 and 33 days, we evaluated the ectopic bone formation through X-ray, histological analysis and gene expression of chondrocytes, osteoblasts, osteoclasts, osteocytes and stem cells recruitment markers. This study is still ongoing, so here we present only completed results obtained at the submission deadline of this thesis.



## 5.2 Materials and methods

### 5.2.1 Materials preparation

Gelatin sponge (GELFOAM – Pfizer®) of 1cm<sup>2</sup> were immersed in 200µL of 30% nano-hydroxyapatite (Fluidinova®) suspension and it was considered as **Control implant**. 200µL was the optimum volume for completed absorption of hydroxyapatite suspension by sponge. For **BMP2 implant**, 0.3 µL of a stock solution 10 µg/µL of recombinant BMP2 (R&D Systems) were added to the hydroxyapatite suspension before the sponge absorption. For the **Sr implant**, 10% of the nano-hydroxyapatite was substituted with Sr100 hydroxyapatite powder and the same procedure was carried out.

### 5.2.2 Animals and Surgery

All animal studies were approved by the Institutional Animal Care and Use Committee at Boston University (BU). Mice were obtained from The Jackson Laboratory (Bar Harbor ME) and housed at the BU Animal facilities under standard conditions. All mice were male between 9-11 weeks and of the strain Pax7cre/Alb 12. Mice were bilaterally implanted with sponges which were inserted surrounding the femur, adjacent to the periosteal surface. Before surgery, mice were subcutaneously injected with a total of 0.1 mL of Buprenex® as pain medication and 0.01mL of Baytril® as antibiotics. At harvest days 16 and 33 post-surgery, three mice were euthanized per condition for RNA and histology analysis. **Fig. 4.1** shows a scheme of the performed experiment.

### 5.2.3 Harvest and X-ray Imaging

Mice were euthanized at a given time points by carbon dioxide inhalation followed by cervical dislocation. Immediately following death, mice were X-rayed using Faxitron MX-20 Specimen Radiography System at 30 kV for 40 seconds using Kodak BioMax XAR Scientific Film. The implant, the surrounding muscle, and the femur from left limb were collected separately for RNA extraction and gene analysis. The samples harvested for RNA analysis were stored at -80 °C. The right limb was recovered for histology analysis and fixed in 4% paraformaldehyde for one week at 4°C.

### 5.2.4 Histology analysis

After fixation in paraformaldehyde, the limb was decalcified in 14% EDTA (pH 7.2) for 1 week at 4°C. Limbs were dehydrated and embedded in paraffin for histology. Fast green and Safranin-O staining was performed on 5µm paraffin sections to observe ectopic bone formation

### 5.2.5 RNA extraction and gene expression

RNA extraction was performed by tissue dissociation and chemical extraction. Samples were snap frozen in 0.75mL of QIAzol® Lysis Reagent using liquid nitrogen. A 5mm Qiagen® stainless steel bead was placed in each tube. Samples were lysed with the Qiagen® Tissue Lyser II using 2-minute intervals at 30Hz; snap freezing the sample again if the sample thawed before being completely lysed. Samples were transferred to a new 2mL tube with the addition 1mL of QIAzol® Lysis Reagent and samples incubated on ice for 2 minutes. After 2 minutes, 200µL of Chloroform (Sigma-Aldrich) was added and the samples vortexed. Again, samples were incubated on ice for 2 minutes followed by vortexing, and centrifuged for 15 minutes at 14000rpm and 4°C. The aqueous phase was transferred to a new 2mL tube, adding an equal volume of isopropanol (Sigma-Aldrich). This new solution was then centrifuged for 30min at 4°C and 14000rpm.

The supernatant was removed and the pellet washed with 500µL of 70% ethanol (Sigma-Aldrich), and centrifuged for 5 minutes at 4°C and 14000rpm. The supernatant was removed and the pellet was washed again. The ethanol was removed and the pellets were left to dry for 20-30 minutes. Once dry, pellets were re-suspended in 30-50 µL of RNase free water by slowly pipetting up and down. The extracted RNA was the stored at -80°C.

In order to ensure the quality and quantity of the extracted RNA, both spectroscopy and gel electrophoresis were used. For the spectroscopy, 1µL of RNA was dissolved in 99 µL of RNase free water. Using a Beckman Coulter™ DU®530 Life Science UV/Vis Spectrophometer, a 260nm/280nm ratio value in the range of 1.7-1.9 indicated an acceptable quality of RNA. The 260nm absorbance value was used to determine the concentration of RNA in the sample. For the gel, 1µL of RNA, 7µL of RNase free water, and 2µL of 6X Agarose Gel Loading Dye were mixed and loaded into 1% agarose gel. The gel was made with UltraPure™ agarose from Invitrogen and GelStar™ Nucleic Acid Gel Stain from Lonza Group to detect the presence of the nucleic acid in the gel. The gel was run at 110V for 60-90 minutes. The presence of two bands under UV light indicates the RNA is intact and not degraded.

RNase free-water was added to 1µg of the extracted RNA in a 0.2mL PCR tube for a total volume of 10.4 µL. The following reagents were mixed in an eppendorf tube to create a mixture with a total volume of 19.6µL: 6.61µL of MgCl<sub>2</sub>, 6.0µL of dNTP Mix, 3.0µL of 10X RT Buffer, 1.5µL of Random Hexamers, 0.6µL of RNase Inhibitor, and 1.89µL of Taqman Reverse Transcriptase. All of the reagents were obtained from the TaqMan® Reverse Transcription Reagents kit from Applied Biosystems®. The master mix was then added to the 0.2mL PCR tube to bring the final volume to 30 µL. The samples were placed in the Eppendorf Mastercycler® Personal thermal cycler. The PCR cycle ran at the following settings: 25°C for 10 minutes, 37°C for 60 minutes, 95°C for 5 minutes,

and finally, a 4°C hold. Following the PCR cycle, RNase free water was used to dilute 1:50, 1:25 and 1:5 the femur, implant and muscle cDNAs, respectively.

For qRT-PCR, a 96-well qPCR plate was used, running doublets of each sample on a single plate. We combined 10 µL TaqMan® Universal PCR Master Mix from Applied Biosystems® and 1 µL TaqMan® Gene Expression Assays primers from Applied Biosystems® for a total of 11µL of per sample. The primers used in this study are listed in **Table 4.1**. In addition to our samples, non-operative femurs and muscle were used as controls. The 11µL of mix was combined with 9µL of cDNA to bring the total volume to 20µL per well. After the plate was filled, it was then centrifuged, covered with clear film and analyzed using ABI 7700 Sequence Detector® from Applied Biosystems®. The qRT-PCR reaction repeated the following cycle 40 times: 50°C for 2 minutes, 95°C for 10 minutes, 95°C for 15 seconds, and 60°C for 1 minute. Target gene expression was normalized for 18S in the same sample using the method of Schmittgen and Livak<sup>19</sup>.

<b>Primer</b>	<b>Catalog Number</b>
<b>Normalization Primer</b>	
<i>18S</i>	Mm03928990_g1
<b>Stem Cell Recruitment Primers</b>	
<i>NANOG</i>	Mm02384862_g1
<b>Chondrogenesis Primers</b>	
<i>SOX9</i>	Mm00448840_m1
<i>COL10A1</i>	Mm00487041_m1
<i>ACAN</i>	Mm00545794_m1
<b>Osteogenic- Associated Primers</b>	
<i>β-GLAP</i>	Mm03413826_mH
<i>RUNX2</i>	Mm00501578_m1
<i>DMP1</i>	Mm00803833_g1
<i>SP7</i>	Mm04209856_s1
<i>IBSP</i>	Mm00492555_m1
<b>Osteoclasts- Associated Primers</b>	
<i>ACP5</i>	Mm00475698_m1
<i>RANKL</i>	Mm00441908_m1
<i>CTSK</i>	Mm00484039_m1
<b>Osteocytes- Associated Primers</b>	
<i>SOST</i>	Mm00470479_m1

**Table 4.1: qRT-PCR Primers.** Primers used with their catalog numbers.

### 5.2.6 Statistics

The statistical analysis of data was accomplished using GraphPad Prism Software, Inc. Quantitative results are expressed as the mean  $\pm$  standard error of the mean (SEM). In order to compare the results between Control, BMP2 and Sr, the one-way ANOVA with post hoc Bonferroni test was applied, with a significance level of 0.05.

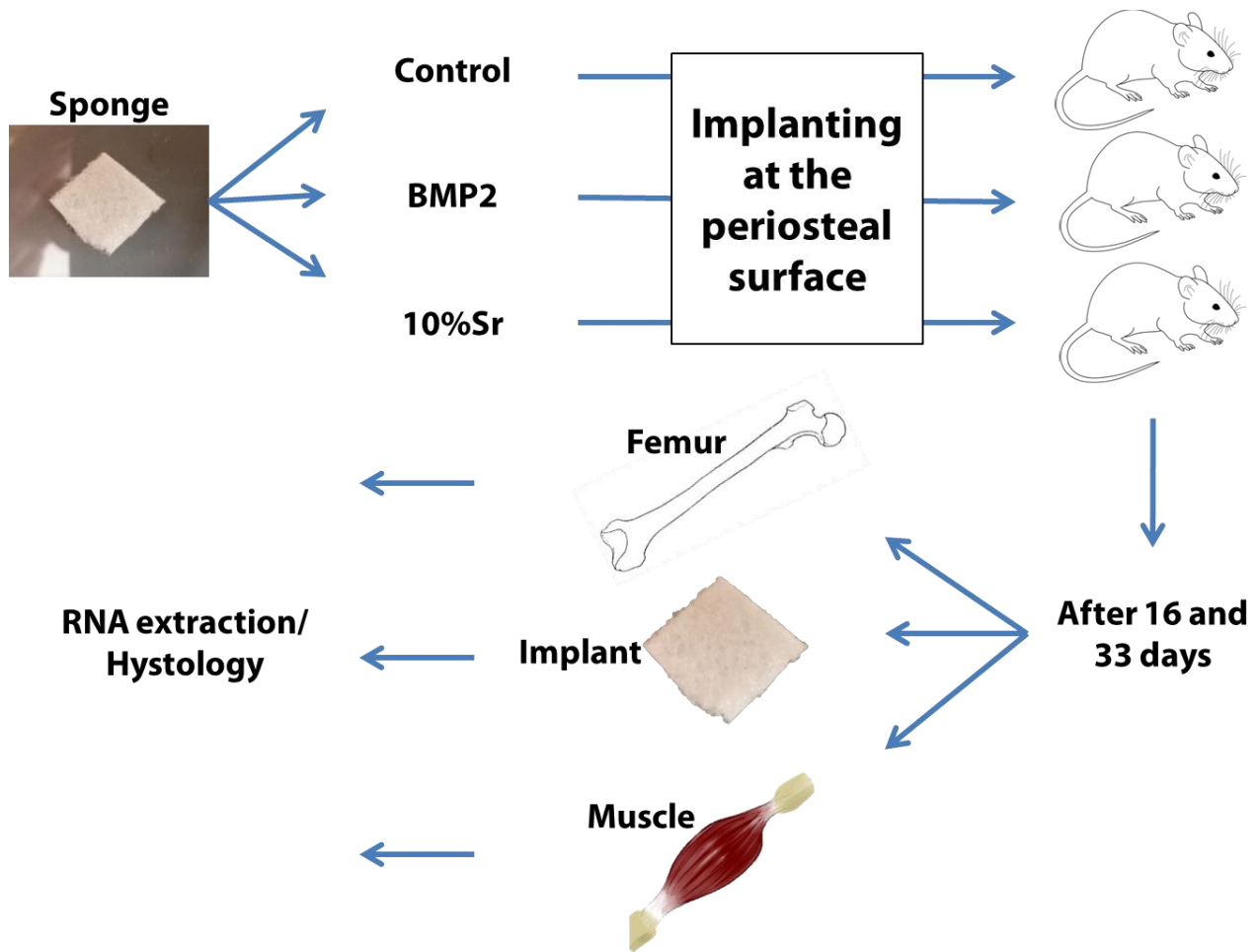
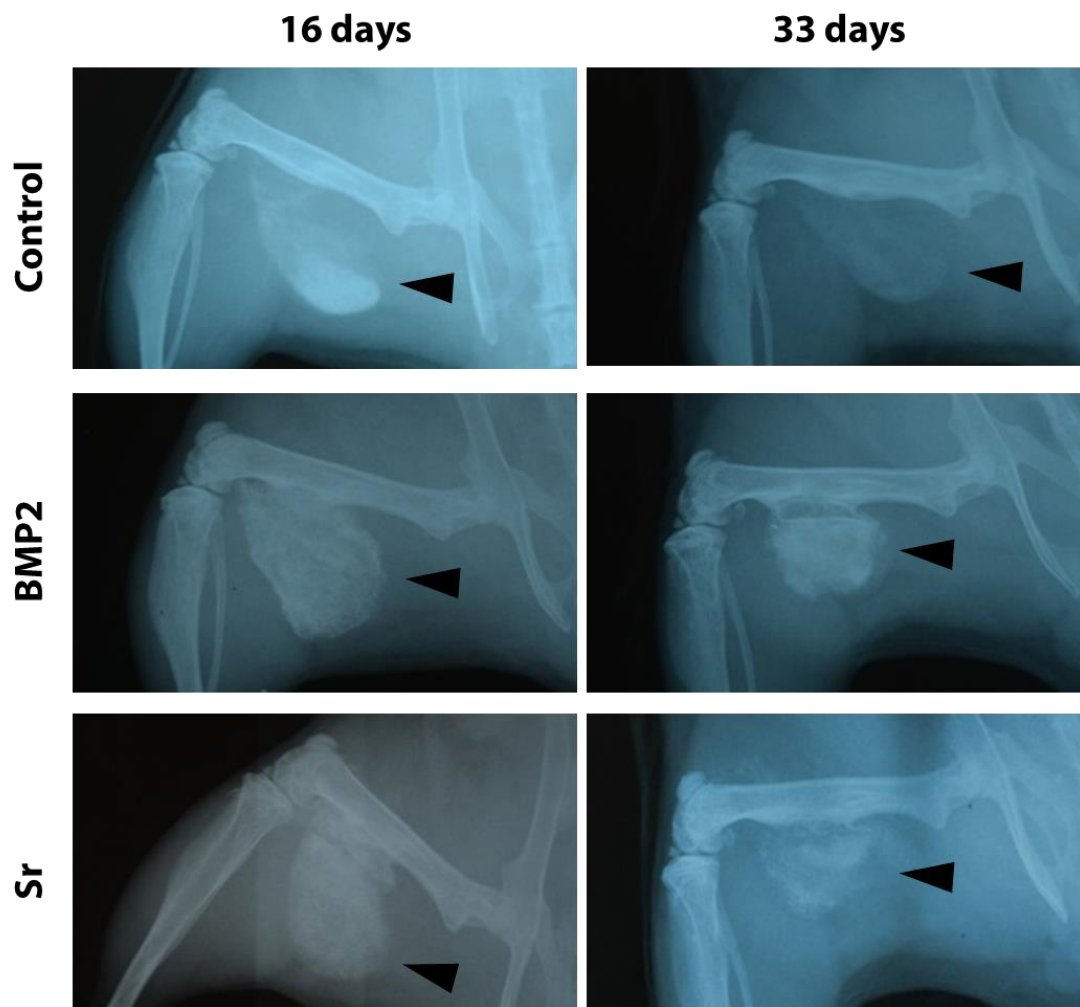


Fig. 4.1 Scheme of *in vivo* experiment to evaluate ectopic bone formation induced by sponge containing Sr-hydroxyapatite in comparison with sponge containing BMP2. The absence of both factors was used as control.

## 5.3 Results

### 5.3.1 X-ray Imaging

**Figure 4.2** shows X-ray images of mice implanted with control, BMP2 and Sr sponges after 16 and 33 days from surgery. The X-ray images showed a formation of new mineralized tissue from the periosteum of femur toward sponges, at both time points. The ectopic bone formation is more evident in BMP2 and Sr implants than in control and it is more extensive after 33 days than 16 days. Moreover, the implanted material is visible at X-ray (**black arrows in Fig. 4.2**), since it contains hydroxyapatite, and a reduction of its dimension can be observed passing from 16 to 33 days. X-ray images support macroscopic observations during harvesting (**Figure 4.3**): implants resulted well integrated with animal tissues with visible nerves and blood vessels all around; implants were strongly attached to femur, especially after 33 days; implants after 33 days resulted smaller than 16 days.



**Fig.4.2** X-ray pics at 16 and 33 days of mice implanted with Control, BMP2 and Sr sponge (black arrows indicate implanted sponge)

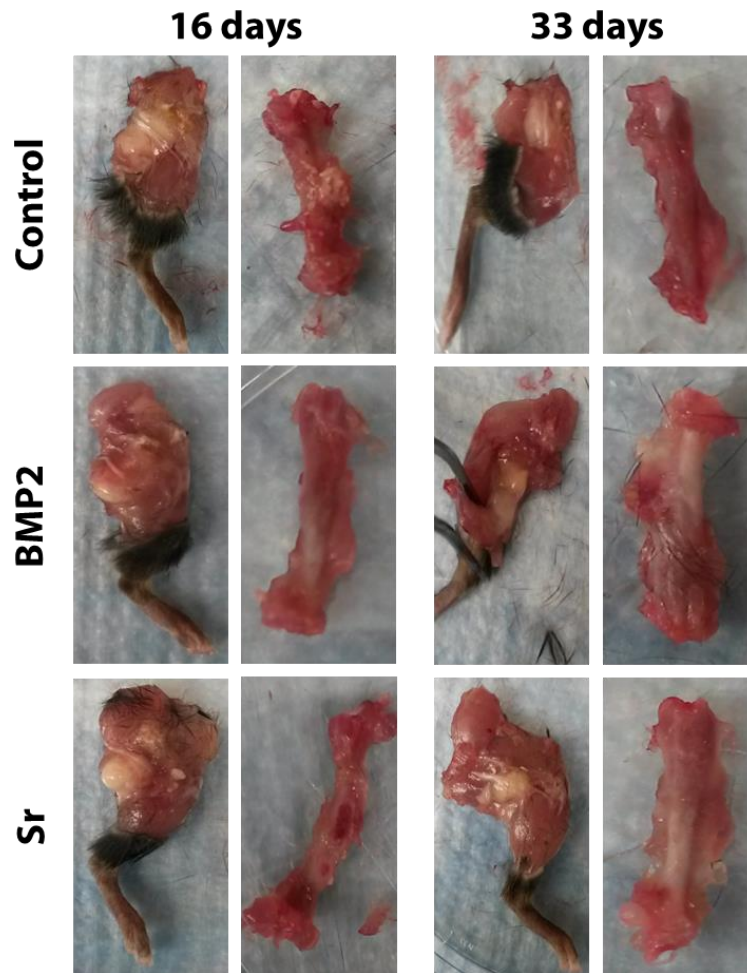
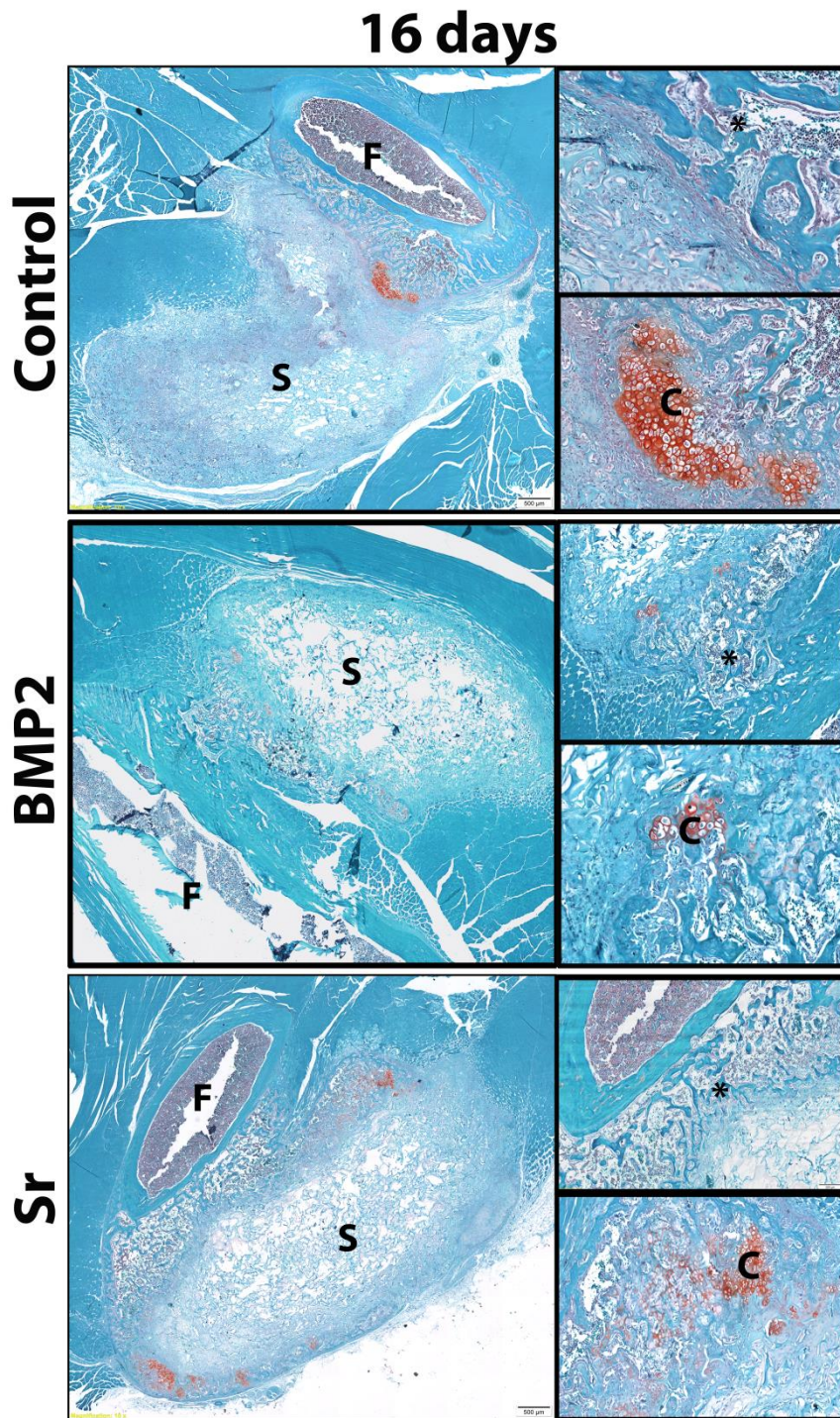


Fig. 4.3 Macroscopic observations at 16 and 33 days of limb and femur of mice implanted with Control, BMP2 and Sr sponges.

### 5.3.2 Histology analysis

Figure 4.4 shows representative images of Fast Green/Safranin-O stained femur, sponge and tissues surrounding of mice implanted with Control, BMP2 and Sr sponges, after 16 days from surgery. The formation of ectopic tissue (indicated with \* in Fig. 4.4) from the femoral cortical bone toward sponges (indicated with S in Fig. 4.4) was observed for all three implants, even if the new tissue formation seems more extended in mice that received Sr implant. Presence of cells was detected in all three types of implants and more extended cartilage tissue (indicated with C in Fig. 4.4), was observed in Sr-containing sponge if compared to BMP2 and control ones.



**Fig. 4.4** Histological observations performed at 16 days with Fast green/Safranin-O staining of limb of mice implanted with Control, BMP2 and Sr sponge. (F = Femur; S = Sponge; \* = ectopic bone; C = Cartilage)

### 5.3.3 Gene expression

In order to study gene expression, after 16 and 33 days, femur, muscle and implant were harvested separately from Control, BMP2 and Sr implanted mice. qRT-PCR was used to evaluate the expression of genes related to chondrocytes, osteoblasts, osteoclasts, osteocytes and stem cells recruitment. While significant expression of these genes was detected in femurs and implants, no

expression was measured in muscles. **Fig. 4.5** shows an overview of all tested genes after 16 and 33 days from femurs and implants of Control, BMP2 and Sr implanted mice. **Figures 4.6** and **4.7** show gene expression results from femurs and implants, respectively, after 16 days. **Figures 4.8** and **4.9** show gene expression results from femurs and implants, respectively, after 33 days.

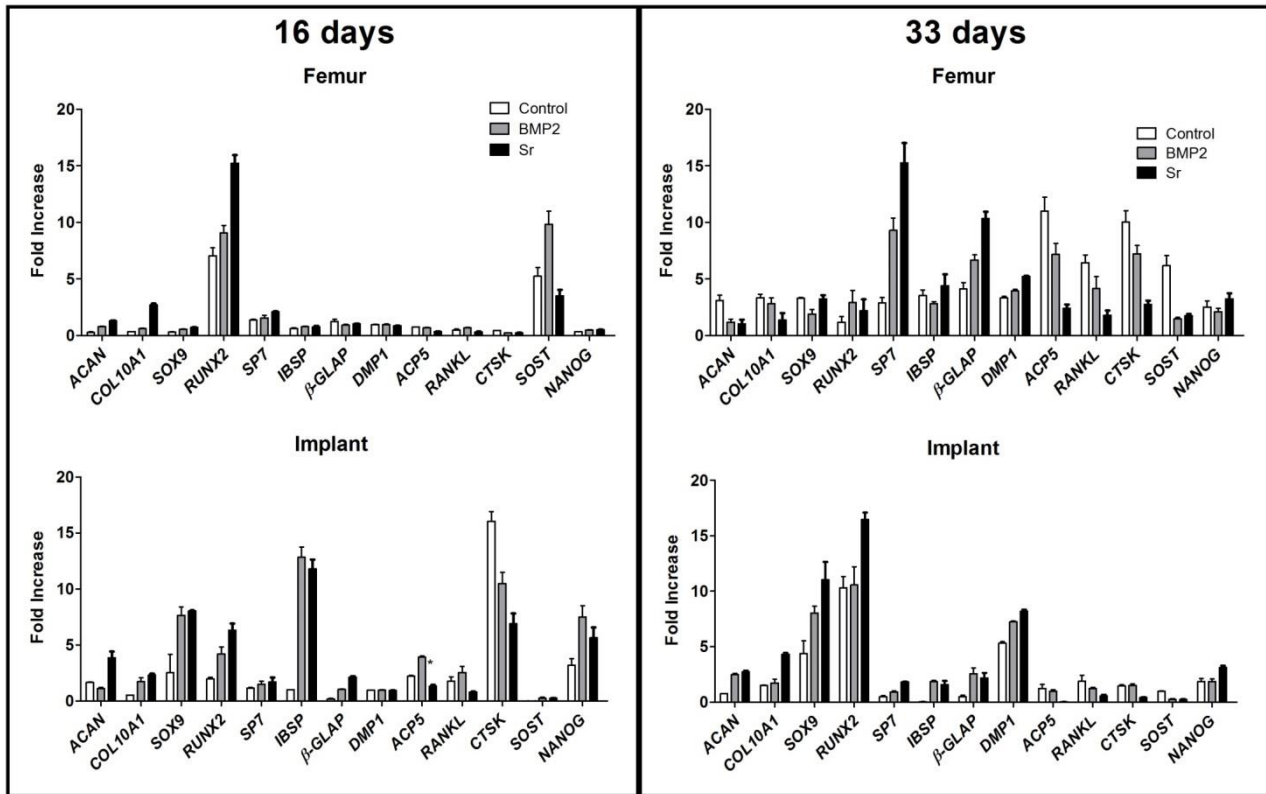


**Fig. 4.5** Gene Expression of chondrogenesis, osteogenic, osteoclasts, osteocytes and stem cell recruitment markers evaluated with qRT-PCR after 16 and 33 days in Femur and Implants.

### *Chondrogenesis Gene Expression*

*ACAN*, *COL10A1* and *SOX9* expression was analyzed as chondrogenesis markers.

After 16 days, all three genes were up-regulated in femur and implants harvested from mice implanted with Sr-containing sponge ( $p < 0.001$ ) if compared to control and BMP2 (**Fig. 4.6** and **4.7**). Up-regulations of *ACAN* and *SOX9* in femur of BMP2 implanted mice ( $p < 0.001$ ) (**Fig. 4.6**), *COL10A1* and *SOX9* in BMP2 sponges ( $p < 0.001$ ) were measured (**Fig. 4.7**), if compared to control. After 33 days, in femur, *ACAN* and *SOX9* resulted down-regulated by BMP2 sponge ( $p < 0.01$ ), whereas *ACAN* and *COL10A1* showed to be down-regulated by Sr sponge ( $p < 0.001$ ), if compared to control (**Fig. 4.8**). In Sr-containing implant, instead, expression of all three genes was up-regulated ( $p < 0.001$ ), if compared to control; whereas in BMP2 sponges, only *ACAN* and *SOX9* were up-regulated ( $p < 0.01$ ) if compared to control (**Fig. 4.9**).



## Osteogenic-associated Gene Expression

*DMP1*, *IBSP*,  $\beta$ -*GLAP*, *RUNX2* and *SP7* expression was analyzed as osteogenic-associated markers. After 16 days, an up-regulation of *RUNX2* and *SP7* in femur of mice that received the Sr implant was observed ( $p < 0.01$ ) if compared to control, instead, *RUNX2* resulted slightly up-regulated in femur of BMP2 implanted mice ( $p < 0.01$ ), if compared to control (**Fig. 4.6**). In BMP2 and Sr sponges, all osteogenic-associated genes, a part from *DMP1*, were up-regulated if compared to control ( $p < 0.05$ ) (**Fig. 4.7**).

After 33 days, in femurs of mice with BMP2 and Sr implants, only  $\beta$ -*GLAP* and *SP7* were up-regulated ( $p < 0.05$ ), if compared to control (**Fig. 4.8**). Furthermore, in Sr sponges, all osteogenic markers genes were up-regulated ( $p < 0.001$ ), while in BMP2 sponge similar up-regulation was observed for *DMP1*, *IBSP*,  $\beta$ -*GLAP* and *SP7* ( $p < 0.01$ ), if compared to control (**Fig. 4.9**).

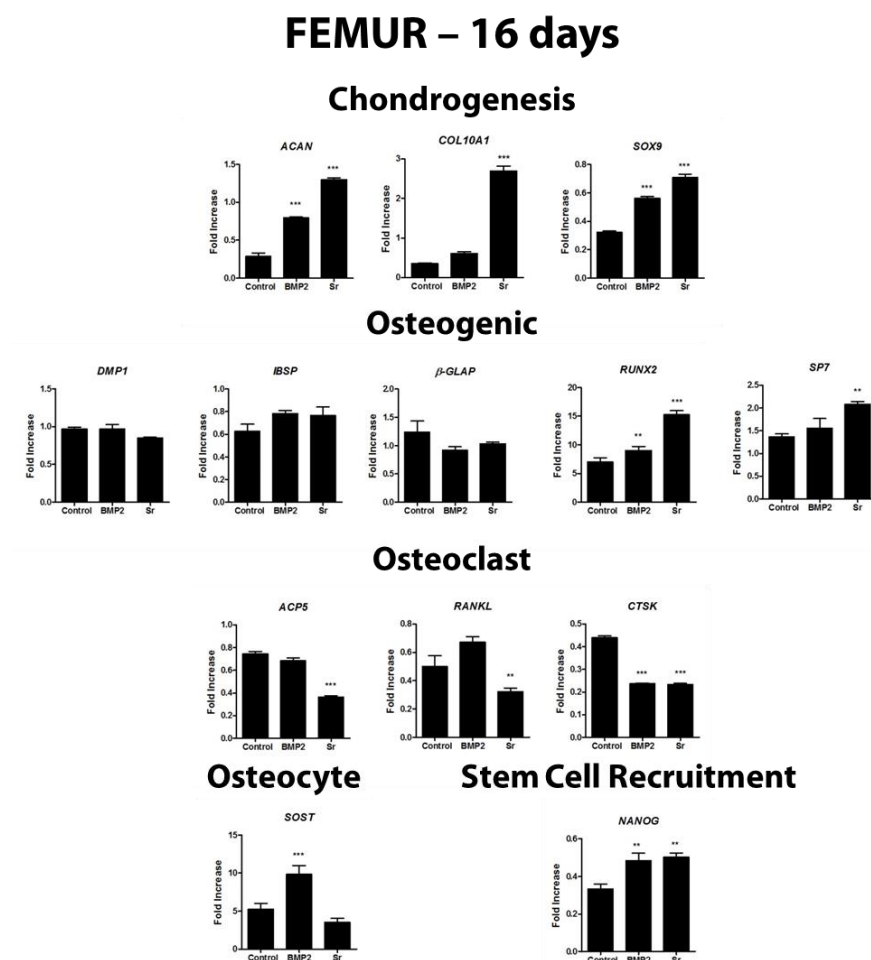


**Fig. 4.6** Gene Expression of chondrogenesis, osteogenic, osteoclasts, osteocytes and stem cell recruitment markers evaluated with qRT-PCR after 16 in femurs of mice that received control, BMP2 and Sr implant. Bars represent mean  $\pm$  SEM. Statistical analysis was performed against control (\* $p < 0,05$ ; \*\* $p < 0,01$ ; \*\*\* $p < 0,001$ )

## Osteoclasts-associated Gene Expression

*ACP5*, *RANKL* and *CTSK* expression was analyzed as marker for osteoclasts.

After 16 days, both in femur and Sr implant, all three genes were down-regulated if compared to control ( $p < 0.01$ ). *CTSK* resulted down-regulated in femur from BMP2 implanted mice and in BMP2 sponge while *ACP5* was up-regulated, if compared to control ( $p < 0.001$ ) (Fig. 4.6 and 4.7).

After 33 days, Sr-hydroxyapatite induced a significative down-regulation of all three genes both in femur and implant, if compared to control ( $p < 0.001$ ) (Fig. 4.8 and 4.9). BMP2 sponges, instead, down-regulated *RANKL* and *ACP5* in femur ( $p < 0.05$ ) (Fig. 4.8), but no big differences were observed in the sponge, if compared to control ( $p > 0.05$ ) (Fig. 4.9).

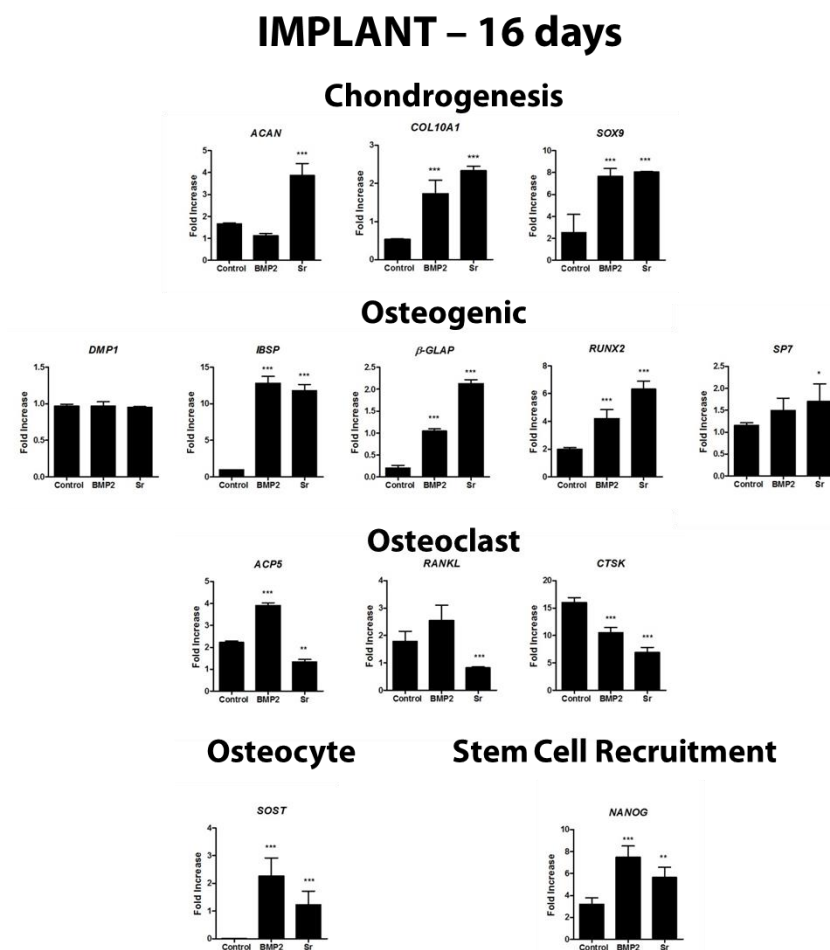


Fig. 4.7 Gene Expression of chondrogenesis, osteogenic, osteoclasts, osteocytes and stem cell recruitment markers evaluated with qRT-PCR after 16 in Control, BMP2 and Sr Implant. Bars represent mean  $\pm$  SEM. Statistical analysis was performed against control (\* $p < 0,05$ ; \*\* $p < 0,01$ ; \*\*\* $p < 0,001$ )

## Osteocytes-associated Gene Expression

*SOST* expression was analyzed as marker for osteocytes.

After 16 days, *SOST* was up-regulated in femurs of BMP2 implanted mice, if compared to control ( $p < 0.001$ ) (**Fig. 4.6**). Instead, in both BMP2 and Sr-containing sponges, up-regulation of *SOST* was observed if compared to control ( $p < 0.001$ ) (**Fig. 4.7**).

After 33 days, a significant down-regulation of *SOST* was observed both in femurs and sponges with BMP2 and Sr, if compared to control ( $p < 0.001$ ) (**Fig. 4.8 and 4.9**).

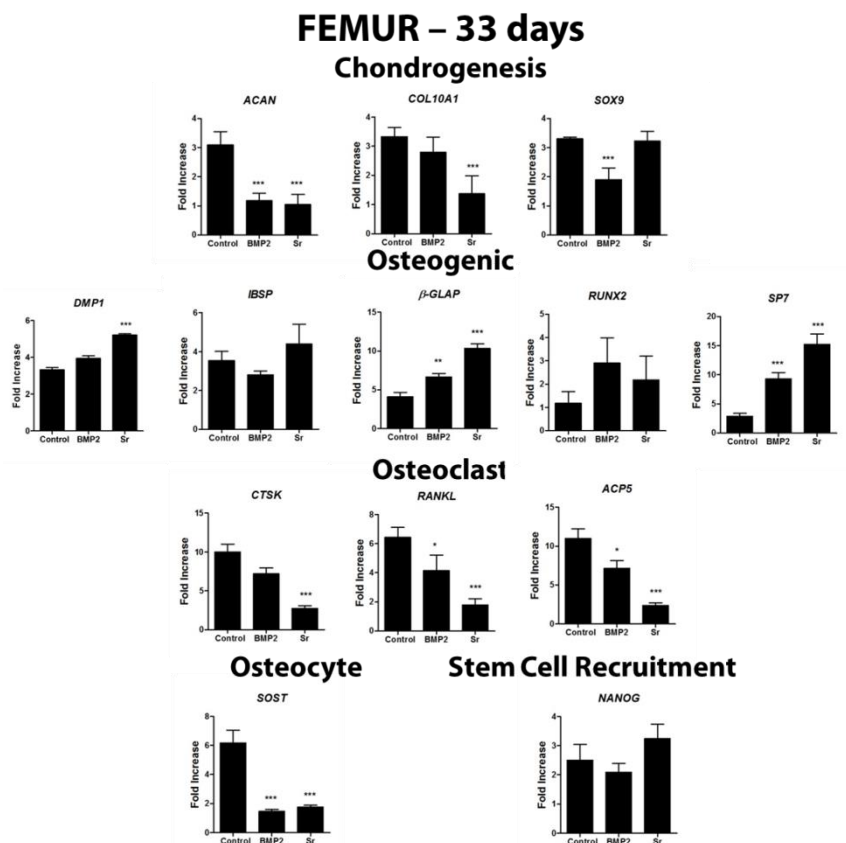


**Fig. 4.8** Gene Expression of chondrogenesis, osteogenic, osteoclasts, osteocytes and stem cell recruitment markers evaluated with qRT-PCR after 33 in Femur of mice that received control, BMP2 and Sr implant. Bars represent mean  $\pm$  SEM. Statistical analysis was performed against control (\* $p < 0.05$ ; \*\* $p < 0.01$ ; \*\*\* $p < 0.001$ )

## Stem cells recruitment Gene Expression

*NANOG* expression was analyzed as marker for stem cells recruitment.

After 16 days, an up-regulation of *NANOG* expression was observed in femur and implants with BMP2 and Sr, if compared to control ( $p < 0.01$ ) (Fig. 4.6 and 4.7).

After 33 days, up-regulation of *NANOG* expression in Sr sponge was observed, if compared to control and BMP2 ( $p < 0.001$ ), while no differences were observed in femurs from Control, BMP2 and Sr implanted mice ( $p > 0.05$ ) (Fig. 4.8 and 4.9).

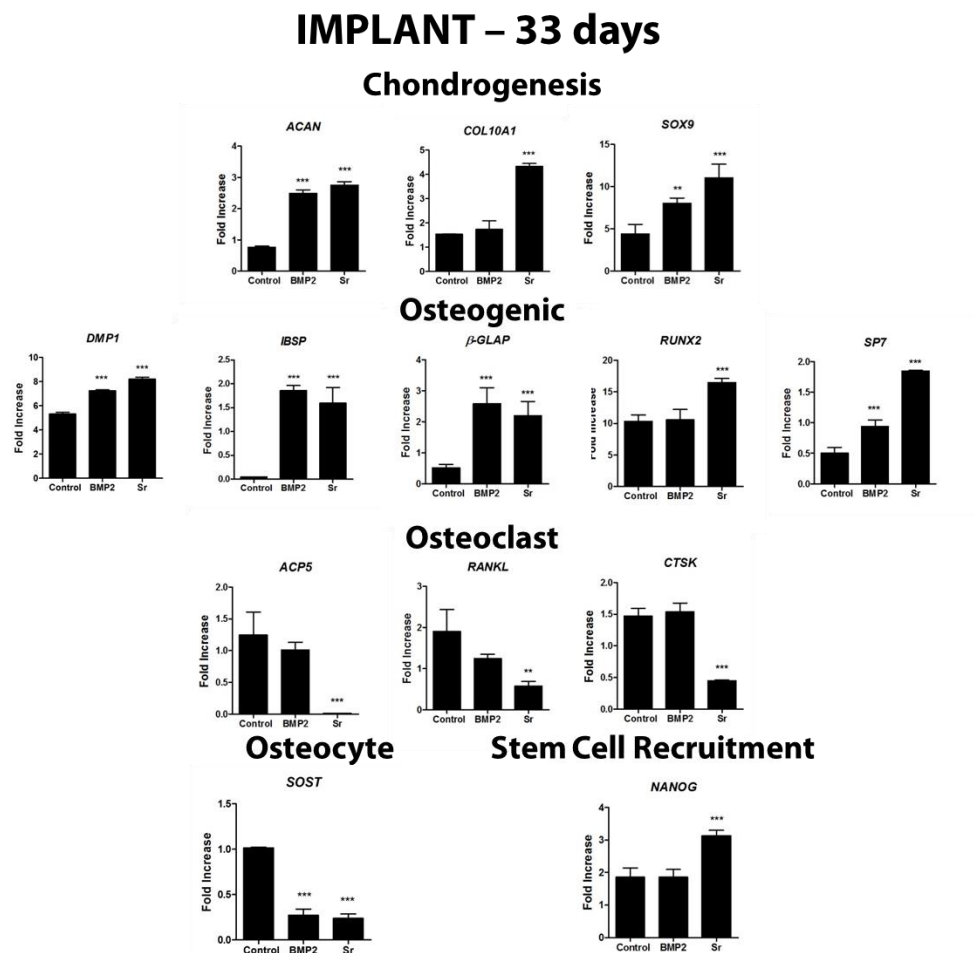


Fig. 4.9 Gene Expression of chondrogenesis, osteogenic, osteoclasts, osteocytes and stem cell recruitment markers evaluated with qRT-PCR after 33 in Control, BMP2 and Sr Implant. Bars represent mean  $\pm$  SEM. Statistical analysis was performed against control (\* $p < 0,05$ ; \*\* $p < 0,01$ ; \*\*\* $p < 0,001$ )

## 5.4 Discussion

In this study, ectopic bone formation induced by gelatin sponge containing BMP2 and Strontium-hydroxyapatite was evaluated. In particular, mice were bilaterally implanted with sponges which were inserted surrounding the femur, adjacent to the periosteal surface. After 16 and 33 days, mice were X-rayed; right limbs were harvested and fixed for histology analysis whereas gene expression from femur, implant and surrounding muscle of left limbs was analyzed.

To assess the effect of BMP2 and Sr, bone ectopic formation was evaluated also in mice implanted with sponges without BMP2 and Sr-hydroxyapatite and used as control. To make sponges harder and to improve their consistency for the surgery, a 30% nano-hydroxyapatite (Fluidinova®) suspension was adsorbed to sponges. For BMP2 implant, 0.3µg of recombinant BMP2 protein was added. This amount was demonstrated to be the minimum to induce femoral ectopic bone formation in mice implanted with BMP2-enriched demineralized bone matrix (data not shown). For Sr implant, instead, 10% of the nano-hydroxyapatite was substitute with Sr100 hydroxyapatite. This amount was extrapolated from *in vitro* studies, estimating the amount of Sr100 nanoparticles administered in 28 days to improve osteoblasts differentiation of hBMSCs.

X-ray revealed induction of ectopic bone formation by all three types of implants at both tested times (**Fig. 4.2**). We observed a more extensive ectopic mineralized tissue in mice implanted with BMP2 and Sr sponges, than the control. Moreover, we observed a reduction of implant dimension passing from 16 to 33 days, suggesting a material degradation and resorption over the time. X-ray data were confirmed by histology observations performed at 16 days: from the femoral cortical bone, new tissue formation toward the sponge and strictly connected to it, was observed (**Fig. 4.4**). Safranin-O staining highlighted a more extensive cartilage tissue in Sr implant than in BMP2 and control. These results were corroborated by gene expression of chondrogenesis markers *ACAN*, *COL10A1* and *SOX9* that were up-regulated by Sr-containing implant, if compared to control and BMP2, suggesting a higher stimulatory effect of Sr-hydroxyapatite to chondrogenesis (**Fig. 4.7 and 4.9**). *SOX9*, the gene responsible for chondrocyte lineage commitment from mesenchymal stem cells<sup>20</sup>, was significant increased by Sr implant at both tested time points. *ACAN* and *COL10A1* are specific late cartilage markers, which are used to assess the progression of chondrogenesis, specifically in endochondral ossification<sup>21</sup>. In this sense, at 33 days, Sr implant down-regulated these two genes in femurs suggesting the reduction of chondrogenesis in advantage to osteogenesis (**Fig. 4.8**). Sr-containing implant seems to stimulate and enhance the endochondral ossification process improving chondrogenesis, the first step toward ossification.

Afterwards, gene expression of osteogenic marker was evaluated. In particular, *RUNX2* and *SP7* are two transcriptional factors activated during osteoblasts differentiation, the first one activated in

earlier stages<sup>22</sup> and the second one in later ones<sup>23</sup>. A time course in activation of these two genes was observed, especially in implants. After 16 days, higher expression of *RUNX2* was observed in Sr containing implant and related treated femur, suggesting a stimulatory effect on osteoblasts differentiation at earlier stages (**Fig. 4.6 and 4.7**). After 33 days, higher increase of *SP7* expression was detected in Sr implant and related treated femur suggesting a stimulatory effect on osteoblasts differentiation also at later stages (**Fig. 4.8 and 4.9**). Moreover, *RUNX2* has also been demonstrated to have significant role in chondrocyte hypertrophy in endochondral ossification<sup>24</sup>. In this sense, *RUNX2* up-regulation by Sr implant corroborates the hypothesis of the stimulatory effect of Sr-hydroxyapatite on chondrogenesis.

Related to mature osteoblasts is the expression and deposition of osteocalcin, a small protein specific constituent of bone mineralized matrix<sup>25</sup> and transcribed by  $\beta$ -*GLAP* gene. Its expression resulted up-regulated in femur by Sr-containing implant after 16 and 33 days (**Fig. 4.6 to 4.9**).

*DMP1* gene expression is strictly related to bone matrix mineralization and later stages of skeletogenesis and it transcribes for dentin matrix protein 1<sup>26</sup>. After 16 days, no differences of *DMP1* expression was observed between control, BMP2 and Sr implants (**Fig. 4.6 and 4.7**), while, after 33 days, both in femur and implants, *DMP1* was up-regulated by Sr-containing implant (**Fig. 4.8 and 4.9**). Increased *DMP1* and  $\beta$ -*GLAP* expression, together with X-ray observations, suggest a higher stimulatory effect of Sr-hydroxyapatite on ectopic tissue formation and mineralization.

Another gene associated to osteogenesis is *IBSP* that transcribes for the bone sialoprotein, the most abundant non-collagenous protein in the bone matrix. Its expression in femurs resulted not modified by BMP2 and Sr implants at both tested time (**Fig. 4.6 and 4.8**), if compared to control, whereas, surprisingly, in BMP2 and Sr implants, *IBSP* expression is significantly increased (**Fig. 4.7 and 4.9**), suggesting bone matrix deposition by osteoblasts inside both types of implants.

To evaluate the effect of BMP2 and Sr implants also on bone resorption, expression of *ACP5*, *CTSK* and *RANKL* were analyzed. Sr implants down-regulated the three osteoclast associated gene, if compared to control and BMP2, at both tested times, with a higher effect at 33 days (**Fig. 4.6 to 4.9**). These data confirm the inhibitory effect of strontium on osteoclasts differentiation and bone resorption highlighting its dual action on osteoblasts and osteoclasts.

Another factor that influences the bone remodeling process is sclerostin/*SOST* expression as inhibitor of osteoblasts differentiation blocking the Wnt pathway<sup>27</sup>. After 16 days, no *SOST* expression was detected in control implant, suggesting absence of osteocytes, unlike to BMP2 and Sr implants (**Fig. 4.7**). After 33 days, BMP2 and Sr implants down-regulated *SOST* expression if compared to control suggesting a promotion of osteoblasts differentiation and bone matrix

deposition (**Fig. 4.8 and 4.9**). In this sense no differences were observed between BMP2 and Sr-hydroxyapatite.

*NANOG* expression was used to evaluate stem cells recruitment by implanted materials. *NANOG* has been demonstrated to be linked to the development and differentiation of cells in the extra-embryonic endoderm and appeared to interact via BMP signaling pathways by interfering with BMP's induction of mesenchymal stem cell differentiation<sup>28</sup>. Increased *NANOG* expression after 16 days in implant containing BMP2 and Sr, suggests higher stem cells recruitment for new tissue formation (**Fig. 4.7**). After 33 days *NANOG* expression decreased because of greater percentage of differentiated cells, unlike to Sr-containing implant, where *NANOG* expression was higher than control and BMP2 suggesting more prolonged stem cell recruitment by Sr-containing implant (**Fig. 4.9**).

In summary, Sr-containing implant induced a greater ectopic bone formation than control and BMP2 implant. The formation of new tissue starts with stem cell recruitment by implant and seems to proceed from chondrogenesis to osteogenesis following the endochondral ossification model. Sr-hydroxyapatite, in this sense, enhanced the differentiation of chondrocyte and the cartilage matrix deposition, as demonstrated by histological observations and chondrogenesis related gene expression. Afterwards, Sr-containing implant improved the osteoblasts differentiation and bone matrix deposition, acting on early and late stages of osteoblasts maturation. X-ray and histology observations revealed the presence of mineralized ectopic bone and Sr-hydroxyapatite, from a macroscopic point of view, showed comparable effect of BMP2. Next to the stimulatory effect on osteoblasts, an increase inhibition on osteoclastogenesis was observed by Sr-hydroxyapatite, if related to control and BMP2, confirming the dual action exerts by strontium on bone formation and bone resorption.

These results are in agreement with recent *in vivo* data showing that incorporation of Sr in bone substitutes<sup>29-31</sup>, collagen membranes<sup>32</sup> and titanium implants<sup>33-35</sup> enhanced bone regeneration and osseointegration. Importantly, the present results extend the previous observation by demonstrating the effect of strontium also on chondrogenesis and so the effect on the endochondral ossification process. Few *in vitro* works have been performed in this sense<sup>36</sup>, but, to the best of our knowledge, no *in vivo* results are present in literature.

## 5.5 Conclusion and Future Perspective

In this first *in vivo* study we demonstrated the ectopic bone formation induced by Strontium-containing implant. To do that, gelatin sponges were enriched with hydroxyapatite to improve their consistency and BMP2 or Sr-hydroxyapatite was added. Sponges were implanted around the femur, adjacent to the periosteal surface of 9-11 weeks old male mice. X-ray at 16 and 33 days revealed BMP2 and Sr-containing implants induced greater mineralized ectopic tissue formation from the femoral cortical bone toward sponge than control. We observed a reduction in implant size over the time suggesting its degradation. Histology analysis and gene expression revealed increased endochondral ossification, with chondrogenesis occurring prior to ossification, induced by Sr-hydroxyapatite. Moreover, Sr-containing implant improved bone formation by up-regulating osteogenic-associated gene expression and down-regulating genes related to osteoclasts differentiation. Sr-hydroxyapatite seems an excellent substituted of BMP2 protein to develop biomaterials for bone tissue regeneration: Sr-hydroxyapatite is more stable and easier to obtain than BMP2 and, moreover, it seems to be effective both on osteoblasts and osteoclasts.

Results presented in this chapter are part of an ongoing study. Histology analysis at 33 days have to be performed as well as other histology staining to evaluate TRAP activity and some cartilage and bone markers observed in gene expression, as type-10 collagen and osteocalcin. Moreover, *in vitro* studies need to be performed to study at cellular level the effect on chondrogenesis and osteoinduction of implanted materials.



## 5.6 References

1. Dimitriou, R., Jones, E., McGonagle, D. & Giannoudis, P. V. Bone regeneration: current concepts and future directions. *BMC Med.* **9**, 66 (2011).
2. Markides, H., McLaren, J. S. & El Haj, A. J. Overcoming translational challenges - The delivery of mechanical stimuli in vivo. *Int. J. Biochem. Cell Biol.* **69**, 162–72 (2015).
3. O’Keefe, R. J. & Mao, J. Bone tissue engineering and regeneration: from discovery to the clinic--an overview. *Tissue Eng. Part B. Rev.* **17**, 389–92 (2011).
4. Mravic, M., Péault, B. & James, A. W. Current trends in bone tissue engineering. *Biomed Res. Int.* **2014**, 865270 (2014).
5. Garreta, E., Gasset, D., Semino, C. & Borrós, S. Fabrication of a three-dimensional nanostructured biomaterial for tissue engineering of bone. *Biomol. Eng.* **24**, 75–80 (2007).
6. Cegielski, M., Izykowska, I., Podhorska-Okolow, M., Zabel, M. & Dziegiel, P. Development of foreign body giant cells in response to implantation of Spongostan as a scaffold for cartilage tissue engineering. *In Vivo* **22**, 203–6
7. Klangjorhor, J. *et al.* Hyaluronan production and chondrogenic properties of primary human chondrocyte on gelatin based hemostatic spongostan scaffold. *J. Orthop. Surg. Res.* **7**, 40 (2012).
8. Anders, J. O., Mollenhauer, J., Beberhold, A., Kinne, R. W. & Venbrocks, R. A. Gelatin-based haemostyptic Spongostan as a possible three-dimensional scaffold for a chondrocyte matrix?: an experimental study with bovine chondrocytes. *J. Bone Joint Surg. Br.* **91**, 409–16 (2009).
9. Chen, S. *et al.* Effect of high molecular weight hyaluronic acid on chondrocytes cultured in collagen/hyaluronic acid porous scaffolds. *RSC Adv.* **5**, 94405–94410 (2015).
10. Paganelli, C. *et al.* Indications on suitable scaffold as carrier of stem cells in the alveoloplasty of cleft palate. *J. Oral Rehabil.* **33**, 625–9 (2006).
11. Cegielski, M. *et al.* Experimental xenotransplantation of antlerogenic cells into mandibular bone lesions in rabbits: two-year follow-up. *In Vivo* **24**, 165–72
12. Arias-Gallo, J., Chamorro-Pons, M., Avendaño, C. & Giménez-Gallego, G. Influence of acidic fibroblast growth factor on bone regeneration in experimental cranial defects using spongostan and Bio-Oss as protein carriers. *J. Craniofac. Surg.* **24**, 1507–14 (2013).
13. Skogh, A.-C. D. *et al.* Variation in calvarial bone healing capacity: a clinical study on the effects of BMP-2-hydrogel or bone autograft treatments at different cranial locations. *J. Craniofac. Surg.* **24**, 339–43 (2013).
14. Moucha, C. S. & Einhorn, T. A. in *Bone Regeneration and Repair* 169–194 (Humana Press,

2005). doi:10.1385/1-59259-863-3:169

15. Carreira, A. C. *et al.* Critical Reviews in Oral Biology & Medicine Bone Morphogenetic Proteins : Facts , Challenges , and Future. *Crit. Rev. oral Biol. Med.* **93**, 335–345 (2014).
16. Bragdon, B. *et al.* Bone Morphogenetic Proteins : A critical review. *Cell. Signal.* **23**, 609–620 (2011).
17. Merino, R., Macias, D., Gañan, Y., Economides, A. N. & Hurle, J. M. The BMP antagonist Gremlin regulates outgrowth , chondrogenesis and programmed cell death in the developing limb. *Development* **126**, 5515–5522 (1999).
18. Zhu, W. *et al.* Noggin regulation of bone morphogenetic protein ( BMP ) 2 / 7 heterodimer activity in vitro. *Bone* **39**, 61–71 (2006).
19. Schmittgen, T. D. & Livak, K. J. Analyzing real-time PCR data by the comparative CT method. *Nat. Protoc.* **3**, 1101–1108 (2008).
20. Provot, S. & Schipani, E. Molecular mechanisms of endochondral bone development. *Biochem. Biophys. Res. Commun.* **328**, 658–65 (2005).
21. Mwale, F., Stachura, D., Roughley, P. & Antoniou, J. Limitations of using aggrecan and type X collagen as markers of chondrogenesis in mesenchymal stem cell differentiation. *J. Orthop. Res.* **24**, 1791–8 (2006).
22. Ducy, P., Zhang, R., Geoffroy, V., Ridall, A. L. & Karsenty, G. Osf2/Cbfa1: A Transcriptional Activator of Osteoblast Differentiation. *Cell* **89**, 747–754 (1997).
23. Nakashima, K. *et al.* The novel zinc finger-containing transcription factor Osterix is required for osteoblast differentiation and bone formation. *Cell* **108**, 17–29 (2002).
24. Kini, U. & Nandeesh, B. N. in *Radionuclide and Hybrid Bone Imaging* 29–57 (Springer Berlin Heidelberg, 2012). doi:10.1007/978-3-642-02400-9\_2
25. Caetano-Lopes, J., Canhão, H. & Fonseca, J. E. Osteoblasts and bone formation. *Acta Reumatol. Port.* **32**, 103–10
26. Sun, Y. *et al.* Roles of DMP1 processing in osteogenesis, dentinogenesis and chondrogenesis. *Cells. Tissues. Organs* **194**, 199–204 (2011).
27. Seme, M. SOST Is a Ligand for LRP5 / LRP6 and a Wnt Signaling Inhibitor \*. *J. Biol. Chem.* **280**, 26770–26775 (2005).
28. Bais, M. *et al.* Transcriptional analysis of fracture healing and the induction of embryonic stem cell-related genes. *PLoS One* **4**, e5393 (2009).
29. Li, Y., Shui, X., Zhang, L. & Hu, J. Cancellous bone healing around strontium-doped hydroxyapatite in osteoporotic rats previously treated with zoledronic acid. *J Biomed Mater Res Part B* **104**, 476–481 (2015).

30. Zhang, Y. *et al.* Evaluation of Injectable Strontium-Containing Borate Bioactive Glass Cement with Enhanced Osteogenic Capacity in a Critical-Sized Rabbit Femoral Condyle Defect Model. *Appl. Mater. Interfaces* **7**, 2393–2403 (2015).
31. Zhang, Y., Wei, L., Wu, C. & Miron, R. J. Periodontal Regeneration Using Strontium-Loaded Mesoporous Bioactive Glass Scaffolds in Osteoporotic Rats. *PLoS One* **9**, e104527 (2014).
32. Kitayama, S. *et al.* Regeneration of rabbit calvarial defects using biphasic calcium phosphate and a strontium hydroxyapatite-containing collagen membrane. *Clin. Oral Implants Res.* **0**, 1–9 (2015).
33. Liang, Y. *et al.* Strontium coating by electrochemical deposition improves implant osseointegration in osteopenic models. *Exp. Ther. Med.* **9**, 172–176 (2015).
34. Zhang, J., Liu, L., Zhao, S., Wang, H. & Yang, G. Characterization and In Vivo Evaluation of Trace Element-Loaded Implant Surfaces in Ovariectomized Rats. *Int J Oral Maxillofac Implant.* (2015).
35. Newman, S. D. *et al.* Enhanced Osseous Implant Fixation with Strontium-Substituted Bioactive Glass Coating. *Tissue Eng. Part A* **20**, 1850–1857 (2014).
36. Okita, N. *et al.* Supplementation of strontium to a chondrogenic medium promotes chondrogenic differentiation of human dedifferentiated fat cells. *Tissue Eng. Part A* **9–10**, 1695–704 (2015).



# Chapter 5

---

## 6. Sr-containing nanoparticles as a potential countermeasure for the bone loss induced by microgravity

### 6.1 Introduction

Many are the studies about bone loss observed in astronauts after spaceflight and in ground simulated microgravity experiments and in the last decades, thanks to the new technologies to simulate microgravity on earth and to the increased possibility to perform experiments on ISS, the number of investigations in this field is grown up exponentially. Bone loss ranges from 1%–2% to 12%–24% per month in space-flown animals<sup>1</sup> and from 2%–9% in astronauts, with slow and often only partial recovery. This degeneration has been mainly attributed to altered bone tissue regenerative growth and repair, and a distorted responsiveness to factors present in the micro-environment: i.e., reduced or absent gravitational forces decrease the integrity of osteoblasts and increase bone resorption by osteoclasts. However, it is only recently that consideration has been given to the possibility that unbalanced bone remodeling in spaceflight may be orchestrated by BMMSCs as well as osteoblasts, osteocytes and osteoclasts<sup>2–5</sup>.

MSCs represent a stem cell population present in adult tissues that can be isolated, expanded in culture, and characterized *in vitro* and *in vivo*. Their ability to self-renew, their multipotent differentiation capacity or simply their stem capability is the main features. BMMSCs can differentiate efficiently and robustly into anchorage-dependent cells, such as osteoblasts, chondrocytes, and adipocytes<sup>6</sup> and also produce active substances regulating bone homeostasis. In terms of bone remodeling, the key components and biological functions of BMMSCs *in vivo* are in part controlled by their niches located mainly in perivascular areas of bone marrow or close to the endosteum<sup>7–10</sup>.

Over the last 10 years, studies have shown that all cells can respond to applied or cell-generated mechanical forces by activating mechanosensors that mediate the complex process of biological mechanotransduction<sup>11–13</sup>. Accordingly, it is widely recognized that defects in mechanotransduction can contribute to human diseases and atypical mechanical stresses, and that the normal mechanotransduction modulate cell processes and cause tissue function impairment or failure<sup>13,14</sup>. The cytoskeleton, ECM, adhesion complexes and membranes are the first and most common cell mechanosensors. As all proteins are deformable and therefore subject to mechanical modulation,

many enzymes that change their conformation in response to force, such as kinases, phosphatases, GTPases, cyclases, and G protein-coupled receptors, create transduction pathways that lead to mechanical stress. Force transduction can also involve changes in the kinetic rate constant of a mechanosensitive enzyme or, more qualitatively, expose cryptic binding sites on a molecule<sup>15</sup>. The mechanotransduction mechanisms involved in bone repair and regeneration have been interpreted on the basis of the tensegrity<sup>16,17</sup> and mechanosome theories<sup>18</sup>. In space research, mechanotransduction has been mainly investigated in studies of bone loss under simulated microgravity conditions, whereas most the studies of flown cells and yeast considered the cytoskeleton the main mechanosensor<sup>19</sup>.

Simulated microgravity reduces osteoblastogenesis of human BMMSCs and induces adipogenesis. Briefly, hBMMSCs failed to express alkaline phosphatase, collagen 1, osteonectin, and Runx2, whereas PPAR- $\gamma$ 2 (which is important for adipocyte differentiation), adipisin, leptin and glut-4 were all highly expressed after 7 d of simulated microgravity. The cells also showed decreased ERK and increased p38 phosphorylation, the pathways that respectively regulate the activity of Runx2 and PPAR- $\gamma$ 2<sup>2</sup>. The reduction in osteoblastic differentiation and induction of adipocytic differentiation, initially associated with reduced integrin signaling<sup>2</sup> was then mainly attributed to the large increase in G-actin, reduced RhoA activity and the subsequent phosphorylation of cofilin<sup>20</sup>.

To address the challenge of microgravity induced musculoskeletal alteration, astronauts usually spend ~2.5 hrs/day of exercising (running and weight lifting). However, this is still not sufficient enough to attenuate bone loss in space. While promising studies have shown anabolic effects using drugs and growth factors, the long-term effects of pharmacological agents are still unclear. Furthermore, drugs have mostly systemic effects, are not as effective in space, and are expensive as a treatment for extended space time<sup>21</sup>. Some authors demonstrated the effect of testosterone and synthetic anabolic steroid (nandrolone decanoate) on musculoskeletal regeneration in hind limb suspended rat model<sup>22</sup> but, these pharmacological treatments are usually hard to translate on humans. Other evidence demonstrated the positive effect *in vitro* and *in vivo* of pulsed ultrasound<sup>23</sup> on bone loss, but all these countermeasure are not sufficient enough to attenuate bone loss in space.

Our group already demonstrated the positive effect of Strontium-containing hydroxyapatite NPs on bone deposition. *In vitro* and *in vivo* results showed increasing in bone deposition by osteoblasts and reduction of osteoclasts differentiation by Sr-containing nanoparticles.

In this chapter encouraging results (FIRST PART) about the effect of Sr100 nanoparticles on hBMMSCs cultured on Random Positioning Machine (RPM) that simulates microgravity on earth are reported. In particular, ECM deposition and mineralization, ALP activity and gene expression were evaluated.

Moreover, it is described the experiment we had the opportunity to perform on ISS (SECOND PART) about the effect exerted by the addition of hydroxyapatite nanoparticles on the differentiation of hBMMSCs to osteoblasts in microgravity. The experiment was launched with the SpX-6 , the 14 April 2015 (Cape Canaveral, Florida, USA).

All data presented in this chapter are the results of a fruitful cooperation among our group in Pavia with the Institute of Crystallography of National Research Council of Italy (CNR) in Rome and with the Department of Pharmacological and Biomolecular Sciences of University of Milan. Furthermore, the hardware used for the experiment on ISS was provided by the industrial partner, Kayser Italia ([www.kayser.it](http://www.kayser.it))

## 6.2 Materials and Methods

### 6.2.1 Isolation, expansion, and culture of hBMMSCs

The design of this study was approved by the Institutional Review Board of the Fondazione IRCCS Policlinico San Matteo and the University of Pavia (2011).

BM aspirates were harvested from healthy pediatric hematopoietic stem cell donors after obtaining written informed consent. Thirty milliliters of BM from each donor was assigned to BM-MSC generation; heparin was added as an anticoagulant. Mononuclear cells were isolated from BM aspirates (30 mL) by Ficoll density gradient centrifugation (density, 1.077 g/mL; Lymphoprep, Nycomed Pharma, Oslo, Norway) and plated in non-coated 75- to 175-cm<sup>2</sup> polystyrene culture flasks (Corning Costar, Celbio, Milan, Italy) at a density of  $16 \cdot 10^4$  cells/cm<sup>2</sup>. Cells were cultured in Mesencult medium (Stem Cell Technologies, Vancouver, Canada) supplemented with 2mM L-glutamine, 50 µg/mL gentamycin, and 10% fetal calf serum. Cultures were maintained at 37°C in a humidified atmosphere containing 5% CO<sub>2</sub>. After 48 h, non-adherent cells were discarded and culture medium was replaced twice a week. After reaching 80% confluence as a minimum, the cells were harvested and replated for expansion at a density of 4000 cells/cm<sup>2</sup> until the fifth passage. The colony-forming unit fibroblast assay (CFU-F) was performed as described previously<sup>24</sup>. CFU-F formation was examined after 12 days of incubation in a humidified atmosphere (37°C, 5% CO<sub>2</sub>); the clonogenic efficiency was calculated as the number of colonies per 10<sup>6</sup> BM mononuclear cells seeded. According to the International Society for Cellular Therapy on the nomenclature of mesenchymal progenitors, the cells cultured for this study were defined as multipotent stromal cells. To phenotypically characterize hBMMSCs and to define their purity, FACS analysis was performed as previously described<sup>24</sup>. After reaching 80% confluence at a minimum, the cells were harvested and replated for expansion at a density of  $2.5 \cdot 10^4$  cells/cm<sup>2</sup>. The cells were cultured at 37°C, 5% CO<sub>2</sub>, and three fifths of the medium was renewed every 3 days.

### 6.2.2 Cell Culture Condition and Nanoparticles treatment

A suspension ( $5 \times 10^5$ ) of hBMMSCs in Mesencult medium was seeded in 25cm<sup>2</sup> tissue culture flasks and allowed to attach and reach the confluence in 72 hours. Then, the medium was replaced with osteogenic medium (OM) and changed 2 times per week:  $\alpha$ -MEM (Invitrogen, Paisley, PENN) supplemented with 10% fetal bovine serum, 50 µg/mL penicillin-streptomycin, 2% L-glutamine, 2% Sodium Pyruvate,  $10^{-7}$  M dexamethasone, 50 µg/mL ascorbic acid, and 5mM  $\beta$ -glycerophosphate<sup>25</sup>.



The osteogenic differentiation of hBMMSCs was performed for 8 and 28 days on the ground (GC) and on the Random Position Machine (RPM) and samples were treated with 3 different nanoparticle (NPs) suspensions: Ca100, Ca50Sr50 and Sr100. To evaluate the effect of nanoparticles on osteoblast differentiation of hBMMSCs, 5 mg of nano-powders (Ca100, Ca50Sr50 and Sr100) were suspended in 4 mL of 5% BSA solution, sonicated for 1 h at 45°C using LBS2 sonicator bath (FALC Instruments) with an operation frequency of 40 kHz and then diluted with Phosphate Buffer Solution (PBS). Nanoparticles suspensions were used at concentration of 62.5 µg/mL in the cell culture medium.

### 6.2.3 Culture on the RPM

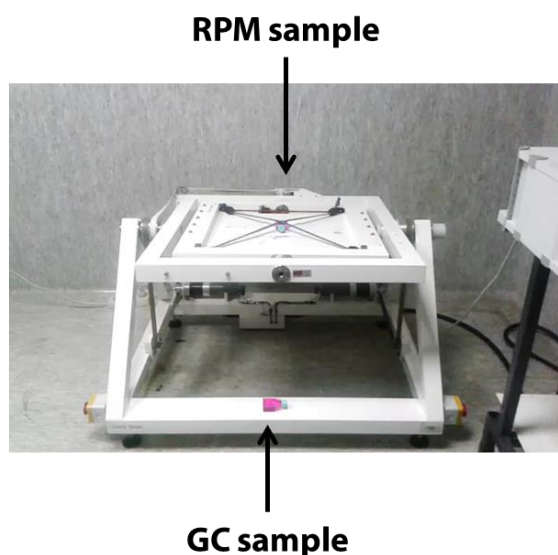


Fig. 5.1 Random positioning Machine (RPM).

Microgravity conditions were simulated using the RPM (Dutch Space, Leiden, Netherlands)<sup>26</sup> (Fig.5.1). The RPM provides continuous random change in orientation relative to the gravity vector of an accommodated experiment. Culture flasks containing confluent monolayers, 72 hours after seeding were completely filled with medium supplemented with 12.5 mM HEPES (Sigma-Aldrich) devoid of air bubbles and fixed on the RPM, as close as possible to the centre of the platform, which was then rotated using the real random mode (random speed and random direction) of the machine. The RPM operated

at 37°C. GC cultures, treated in parallel in identical equipment, were placed on the basis of the RPM.

### 6.2.4 Resazurin-based assay

The resazurin-based assay was used to estimate the number of viable cells by measuring the reduction of resazurin into resorufin. Resazurin solution (Sigma-Aldrich) was added as one-tenth of culture volume to each flask, which was then incubated for 3 h at 37°C and 5% CO<sub>2</sub>. Optical measurements were run on aliquots of 100 µL by a microplate reader (BioRad Laboratories, Hercules, CA, USA) at reference wavelengths of 600 nm and 690 nm at day 8 and 28 on NPs treated and untreated cells cultured on ground and on RPM. A cell viability standard curve was used to express the results as number of live cells.

### **6.2.5 Alkaline Phosphatase (ALP) Activity**

ALP activity was determined using a colorimetric end point assay<sup>27</sup>. The assay measures the conversion of the colorless substrate p-nitrophenol phosphate (pNPP) by the enzyme ALP to the yellow product p-nitrophenol; the rate of color change corresponds with the amount of enzyme present in solution. The test was performed as previously described<sup>28</sup> on cells cultured in presence or absence of NPs on ground and on RPM at 8 and 28 days. Samples were run in triplicate and compared with the calibration curve of p-nitrophenol standards. The enzyme activity was expressed as micromoles of p-nitrophenol produced per minute per milligram of enzyme.

### **6.2.6 Quantification of calcium – Alizarin Red Staining**

To analyze calcium (Ca) deposition by hBMMSCs, after 8 and 28 days of culture in GC and RPM condition, cells were rinsed with PBS, fixed for 30 min at 4°C with 4% PFA and stained for 10 min with 40 mM Alizarin Red S (pH 4.2, Sigma-Aldrich)<sup>29</sup>. Alizarin Red S staining was released from the cell matrix by incubation in 10% cetylpyridinium chloride (Sigma-Aldrich) in 10 mM sodium phosphate (pH 7.0), for 15 min and the absorbance measured at 562 nm.

### **6.2.7 Extraction of ECM proteins and enzyme-linked immunosorbent assay**

Protein precipitation with acetone was performed from flow-through of the RNA binding step during the total RNA extraction procedure (see below). Four volumes of acetone were added to the flow-through and incubated for 30 minutes at -20°C. Samples were allowed to thaw and centrifuged for 10 minutes at 16000g. Pellet was washed 1 time with 50% Ethanol, resuspended in 2% SDS solution and the total protein concentration was evaluated with the BCA Protein Assay Kit (Pierce Biotechnology, Inc., Rockford, IL).

Calibration curves to measure type-I and -III collagens, decorin, osteopontin, osteocalcin, osteonectin, FN, and ALP were performed. Microtiter wells were coated with increasing concentrations of each purified protein, from 10 ng to 2 mg, in coating buffer (50mM Na<sub>2</sub>CO<sub>3</sub>, pH 9.5) overnight at 4°C. Control wells were coated with bovine serum albumin (BSA) as a negative control. To measure the ECM amount of each protein by ELISA, microtiter wells were coated, overnight at 4°C, with 100 µL of the previously extracted ECM (20 µg/mL in coating buffer). After three washes with PBS containing 0.1% (v/v) Tween 20, the wells were blocked by incubating with 200 µL of PBS containing 2% (w/v) BSA for 2 h at 22°C. The wells were subsequently incubated for 1.5 h at 22°C with 100 µL of the anti-type-I and -III collagens, antidecorin, anti-osteopontin, anti-osteocalcin, anti-osteonectin, and anti-ALP rabbit polyclonal antisera (1:500 dilution in 1% BSA), kindly provided by L. Fisher. The same dilution was used for the anti-FN rabbit polyclonal IgG. After washing, the wells were incubated for 1 h at 22°C with 100µL of horseradish peroxidase

(HRP)-conjugated goat anti-rabbit IgG (1:1000 dilution in 1% BSA). The wells were finally incubated with 100 mL of the development solution (phosphate-citrate buffer with o-phenylenediamine dihydrochloride substrate). The color reaction was stopped with 100  $\mu$ L of 0.5 M H<sub>2</sub>SO<sub>4</sub>, and the absorbance values were measured at 490nm with a microplate reader (BioRad Laboratories). An underestimation of the absolute protein deposition is possible because the sample buffer, used for matrix extraction, contained sodium dodecyl sulfate, which may interfere with the protein adsorption during ELISA. The amount of ECM constituents was expressed as pg/cell.

### **6.2.8 Fluorescence microscopy analysis**

After 28 days of culture on ground and on RPM, untreated and NPs treated samples were fixed with 4% (w/v) paraformaldehyde solution in 0.1M phosphate buffer (pH 7.4) for 30 min at 4°C and washed with PBS three times. For immunological studies, paraformaldehyde fixed cells were blocked by incubating with PAT (PBS containing 1% [w/v] bovine serum albumin and 0.02% [v/v] Tween 20) for 2 h at room temperature and washed. Anti-type-I collagen and anti-osteocalcin rabbit polyclonal antisera were used as the primary antibodies diluted to 1:500 in PAT. The incubation with the primary antibodies was performed overnight at 4°C, whereas the negative controls were incubated with PAT alone. The samples and the negative controls were washed and incubated with Alexa-Fluor-488 goat anti-rabbit IgG (H<sub>β</sub>L; Invitrogen) at a dilution of 1:750 in PAT for 1 h at room temperature. At the end of the incubation, the samples were washed in PBS, counterstained with a Hoechst solution (2  $\mu$ g/mL) to target the cellular nuclei, and then washed. The images were taken by the Fluorescence microscope (Leica Microsystems, Bensheim, Germany) equipped with a digital image capture system at 40X magnification.

### **6.2.9 Gene expression analyses**

Total RNA from samples cultured in presence and absence of NPs, on ground and on RPM for 8 and 28 days in DM was extracted with the RNeasy Plus Mini Kit (Qiagen) and retrotranscribed into cDNA with the iScript cDNA Synthesis Kit (BioRad Laboratories) as previously reported<sup>28</sup>. Quantitative reverse-transcription polymerase chain reaction (qRT-PCR) analysis was performed in a 48-well optical reaction plate using a MiniOpticon Real-Time PCR System (BioRad Laboratories). Oligonucleotide primers were designed with gene sequences published in GenBank and are indicated in Table 5.1. Reactions were performed in 20  $\mu$ L with 2  $\mu$ L of cDNA, 10  $\mu$ L Brilliant SYBER Green qPCR Master Mix (Stratagene, La Jolla, CA), 0.4  $\mu$ L of each primer, and 7.2  $\mu$ L H<sub>2</sub>O. PCR conditions were as follows: 3 min at 95°C, 40 cycles of 5 sec at 95°C, and 23 sec at 60°C. Gene expression was normalized to the 18S housekeeping gene expression. Each sample

was analyzed in triplicate and correlated against a standard curve. The reaction mixture, without cDNA, was used as a negative control in each run.

Gene	Forward primer	Reverse Primer
<b>IBSP</b>	5'-GGGCAGTAGTGACTCATCCG-3'	5'-TCAGCCTCAGAGTCTTCATCTTC-3'
<b>ALP</b>	5'- ACCTCGTTGACACCTGGAAG-3'	5'- CCACCATCTCGGAGAGTGAC-3'
<b>COL1A1</b>	5'-TGTAAGCGGTGGTGGTTATG-3'	5'-GGTAGCCATTTTCCTTGGAAG-3'
<b>COL3A1</b>	5'-TGGATCAGATGGTCTTCCA-3'	5'-TCTCCATAATACGGGGCAA-3'
<b>DCN</b>	5'-CGAGTGGTCCAGTGTCTGA-3'	5'-AAAGCCCCATTTTCAATTCC-3'
<b>RUNX2</b>	5'-ACAGTAGATGGACCTCGGGA-3'	5'-ATACTGGGATGAGGAATGCG-3'
<b>BMP2</b>	5'-AACGGACATTCGGTCCTTGC-3'	5'-CGCAACTCGAACTCGCTCAG-3''
<b>18S</b>	5'-GTAACCCGTTGAACCCCAT-3'	5'-CCATCCAATCGGTAGTAGCG-3'

Tab.5.1 Primers used for Quantitative Reverse-Transcription Polymerase Chain Reaction

### 6.2.10 Experiment performed on ISS

In order to study the effect of Sr100 hydroxyapatite nanoparticles on hBMMSCs differentiation to osteoblasts on ISS, 12 STROMA experimental units (EU) provided by Kyser Italia were used to cultivate cells in absence and presence of Ca100 and Sr100 nanoparticles: 6 were launched on ISS and 6 were cultured on ground. **Fig. 5.2** shows the closed EU with the electronic part built on (**Fig. 5.2A**) and the KIC (**Fig. 5.2B**) that contains the EU and allows the connection to the incubator, KUBIK (**Fig. 5.3B**) and to the software for the experiment control and the inner part of STROMA EUs with five independent reservoirs (**Fig. 5.2C**).

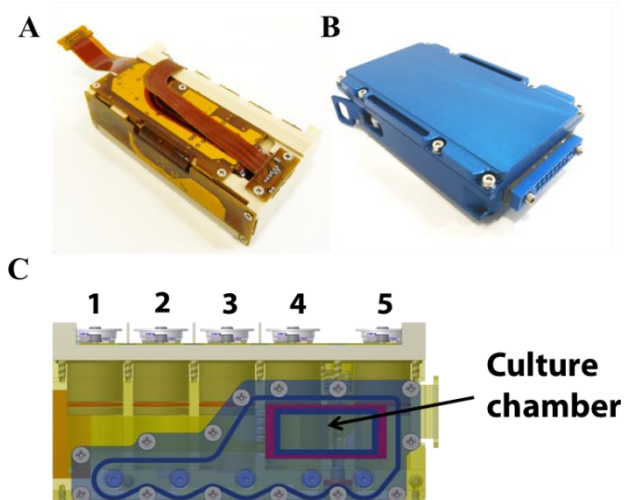


**Fig. 5.2 STROMA Experimental Units used for experiment on ISS. A) External view of EU with electronic part built; B) KIC containing EU and that allow the connection with KUBIK; C) Inner part of STROMA Eus with five independent reservoirs and Culture Chamber**

$3 \times 10^5$  cells were seeded on 12 thermanox coverslips (Nunc) and let them attach for 48h. Than the medium was replaced with OM without/with Ca100 or Sr100 nanoparticles at the same concentration. After 8 days, few samples were fixed for SEM observation. Then, for the other samples media were collected and kept at  $-80^{\circ}\text{C}$  and thermanox were built inside the Culture chamber of the EU with fresh medium without/with nanoparticles plus the addition of 12.5 mM HEPES (Sigma).

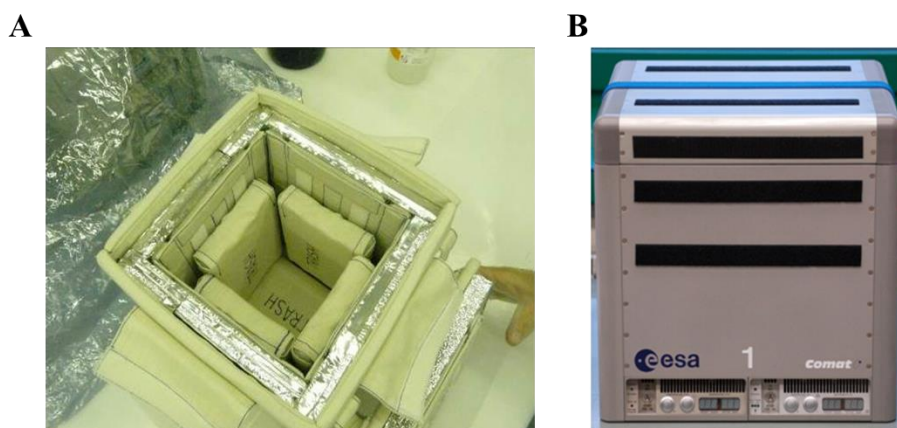


Fig.3 A) BLOKIT and B) KUBIK incubator

RESERVOIRS FILLING OF THE EU: Four of the five EU reservoirs were filled in this order: #2 with fresh medium without or with nanoparticles (depending of the EU) , #3 PBS (first washing), #4 PBS (second washing) and #5 RNA Cell Protector (Qiagen). 6 EUs inside 6 KICs were shipped inside BLOKIT (Fig. 5.3A), that ensured the temperature constant at 37°C, to ISS through the space vector Falcon 9 of the SpaceX CRS6, launched from SLC-40 (Space Launch Complex 40) on 14<sup>th</sup> of April 2015 from Kennedy Space Center – Cape Canaveral – Florida. The payload reached the ISS on 17<sup>th</sup> of April and it was docked by Captain Samantha Cristoforetti who inserted KICs inside the KUBIK, the incubator present on ISS. When the KICs were inserted in the KUBIK, the first medium change from reservoir #2 occurred. Cells were cultivated for 88 hours and then washed two times with PBS from reservoirs #3 and #4 and, finally, RNA Cell Protector was inserted in culture chamber to stabilize RNA. EUs were then transferred by Captain Samantha Cristoforetti from the KUBIK to -95 °C. The 6 KICs of GC followed the same procedures but manually.

On 21<sup>st</sup> of May 2015 freeze samples were carried down to earth by Dragon 6 vector that splashed down in Pacific Ocean at 12.58 pm. Samples were then shipped to Italy. The KICs were opened and the RNA cell protector from the culture chambers, the thermanox and culture media from washings were recovered.

RNA and proteins were extracted from RNA cell protector using RNeasy Mini Kit (Qiagen), RNA qualitatively analyzed by Agilent BioAnalyzer 2100 in order to perform RNAseq.

Pics of thermanox were acquired, media were stored at -80°C to analyze cytokine release and proteins will be used for a proteomic study.

### 6.2.11 Human Cytokine Antibody Array

Media collected during the first 8 days of culture before the EU building of untreated and NPs treated cells, were analyzed to study the release of 36 cytokines using the Human Cytokine

Antibody Array (Affimetrix). Cytokines were evaluated also in basal medium without cells and subtracted as background.

It is still incomplete the experiment with the culture medium of the samples performed on the ISS experiment.

#### **6.2.12 Statistics**

Each experiment was repeated three times. Quantitative results are expressed as the mean  $\pm$  standard error of the mean (SEM). In order to compare the results between untreated, Ca100, Ca50Sr100 and Sr100 treated samples, the one-way ANOVA with post hoc Bonferroni test was applied, with a significance level of 0.05.

## 6.3 Results

### 6.3.1 FIRST PART: Experiment on simulated microgravity (RPM)

#### *Alkaline Phosphatase (ALP) Activity*

In order to evaluate the effect of simulated microgravity (by using RPM) on osteoblasts differentiation, ALP activity of cells cultured on GC and RPM was measured at 8, 14, 21 and 28 days, respectively. **Fig. 5.4** shows results expressed as ALP specific activity. We observed an increase in ALP activity over the time in both culture conditions but a significant reduction of enzyme activity in RPM ( $p < 0.05$ ) was determined as related to GC.

In order to evaluate the effect exerted by the addition of Ca100, Ca50Sr50 and Sr100 NPs on osteoblasts differentiation in GC and RPM, ALP activity was evaluated after 8 and 28 days of cell cultures. **Figure 5.5** shows results expressed as ALP specific activity. After 8 days, an increase in ALP activity was observed in Ca50Sr50 and Sr100 treated cells cultured on GC ( $p < 0.05$ ) while no differences were observed between treated and untreated cells cultured on RPM ( $p > 0.05$ ). After 28 days the same statistically significant increase was observed in samples cultured on GC, whereas on RPM only cells treated with Sr100 nanoparticles showed an increase in ALP activity related to untreated cells ( $p < 0.001$ ). At both time points, enzyme activities measured in samples cultured on RPM were lower than those cultured on GC.

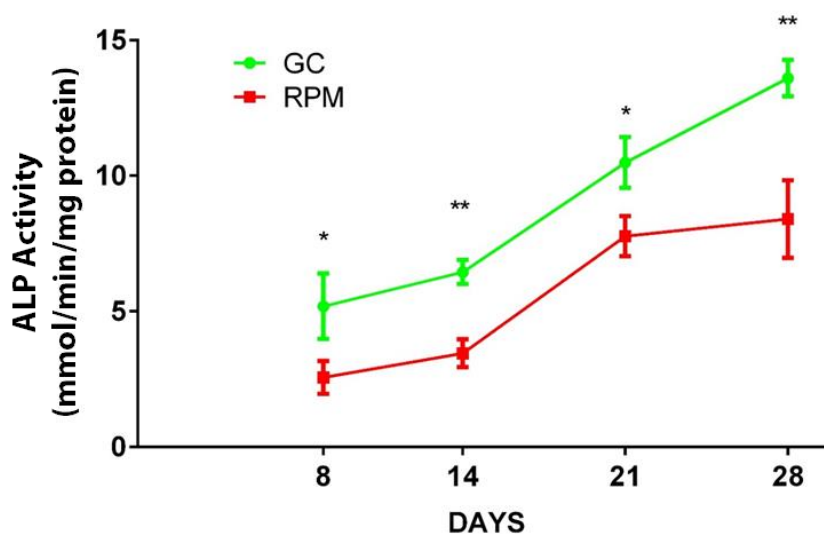


**Fig. 5.4** ALP activity of cells cultured on ground and on RPM at 8, 14, 21 and 28 days of culture. (\* $p < 0.05$ ; \*\* $p < 0.01$ )

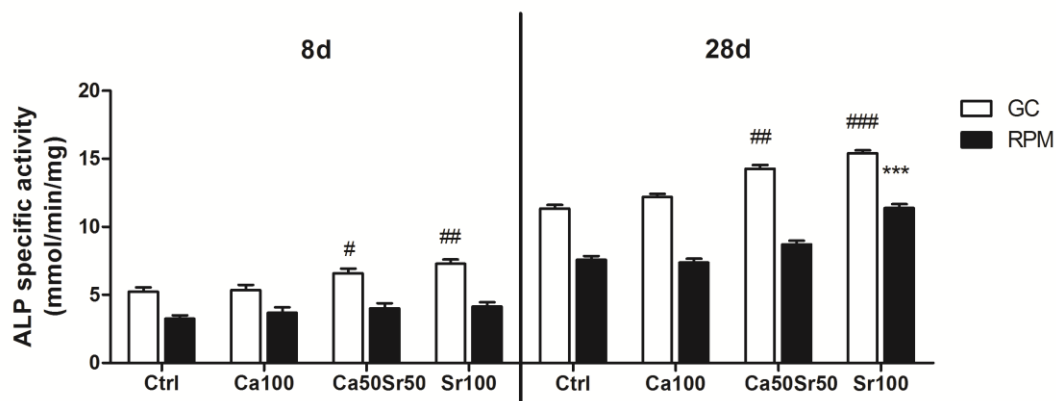


Fig. 5.5 ALP activity measured after 8 and 28 days of hBMMSCs cultured on ground and on RPM, untreated and treated with NPs. Statistical analysis performed against the GC Ctrl (#) and RPM Ctrl (\*) (# p<0,05; ## p<0,01; ### and \*\*\* p<0,001)

### Calcium deposition

After 8 and 28 days of cultures, ECM mineralization was evaluated on samples cultured on GC and RPM, untreated and treated with Ca100, Ca50Sr50 and Sr100 nanoparticles, by using Alizarin red staining. Calcium deposition was, then, quantified after cetylpyridinium dissolution of Alizarin Red crystals. **Figure 5.6** shows representative images of Alizarin Red stained samples (**Fig. 5.6A**) and the absorbance readings at 562 nm obtained after dissolution of Alizarin red crystals (**Fig. 5.6B**).

After 8 days, we observed an increase of calcium deposition in Sr100 treated samples in both culture conditions, GC and RPM, if compared to their controls. This slight increase was confirmed quantitatively by absorbance values (p<0.01). After 28 days, Sr100 treated samples showed in general a higher mineralization (p<0.01), if compared to control. Quantitative results showed a decrease in ECM mineralization in RPM samples, if compared to GC, but confirmed the increase in Sr100 treated samples for both culture conditions.

### ECM proteins deposition

After 8 and 28 days of cultures, ECM protein deposition was evaluated on samples cultured on GC and on RPM, untreated and treated with Ca100, Ca50Sr50 and Sr100 nanoparticles, by using ELISA (**Fig. 5.7**).

After 8 days, ALP protein expression was increased by Sr100 treatment in both culture conditions, GC and RPM (p<0.01) if compared to control; OPN deposition was enhanced by all nanoparticles types related to untreated cells (p<0.001), while DCN resulted increased by Ca50Sr50 and Sr100 nanoparticles (p<0.001), if compared to control.

After 28 days, a larger number of proteins resulted more expressed in treated samples than control. In particular, DCN and type-III Collagen were more abundant in Ca50Sr50 and Sr100 treated samples (p<0.001), both cultured in GC and RPM, if compared to controls; increased deposition of



type-I collagen and osteonectin was measured in Ca50Sr50 and Sr100 treated samples cultured on ground ( $p<0.001$ ), if compared to control; OPN deposition resulted enhanced by all nanoparticles treatment in particular for Sr-containing samples ( $p<0.001$ ), if compared to control; finally, deposition of OCN resulted enhanced only in Sr100 treated samples ( $p<0.001$ ), cultured on ground and on RPM, in comparison to control.

Quantitative results were corroborated by immune-localization of type-I collagen and osteocalcin evaluated at 28 days on NPs treated or untreated samples, cultured in GC or RPM. **Figure 5.8** shows representative images of samples cultured on GC and RPM. A more intense and diffuse green fluorescence for both types of proteins in samples cultured on GC than on RPM was observed. Moreover, the addition of Sr100 nanoparticles in both cell cultures conditions showed to improve the expression of these proteins, in comparison to control.

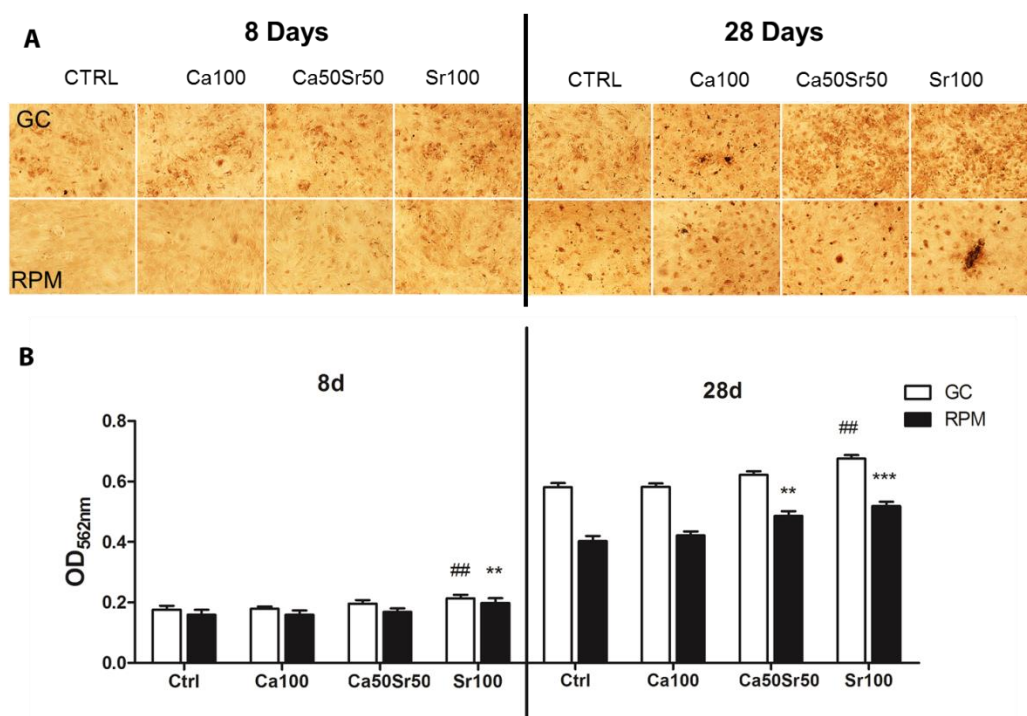


**Fig. 5.6 Extracellular Matrix Mineralization of NPs treated and untreated samples cultured on ground and on RPM. (A) Representative images of samples stained with Alizarin Red untreated and treated with NPs, cultured on ground (GC) and on Random Positioning Machine (RPM) at 8 and 28 days, 20X Magnification; (B) Quantitative evaluation of Alizarin Red stained calcium deposits after cetylpyridinium dissolution. Statistical analysis performed against the GC Ctrl (#) and RPM Ctrl (\*) (## and \*\*  $p<0,01$ ; \*\*\*  $p<0,001$ )**

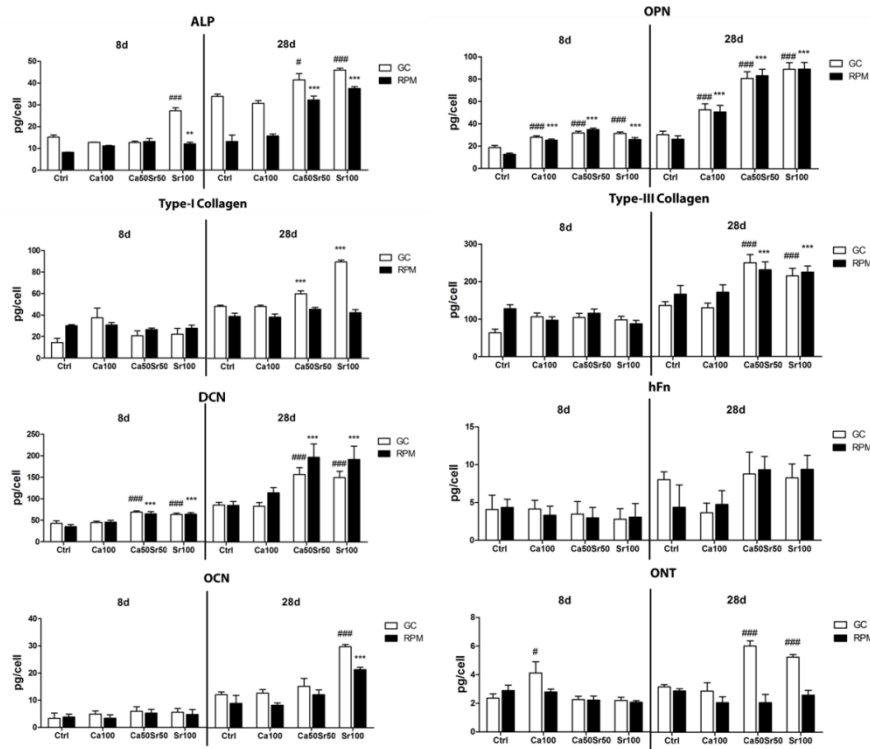


**Fig. 5.7 Bone Extracellular Matrix proteins deposition. Quantitative evaluation at 8 and 28 days of ALP, OPN, DCN, hFN, OCN, ONT, type-I and type-III collagenes in sample untreated and treated with NPs, cultured on ground and on RPM. Statistical analysis performed against the GC Ctrl (#) and RPM Ctrl (\*) (# and \*  $p < 0,05$ ; ## and \*\*  $p < 0,01$ ; ### and \*\*\*  $p < 0,001$ )**

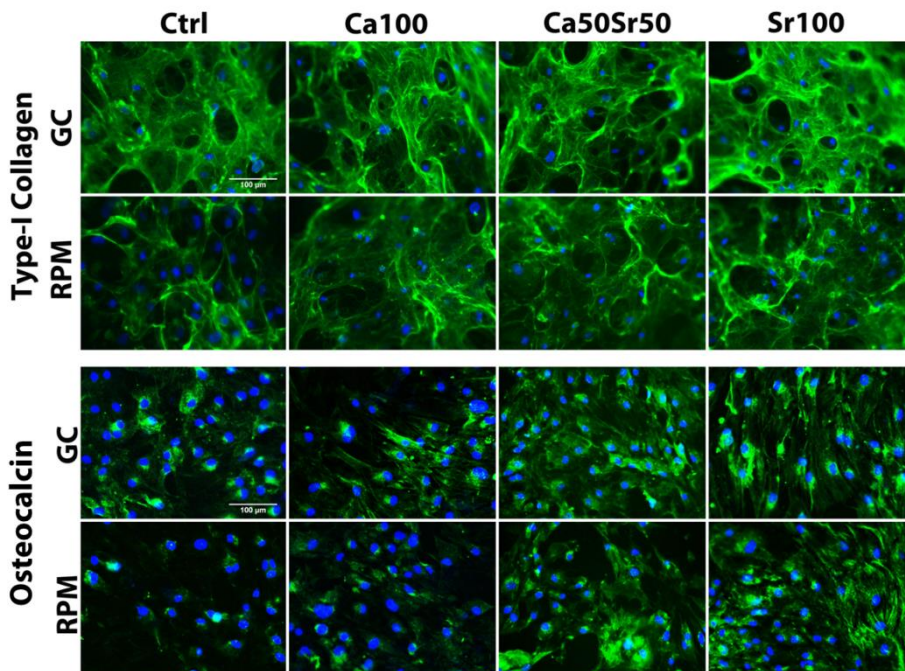


**Fig. 5.8 Extracellular matrix proteins immunostaining. Representative fluorescence images of Type-I Collagen and Osteocalcin immuno-localization (green) in samples untreated and treated with NPs, cultured for 28 days on ground (GC) and on RPM. Nuclei were counterstained with Hoechst 33342 (blue). 40X magnification.**

## Gene expression

After 8 and 28 days of cultures in GC or RPM experimental conditions, the expression of specific marker genes of untreated or treated samples with Ca100, Ca50Sr50 or Sr100 nanoparticles was evaluated by qRT-PCR. **Fig. 5.9** shows relative expression of indicated genes normalized with untreated samples at 8 and 28 days, respectively. After 28 days, in samples cultured in both culture conditions, expression of *IBSP* and *ALP* was slightly enhanced by nanoparticles treatment, especially with Sr100 nanoparticles ( $p < 0.001$ ), if compared to control. Interestingly, after 8 days, a slight down-regulation of *RUNX2*, *COL1A1* and *COL3A1* induced by Sr100 treatment was observed ( $p < 0.001$ ), if compared to control. After 28 days, the expression of *RUNX2*, *COL1A1* and *COL3A1* in Sr100 treated samples resulted comparable or even increased ( $p < 0.05$ ), if related to untreated samples at similar time of incubation. Regarding *BMP2* and *DCN* expression, a slight increase was observed in Sr100 treated samples cultured on RPM ( $p < 0.01$ ).

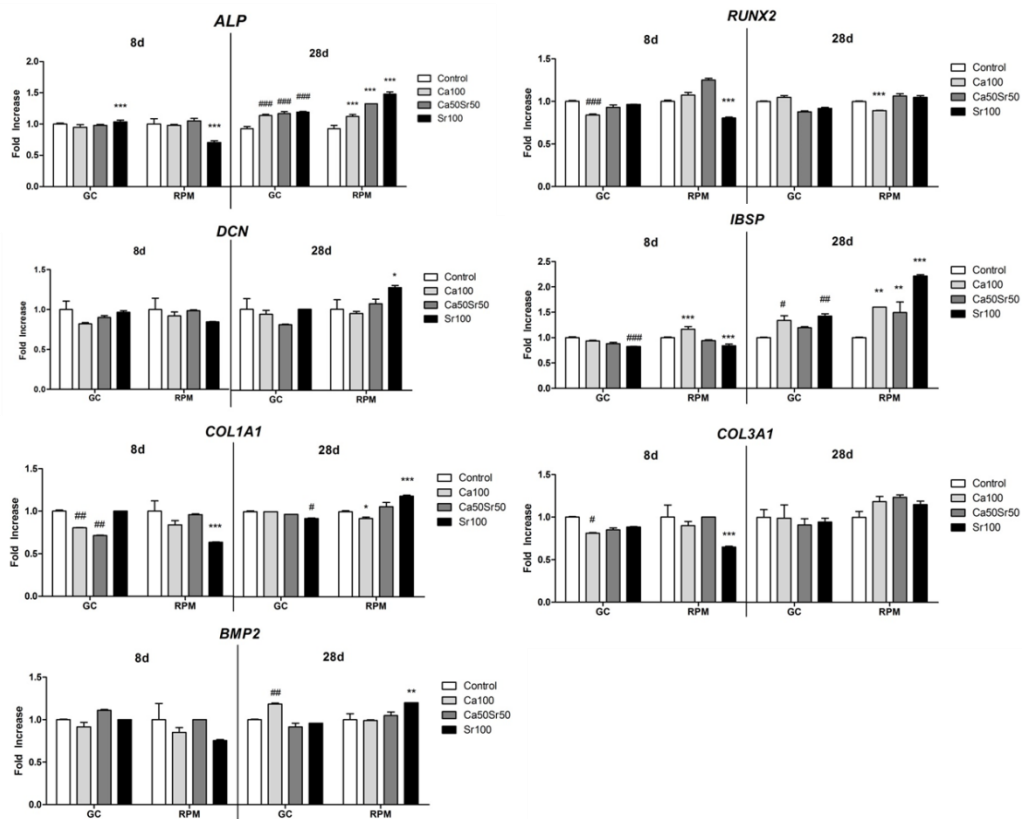


**Fig. 5.9** Gene expression of indicated bone specific markers as determined by qRT-PCR. Gene expression of GC samples are normalized to the GC untreated samples (#); gene expression of RPM samples are normalized to the untreated RPM sample (\*); (# and \*  $p < 0,05$ ; ## and \*\*  $p < 0,01$ ; ### and \*\*\*  $p < 0,001$ )

## 6.3.2 SECOND PART: Experiment performed on ISS

In order to visualize cells adherent on thermanox coverslip, SEM observation of duplicates were performed. **Figure 5.10** shows representative images of hBM MSCs seeded on thermanox coverslips, cultured for 8 days in absence (**Fig. 5.10A and B**), presence of Ca100 (**Fig. 5.10C and**

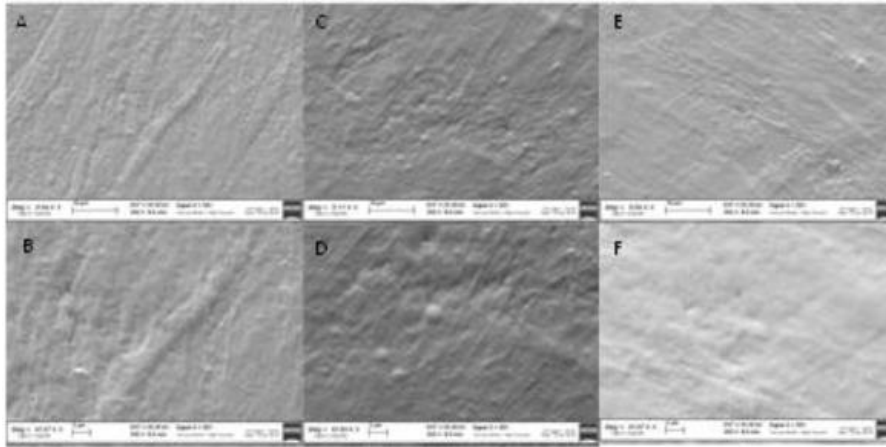


**Fig 5.10** Representative images of hBMMSCs seeded on thermanox coverslips, cultured for 8 days in absence (A and B), presence of Ca100 (C and D) and Sr100 (E and F) nanoparticles. Observed samples are duplicates of those built in EUs. Magnification 5000X (A, C and E) and 10000X (B, D and F).

**D**) and Sr100 (**Fig. 5.10E and F**) nanoparticles. Cells covered completely the Thermanox coverslip surface and showed a more round-shape morphology typical of first stages of osteoblasts differentiation.

In order to evaluate the influence of nanoparticles on osteoblasts differentiation in space environment, 6 EU after space flight on ISS and 6 EU from GC were opened and RNA cell protector was recovered. Unfortunately, in two of the 6 EUs from ISS, an evident contamination was observed. RNA cell protector was recovered from culture chambers, allowing the isolation of both proteins and RNAs. The quality of RNA was, then, evaluated by Agilent BioAnalyzer 2100 (IC- CNR, Rome) and **Figure 5.11** shows relative results. Four samples showed good quality RNA

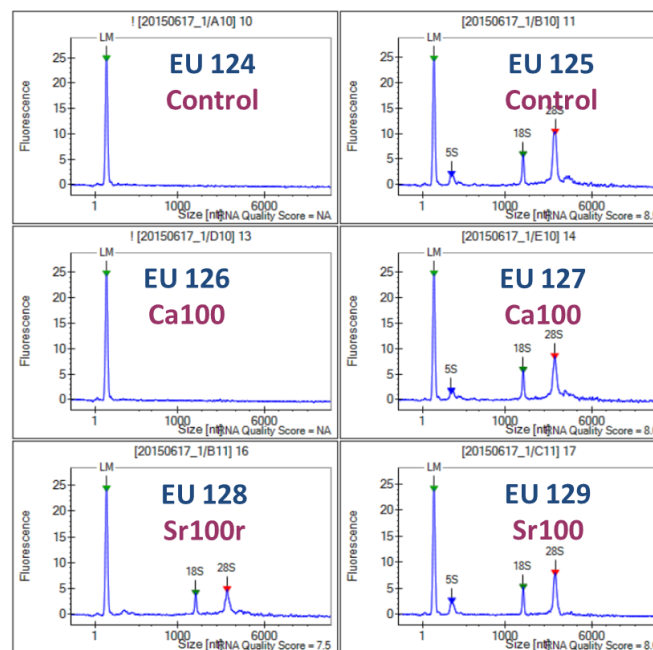


**Fig. 5.11** Qualitative analysis of RNA extracted from EU from ISS evaluated by Agilent BioAnalyzer 2100

(RNA integrity numbers between 7.5 and 8.6) while in the two contaminated EUs, RNA was completely degraded.

**Tab. 5.2** shows quantitative results of proteins isolated from 6EU after space flight on ISS and 6 EU from GC and that will be analyzed by mass spectrometry to perform proteomic study in collaboration with Immunotechnology Department, Lund University, Sweden.

	EU	Protein amount ( $\mu\text{g}$ )
ISS SAMPLES	124	$135.57 \pm 0.41$
	125	$103.67 \pm 0.51$
	126	$162.15 \pm 0.91$
	127	$116.96 \pm 0.7$
	128	$177.43 \pm 1.02$
	129	$182.08 \pm 0.71$
GC SAMPLES	116	$82.4 \pm 0.6$
	117	$101.01 \pm 1.52$
	118	$158.82 \pm 0.64$
	119	$164.14 \pm 0.91$
	120	$210.66 \pm 0.41$
	121	$174.11 \pm 0.36$

**Tab. 5.2 Protein amount isolated from EU after space flight on ISS and from EU from GC**

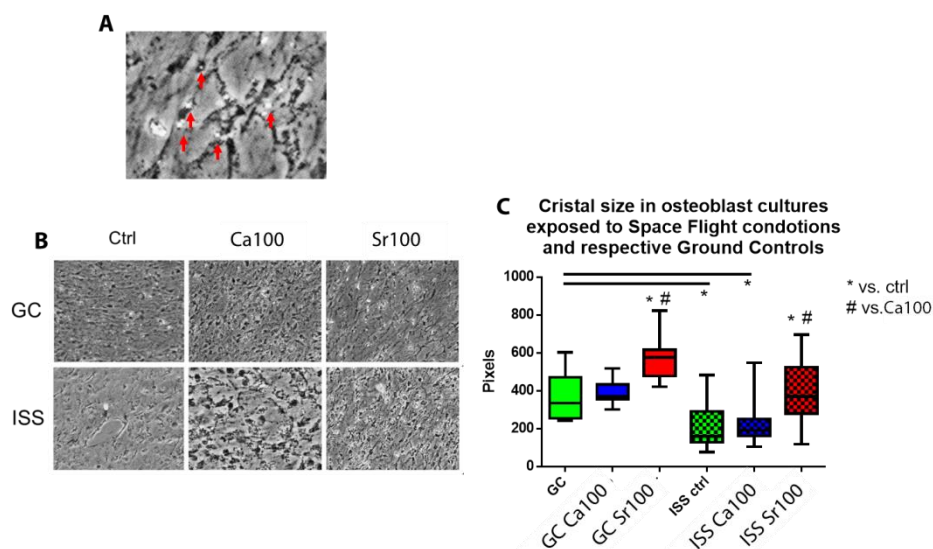


**Fig. 12 Crystal size evaluation of hBMMSCs cultivated on ground and on ISS. (A) Crystals (red arrows) visible in thermanox after RNA Cell protector treatment; (B) Representative pics of thermanox recovered from EUs from ISS and GC; (C) Quantitative evaluation of crystal sizes. Statistical analysis performed against untreated (\*) and Ca100 treated (#) cells. (\* $p < 0.05$ ; # $p < 0.05$ )**

Furthermore, Thermanox from EU were recovered and observed under inverted microscope and crystal size (Fig. 5.12A) was evaluated (UniMi, Milan). Figure 5.12 shows pics of recovered thermanox (Fig. 5.12B) and the results extrapolated by crystal size quantitative analysis (Fig. 5.12C). In both culture conditions (ISS and GC), an increment in crystal size for Sr100 treated samples in comparison to Ca100 and control ( $p < 0.05$ ) was observed. Moreover, the crystals' size for ISS's samples was smaller if related to those on GC ( $p < 0.05$ ).

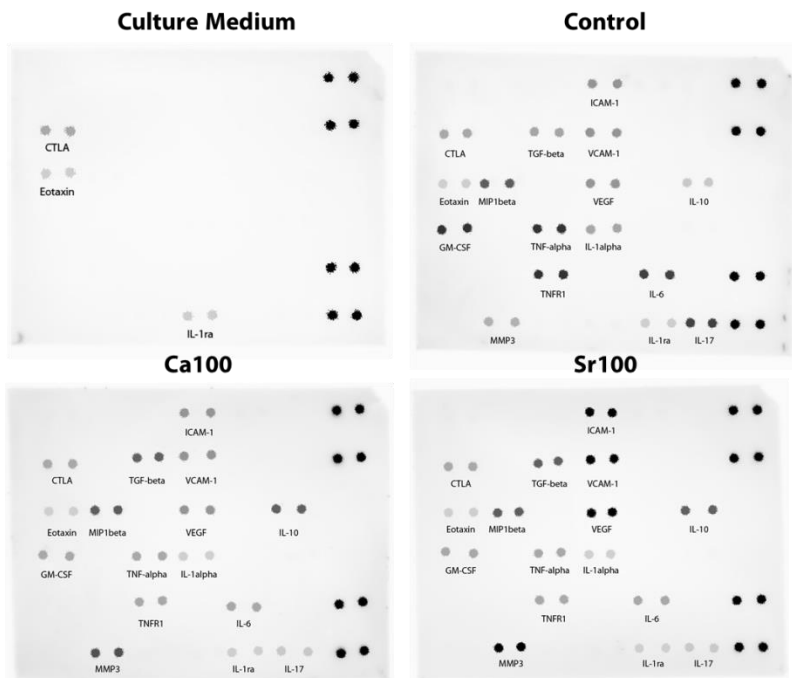
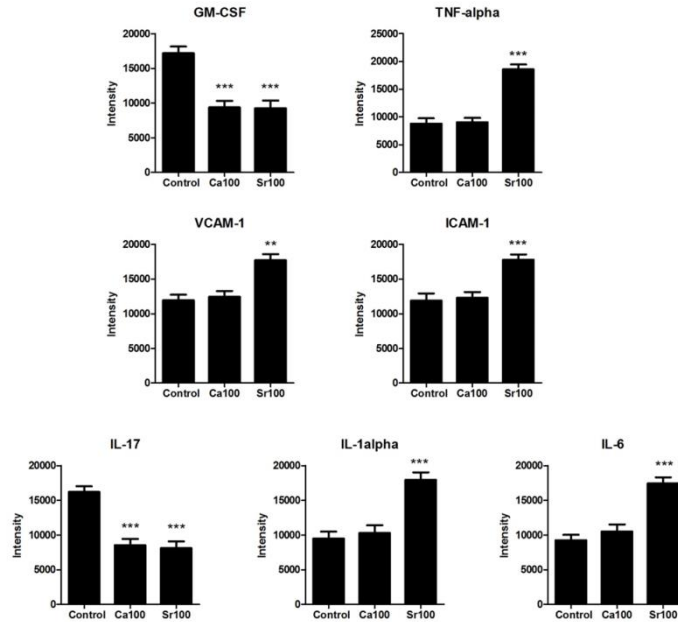


Fig. 5.13 Arrays for cytokines determination in culture medium, untreated, Ca100 and Sr100 treated cells for 8 days.

### Cytokines Release

During the first 8 days of cell cultures, the collected medium from samples that were then built in EUs, was evaluated for cytokines and chemokines determination. Media collected from untreated, Ca100 and Sr100 treated cells were incubated with Affimetrix membranes to detect 36 different cytokines. The presence of cytokines was visualized using chemiluminescent system (Fig. 5.13). The same procedure was

used for basal medium to detect the presence of cytokines in medium without cells. Results from basal medium were subtracted as background. 16 different cytokines were detected in samples, three were subtracted because already present in basal medium and differences in release between control and treated samples were observed for 11 cytokines (Figures 5.14 and 5.15). In particular, about 2-times lower levels of granulocyte-macrophage colony-stimulating factor (GM-CSF) and IL-17 were detected in treated samples related to control ( $p < 0.001$ ) and no differences were observed between the two different nanoparticles treatments (Fig. 5.14). Intercellular Adhesion Molecule 1 (ICAM-1), vascular cell adhesion molecule 1 (VCAM-1), VEGF, TNF- $\alpha$ , IL-1 $\alpha$  and IL-6 were measured around 1.5-times higher in Sr100 treated samples than in control and Ca100 treated ones ( $p < 0.001$ ). An increment between 2- and 3-times of TGF- $\beta$ , IL10 and MMP3 cytokines were observed in treated samples related to untreated ones ( $p < 0.001$ ) (Fig. 5.15).



**Fig. 5.14** Pro-inflammatory cytokines released in the medium by BM-MSCs untreated and treated with NPs cultured for 8 days on ground. Data represent intensities of spots detected by Human Antibody Array (Affimetrix). Statistical analysis was performed between treated and untreated samples (\* $p < 0,05$ ; \*\* $p < 0,01$ ; \*\*\* $p < 0,001$ ).

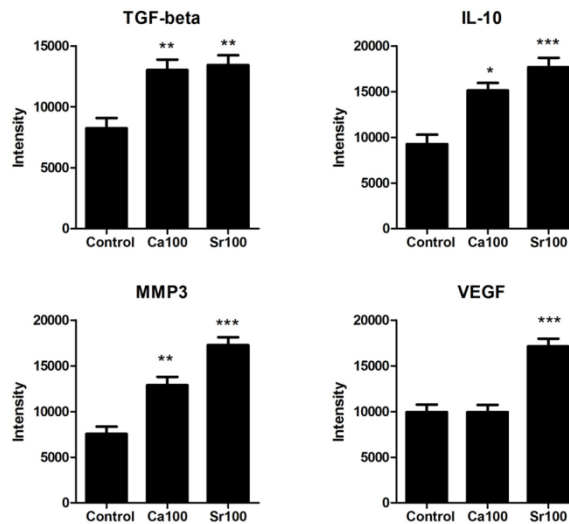


**Fig. 5.15** Anti-inflammatory cytokines released in the medium by BM-MSCs untreated and treated with NPs cultured for 8 days on ground. Data represent intensities of spots detected by Human Antibody Array (Affimetrix). Statistical analysis was performed between treated and untreated samples (\* $p < 0,05$ ; \*\* $p < 0,01$ ; \*\*\* $p < 0,001$ )

## 6.4 Discussion

The *in vitro* effect of Sr-containing nanoparticles on mesenchymal stem cells differentiation to osteoblasts cultured in microgravity condition was evaluated.

It is widely demonstrated that microgravity or simulated microgravity environment reduces differentiation of osteoblasts and their activity leading to reduction of bone mass. In this process also osteoclasts are affected: some evidence pointed out an increase in osteoclastogenesis *in vitro*<sup>30</sup> and *in vivo*<sup>31</sup>. On the other hand, it has been widely accepted that reduced bone formation is the main cause of bone loss under microgravity<sup>32</sup>. Thus, it is a significant possibility that decreased activity of functional cells and a decrease in new osteoblasts from progenitors play a vital role in this process. hBMMSCs act as a major source for osteoblasts and have a significant role in bone remodeling and repair<sup>33</sup>. Here, we observed that RPM reduced significantly ALP activity, the ECM deposition and mineralization, the gene expression of some osteogenic markers.

Random positioning machine rotates biological samples along two independent axes to change their orientation in space in complex ways and so eliminate the effect of gravity<sup>34</sup>. The RPM is a more sophisticated development of the single-axis clinostat. RPM consists of two independently rotating frames. One frame is positioned inside the other giving a very complex net change of orientation to a biological sample mounted in the middle. It is a microgravity simulator that is based on the principle of 'gravity-vector-averaging'<sup>35</sup>.

Sr-substitute hydroxyapatite nanoparticles have shown to accelerate and enhance the osteoblasts differentiation and their ability to deposit and mineralize ECM. For this reason, we investigated the effect of Sr-containing nanoparticles on osteoblasts differentiation in microgravity condition.

To do that, we evaluated ALP activity of cells cultured on ground and on RPM in absence or presence of nanoparticles. We observed that Sr100 nanoparticles increased ALP activity, both in microgravity and on ground. Moreover, after 28 days, Sr100 nanoparticles induced higher *ALP* gene expression and higher deposition of ALP protein, following the enzyme activity data. ALP is a marker of osteoblasts differentiation and Sr100 nanoparticles seem to counterbalance the inhibitory effect of microgravity. Similar results showed reduced osteoblasts differentiation of hBMMSCs cultivated on Rotary Wall Vessel bioreactor with reduced ALP activity<sup>36</sup>.

Strictly related to the osteoblasts differentiation is their ability of bone matrix deposition and mineralization. We observed a reduction of ECM protein deposition and mineralization induced by microgravity, as already widely reported<sup>2,36</sup>. The treatment with Sr-containing nanoparticles increased the ECM deposition and mineralization, in some cases counterbalancing completely the reduction due to microgravity exposure. In Sr100 treated samples cultured on RPM, deposition of osteopontin was comparable to the GC and significantly higher than untreated cells. Similar results



were obtained for decorin and type-III collagene. Regarding osteonectin, osteocalcein and type-I collagen, instead, an increase in Sr100 treated samples related to untreated cells was observed but the deposition in RPM cell cultures was much lower than those cultured on ground. Some of the gene expressions seem to follow the protein results, like *DCN* and *COL1A1* but no significant differences were observed in *COL3A1* expression suggesting that Sr100 nanoparticles may act both at transcriptional and translational level.

Significant increase of *IBSP* transcription was observed after 28 days in Sr100 treated samples. *IBSP* gene transcribes for bone sialo-protein, the most abundant non-collagen protein present in bone matrix<sup>37</sup>. This result is in accordance with our previous observation on the effect of Sr100 nanoparticles on the expression of this gene. Another gene found slightly up-regulated by Sr100 nanoparticles on RPM was *BMP2*, a powerful modulator of osteogenesis<sup>38</sup>.

Sr100 nanoparticles increased not only the ECM deposition in terms of proteins but also its bone matrix mineralization. Alizarin Red staining, in fact, revealed greater calcium deposition in Sr100 treated samples both in ground and in RPM experimental conditions. The reduced matrix mineralization observed in microgravity is strictly related to the lower level of osteoblasts differentiation since calcium deposition occurs in the later stages of differentiation. We demonstrated that Sr100 nanoparticles push the hBMMSCs differentiation toward more mature osteoblasts, so this treatment increases ECM deposition and mineralization even in simulated microgravity counterbalancing its inhibitory effect.

Regarding results obtained from experiment performed on ISS, RNAseq of isolated RNAs that were not degraded is still under analysis and no results are evaluable in both culture conditions (ISS and GC). Similar situation can be considered for proteomic studies on isolated proteins that will be performed in collaboration with Immunotechnology Department, Lund University, Sweden.

We observed increased crystal size in those samples cultivated in presence of Sr100 nanoparticles both on ISS and on ground, and that could be due to Sr incorporation, as has been already demonstrated in previous *in vitro* work (described in chapter 3) with SAOS-2 cells.

We performed a cytokine release analysis in media of cells on thermanox before inserting in EUs, at 8 days of differentiation in absence and presence of Ca100 and Sr100 nanoparticles. This is a not very explored field, but it is possible to group cytokines in anti-inflammatory and pro-inflammatory and some works focused on different expression during osteoblast differentiation<sup>39</sup>. hBMMSCs treated with TNF- $\alpha$  resulted in the activation of nuclear factor kappa-light-chain-enhancer of activated B cells (NF- $\kappa$ B), leading to increased mineralization and enhanced expression of osteogenic proteins, such as BMP2 and ALP, and transcription factors such as Runx2 and

Osterix<sup>40,41</sup>. Ferreira et al. found that IL-1 also enhanced mineralization through both NF- $\kappa$ B and MAPK pathways<sup>42</sup>. It has been previously shown that cytokines such as IL-1, IL-6, and TNF- $\alpha$  have the ability to inhibit adipogenic differentiation of hBMMSCs. In Sr100 treated samples, an increase in TNF- $\alpha$ , IL-1 $\alpha$  and IL-6 were observed and these increases should result in decrease of adipogenesis and in enhancing of osteoblast differentiation. Moreover, increasing in anti-inflammatory cytokines (like IL-10, MMP3, TGF- $\beta$ ) was observed in Sr100 treated sample. These cytokines reduce the inflammatory status that has been shown to contribute to a decrease in bone mineral density by inhibiting osteoblast proliferation and differentiation and enhancing the rate of osteoclast differentiation in patients with severe inflammatory disease<sup>39</sup>.

## 6.5 Conclusion and Future Perspectives

In this chapter we presented results about the effect of Sr-substituted hydroxyapatite nanoparticles on hBMMSCs differentiation to osteoblasts in microgravity conditions, simulated (RPM) or on ISS. For simulated microgravity, mesenchymal stem cells isolated from human bone marrow were cultivated in RPM and GC, in absence and presence of Ca100, Ca50Sr50 and Sr100 nanoparticles. Sr100 nanoparticles improved the expression and activity of alkaline phosphatase on sample cultured on RPM suggesting a positive effect on osteoblast differentiation even in microgravity condition. Moreover, in samples cultured on RPM and treated with Sr100 nanoparticles, higher ECM deposition was measured, with higher amount of bone matrix proteins deposition as well as the related gene expression, like *ALP* and *IBSP*. An increase in bone matrix mineralization was detected in Sr100 nanoparticles treated samples cultured on RPM.

Further investigation about the effect of nanoparticles on proteome modification of hBMMSCs cultured in RPM and GC will be performed in collaboration with Immunotechnology Department, Lund University, Sweden.

Future works will focus on the effect of Sr-containing nanoparticles also on osteoclastogenesis in microgravity condition to evaluate if the observed dual action of Sr100 nanoparticles occurs also in microgravity condition.

Sr-containing nanoparticles affect also the release of several cytokines that were demonstrated to be involved in osteoblasts differentiation like IL-1, IL-6, and TNF- $\alpha$  and increase the release of anti-inflammatory cytokines that are strictly correlated with osteoclastogenesis. It seems that nanoparticles effect on bone remodeling could be related also to the modulation of cytokines release by cells.

All these data suggest that Sr100 nanoparticles improve the differentiation and activity of human osteoblasts and can be a powerful tool to reduce the bone loss induced by microgravity. Moreover, it is quite interesting to highlight that all these data demonstrated a positive effect of Sr-containing nanoparticles on human osteoblasts differentiation also in a non-physiological condition. Microgravity, in fact, is a model used to mimic the osteoporosis condition, so it can be speculated that this data suggest a possible stimulatory effect of Sr-containing nanoparticles in an osteoporotic model.

## 6.6 References

1. Blaber, E. A. *et al.* Microgravity Induces Pelvic Bone Loss through Osteoclastic Activity , Osteocytic Osteolysis , and Osteoblastic Cell Cycle Inhibition by CDKN1a / p21. *PLoS One* **8**, (2013).
2. Meyers, V. E., Zayzafoon, M., Gonda, S. R., Gathings, W. E. & McDonald, J. M. Modeled Microgravity Disrupts Collagen I / Integrin Signaling During Osteoblastic Differentiation of Human Mesenchymal Stem Cells. *J. Cell. Biochem.* **707**, 697–707 (2004).
3. Monticone, M., Liu, Y., Pujic, N. & Cancedda, R. Activation of Nervous System Development Genes in Bone Marrow Derived Mesenchymal Stem Cells Following Spaceflight Exposure. *J. Cell. Biochem.* **111**, 442–452 (2010).
4. Klein-nulend, S. V. J., Loon, J. Van & Bradamante, S. Influence of Oxygen in the Cultivation of Human Mesenchymal Stem Cells in Simulated Microgravity : An Explorative Study. *Microgravity Sci. Technol.* **25**, 59–66 (2013).
5. Wang, N., Wang, H., Chen, J., Wang, W. & Wang, Z. The simulated microgravity enhances multipotential differentiation capacity of bone marrow mesenchymal stem cells. *Cytotechnology* **66**, 119–131 (2014).
6. Bianco, P. *et al.* The meaning, the sense and the significance: translating the science of mesenchymal stem cells into medicine. *Nat. Med.* **19**, 35–42 (2013).
7. Ehninger, A. & Trumpp, A. The bone marrow stem cell niche grows up : mesenchymal stem cells and macrophages move in. *J. Exp. Med.* **208**, 421–428 (2011).
8. Nombela-Arrieta, C., Ritz, J. & Silberstein, L. E. The elusive nature and function of mesenchymal stem cells. *Nat. Rev. Mol. Cell Biol.* **12**, 126–131 (2011).
9. Frenette, P., Pinho, S., Lucas, D. & Scheiermann, C. Mesenchymal stem cell: keystone of the hematopoietic stem cell niche and a stepping-stone for regenerative medicine. *Annu Rev Immunol.* **31**, 285–316 (2013).
10. Morrison, S. J. & Scadden, D. T. The bone marrow niche for haematopoietic stem cells. *Nature* **505**, 327–334 (2014).
11. DuFort, C. C., Paszek, M. J. & Weaver, V. M. Balancing forces: architectural control of mechanotransduction. *Nat. Rev. Mol. Cell Biol.* **12**, 308–319 (2011).
12. Hoffman, B. D., Grashoff, C. & Schwartz, M. A. Dynamic molecular processes mediate cellular mechanotransduction. *Nature* **475**, 316–323 (2011).
13. Jaalouk, D. E. & Lammerding, J. Mechanotransduction gone awry. *Nat. Rev. Mol. Cell Biol.* **10**, 63–73 (2009).
14. Janmey, P. A. & Miller, R. T. Mechanisms of mechanical signaling in development and

- disease. *J. Cell Sci.* (2011). doi:10.1242/jcs.071001
15. Sukharev, S. & Sachs, F. Molecular force transduction by ion channels – diversity and unifying principles. *J. Cell Sci.* **d**, (2012).
  16. Huang, C. & Ogawa, R. Mechanotransduction in bone repair and regeneration. *FASEB J.* **24**, 3625–3632 (2016).
  17. Ingber, D. E. Tensegrity II . How structural networks influence cellular information processing networks. *J. Cell Sci.* (2003). doi:10.1242/jcs.00360
  18. Pavalko, F. M. *et al.* A Model for Mechanotransduction in Bone Cells : The Load-Bearing Mechanosomes. *J. Cell. Biochem.* **112**, 104–112 (2003).
  19. Vorselen, D., Roos, W. H., Mackintosh, F. C., Wuite, G. J. L. & Loon, J. J. W. A. Van. The role of the cytoskeleton in sensing changes in gravity by nonspecialized cells. *FASEB J.* **28**, 536–547 (2016).
  20. Meyers, V. E., Zayzafoon, M., Douglas, J. T. & McDonald, J. M. RhoA and cytoskeletal disruption mediate reduced osteoblastogenesis and enhanced adipogenesis of human mesenchymal stem cells in modeled microgravity. *J. Bone Miner. Res.* **20**, 1858–1866 (2005).
  21. Shapiro, J. R. Microgravity and drug effects on bone. *J Musculoskelet Neuronal Interact* **6**, 322–323 (2006).
  22. Wimalawansa, S. M. & Wimalawansa, S. J. A novel pharmacological approach of musculoskeletal losses associated with simulated microgravity. *J Musculoskel Neuron Interact* 35–41 (2000).
  23. Uddin, S. M. Z. *et al.* Reversal of the Detrimental Effects of Simulated Microgravity on Human Osteoblasts by Modified Low Intensity Pulsed Ultrasound. *Ultrasound Med Biol* **39**, 804–812 (2013).
  24. Bernardo, M. E. *et al.* Human bone marrow derived mesenchymal stem cells do not undergo transformation after long-term in vitro culture and do not exhibit telomere maintenance mechanisms. *Cancer Res.* **67**, 9142–9 (2007).
  25. Bernardo, M. E. *et al.* Optimization of in vitro expansion of human multipotent mesenchymal stromal cells for cell-therapy approaches: further insights in the search for a fetal calf serum substitute. *J. Cell. Physiol.* **211**, 121–30 (2007).
  26. Benavides Damm, T., Walther, I., Wüest, S. L., Sekler, J. & Egli, M. Cell cultivation under different gravitational loads using a novel random positioning incubator. *Biotechnol. Bioeng.* **111**, 1180–1190 (2014).
  27. Saino, E. *et al.* In vitro calcified matrix deposition by human osteoblasts onto a zinc-

- containing bioactive glass. *Eur. Cell. Mater.* **21**, 59–72; discussion 72 (2011).
28. Saino, E. *et al.* In Vitro Enhancement of SAOS-2 Cell Calcified Matrix Deposition onto Radio Frequency Magnetron Sputtered Bioglass-Coated Titanium Scaffolds. *Tissue Eng. Part A* **16**, 995–1008 (2010).
  29. Gregory, C. A., Gunn, W. G., Peister, A. & Prockop, D. J. An Alizarin red-based assay of mineralization by adherent cells in culture: comparison with cetylpyridinium chloride extraction. *Anal. Biochem.* **329**, 77–84 (2004).
  30. Tamma, R. *et al.* Microgravity during spaceflight directly affects in vitro osteoclastogenesis and bone resorption. *FASEB J.* **23**, 2549–54 (2009).
  31. Saxenaa, R., Panb, G., Dohmc, E. D. & McDonald, J. M. Modeled microgravity and hindlimb unloading sensitize osteoclast precursors to RANKL mediated osteoclastogenesis. *J. bone Miner. Res.* **29**, 111–122 (2011).
  32. Lloyd, S. A. *et al.* Osteoprotegerin is an effective countermeasure for space flight-induced bone loss in mice. *Bone* **81**, 562–572 (2015).
  33. See, E. Y. *et al.* Multilineage Potential of Bone-Marrow-Derived Mesenchymal Stem Cell Cell Sheets : Implications for Tissue Engineering. *Tissue Eng. Part A* **16**, (2010).
  34. van Loon, J. J. W. A. Some history and use of the random positioning machine , RPM , in gravity related research. *Adv. Sp. Res.* **39**, 1161–1165 (2007).
  35. Borst, A. G. & van Loon, J. J. W. A. Technology and Developments for the Random Positioning Machine , RPM. *Microgravity Sci. Technol.* **21**, 287–292 (2009).
  36. Zayzafoon, M., Gathings, W. E. & Donald, J. A. Y. M. M. C. Modeled Microgravity Inhibits Osteogenic Differentiation of Human Mesenchymal Stem Cells and Increases Adipogenesis. *Endocrinology* **145**, 2421–2432 (2004).
  37. Caetano-Lopes, J., Canhão, H. & Fonseca, J. E. Osteoblasts and bone formation. *Acta Reumatol. Port.* **32**, 103–10
  38. Bragdon, B. *et al.* Bone Morphogenetic Proteins : A critical review. *Cell. Signal.* **23**, 609–620 (2011).
  39. Strong, A. L., Gimble, J. M. & Bunnell, B. a. Analysis of the Pro- and Anti-Inflammatory Cytokines Secreted by Adult Stem Cells during Differentiation. *Stem Cells Int.* **2015**, 1–12 (2015).
  40. Hess, K., Ushmorov, A., Fiedler, J., Brenner, R. E. & Wirth, T. TNFalpha promotes osteogenic differentiation of human mesenchymal stem cells by triggering the NF-kappaB signaling pathway. *Bone* **45**, 367–76 (2009).
  41. Osta, B., Lavocat, F., Eljaafari, A. & Miossec, P. Effects of Interleukin-17A on Osteogenic

- Differentiation of Isolated Human Mesenchymal Stem Cells. *Front. Immunol.* **5**, 425 (2014).
42. Ferreira, E. *et al.* Inflammatory Cytokines Induce a Unique Mineralizing Phenotype in Mesenchymal Stem Cells Derived from Human Bone Marrow. *J. Biol. Chem.* **288**, 29494–29505 (2013).





# Chapter 6

---

## 7. Summary, closing remarks and future perspectives

### 7.1 Summary and address to the aims

#### Chapter 1 – General introduction (pag. 2)

The change in living conditions during the twentieth century, compared to the previous centuries, has brought major benefits to the welfare and health of mankind. However, the increased life-expectancy, the dynamism of activities (e.g. transportation methods and sport activities), and the growing world population lead to a substantial increase in patients who suffer from damaged, malfunctioning or diseased tissues or body parts. In the case of bone tissue, the normal function of it can be impaired by many traumatic injuries and some pathological disorders, such as osteoarthritis, osteoporosis, osteogenesis imperfecta, and Paget's disease and tumor. These malfunctions cause nonunion bone fractures, bone deformation, severe pain, and loss of mobility<sup>1</sup>. For this reason, research in bone field is growing up very quickly in last few years with the aim of discovering new factors that modulate bone remodeling to be addressed by new drugs. In this sense, many efforts have been made to study new strontium-based drugs to enhance the pharmacological effect of this element on bone cells.

#### Chapter 2 - Synthesis and Characterization of Strontium-substituted hydroxyapatite nanoparticles for bone regeneration (pag. 44)

Chapter 2 presents a deep and complete physical-chemical characterization of strontium(Sr)-substituted hydroxyapatite (HA) nanopowders, stable nanoparticle suspension preparation and the evaluation of their biocompatibility. In particular, Sr-substituted hydroxyapatite nanopowders were systematically synthesized by aqueous precipitation in the range of 0-100 mol% Sr. The replacement of  $\text{Ca}^{2+}$  by  $\text{Sr}^{2+}$  ions with different ionic radius and electronegativity leads to the nanopowders modification at different structural levels. Pure Sr-HA and Ca-HA nanopowders are characterized by larger crystallite size (50 – 60 nm) with respect to intermediate compositions (20-30 nm). Crystalline unit cells are subjected to an expansion which is larger along  $c$  than along  $a$ ; this leads to functional group rearrangements, responsible for weaker P-O bonds and, above all, for evident OH spatial density changes and their local environment.

The synthesized powders can be easily used for the preparation of water suspensions with the addition of Bovine Serum Albumin. The produced suspensions are biocompatible with no apoptotic effect on osteoblast cells. Suspensions prepared with nanopowders containing larger Sr amount clearly promote osteoblast viability and proliferation. Moreover, we demonstrated that Sr-containing hydroxyapatite nanoparticles have higher biocompatibility and stimulatory effect on osteoblasts proliferation if compared with strontium ranelate and strontium chloride.

### **Chapter 3 - Effect of Strontium-containing nanoparticles on Bone Remodelling: in vitro cell studies (pag. 73)**

Chapter 3 presents a wide *in vitro* investigation of Sr-containing nanoparticle effect on bone remodelling, performing studies on pre-osteoblasts, hBMMSCs, murine osteocytes and osteoclasts.

We observed enhanced osteoblasts differentiation induced by Sr-containing nanoparticles. In particular, we observed an increment in ALP activity, greater ECM bone matrix deposition and mineralization and an increased gene expression of specific markers for osteogenesis in Sr-containing nanoparticles treated samples, in comparison to Ca100 nanoparticles and untreated samples (control). Pathway involved in nanoparticle uptake was shown to be micropinocytosis and deposition of strontium was observed also in mineralized bone matrix at the end of cell culture.

Sr-containing nanoparticles reduced the differentiation of osteoclasts, the cells responsible for bone resorption. Reduction of osteoclasts differentiation markers, like TRAP, was observed in Sr treated samples. Moreover, Sr-containing nanoparticles prevent cell fusion and adhesion inhibiting the multinucleated cells formation, typical of osteoclasts.

In our studies we also demonstrated that Sr-containing nanoparticles push the osteocytes differentiation toward more mature stages and improved their ability to deposit a mineralized bone matrix. A modulation in molecules that influence osteoblasts and osteoclasts differentiation was observed with a decrease of *RANKL* and increase of *SOST* expression. Preliminary results about the molecular mechanism involved in this process, suggest a role of calcium sensing receptor and in particular the possibility to use Sr100 nanoparticles to reduce the negative effect of calcilytics drugs.

### **Chapter 4 - Effect of Strontium-containing gelatine sponge on ectopic bone formation (pag.127)**

Chapter 4 presents *in vivo* results about the ectopic bone formation induced by gelatin sponge enriched with Sr-containing hydroxyapatite and the comparison with gelatin sponge enriched with

BMP2. To do that, gelatin sponges with BMP2 or Sr-hydroxyapatite were implanted around the femur, adjacent to the periosteal surface of 9-11 weeks old male mice. X-ray at 16 and 33 days revealed the induction of mineralized tissue from the femur toward sponge in a more evident way in BMP2 and Sr-hydroxyapatite containing materials. Histology analysis and gene expression revealed increased endochondrial ossification induced by Sr-hydroxyapatite. Moreover, Sr-hydroxyapatite enriched sponges improved bone formation enhancing osteogenic-associated gene expression and reducing those related to osteoclasts differentiation.

## **Chapter 5 - Sr-containing nanoparticles as a potential countermeasure for bone loss induced by microgravity (pag. 150)**

Chapter 5 presents results related to the effect of Sr-containing nanoparticles on osteoblasts differentiation from human mesenchymal stem cells cultured in simulated (RPM) and space microgravity (ISS) conditions. Sr-containing nanoparticles improved the expression and activity of alkaline phosphatase on samples cultured on Random Positioning Machine (RPM) suggesting a positive effect on osteoblast differentiation even in simulated microgravity condition. Moreover, in samples cultured on RPM, Sr-containing nanoparticles induced higher ECM bone matrix deposition and mineralization like as gene expression of specific bone markers, such as *ALP* and *IBSP*.

Sr-containing nanoparticles affected also the release of several cytokines that were demonstrated to be involved in osteoblasts differentiation like IL-1, IL-6, and TNF- $\alpha$  and increased the release of anti-inflammatory cytokines. It seems that nanoparticles' effect on bone remodeling could be related also to the modulation of cytokines release by cells. The *in vitro* experiment performed on the ISS to study the effect of Sr-containing nanoparticles on osteoblasts differentiation in space condition, is also described and preliminary results (RNA quality, proteins quantifications and culture medium) are shown. Further studies (RNASeq results, proteomic studies) are still on going on the space flight experiments.

## **7.2 Closing remarks and Future Perspectives**

In this thesis, research efforts focused on the development of a new nanosystem for the delivery of strontium to improve bone formation are reported. Strontium-substitute hydroxyapatite nanoparticles were synthesized and deeply physical-chemical characterize. The effect of nanoparticles on bone remodeling was evaluated using four different *in vitro* models that allowed investigations on every single bone cell type: BMMSCs, osteoblasts, osteocytes and osteoclasts. It is quite remarkable that, for the first time, results about the effect of Sr on osteocytes are here presented. In future studies the specificity of these nanoparticles needs to be improved to have a

more effective delivery of strontium in an *in vivo* systemic administration. To do that, peptides specific for bone matrix recognition could be conjugated to the external shell of nanoparticles to target them directly to bone tissue. Comparing to the existing drugs used to improve bone formation, Sr-NPs showed to be effective on both osteoblasts and osteoclasts, producing a synergic effect toward increased bone matrix deposition and reducing rebound effect caused by stimulation of only one cell type. Moreover, some steps ahead to the molecular mechanism were performed, but the complete understanding still needs to be addressed.

Moving from *in vitro* to *in vivo*, a new material was developed made of gelatin sponge and enriched with Sr-hydroxyapatite and its effect on ectopic bone formation was evaluated in mice. Ectopic bone formation induced by Sr-hydroxyapatite resulted comparable, even greater in some cases, to BMP2 effect. In this sense, Sr-hydroxyapatite is easier to obtain, cheaper and more stable than BMP2. These studies need to be completed but promising results came out and they can be the platform to develop a material useful in orthopedic field to promote fracture healing or bone reconstruction.

The bone loss is one of the main problems for astronauts who spend long period on ISS. Besides, microgravity is an ideal model to study the inhibition of osteoblast differentiation. Sr-containing nanoparticles showed to be a useful countermeasure to the bone reduction induced by microgravity, with lower side effects of pharmacological treatments. Also in this sense a deeper understanding of the molecular mechanism involved is necessary as well as translational studies on animal models.

## 8. List of Abbreviations

<sup>31</sup> P cross-polarization spectra	
31P CP-MAS .....	47
3-dimensional	
3D .....	128
Acid Phosphatase 5	
ACP5 .....	107
Activating protein 1	
AP-1 .....	8
Activating-transcription factor 4	
ATF4 .....	5
Alkaline phosphatase	
ALP .....	5
Analysis of variance	
ANOVA .....	49
Basic multicellular unit	
BMU .....	12
Bone Marrow	
BM .....	75
Bone Mineral Density	
BMD .....	17
Bone Morphogenetic Protein 2	
BMP2 .....	1
Bone morphogenetic proteins	
BMPs .....	4
Bone sialo protein	
BOSP .....	5
Bovine serum albumin	
BSA .....	47
Calcium-calmodulin dependent kinases typeII	
CaMKII .....	109
Calcium-sensing receptor	
CaSR .....	24
Cathepsin K	
CTSK .....	107
Collagen type I	
(Col I) .....	5
Colony-forming unit fibroblasts	
CFU-F .....	75
Confocal Laser Scanning Microscopy	
CLSM .....	77
CREB-binding protein	
CBP .....	8
d2 isoform of vacuolar ATPase V <sub>o</sub> domain	
Atp6v0d2 .....	116
Decorin	
DEC .....	82
Dendritic cell-specific transmembrane protein	
DC-STAMP .....	8
Dentin matrix protein 1	
DMP1 .....	74
Distal-less homeobox 5	
Dlx5 .....	5
DNAX-activating protein 12	
DAP12 .....	9
Dulbecco's modified Eagle's medium	
DMEM .....	76
Dynamic light scattering	
DLS .....	48
Energy dispersive X-ray spectroscopy	
EDS .....	81
European Medicines Agency	
EMA .....	25
Experimental units	
EU .....	157

Extracellular matrix (ECM).....	5	Inductively coupled plasma optical emission spectrometry ICP-OES.....	46
Fc receptor common $\gamma$ subunit (FcR $\gamma$ ).....	9	Insulin-like Growth Factor IGF .....	5
Fibroblast growth factor 23 FGF23.....	14	Integrin binding Sialoprotein IBSP .....	100
Fibronectin FN.....	82	Intercellular Adhesion Molecule 1 ICAM-1 .....	167
Fourier transform infrared spectroscopy FTIR .....	47	Interleukin IL.....	6
Frizzled Fz .....	4	International Space Station ISS.....	16
G-protein coupled receptor GPCR.....	24	Lipoprotein receptor related protein 5/6 LRP5/6 .....	4
Granulocyte-macrophage colony-stimulating factor GM-CSF.....	167	Lymphoid enhancer factor/T cell factor Lef/Tcf .....	4
Green fluorescent protein GFP.....	101	Macrophage colony stimulating factor M-CSF.....	7
Ground control GC .....	154	Magic Angel Spinning MAS .....	47
Guided bone regeneration GBR.....	127	Matrix metalloproteinases MMP .....	11
Horseradish peroxidase HRP .....	156	Matrix vesicles MVs.....	6
Human Bone Marrow Mesenchymal Stem Cells hBMMSCs.....	75	Mesenchymal stem cell MSC .....	4
Hydroxyapatite HA .....	6	Microphthalmia-associated transcription factor MITF .....	9
Immunoreceptor tyrosine-based activation motif ITAM.....	9	Mitogen-activated protein kinase MAPK .....	25
		Msh homeobox homologue-2 Msx2.....	73

Myocardial infarction	
MI.....	25
Nano-Hydroxyapatites	
nHAp.....	22
Nanoparticles	
NPs .....	22
Nuclear factor of activated T-cells, cytoplasmic 1	
NFATc1 .....	8
Nuclear factor of activated T-cells, cytoplasmic 2	
NFATc2.....	8
Nuclear magnetic resonance	
NMR.....	47
Octacalcium phosphate	
OCP .....	28
Osteocalcin	
(OCN).....	5
Osteoclast-specific immunoreceptor osteoclast associated receptor	
OSCAR.....	8
Osteonectin	
ONT.....	5
Osteopontin	
OPN .....	5
Osteoprotegerin	
OPG .....	10
Osterix	
Osx.....	5
p300/CBP-associated factor	
PCAF .....	8
Paired immunoglobulin-like receptor-A	
PIR-A.....	9
Paraformaldehyde	
PFA .....	77
Parathyroid hormone	
PTH .....	12
Phosphate Buffer Solution	
PBS.....	77
Phospholipase C $\gamma$	
PLC $\gamma$ .....	10
p-nitrophenol phosphate	
pNPP .....	80
Poly(glycolic acid)	
PGA.....	22
Poly(lactic acid)	
PLA .....	22
Protein kinase A	
PKA.....	5
Quantitative reverse-transcription polymerase chain reaction	
qRT-PCR.....	83
Random Positioning Machine	
RPM .....	151
Receptor activator of nuclear factor- $\kappa$ B ligand	
RANKL.....	7
Runt-related transcription factor 2 / core binding factor alpha 1	
Runx2/Cbfa1 .....	5
Scanning electron microscopy	
SEM .....	49
Sclerostin	
SOST .....	6
Selected area electron diffraction	
SAED .....	27
Selective oestrogen receptor modulators	
SERMs .....	18
Signal-regulatory protein $\beta$ 1	

SIRP $\beta$ 1.....	9	TEM .....	27
Small, Integrin-Binding Ligand, N-linked Glycoprotein		Triggering receptor expressed in myeloid cells-2	
SIBLINGs.....	113	TREM-2 .....	9
Strontium		Tumor necrosis factor	
Sr. ....	23	TNF .....	6
Strontium chloride		Tumor necrosis receptor-associated factor	
SrCl <sub>2</sub> .....	26	TRAF .....	7
Strontium ranelate		US Food and Drug Administration	
SrR.....	24	USFDA.....	127
Strontium-Hydroxyapatite		Vascular cell adhesion molecule 1	
Sr-HAp .....	23	VCAM.....	167
Tartrate-resistant acid phosphatase		Vascular endothelial growth factor	
TRAP .....	8	VEGF .....	12
Tetramethylrhodamine		Venous thromboembolism	
TRITC .....	77	VTE.....	25
Transforming growth factor beta		X-ray diffraction	
TGF- $\beta$ .....	4	XRD .....	27
Transmission Electron Microscopy			



## 9. Acknowledgements

At the end of this thesis and my doctoral path, I want to thank Professor Livia Visai to whom I owe most of my professional and scientific advances during the past three years. Thank to her I had the opportunity to take part to the NATO project, one of the most exciting experience in my life. All my respect and my admiration are for the tenacity that she shows every day in the lab and I hope, one day, to have the same determination and strength of character.

I also want to thank all the people with whom I worked in Pavia for the several research projects that we carried out especially my research group so young and so thrilled.

I want to thank the research groups in Trento, Rome and Milan, with whom we shared a few pieces of this research work. A special thank goes to the NATO team members in Rome and Milan.

I also thank the research teams of the Boston University with whom I worked for six months. I thank Professor Louis Gerstenfeld, Professor Paola Divieti Pajevic and Dr. Beth Bragdon for their helpfulness, professionalism and competence that they shared with me. To them, my most sincere and profound gratitude.

I want to thank my parents. They are the cornerstones of my life, those who have made possible every step so far, they have taught me the curiosity and the commitment to the achievement of the goals. I want to thank my sister and her husband for their constant presence in my life, a source of serenity and love.

I want to thank all the friends from Pavia, Taranto and Boston whose support had and has a vital importance in my life.

*PAR INGENIO VIRTUS*

## 10. Publications

### Articles

**Cristofaro F**, Frasnelli M, Sglavo VM, Dirè S, Callone E, Ceccato R, Bruni G, Icaro Cornaglia A, Visai L; Strontium-substituted hydroxyapatite nanoparticles for bone regeneration; *Material Science and Engineering C* 71 (2017) 653–662; doi: 10.1016/j.msec.2016.10.047

Vercellino M, Ceccarelli G, **Cristofaro F**, Balli M, Bertoglio F, Bruni G, Benedetti L, Avanzini MA, Imbriani M, Visai L; Nanostructured TiO<sub>2</sub> Surfaces Promote Human Bone Marrow Mesenchymal Stem Cells Differentiation to Osteoblasts; *Nanomaterials* 2016, 6, 124

Rea G, **Cristofaro F**, Pani G, Pascucci B, Ghuge SA, Corsetto PA, Imbriani M, Visai L, Rizzo AM; Microgravity-driven remodeling of the proteome reveals insights into molecular mechanisms and signal networks involved in response to the space flight environment; *Journal of Proteomics*, 137 (2016) 3–18

Patrucco A, **Cristofaro F**, Simionati M, Zoccola M, Bruni G, Fassina L, Visai L, Mossotti R, Montarsolo A, Tonin C; Wool fibrils sponges with perspective biomedical applications; *Materials Science and Engineering C* 61 (2016) 42–50

Scavone M, Armentano I, Fortunati E, **Cristofaro F**, Mattioli S, Torre L, Kenny JM, Imbriani M, Arciola CR and Visai L; Antimicrobial Properties and Cytocompatibility of PLGA/Ag Nanocomposites; *Materials* 2016, 9, 37;

Burgos N, Armentano I, Fortunati E, Dominici F, Luzi F, Fiori S, **Cristofaro F**, Visai L, Jiménez A, Kenny JM; Functional properties of plasticized bio-based Poly(lactic acid)\_Poly(hydroxybutyrate) (PLA\_PHB) films for active food packaging; *Food and Bioprocess Technology* (2017); doi 10.1007/s11947-016-1846-3

### Abstract on proceedings

**Cristofaro F**, Patrucco A, Simionati M, Zoccola M, Bruni G, Fassina L, Magenes G, Mossotti R, Montarsolo A, Tonin C, Visai L; A new keratin-based scaffold with promising features for biomedical application; *J Appl Biomater Funct Mater* 2016; doi: 10.5301/jabfm.5000321

**Cristofaro F**, Pani G, Pascucci B, Rizzo AM, Rea G, Vukic M, Visai L; *In vitro* effects of nanoparticles on osteoblasts differentiation in microgravity; *Proceedings of the XXXIII National Conference of the Italian Society of Cytometry*, pag 6

**Cristofaro F**, Cambarau M, Grandi S, Fassina L, Omes C, Bruni G, Mustafazade G, Riva F, Mustarelli P, Visai L; An *In vitro* biochemical study of Mesenchymal Stem Cells differentiation on Bioglass Coated Titanium Scaffold; *I materiali Biocompatibili per la medicina*, pag. 230-234; ISBN 9788897683520

Patrucco A, **Cristofaro F**, Bloise N, Simionati M, Zoccola M, Bruni G, Fassina L, Visai L, Magenes G, Mossotti R, Montarsolo A, Tonin C; Fabrication of wool fibrils micro- and macroporous scaffold for bone tissue engineering, 9th International Conference on Fiber and Polymer Biotechnology, pag 51

## Oral Communication

Workshop: Research and Nanomedicine, 20 June 2016, Pavia – Italy  
Nanoparticles for bone regeneration

National Congress of Italian Society of Biomaterials, 02 – 04 July 2014, Palermo - Italy  
An *In vitro* biochemical study of Mesenchymal Stem Cells differentiation on Bioglass Coated Titanium Scaffold

## Poster Communication

Conference of European Centre for Nanomedicine, 18 June 2016, Milan - Italy  
**Cristofaro F**, Frasnelli M, Dirè S, Sglavo V, Bloise N, Bertoglio F, Visai L; Strontium-containing nanoparticles improve osteoblast proliferation and differentiation

National Congress of Italian Society of Biomaterials (SIB), 13-15/0/2015 Ischia Porto - Italy  
**Cristofaro F**, Patrucco A, Simionati M, Zoccola M, Bruni G, Fassina L, Magenes G, Mossotti R, Montarsolo A, Tonin C, Visai L; A NEW KERATIN-BASED SCAFFOLD WITH PROMISING FEATURES FOR BIOMEDICAL APPLICATION

International Conference, NanotechItaly2015  
**Cristofaro F**, Pani G, Pascucci B, Rizzo AM, Rea G, Vukich M, Visai L; In vitro effects of nanoparticles on bone remodelling in microgravity

XVIII International School of “NANOMECHANICS IN BIOMOLECULAR ADHESION”, Franchetti building, 27-31 January 2014, Venice - Italy  
**Cristofaro F**, Dirè S., Visai L. Bone remodelling study using Strontium enriched Hydroxyapatite Nanoparticles

International Symposium of European Materials Research Society; Congress Center, 26th – 30th May 2014, Lille - France  
S. Grandi, **Cristofaro F**, Mustarelli P., Bruni G., Cermola G., Visai L.; In Vitro Studies of 58S Bioglass coating by sol-gel Process Onto Titanium Alloy Scaffolds

International Conference, NanotechItaly2014 26 – 28 November 2014, Venice – Italy  
**Cristofaro F**, Rizzo AM, Pani G, Dirè S, Rea G, Bruni G, Vukich M, Visai L; Bone Remodeling study using Strontium enriched hydroxyapatite nanoparticles (nHAPs)

National Congress of Italian Society of Biomaterials (SIB), 03-05/06/2015 Portonovo - Italy  
**Cristofaro F**, Frasnelli M, Bloise N, Cornaglia A I, Dirè S, Sglavo V, Visai L. *In vitro study of Strontium-enriched Hydroxyapatite on osteoblast differentiation*  
NanotechITALY2015 Congress,

EMRS Spring meeting, Simposium X, 11-15/05/2015  
**Cristofaro F**, Dirè S, Bruni G, Ceccarelli G, Cornaglia AI, Imbriani M, Visai L, *An in vitro study of Strontium-enriched Hydroxyapatite effects on osteoblast cultures*; Published in Polimer International (Wiley)

# 11. Curriculum Vitae

## PERSONAL INFORMATION

Name and Surname **Francesco CRISTOFARO**  
Date of birth (dd/mm/yyyy) 26 / 01 / 1990  
Nationality Italian  
Permanent Address Via golfo di Taranto, 5/H, 74121 Taranto - Italy  
Current Residential Address (until 31/12/2016) Via Don Giovanni Minzoni 7, 27100 Pavia - Italy  
Mobile phone +39 329 54 46 519  
E-mail [francesco.cristofaro01@ateneopv.it](mailto:francesco.cristofaro01@ateneopv.it);  
Linkedin [www.linkedin.com/in/francesco-cristofaro-6962b591](http://www.linkedin.com/in/francesco-cristofaro-6962b591)



## EDUCATION, TRAINING AND PROFESSIONAL EXPERIENCES

November 2013 – October 2016 **Ph.D. Student**  
(3 years)

University of Pavia – PhD School in **Biomedical Science**  
Molecular Medicine Department, Biochemistry Unit, Viale taramelli 3/B, Pavia - Italy  
Prof. Livia Visai Labs  
+39 0382 987725  
<http://molecularmedicine.unipv.it/research-groups/biochemistry/l-visai/>

My PhD project is about the effect of nanoparticles on bone remodelling process. In particular, we developed nanoparticles to modulate bone cells activity to improve bone matrix deposition. To do this we used *in vitro* models like osteoblast-like cell lines, primary human mesenchymal stem cells, osteoclasts precursor and osteocytes.

### Hard Skills acquired:

- Cell culture techniques focusing on bone cells culture
- Biochemical techniques (Protein Extraction, ELISA, Electrophoresis, Western Blot, Protein Purification, FPLC, HPLC, Mass Spectrometry)
- Cyto-morphometric analysis (cyto-chemical staining, immunostaining)
- Extracellular Bone matrix analysis (Protein quantification and mineralization)
- Molecular Techniques (DNA and RNA extraction, PCR, qRT-PCR)
- Nanoparticles/Biomaterials preparation and Physical-chemical characterization (DLS, Z-potential, SEM, TEM, FT-IR)
- Peer-reviewed paper preparation

### Soft Skills acquired:

- Experiments Design
- Team work and Students Mentoring
- Data Presentation (oral and written)
- Time Management (Creating schedules; Setting daily, weekly and monthly goals)
- Problem solving

December 2015 – May 2016  
(6 months)

### Visiting PhD Student

**Boston University – School of Medicine**  
Orthopedic Surgery Department, 715 Albany St, E-243 - Boston MA 02118 - USA  
Prof. Louis C. Gerstenfeld

In those six months, we developed a collagen based nanomaterials for the bone regeneration. We used *in vivo* model to study the ectopic bone formation induced by the material.

**Hard Skills** acquired:

- Aseptic surgeries on mice
- Mice tissues harvesting
- RNA extraction from bone and muscle tissues and histological assays

---

December 2015 – May 2016  
(6 months)

**Boston University – School of Dental Medicine**

Molecular and Cell Biology Department, 700 Albany St. Boston, MA 02118 - USA  
Prof. Paola Divieti Pajevic

Nanoparticles effects on murine osteocytes activity.

**Hard Skills** acquired:

- *In vitro* Osteocytes culture
- Bone cells signaling (sclerostin, RANKL)
- Cyto-morphometric analysis (cyto-chemical staining, immunostaining)
- Extracellular Bone matrix analysis (Protein quantification and mineralization)

**Soft skills** acquired in Boston:

- *In vivo* experiments design
- Ability to work in an international research group
- Communicative Skills
- Adapt to a new work environment

---

March 2015 – April 2015  
(2 months)

**Visiting Scientist**

NASA Space Kennedy Center  
Cape Canaveral  
Florida - USA.

We studied the effect of nanoparticles on osteoblasts differentiation in absence of gravity force. We cultured Mesenchymal Stem Cells on International Space Station and we analysed transcriptome through RNAseq technique, proteome and cytokine release.

Italian Space Agency (ASI), "Nanoparticles based countermeasures for treatment of microgravity induced osteoporosis" (Nanoparticles and Osteoporosis — NATO project) contract n. 2013-060-I.0

**Skills** acquired:

- Space biology
- Problem Solving in not ordinary lab environment

<http://nanospace.unipv.it/>

[https://youtu.be/ankuD-q8e\\_M](https://youtu.be/ankuD-q8e_M)

---

November 2013 – Present  
(3 years)

**College Students' Tutor** for Chemistry and Biochemistry Courses

University of Pavia, School of Medicine - Italy

**Skills** acquired:

- Students Mentoring
- Lesson Preparation
- Effective Communication

---

September 2016 - Present

**Member of Editorial Board** of "Insights in Biomedical Engineering" Journal

Responsibilities:

- **Peer reviewing** from 3 to 5 high impact scientific articles

October 2011 – September 2013 (2 years)	<b>Master Degree in Sperimental and Applied Biology (110/110 cum laudem)</b>
	University of Pavia – Italy
	<b>Skills</b> acquired: <ul style="list-style-type: none"> <li>• Toxicological Analysis</li> <li>• Food and Drug Quality Control</li> <li>• Microbiological, Biochemical and molecular Analysis</li> </ul>
March 2013 – August 2013 (6 months)	<b>Visiting Master Student</b> University of Brighton – UK School of Pharmacy and Biomolecular Sciences, Moulsecoomb, Brighton BN2 4GJ Prof. Matteo Santin  We developed a drug delivery vector gold nanoparticles-based for breast cancer treatment.  <b>Skills</b> acquired: <ul style="list-style-type: none"> <li>• Solid Phase Polymer synthesis and characterization</li> <li>• Gold Nanoparticles Synthesis and characterization</li> <li>• Breast cancer cell lines (SK-BR-3, MCF-7) culture</li> </ul>
October 2008 – July 2011 (3 years)	<b>Bachelor Degree in Biological Science (110/110 cum laudem)</b>  <i>University of Bari “Aldo Moro” - Italy</i>  Basic knowledge in biological science with insights into the biochemistry. Bachelor thesis in Mass Spectrometry techniques applied to biochemistry field.
Professional Referees	Livia <b>VISAI</b> , PhD – University of Pavia – Molecular medicine Department, Biochemistry Unit – Via Taramelli 3/B, 27100 Pavia – Italy. E-mail: <a href="mailto:livia.viasi@unipv.it">livia.viasi@unipv.it</a> ; Tel: +38 0382 987725; Skype ID: livia.visai  Louis C. <b>GERSTENFELD</b> , Ph.D. – Boston University – School of Medicine, Orthopedic Surgery Department – 715 Albany St, E-243 - Boston MA 02118 – USA e-mail: <a href="mailto:lgersten@bu.edu">lgersten@bu.edu</a> ; Tel. +1 617 414 1660; Fax: +1 617 414 1661  Paola <b>DIVIETI</b> Pajavic – Boston University - School of Dental Medicine, Molecular and Cell Biology Department, 700 Albany St. - Boston MA 02118 – USA e-mail: <a href="mailto:pdivieti@bu.edu">pdivieti@bu.edu</a> ; Tel +1 617 414 1040; Skype ID: ppajeivic

### SCIENTIFIC PUBLICATIONS

Articles	<p><b>Cristofaro F</b>, Frasnelli M, Sglavo VM, Dirè S, Callone E, Ceccato R, Bruni G, Icaro Cornaglia A, Visai L; Strontium-substituted hydroxyapatite nanoparticles for bone regeneration; <i>Material Science and Engineering C</i> 71 (2017) 653–662; doi: 10.1016/j.msec.2016.10.047</p> <p>Burgos N, Armentano I, Fortunati E, Dominici F, Luzi F, Fiori S, <b>Cristofaro F</b>, Visai L, Jiménez A, Kenny JM; Functional properties of plasticized bio-based Poly(lactic acid)_Poly(hydroxybutyrate) (PLA_PHB) films for active food packaging; <i>Food and Bioprocess Technology</i>; <u>Submitted</u></p> <p>Vercellino M, Ceccarelli G, <b>Cristofaro F</b>, Balli M, Bertoglio F, Bruni G, Benedetti L, Avanzini MA, Imbriani M, Visai L; Nanostructured TiO<sub>2</sub> Surfaces Promote Human Bone Marrow Mesenchymal Stem Cells Differentiation to Osteoblasts; <i>Nanomaterials</i> 2016, 6, 124</p> <p>Rea G, <b>Cristofaro F</b>, Pani G, Pascucci B, Ghuge SA, Corsetto PA, Imbriani M, Visai L, Rizzo AM; Microgravity-driven remodeling of the proteome reveals insights into molecular mechanisms and signal networks involved in response to the space flight environment; <i>Journal of Proteomics</i>, 137 (2016) 3–18</p>
----------	--

---

Patrucco A, **Cristofaro F**, Simionati M, Zoccola M, Bruni G, Fassina L, Visai L, Mossotti R, Montarsolo A, Tonin C; Wool fibrils sponges with perspective biomedical applications; *Materials Science and Engineering C* 61 (2016) 42–50

Scavone M, Armentano I, Fortunati E, **Cristofaro F**, Mattioli S, Torre L, Kenny JM, Imbriani M, Arciola CR and Visai L; Antimicrobial Properties and Cytocompatibility of PLGA/Ag Nanocomposites; *Materials* 2016, 9, 37;

Burgos N, Armentano I, Fortunati E, Dominici F, Luzi F, Fiori S, Cristofaro F, Visai L, Jiménez A, Kenny JM; Functional properties of plasticized bio-based Poly(lactic acid)\_Poly(hydroxybutyrate) (PLA\_PHB) films for active food packaging; *Food and Bioprocess Technology* (2017); doi 10.1007/s11947-016-1846-3

Activity of **peer-reviewing** for Journal of Applied Biomaterials & Functional Materials and

---

Abstract on Proceeding

**Cristofaro F**, Patrucco A, Simionati M, Zoccola M, Bruni G, Fassina L, Magenes G, Mossotti R, Montarsolo A, Tonin C, Visai L; A new keratin-based scaffold with promising features for biomedical application; *J Appl Biomater Funct Mater* 2016; doi: 10.5301/jabfm.5000321

**Cristofaro F**, Pani G, Pascucci B, Rizzo AM, Rea G, Vukic M, Visai L; *In vitro* effects of nanoparticles on osteoblasts differentiation in microgravity; Proceedings of the XXXIII National Conference of the Italian Society of Cytometry, pag 6

**Cristofaro F**, Cambarau M, Grandi S, Fassina L, Omes C, Bruni G, Mustafazade G, Riva F, Mustarelli P, Visai L; An *In vitro* biochemical study of Mesenchymal Stem Cells differentiation on Bioglass Coated Titanium Scaffold; *I materiali Biocompatibili per la medicina*, pag. 230-234; ISBN 9788897683520

Patrucco A, **Cristofaro F**, Bloise N, Simionati M, Zoccola M, Bruni G, Fassina L, Visai L, Magenes G, Mossotti R, Montarsolo A, Tonin C; Fabrication of wool fibrils micro- and macroporous scaffold for bone tissue engineering, 9th International Conference on Fiber and Polymer Biotechnology, pag 51

Oral Communication

Workshop: Research and Nanomedicine, 20 June 2016, Pavia – Italy  
Nanoparticles for bone regeneration

National Congress of Italian Society of Biomaterials, 02 – 04 July 2014, Palermo - Italy  
An *In vitro* biochemical study of Mesenchymal Stem Cells differentiation on Bioglass Coated Titanium Scaffold

Poster communication

Conference of European Centre for Nanomedicine, 18 June 2016, Milan - Italy

**Cristofaro F**, Frasnelli M, Dirè S, Sglavo V, Bloise N, Bertoglio F, Visai L; Strontium-containing nanoparticles improve osteoblast proliferation and differentiation

National Congress of Italian Society of Biomaterials (SIB), 13-15/0/2015 Ischia Porto - Italy

**Cristofaro F**, Patrucco A, Simionati M, Zoccola M, Bruni G, Fassina L, Magenes G, Mossotti R, Montarsolo A, Tonin C, Visai L; A NEW KERATIN-BASED SCAFFOLD WITH PROMISING FEATURES FOR BIOMEDICAL APPLICATION

International Conference, NanotechItaly2015

**Cristofaro F**, Pani G, Pascucci B, Rizzo AM, Rea G, Vukich M, Visai L; In vitro effects of nanoparticles on bone remodelling in microgravity

XVIII International School of “NANOMECHANICS IN BIOMOLECULAR ADHESION”, Franchetti building, 27-31 January 2014, Venice - Italy

**Cristofaro F**, Dirè S., Visai L. Bone remodelling study using Strontium enriched Hydroxyapatite Nanoparticles

International Symposium of European Materials Research Society; Congress Center, 26th – 30th May 2014, Lille - France

S. Grandi, **Cristofaro F**, Mustarelli P., Bruni G., Cermola G., Visai L.; In Vitro Studies of 58S

Bioglass coating by sol-gel Process Onto Titanium Alloy Scaffolds

International Conference, NanotechItaly2014 26 – 28 November 2014, Venice – Italy

**Cristofaro F**, Rizzo AM, Pani G, Dirè S, Rea G, Bruni G, Vukich M, Visai L; Bone Remodeling study using Strontium enriched hydroxyapatite nanoparticles (nHAPs)

National Congress of Italian Society of Biomaterials (SIB), 03-05/06/2015 Portonovo - Italy

**Cristofaro F**, Frasnelli M, Bloise N, Cornaglia A I, Dirè S, Sglavo V, Visai L. *In vitro study of Strontium-enriched Hydroxyapatite on osteoblast differentiation*  
NanotechITALY2015 Congress,

EMRS Spring meeting, Simposium X, 11-15/05/2015

**Cristofaro F**, Dirè S, Bruni G, Ceccarelli G, Cornaglia AI, Imbriani M, Visai L, *An in vitro study of Strontium-enriched Hydroxyapatite effects on osteoblast cultures*; Published in Polimer International (Wiley)

<b>PERSONAL SKILLS</b>	
------------------------	--

FIRST LANGUAGE *ITALIAN*

OTHER LANGUAGES *ENGLISH*

- **TRINITY CERTIFICATION - VIII GRADE.**

	<b>Understanding</b>		<b>Speaking</b>		<b>Writing</b>
	<i>listening</i>	<i>Reading</i>	<i>Spoken Interaction</i>	<i>Spoken Production</i>	
European Level	<i>B1</i>	<i>B2</i>	<i>B1</i>	<i>B1</i>	<i>C1</i>

- ✓ **Enthusiastic:** Always willing to build morale and improve work environment by showing enthusiasm for all tasks and responsibilities.
- ✓ **Effective Communication Skills:** Articulate communicator with appreciation for the different communication styles required when working with other team members.
- ✓ **Honest and Reliable:** Strong morals and ethics ensure honesty, reliability and ability to undertake tasks responsibly.
- ✓ **Flexible:** Understanding of need to remain flexible to support last-minute demands and changes. Comfortable in changing environments and situations, ensuring ability to remain flexible and adaptable at all times.
- ✓ **Problem Solving:** Applied a logical approach to problem solving to minimise conflict and create positive outcomes. Commended for helping others understand reasons for proposed resolutions.

Pavia, 15 / 01 / 2017

Francesco Cristofaro



